

## Atmospheric nanoparticle growth

Dominik Stolzenburg <sup>\*</sup>

*Institute for Atmospheric and Earth System Research/Physics, University of Helsinki, 00560 Helsinki, Finland and Institute for Materials Chemistry, TU Wien, 1060 Vienna, Austria*

Runlong Cai <sup>†</sup>

*Institute for Atmospheric and Earth System Research/Physics, University of Helsinki, 00560 Helsinki, Finland*

Sara M. Blichner 

*Department of Environmental Science (ACES), Stockholm University, 10691 Stockholm, Sweden*

Jenni Kontkanen  and Putian Zhou 

*Institute for Atmospheric and Earth System Research/Physics, University of Helsinki, 00560 Helsinki, Finland*

Risto Makkonen

*Finnish Meteorological Institute, 00560 Helsinki, Finland*

Veli-Matti Kerminen 

*Institute for Atmospheric and Earth System Research/Physics, University of Helsinki, 00560 Helsinki, Finland*

Markku Kulmala 

*Institute for Atmospheric and Earth System Research/Physics, University of Helsinki, 00560 Helsinki, Finland, Aerosol and Haze Laboratory, Beijing University of Chemical Technology (BUCT), 100029 Beijing, China, and Joint International Research Laboratory of Atmospheric and Earth System Sciences, Nanjing University, 210023 Nanjing, China*

Ilona Riipinen

*Department of Environmental Science (ACES), Stockholm University, 10691 Stockholm, Sweden*

Juha Kangasluoma 

*Institute for Atmospheric and Earth System Research/Physics, University of Helsinki, 00560 Helsinki, Finland*

 (published 9 November 2023)

New particle formation of liquid or solid nanoparticles from gas-phase precursors is a decisive process in Earth's atmosphere and is considered one of the largest uncertainties in climate change predictions. Key for the climate relevance of new particle formation is the growth of freshly formed molecular clusters, as it determines the survival of these particles to cloud condensation nuclei sizes, where they can contribute to the aerosol-indirect effect. This review lays out the fundamental definitions of nanoparticle growth and addresses the rapidly emerging field of new particle formation studies with a focus on the diverse processes contributing to nanoparticle growth, explicitly comparing the latest experimental findings and their implementation in large-scale models. Atmospheric nanoparticle growth is a complex phenomenon including condensational and reactive vapor uptake, aerosol

<sup>\*</sup>dominik.stolzenburg@tuwien.ac.at

<sup>†</sup>runlong.cai@helsinki.fi

coagulation, and sink processes. It is linked to thermodynamics, cluster- and phase-transition physics. Nanoparticle growth rates measured from the evolution of the particle-size distribution describe growth as a collective phenomenon, while models often interpret them on a single-particle level and incorporate it into highly simplified size-distribution representations. Recent atmospheric observations show that sulfuric acid together with ammonia and amines, iodic acid, and oxidized organic species can contribute to nanoparticle growth, whereas most models describe the growth effects from a limited subset of this variety of condensable vapors. Atmospheric simulation chamber experiments have clarified the role of ions, intermolecular forces, the interplay of acids and bases, and the contribution of different types of organic vapors. Especially in the complex thermodynamics of organic vapor condensation, the field has had noteworthy advances over the last decade. While the experimental field has achieved significant progress in methodology and process level understanding, this has not led to a similar improvement in the description of the climate impact of nanoparticle formation in large-scale models. This review sets the basis to better align experimental and modeling studies on nanoparticle growth, giving specific guidance for future studies aiming to resolve the questions as to why the climate response in large-scale models seems to be buffered against high survival probabilities and why the global growth observations herein show surprisingly low variation.

DOI: [10.1103/RevModPhys.95.045002](https://doi.org/10.1103/RevModPhys.95.045002)

## CONTENTS

I. Introduction	3	3. Other causes of apparent growth: Transport, emissions, and variations in vapor concentration	22
II. Definition: Growth in Models and Experiments	5	C. Mechanistic understanding of condensational growth	23
A. Collective phenomenon and single-particle approximation	5	1. Growth at the kinetic collision limit	23
1. The growth of a single particle	5	a. Hard-sphere approximation	23
2. The growth of a population of particles	7	b. Intermolecular forces	24
B. Definitions with respect to the relevance of nanoparticle growth in the climate system	8	2. Nonvolatile acids: Sulfuric and iodic acid	25
III. Measuring Nanoparticle Growth: Methodology	9	a. Sulfuric acid	25
A. Instrumentation for the measurement of atmospheric nanoparticle growth	9	b. Iodic acid	27
1. Electrical mobility analysis	9	c. Hygroscopicity effects	27
2. Condensation particle counters	10	3. Acid-base interactions: Sulfuric acid with ammonia and amines	28
3. Measurement of trace vapors, particle-phase composition, hygroscopicity, and volatility	10	a. Equilibrium thermodynamics	28
4. Instrumental limitations in measuring nanoparticle growth	11	b. Ammonia	28
B. Analysis methods applied to estimating nanoparticle growth rates	12	c. Amines	29
1. Collective approaches: Mode fitting, maximum concentration, and appearance time	12	4. Contribution of clusters to particle growth	29
a. Mode-fitting method	12	5. Other acids: Nitric acid, methanesulfonic acid, and organic acids	30
b. Maximum concentration and appearance time method	13	a. Nitric acid	30
c. Applicability of collective methods	13	b. Methanesulfonic acid	30
2. Dynamic approaches based on the aerosol general dynamic equation	14	c. Small organic acids	31
C. Method performance under varying conditions: From rural backgrounds to highly polluted megacities	15	6. Reversible condensation of oxidized organics: Semivolatile partitioning and low-volatility growth	32
D. Analysis methods for estimating particle survival probabilities	16	a. Kinetic condensation versus thermodynamic equilibrium	32
IV. Understanding Nanoparticle Growth: From Measurements to Process Models	17	b. Volatility basis set	33
A. Overview of ambient observations of nanoparticle growth	17	7. Gas- and particle-phase chemistry influencing oxygenated-organic-molecule-driven growth	35
B. Growth as a collective phenomenon	19	a. Gas-phase chemistry	35
1. Apparent and real growth due to coagulation	22	b. Particle-phase reactions	36
2. Growth driven by diffusion in the particle-size space	22	V. Large-Scale Modeling of Nanoparticle Growth: The Current State	36
		A. Representation of growth in large-scale models	36
		1. Representation of the particle number size distribution and aerosol dynamics	37
		2. Condensable vapors considered for growth processes	37
		B. Importance of nanoparticle growth in global and regional scale atmospheric predictions	38
		C. Testing the sensitivity to early growth in Earth system models	41
		1. Model descriptions	41

a. NorESM (OsloAero and OsloAeroSec)	41
b. TM5	41
c. ECHAM	42
2. Model results	42
VI. Conclusion and Outlook	44
A. Summary	44
B. Recommendations for future growth studies	46
1. Experimental requirements	46
2. Recommendations for model setup	47
C. Future work	48
List of Symbols and Abbreviations	49
Acknowledgments	50
References	50

## I. INTRODUCTION

Aerosols, defined as a two-phase system of liquid or solid particles suspended in a carrier gas, are ubiquitous in Earth's atmosphere. Aerosol particles influence the global climate (Masson-Delmotte *et al.*, 2023) and impact human health (Lelieveld *et al.*, 2015; Apte *et al.*, 2018). In fact, they are recognized as a major source of uncertainty in climate change predictions (Boucher *et al.*, 2013). Aerosols can alter Earth's radiation budget directly by scattering or absorbing incoming solar radiation (Charlson *et al.*, 1992; Haywood and Shine, 1995; Myhre, 2009), and indirectly by affecting cloud properties (Twomey, 1974; Albrecht, 1989).

The emission of volatile gases into the atmosphere from a variety of sources from the biosphere and anthroposphere [such as SO<sub>2</sub>, NH<sub>3</sub>, or volatile organic compounds (VOCs)] can result in the formation of low volatile trace vapors through atmospheric oxidation, which are able to form a new aerosol phase. This phase-transition process, called new particle formation (NPF), includes both the formation of stable molecular clusters, a process commonly referred to as nucleation, and the subsequent growth of the newly formed particles to larger sizes (Kulmala, 2003). For most parts of the troposphere, the dominant source with respect to aerosol number concentration is NPF (Yu and Luo, 2009; Spracklen *et al.*, 2010; Gordon *et al.*, 2017). These newly formed particles can even grow to sizes where they can be efficiently activated by water and become cloud droplets (Andreae and Rosenfeld, 2008); i.e., they act as cloud condensation nuclei (CCN), thereby influencing the properties of clouds (Ackerman *et al.*, 2000; Mauritsen *et al.*, 2011; Bellouin *et al.*, 2020; Quaas *et al.*, 2020), and hence the global climate (Boucher *et al.*, 2013). In addition, NPF can contribute to severe air pollution with high mass concentrations of particulate matter (Guo *et al.*, 2014; Kulmala *et al.*, 2021) and can influence human health through higher abundances of ultrafine particles (< 100 nm), which are able to penetrate deep into the human lung (Pedata *et al.*, 2015; Kwon, Ryu, and Carlsten, 2020). Figure 1 illustrates that connection between vapor emissions and their severe impact on climate and human health via NPF. NPF occurs frequently at many locations around the globe (Kerminen *et al.*, 2018; Nieminen *et al.*, 2018). It is often observed in the daytime and hence is associated with enhanced photochemical activity in the atmosphere (Kulmala *et al.*, 2013). The direct observation of molecular cluster formation has greatly improved our understanding of the most important atmospheric nucleation mechanisms (Sipilä *et al.*, 2010, 2016; Bianchi *et al.*, 2016;

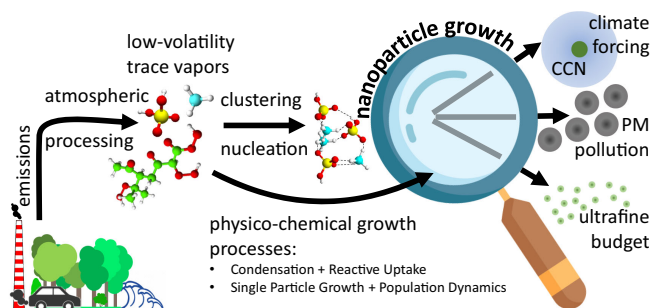


FIG. 1. Link between vapor emissions, their atmospheric processing (oxidation) into low-volatility trace vapors (H<sub>2</sub>SO<sub>4</sub>, NH<sub>3</sub>, and oxidized organics are shown), and subsequent clustering and growth that can lead to severe impacts on the climate system and human health via both air pollution from particulate matter (PM) and the ultrafine (< 100 nm) aerosol burden.

Yao *et al.*, 2018; Beck *et al.*, 2021; Yan *et al.*, 2021). However, the newly formed small particles are highly diffusive and quickly get removed from the number budget by coagulation with larger preexisting aerosol particles, and they therefore need to grow fast in order to avoid that scavenging (Pierce and Adams, 2007). The characteristic scavenging time is determined by the background aerosol concentration and the collision rate coefficient of the growing particles with that background population. Since the collision rate coefficient decreases significantly with increases in particle size, by the time the particle reaches the Aitken mode (> 25 nm in particle diameter), the characteristic scavenging time typically becomes longer than the time it takes for the particle to grow to sizes relevant for climate and air quality. Thus, their survival probability will be greatly enhanced (McMurry and Friedlander, 1979; McMurry, 1983; Kerminen and Kulmala, 2002; Kuang *et al.*, 2010). Large-scale model simulations suggest that atmospheric NPF via growth of the formed particles to larger sizes is the main contributor to the global CCN budget (Merikanto *et al.*, 2009; Pierce and Adams, 2009; Makkonen *et al.*, 2012a; Gordon *et al.*, 2017). Observations made in continental boundary layers confirm the important contribution of atmospheric NPF to the CCN population in different environments ranging from forested regions to moderately polluted rural areas even to polluted urban locations (Kuang, McMurry, and McCormick, 2009; Sihto *et al.*, 2011; Kerminen *et al.*, 2012; Peng *et al.*, 2014; Yu *et al.*, 2014; Zheng *et al.*, 2020). In addition, it was shown that NPF at high altitudes can also lead to increased CCN numbers (Williamson *et al.*, 2019). Therefore, the contribution of NPF to the global budget of CCN establishes a crucial link between particle nucleation and the radiative balance of the atmosphere (Boucher *et al.*, 2013; Carslaw *et al.*, 2013), where fast aerosol growth processes might be of even larger importance than the nucleation mechanism responsible for cluster formation. In the same way, enhanced aerosol survival potentially via fast growth processes is also crucial for the contribution of NPF to air pollution, as the characteristic scavenging time under polluted conditions with a high preexisting sink is even longer (Kulmala *et al.*, 2017, 2021; Kulmala, Cai *et al.*, 2022).

In this review, we focus on the sub-25-nm range when discussing atmospheric nanoparticle growth, as this is the crucial range determining particle survival. The growth of sub-25-nm aerosol particles is a highly complex physico-chemical process including the phase transition through

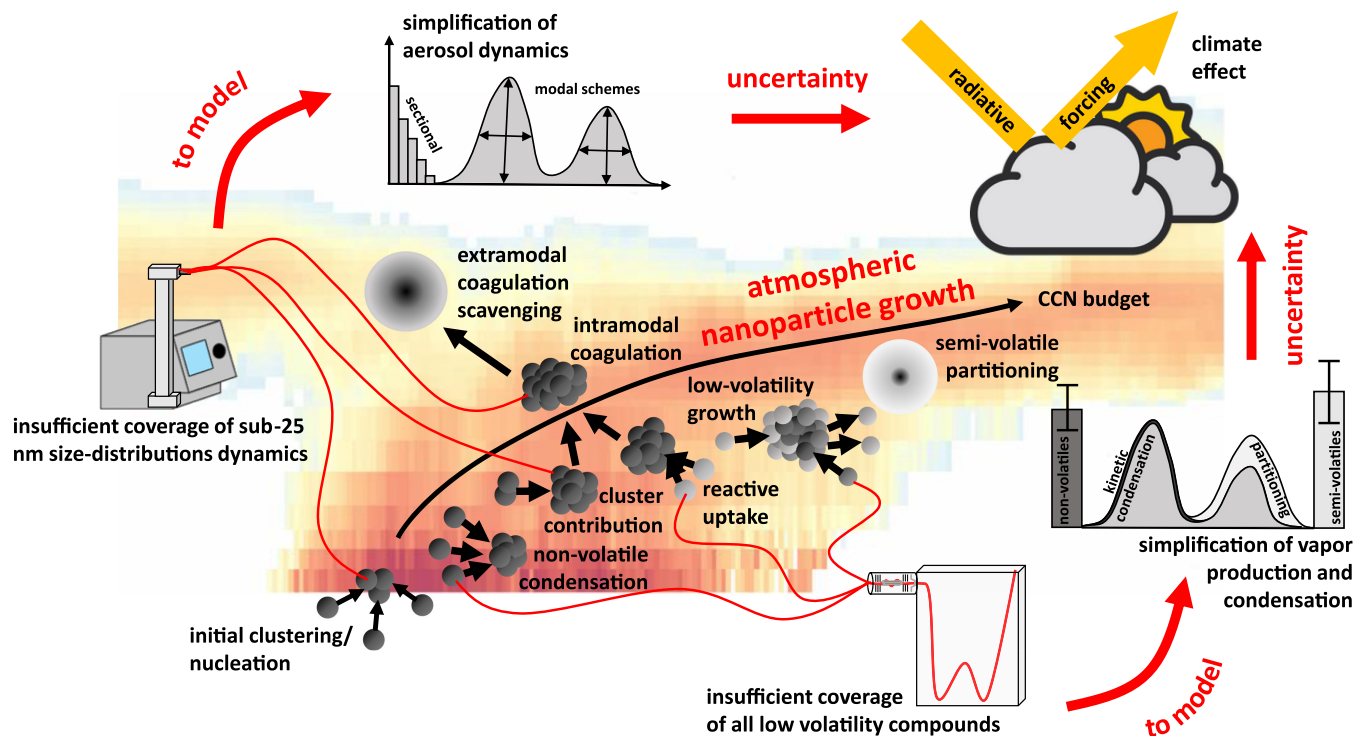


FIG. 2. Overview of the physicochemical processes involved in atmospheric nanoparticle growth, the related experimental approaches in assessing contributing vapors, and the particle-size-distribution dynamics illustrating their limitations. Together with common model simplifications this translates into a major source of uncertainty for climate forcing predictions. The background shows a typical new particle formation event recorded in the Finnish boreal forest at Hyytiälä, with the color code representing the number concentration of a certain particle size (vertical axis) and time instant (horizontal axis).

vapor condensation, molecular interaction kinetics, coagulation, and chemically induced reactive uptake (Kulmala, Laakso *et al.*, 2004; Wang *et al.*, 2010; Vehkamäki and Riipinen, 2012; Zhang *et al.*, 2012), which is illustrated in Fig. 2.

Owing to this complexity, there is no unambiguous definition of atmospheric nanoparticle growth rates (GRs), which are measured from the evolution of the particle number size distribution (PNSD) as a collective phenomenon (Kulmala *et al.*, 2012), whereas models interpret them on a single-particle level (Stolzenburg *et al.*, 2005) and, as shown in Fig. 2, have simplified representations of aerosol dynamics to calculate particle survival (Kuang, McMurry, and McCormick, 2009). However, the descriptions of growth need to be aligned in order to reduce the significant bias in model and experimental CCN number predictions (Westervelt *et al.*, 2013; Fanourgakis *et al.*, 2019). This in turn relies on a better theoretical understanding of the involved dynamics ranging from the molecular collision rates to cluster-cluster coagulation to the contribution of different vapors. A variety of approaches to analyze experimental data exist (Kulmala *et al.*, 2012; Dada *et al.*, 2020b), and some recent developments start to disentangle different growth processes including the contribution of cluster coagulation (Kuang, Chen, Zhao *et al.*, 2012; Pichelstorfer *et al.*, 2018). As shown in Fig. 2, this relies on accurate aerosol size-distribution measurements, but the methodology used for quantifying nanoparticle growth in experiments is still limited.

The decisive size range for the survival of newly formed particles,  $< 10$  nm in diameter, is difficult to measure

accurately (Kangasluoma *et al.*, 2020) and, despite significant advances in the available instrumentation, large uncertainties remain (Kangasluoma and Kontkanen, 2017). In addition, as shown in Fig. 2, it is challenging to cover the wide variety of low volatile trace vapors with individual experimental techniques, and knowledge about the sub-10-nm particle composition remains sparse (Smith *et al.*, 2021). Nevertheless, recent atmospheric observations were able to show that sulfuric acid together with ammonia and amines (Smith *et al.*, 2010; Chen *et al.*, 2012; Kulmala *et al.*, 2013; Yao *et al.*, 2018; Brean *et al.*, 2021; M. Cai *et al.*, 2021; Yan *et al.*, 2021), iodic acid (Sipilä *et al.*, 2016; Baccarini *et al.*, 2020; Beck *et al.*, 2021), and oxidized organic species formed through atmospheric oxidation of VOCs released by both the anthroposphere and the biosphere (Kulmala *et al.*, 1998, 2013; Bianchi *et al.*, 2016) can contribute to nanoparticle growth, whereas most models need to describe the growth using a limited subset of condensable vapors (Fanourgakis *et al.*, 2019), as shown in Fig. 2. Moreover, laboratory studies and field measurements have greatly enhanced our understanding of the involved physicochemical processes in the last decade, for instance, the role of ions (Yli-Juuti *et al.*, 2011; Gonser *et al.*, 2014; Svensmark *et al.*, 2017; Wagner *et al.*, 2017), intermolecular forces (Stolzenburg *et al.*, 2020), the interplay between acids and bases (Yli-Juuti *et al.*, 2013; Lehtipalo *et al.*, 2016; Wang *et al.*, 2020b), and the contribution of different types of organic vapors (Tröstl *et al.*, 2016a; McFiggans *et al.*, 2019; Mohr *et al.*, 2019). Large-scale atmospheric models have recently started to implement more complex schemes for

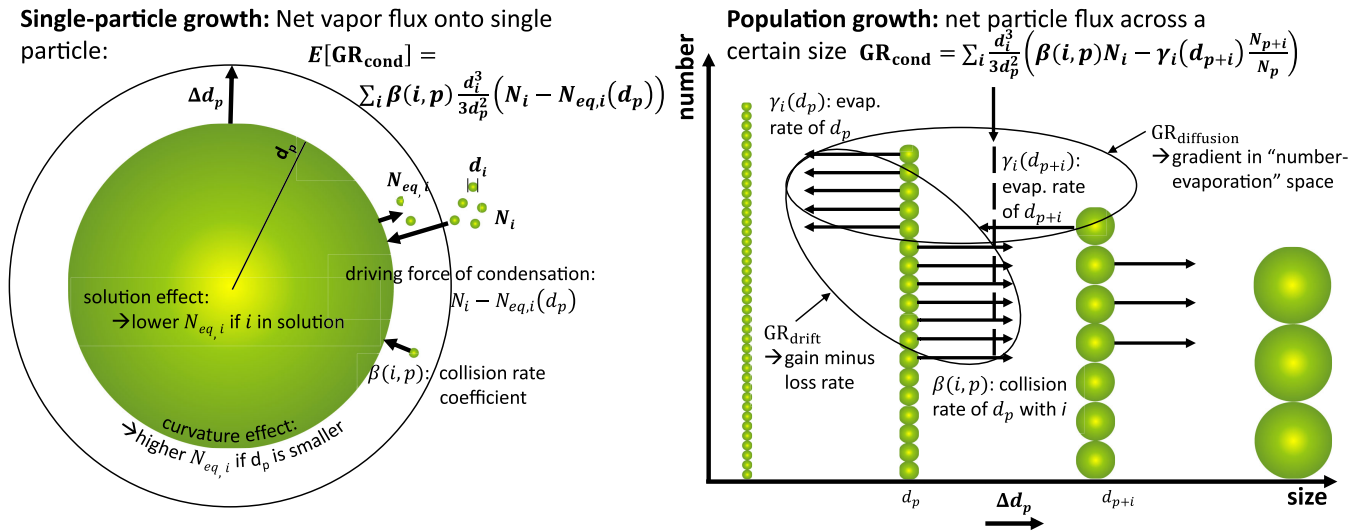


FIG. 3. Contrasting definitions of nanoparticle growth. Left diagram: single-particle growth definition that focuses on the mass balance between the gas and particle phases and defines growth as the net gain in particle mass through vapor addition, including solution and curvature effects that influence the vapor pressure above the investigated growing particle. This definition takes a Lagrangian perspective following the size-time trajectory of an individual particle. Right diagram: the definition of growth from a Eulerian perspective tracking the change of particle concentration vs size. The growth rate is defined as the flux through a given size. As a result, growth can also occur through diffusion in particle-size space. This is induced by gradients in the “number concentration–evaporation” space (evaporation rates can be defined to also include curvature and solution effects), where some particles might grow faster than their expected value due to stochastics, leading to the fact that an original monodisperse particle population will not remain monodisperse over time.

organic growth (Gordon *et al.*, 2016; Patoulias and Pandis, 2022) and have improved the description of their sub-25-nm dynamics (Blichner *et al.*, 2021) but still do not reproduce the variety of potential growth mechanisms, which results in significant uncertainties on the role of NPF in the climate system, as illustrated in Fig. 2.

## II. DEFINITION: GROWTH IN MODELS AND EXPERIMENTS

Since the postulation of the aerosol growth laws (Brock, 1972) and their extension to all particle growth mechanisms by Kerminen and Wexler (1995), the GR is widely used to characterize atmospheric nanoparticle growth. However, the meaning of GR varies with its usage: the GR retrieved from experiments or observations often differs from the GR used in an aerosol dynamics model. Here we lay out the various definitions of growth and clarify their differences.

### A. Collective phenomenon and single-particle approximation

The GR refers to the rate of increase in particle size as a function of time; its expression is given as

$$\text{GR} = \frac{\Delta d_p}{\Delta t}, \quad (1)$$

where  $\Delta d_p$  is the increase of particle diameter (in nanometers) during a given time period  $\Delta t$  (in hours). Assuming a certain particle geometry such as a sphere, Eq. (1) can be readily related to the growth with respect to the particle volume, which was used in earlier definitions (Heisler and Friedlander, 1977).

Although Eq. (1) seems to be straightforward, it does not provide an unambiguous definition of GR. Are we interested in the rate at which a single aerosol particle grows? But what happens if that particle collides with another, with both gaining in size, but where the total number concentration is reduced? And how do we obtain this rate of growth when we cannot track an individual particle in our measurements or when we need to calculate the gain in size from known vapor and particle concentrations?

We see that the exact meaning of GR varies with the scope of the studied system and the method to calculate  $\Delta d_p$ . The GR may characterize either a collective phenomenon of a shifting particle-size distribution, the contributions to growth from certain mechanisms and vapors, or the growth of a single particle within the population. The difference in scope will cause a discrepancy when the GR is compared or used while taking the wrong perspective. Figure 3 summarizes the two most popular definitions of nanoparticle growth, the single-particle and population perspectives, which are explained in the following.

### 1. The growth of a single particle

In the microscopic scale, the association of a condensable vapor molecule to a given particle results in an increase in both the size and mass of the particle. The GR contributed by the association of vapors is determined by the association rate and increase in particle size by the added vapor molecular mass. In addition to association, volatile vapors may dissociate from a particle. The net GR is therefore determined by the competition between association and dissociation, which is correspondingly characterized by the vapor concentration and the equilibrium vapor concentration, respectively. With

a spherical particle assumption, the formula for the expected value of the net GR for a single particle is

$$E[\text{GR}_{\text{cond}}(d_p)] = \sum_i \beta(i, p) \left( \sqrt[3]{d_p^3 + d_i^3} - d_p \right) \times [N_i - N_{\text{eq},i}(d_p)], \quad (2)$$

where  $\text{GR}_{\text{cond}}(d_p)$  is the net condensational GR of particles with diameter  $d_p$ .  $E$  represents the expected value, and it emphasizes that vapor association and dissociation are stochastic processes. Hence,  $\text{GR}_{\text{cond}}(d_p)$  is a random variable rather than a constant.  $N_i$  and  $d_i$  are the number concentration and diameter of vapor  $i$ , respectively.  $\beta(i, p)$  is the association coefficient between the particle  $p$  with size  $d_p$  and vapor  $i$ .  $N_{\text{eq},i}$  is the equilibrium concentration of vapor  $i$  for the given particle with size  $d_p$ . The dissociation rate is assumed to be given by the equilibrium concentration; i.e., the expected value of the dissociation rate of molecules from a given particle is equal to the association rate of vapor molecules within the corresponding equilibrium. This assumption of detailed balance is based on the logic that the vapor dissociation rate in equilibrium is the same as the dissociation rate outside equilibrium.

Owing to the Kelvin effect, the equilibrium concentration above a curved surface, for instance, a single-component particle, is usually higher than the saturation concentration of the substance, which is defined as the equilibrium concentration  $N_{\text{eq},0}$  over a flat surface,

$$N_{\text{eq},i}(d_p) = N_{\text{eq},0,i} \exp\left(\frac{4\sigma_i M_i}{RT\rho_i d_p}\right). \quad (3)$$

In Eq. (3)  $\sigma_i$  is the surface tension,  $M_i$  is the molecular mass, and  $\rho_i$  is the density of the substance  $i$ . The expression  $d_k = 4\sigma_i M_i / RT\rho_i$  in the exponent has the dimension of a diameter, and is hence often referred to as the Kelvin diameter, i.e., the size scale at which the curvature effect for a specific vapor  $i$  becomes important.

In addition, the presence of multiple vapors in the particle phase can also affect the equilibrium vapor concentration via the solution or the Raoult effect (Raoult, 1886). Assuming a solution of the different condensable vapors in the particle phase, their equilibrium vapor pressure is reduced by the mole fraction of the particles within the particle phase,

$$N_{\text{eq},i}(d_p) = N_{\text{eq},0,i} \gamma_{\text{act},i} \frac{N_i}{N_{\text{tot}}}, \quad (4)$$

where  $N_i$  is the number concentration of the condensable vapor  $i$  in the particle phase and  $N_{\text{tot}}$  is the total particle-phase number concentration of all solution constituents, including the condensable vapor of interest  $i$  (both quantities are often expressed in amounts of substance, i.e., in moles).  $\gamma_{\text{act},i}$  is the so-called activity coefficient of substance  $i$  in the particle phase accounting for nonideal solutions and is set to unity for ideal solutions. In practice, the Raoult effect is known to facilitate the activation of aerosol particles to CCN and it can also be important on the nanometer scale, where

it could enhance the condensation of vapors, which would otherwise not overcome the Kelvin barrier (Kulmala, Kerminen *et al.*, 2004).

The condensational GR usually refers to the net condensational GR in Eq. (2) including Kelvin and Raoult effects, although there are sometimes ambiguities in the definitions of condensation rate and evaporation rate. The condensation rate may refer to a positive net condensation rate (Tröstl *et al.*, 2016a) or the association rate only (Li and Cai, 2020). Similarly, the evaporation rate may refer to the dissociation rate (Ortega *et al.*, 2012) or a negative net condensation rate (Wang, McGraw, and Kuang, 2013). In this review, if not otherwise specified, condensation is referred to as net condensation and evaporation is referred to as vapor dissociation.

$\text{GR}_{\text{cond}}(d_p)$  is characterized by its expected values in Eq. (2) because the association and dissociation of a molecule are stochastic processes. That is, for a nanoparticle containing only a handful of molecules, the observed  $\text{GR}_{\text{assoc}}(d_p)$  and  $\text{GR}_{\text{cond}}(d_p)$  may deviate from their expected values, i.e., there is a probability that a particle grows despite a negative expected value. Owing to the Kelvin effect, the equilibrium vapor concentration with respect to a particle decreases with its diameter. Therefore, the stochastic nature of growth might overcome an initial negative  $E[\text{GR}_{\text{cond}}(d_p)]$ , growing a particle by fluctuations up to the diameter  $d_p$  at which the ambient vapor concentration is equal to the saturation vapor concentration [ $N_{\text{eq},i}(d_p) = N_i$ ]. Particles at this critical diameter become semistable from a net condensation point of view ( $E[\text{GR}_{\text{cond}}(d_p)] = 0$ ). In the case of a single vapor, reaching the critical diameter is called homogeneous homomolecular nucleation (Seinfeld and Pandis, 2016). If the evaporation rates are negligible for all sizes,  $E[\text{GR}_{\text{cond}}(d_p)]$  is always non-negative; i.e., that barrier does not exist, and the nucleation is a condensation process from the monomer onward. In atmospheric NPF studies (in both experiments and models), nucleation and growth are usually treated as two separate processes. The previous discussion indicates that this separation is a reasonable convention, although nucleation and condensation growth of a single particle are governed by the same equation [Eq. (2)].

Separating condensation growth from nucleation usually facilitates NPF studies because the formulas for  $\text{GR}_{\text{cond}}$  can be further simplified with reasonable assumptions for sizes well beyond typical critical diameters. The increment in particle size due to the association of a single vapor molecule can be simplified using the first-order term of its Taylor series (R. Cai *et al.*, 2021a) when  $d_p \gg d_i$  in Eq. (2). The simplified formula is

$$E[\text{GR}_{\text{cond}}(d_p)] = \sum_i \beta(i, p) \frac{d_i^3}{3d_p^2} [N_i - N_{\text{eq},i}(d_p)]. \quad (5)$$

Equation (5) is the most common way to describe condensation growth, as the underlying continuity assumption for the size distribution is generally preferred due to its reduced complexity (Seinfeld and Pandis, 2016). The errors introduced by the simplification in Eq. (5) decrease with increasing particle diameter. For instance, assuming vapor species of a diameter  $d_i = 0.7$  nm, the errors for

$E[\text{GR}_{\text{cond}}(1 \text{ nm})]$ ,  $E[\text{GR}_{\text{cond}}(3 \text{ nm})]$ , and  $E[\text{GR}_{\text{cond}}(10 \text{ nm})]$  in Eq. (2) are 10%, 0.4%, and 0.01%, respectively. Moreover, the potential fluctuation in  $\text{GR}_{\text{cond}}(d_p)$  due to stochastic effects decreases with particle size, as for a large particle it is reasonable to assume that there are large amounts of molecules associating and dissociating during a short  $\Delta t$ . And, as with every stochastic process, for large numbers of association and dissociation reactions  $\text{GR}_{\text{cond}}(d_p)$  hence converges to its expected value.

In addition to growth by condensation, a particle may also grow by coagulating with clusters of vapor molecules and other small particles. Conventionally coagulation refers to the coalescence of two particles upon collision, whereas condensation refers to the uptake of vapors by a large surface. Using the Fuchs-Sutugin correction (Fuchs and Sutugin, 1965) that covers the free-molecular, transition, and continuous regimes, coagulation and condensation can be unified. The association coefficient for vapor molecules is then described using the coagulation coefficient, assuming spherical particles and vapor molecules and simple collision kinetics. Therefore, Eq. (2) can be generalized to characterize the overall GR contributed by both the condensation of vapors and the coagulation of clusters and particles:

$$E[\text{GR}_{\text{tot}}(d_p)] = \sum_{d_i < d_p} \left\{ \beta(i, p) \left( \sqrt[3]{d_p^3 + d_i^3} - d_p \right) \times [N_i - N_{\text{eq},i}(d_p)] \right\}, \quad (6)$$

where  $d_i$  is the diameter of condensable vapors, clusters, and particles. The most widely applied convention is that the coagulation between a small particle and a large particle is considered the loss of the small particle and growth of the large one, not vice versa. Therefore, the criterion  $d_i < d_p$  is used in Eq. (6) to distinguish coagulation growth from coagulation loss. However, unlike vapor association, coagulation is usually considered to be an irreversible process. Correspondingly, the equilibrium concentration  $N_{\text{eq},i}(d_p)$  for a cluster in Eq. (6) is usually assumed to be zero (Stolzenburg *et al.*, 2005; R. Cai *et al.*, 2021a).

## 2. The growth of a population of particles

Atmospheric NPF studies usually focus on the growth of a large number of new particles. Correspondingly, GR is used to characterize the growth of an aerosol population rather than a single particle. According to the law of large numbers, the average GR of particles with the same size converges to its expected value (Olenius *et al.*, 2014). Hence,  $E[\text{GR}_{\text{cond}}(d_p)]$  for a single particle is replaced with  $\text{GR}_{\text{cond}}(d_p)$  for an aerosol population and  $\Delta d_p$  and  $\Delta t$  in Eq. (1) can be replaced by their corresponding infinitesimal values  $dd_p$  and  $dt$ .

The evolution of a population of particles can be characterized by population balance equations for each particle size or size interval. The population balance equation for the vapor association, vapor dissociation, and coagulation processes is named the aerosol general dynamic equation (GDE) (Gelbard and Seinfeld, 1979). Some (Goodrich, 1964; Wyslouzil and Wilemski, 1995; McGrath *et al.*, 2012) have also referred to

the population balance equations as birth-death equations since vapor association, vapor dissociation, and coagulation can be considered Markov processes. An example of a population balance equation for the homomolecular growth of single-component particles in the discrete form is

$$\frac{dN_k}{dt} = \beta(1, k-1)N_1N_{k-1} - \gamma_k N_k - \beta(1, k)N_1N_k + \gamma_{k+1}N_{k+1} + \text{CoagSrc}_k - \text{CoagS}_kN_k, \quad (7)$$

where  $N_k$  and  $N_1$  are the concentrations of particles containing  $k$  molecules and the vapor monomer, respectively.  $\gamma_k$  and  $\gamma_{k+1}$  are the evaporation (dissociation) rates of particles with  $k$  and  $k+1$  molecules, respectively. By setting Eq. (2) to zero, the equilibrium vapor concentration can be related to  $\gamma_k$  with  $\gamma_k = \beta(i, k)N_{\text{eq},k}$ .  $\text{CoagSrc}_k$  and  $\text{CoagS}_kN_k$  are the sums of sources and sinks (Kuang, Chen, Zhao *et al.*, 2012) for particles  $k$ , with  $\text{CoagSrc}_k$  accounting for all coagulation that forms particles  $k$  and  $\text{CoagS}_k$  accounting for all coagulation between a particle  $k$  and any other cluster or particle. As previously, the fission of clusters and particles are usually assumed to be negligible, and hence they are not accounted for in Eq. (7). The first four terms on the right-hand side of Eq. (7) characterize the formation of particles  $k$  due to vapor association, the dissociation of vapor molecules from particles  $k$ , the growth particles  $k$  into particles  $k+1$  via vapor association, and the evaporation (vapor dissociation) of particles  $k+1$  into particles  $k$ , respectively.

The GR of an aerosol population is usually defined by the net flux through a given particle size, i.e., the net change in the number concentration of particles into larger sizes per unit time (Olenius *et al.*, 2014; Li and McMurry, 2018). Accordingly,  $\text{GR}(d_p)$  can be expressed as follows:

$$\text{GR}_{\text{tot}}(d_p) = \text{GR}_{\text{cond}}(d_p) + \text{GR}_{\text{coag}}(d_p), \quad (8)$$

$$\begin{aligned} \text{GR}_{\text{cond}}(d_p) &= \sum_i \frac{d_i^3}{3d_p^2} \left[ \beta(i, p)N_i - \gamma_i(d_{p+i}) \frac{N_{p+i}}{N_p} \right] \\ &= \underbrace{\sum_i \frac{d_i^3}{3d_p^2} [\beta(i, p)N_i - \gamma_i(d_p)]}_{\text{GR}_{\text{drift}}} \\ &\quad + \underbrace{\sum_i \frac{d_i^3}{3d_p^2} \frac{1}{N_p} [N_p \gamma_i(d_p) - N_{p+i} \gamma_i(d_{p+i})]}_{\text{GR}_{\text{diffusion}}}, \quad (9) \end{aligned}$$

$$\text{GR}_{\text{coag}}(d_p) = \sum_{d_j < d_p} \beta(j, p) \left( \sqrt[3]{d_p^3 + d_j^3} - d_p \right), \quad (10)$$

where  $d_{p+i} = \sqrt[3]{d_p^3 + d_i^3}$  is the diameter of the particle after the condensation of vapor  $i$  and  $N_{p+i}$  is the corresponding number concentration.  $\gamma_i(d_p)$  and  $\gamma_i(d_{p+i})$  are the evaporation rate of vapor  $i$  from particles at sizes  $d_p$  and  $d_{p+i}$ , respectively. The contributions of condensation and coagulation to  $\text{GR}_{\text{tot}}(d_p)$  are correspondingly separated into  $\text{GR}_{\text{cond}}(d_p)$

and  $\text{GR}_{\text{coag}}(d_p)$  in Eq. (8). The coagulation process is again assumed to be irreversible in Eq. (10).

Contrasting Eq. (9) for an aerosol population with Eq. (5) for a single particle shows that the first summation term on the right-hand side of Eq. (9) is equal to  $E[\text{GR}_{\text{cond}}(d_p)]$  in Eq. (5), yet there is a second summation term in Eq. (9) characterizing the gradient between the evaporation rates and particle concentrations for  $d_p$  and  $d_{p+i}$ . This is because  $\text{GR}(d_p)$  for an aerosol population is defined based on the flux between two different particle sizes rather than the mass balance of particles at a given size. These first and second terms are called the drift-driven (or sometimes deterministic) term and diffusion-driven (or sometimes stochastic) term, as their corresponding expressions for the change of particle concentration in the continuous form are analogous to the formulas for particle drift and diffusion in a flow field (Goodrich, 1964; Clement, Lehtinen, and Kulmala, 2004; Wang, McGraw, and Kuang, 2013; Olenius *et al.*, 2018).

Using the same analogy, the methods to characterize the growth of aerosols can be classified into Eulerian methods and Lagrangian methods (Olenius *et al.*, 2014; R. Cai *et al.*, 2021a). Lagrangian methods track the change of particle diameter as a function of time. In contrast, a Eulerian method focuses on the particle-size space and tracks the change of particle concentration at each size bin. In the Eulerian specification, the evolution of particle concentration for each size or size interval is calculated using the GDE in Eq. (7) or its continuous form,

$$\begin{aligned} \frac{\partial n(v)}{\partial t} = & \frac{1}{2} \int_0^v \beta(v-q, q) n(v-q) n(q) dq \\ & - n(v) \int_0^\infty \beta(q, v) n(q) dq \\ & - \frac{\partial}{\partial v} [I(v) n(v)], \end{aligned} \quad (11)$$

which is expressed in terms of the number volume distribution  $n(v) = dN/dv$ , and the first two terms now correspond to  $\text{CoagSrc}(v)$  and  $\text{CoagS}(v)N(v)$  for the particle volume of interest  $v$ . The third term incorporates the net number flux out of that volume due to net condensation growth with a volume  $\text{GR } I(v) = (\pi/2d_p^2)\text{GR}$ .

The aerosol dynamics models corresponding to the discrete and continuous forms of the GDE are called discrete and sectional models, respectively (Gelbard, Tambour, and Seinfeld, 1980; Li and Cai, 2020). Both the drift-driven and diffusion-driven growth terms are accounted for in a discrete model. A sectional model is not naturally compatible with growth driven by diffusion in the particle-size space because  $\gamma_i(d_{p+i})$  and  $N_{p+i}$  in Eq. (9) converge to  $\gamma_i(d_p)$  and  $N_p$ , respectively, as  $d_{p+i} - d_p$  approaches 0. Therefore, the continuous GDE given in Eq. (11) often does not include the higher-order fluxes (Olenius *et al.*, 2018), even if this diffusion term for the stochastic growth can be incorporated into the GDE, resulting into the so-called Fokker-Planck equation (Goodrich, 1964).

The diffusion-driven term often remains difficult to estimate, as the evaporation rates and particle concentrations for each cluster are difficult to access experimentally. As a result,

drift-driven  $\text{GR}_{\text{cond}}(d_p)$  is favored for its simplicity for calculation and low expenses for aerosol dynamics modeling, especially as it implies that any monodisperse subpopulation remains monodisperse during their growth or evaporation. However, neglecting it may introduce significant error. The most extreme example is for particles smaller than the critical diameter [i.e., with  $N_i < N_{\text{eq},i}(d_p)$ ]. Here the usage of only the drift term leads to the wrong conclusion that these particles are unable to grow large (Holten and Van Dongen, 2009), whereas  $\text{GR}_{\text{cond}}(d_p)$  can be positive due to the contribution of growth driven by diffusion in the particle-size space (Olenius *et al.*, 2018). To avoid such bias, Olenius *et al.* (2018) applied a metric on the PNSD to estimate at least the magnitude of this term. Generally for large particles sizes well beyond the critical diameter (for instance,  $\sim 5 \text{ nm} \gg d_{p,\text{crit}}$  for low-volatility vapors), the drift-driven  $\text{GR}_{\text{cond}}(d_p)$  is sufficiently accurate to characterize particle growth (Holten and Van Dongen, 2009; Wang, McGraw, and Kuang, 2013; Olenius *et al.*, 2018).

## B. Definitions with respect to the relevance of nanoparticle growth in the climate system

NPF affects climate by contributing to the global CCN budget through its influence on the average aerosol number size distribution. A population of new particles at the critical diameter need to grow efficiently so that a proportion of them can reach sizes where typical atmospheric water supersaturation is sufficient to activate these particles, thus seeding cloud droplets (McFiggans *et al.*, 2006). Depending on the chemical composition, the availability of additional soluble vapors (Kulmala *et al.*, 1997), the overall aerosol size distribution, and the maximum water supersaturation, particles typically need to reach the accumulation or Aitken-mode sizes in order to become CCNs (Petters and Kreidenweis, 2007; Lowe *et al.*, 2019; Bulatovic *et al.*, 2021). However, depending on the atmospheric conditions, some portion of the growing particles will be scavenged by larger aerosols during the growth process (Pierce and Adams, 2007). The survival probability is hence the key parameter and characterizes the fraction of new particles scavenged during a growth process, indicating their influences on the aerosol PNSD at the relevant CCN sizes. It is defined as the probability of a single particle with size  $d_{p1}$  growing up to  $d_{p2}$  without being scavenged by larger particles. Equivalently, as shown in Eq. (12), the survival probability is equal to the fraction of a large population of particles with size  $d_{p1}$  that survive to  $d_{p2}$ ,

$$P(d_{p1} \rightarrow d_{p2}) = \frac{N(d_{p2}, t_2)}{N(d_{p1}, t_1)}, \quad (12)$$

where  $P(d_{p1} \rightarrow d_{p2})$  is the survival probability of particles during the growth process from  $d_{p1}$  to  $d_{p2}$ .  $N(d_{p1}, t_1)$  is the initial number concentration of the growing particle mode with size  $d_{p1}$  at  $t_1$  and  $N(d_{p2}, t_2)$  is the remaining number concentration of this mode when grown to  $d_{p2}$  at  $t_2$ .

The survival probability of a particle can be derived from known growth and scavenging rates as a function of  $d_p$ . For

atmospheric NPF events, the scavenging losses of new particles is usually dominated by Brownian coagulation losses. The coagulation loss is characterized by the coagulation sink  $\text{CoagS}(d_p)$ , which accounts for the loss rate of particles of size  $d_p$  due to the Brownian coagulation with larger particles (Kulmala *et al.*, 2001, 2012). Tracking the probability of a particle growing against the coagulation loss at any particle diameter from  $d_{p1}$  to  $d_{p2}$  yields the formula for  $P(d_{p1} \rightarrow d_{p2})$ , as given by (McMurry and Friedlander, 1979; Weber, Marti, and McMurry, 1997; Kerminen and Kulmala, 2002; Lehtinen *et al.*, 2007; Kuang *et al.*, 2010)

$$P(d_{p1} \rightarrow d_{p2}) = \exp \left( \int_{d_{p1}}^{d_{p2}} - \frac{\text{CoagS}(d_p)}{\text{GR}_{\text{tot}}(d_p)} \right). \quad (13)$$

The integration in the exponent can be simplified by assuming a certain diameter dependence of the sink and using an average GR that results in

$$\begin{aligned} P(d_{p1} \rightarrow d_{p2}) & \approx \exp \left( \frac{\{[(d_{p1}^m/d_{p2}^{m-1}) - d_{p1}]/(m-1)\} \text{CoagS}(d_{p1})}{\text{GR}_{\text{tot}}([d_{p1}, d_{p2}])} \right) \\ & = \exp \left[ \left( \frac{1}{d_{p2}} - \frac{1}{d_{p1}} \right) \frac{d_{p1}^2 \text{CoagS}(d_{p1})}{\text{GR}_{\text{tot}}([d_{p1}, d_{p2}])} \right] \quad (\text{for } m = 2). \end{aligned} \quad (14)$$

In Eq. (14)  $m$  is the slope of  $\text{CoagS}(d_p)$  vs  $d_p$ .  $m$  is theoretically a function of  $d_p$  defined by  $m = -d \ln \text{CoagS}(d_p) / d \ln d_p$ . It is practically approximated as a constant value in the range of 1.5 to 2, depending on the size distribution (Kerminen and Kulmala, 2002; Lehtinen *et al.*, 2007), further simplifying Eq. (14) together with the approximation of the size-dependent  $\text{GR}_{\text{tot}}(d_p)$  by the average  $\text{GR}_{\text{tot}}([d_{p1}, d_{p2}])$  in the size range of concern. By definition, the average  $\text{GR}_{\text{tot}}([d_{p1}, d_{p2}])$  is the harmonic mean of the size-segregated GR. The corresponding formula in the continuous size space is given by

$$\text{GR}_{\text{tot}}([d_{p1}, d_{p2}]) = \frac{d_{p2} - d_{p1}}{\int_{d_{p1}}^{d_{p2}} [1/\text{GR}_{\text{tot}}(d_p)] dd_p}, \quad (15)$$

where  $d_{p1}$  and  $d_{p2}$  are the lower and upper size limits of the particle-size range of concern and  $\text{GR}_{\text{tot}}([d_{p1}, d_{p2}])$  is the average total GR for this size range. The advantage of the average GR is that this quantity is often directly retrieved with the most widely applied methodology. However, note that the particle population is assumed to maintain monodispersity in the derivations of  $P(d_{p1} \rightarrow d_{p2})$ , as indicated by  $\approx$  in Eq. (14), and hence the  $\text{GR}_{\text{tot}}([d_{p1}, d_{p2}])$  here is correspondingly the drift-driven GR only, which is in turn often not disentangled from the diffusion-driven GR in the GR retrieval methods used; see Sec. III.

Korhonen *et al.* (2014) derived an analytical solution similar to Eq. (14) for the case of typical size-dependent GRs. The simplified Eq. (14) is known as the Kerminen-Kulmala equation (Kerminen and Kulmala, 2002), in which the  $d_{p1}^2 \text{CoagS}(d_{p1})$  term is usually replaced by an equivalent

condensation sink (CS) term for gas-phase sulfuric acid molecules. Hence, the CS in the Kerminen-Kulmala equation characterizes the coagulation scavenging of new particles rather than the condensation of the vapor, and it should always be calculated for sulfuric acid regardless of the condensing vapor driving particle growth.

The usage of the concept of particle survival as laid out in Eq. (14) and its various derivatives (Lehtinen *et al.*, 2007) is often used within large-scale models due to its simplicity. It allows one to scale the nucleation rate derived from a parametrization or theoretical concept toward larger sizes at low computational burden with the use of a GR that is derived from vapor concentrations and applied in the sense of Eq. (5). We see in Sec. III that this is in contrast to the methodology used for experimental GR determination.

### III. MEASURING NANOPARTICLE GROWTH: METHODOLOGY

#### A. Instrumentation for the measurement of atmospheric nanoparticle growth

The most common approach for the estimation of nanoparticle GRs is the analysis of the collective phenomenon of a shifting PNSD due to growth discussed in Sec. II. Hence, the precise measurement of the PNSD is the most important prerequisite for a solid estimate of the GR. The instrumentation used for the nanoparticle growth measurements are mostly limited to electrical mobility spectrometers and size-dependent particle activation due to the Kelvin effect via a controlled vapor supersaturation. Detailed instrumental aspects for PNSD measurements in the nucleation mode size range were given by Kangasluoma *et al.* (2020).

#### 1. Electrical mobility analysis

Electrical mobility analysis generally refers to type of instruments in which sampled particles are brought to a supposedly known steady-state charge distribution using an aerosol charger, sizing of the charged particles is conducted using one or more differential mobility analyzers (DMAs), and particle counting is done with an electrometer or a condensation particle counter (CPC). The PNSD is obtained by scanning the particle size given by the DMA, and continuous observation of the particle population reveals the particle dynamics. Three different types of electrical mobility spectrometers have been used to obtain particle GRs in the sub-25-nm size range.

Scanning mobility particle sizer (SMPS) and differential mobility particle sizer (DMPS) spectrometers are the most established instruments for measuring the evolution of nucleation mode particle-size distributions (Wang and Flagan, 1990), and they both consist of a bipolar charger, a DMA, and a CPC. The first variants of SMPS focusing on the ultrafine particle range were limited to  $\sim 3$  nm due to the lowest detectable diameter of the CPC and low counting statistics from large diffusion and charging losses in the system (Covert *et al.*, 1996; Aalto *et al.*, 2001). During the last two decades, improvements in the CPC detection

(Vanhanen *et al.*, 2011; Kuang, Chen, McMurry, and Wang *et al.*, 2012; Wimmer *et al.*, 2013), advances in particle sampling (Kangasluoma *et al.*, 2016; Fu *et al.*, 2019), DMA technology (Cai *et al.*, 2017; Cai, Attoui *et al.*, 2018), and configuration optimizations (Stolzenburg, Steiner, and Winkler, 2017; Cai *et al.*, 2019) extended the size-distribution measurements with the SMPS down to sizes approaching 1 nm (Jiang, Chen *et al.*, 2011; Kuang, Chen, Zhao *et al.*, 2012; Kangasluoma *et al.*, 2018; Kong *et al.*, 2021). Low signals due to low charging efficiency and inefficient particle detection with the CPC and overlap of charger ions typically limit the measurements with the SMPS in the lower size end to 1 to 2 nm.

A variant of the electrical mobility spectrometer to reach high time resolution for more accurate GR measurements is the so-called DMA train (Flagan *et al.*, 1991; Stolzenburg, Steiner, and Winkler, 2017), in which size classification is conducted using several pairs of DMAs and CPCs in parallel that monitor only a single particle size. The DMA train also reaches lower detection limits than traditional SMPS systems because of the long averaging time and higher counting statistics at each measured particle size (Cai *et al.*, 2019).

The neutral cluster and air ion spectrometer (NAIS) (Mirme *et al.*, 2007; Manninen *et al.*, 2009) includes two unipolar corona needle chargers and two DMA columns in which a series of electrometers have been placed at the inner surface. The design is based on a large inlet flow rate to overcome the electrical noise in the electrometers. The measurement cycle of the NAIS allows GR measurements of the total particle populations in the size range of 2–40 nm. The lower limit at ~2 nm is caused by the size of the largest charger ions of the used unipolar corona chargers. Kangasluoma *et al.* (2020) showed that the NAIS particle mode often overestimates aerosol number concentrations compared to other mobility spectrometers. However, the NAIS is often used in ion mode as an air ion spectrometer (AIS), where the corona chargers are switched off and the ambient ion size distribution is measured, yielding a lower limit of detection of 0.8 nm. Ion GRs have been inferred using the NAIS in many studies (Hirsikko *et al.*, 2005; Manninen *et al.*, 2010). Like the NAIS without the chargers, the balanced scanning mobility analyzer (Tammiet, 2006) is an air ion spectrometer based on a parallel plate DMA design, which has also been used for studying the growth of atmospheric ions (Yli-Juuti *et al.*, 2011).

## 2. Condensation particle counters

CPCs detect particles by growing them through vapor condensation and subsequent optical detection. The Kelvin effect determines the smallest particle onto which a vapor can condense at a given supersaturation, and this threshold particle size decreases with increasing supersaturation. By continuously scanning the supersaturation in a single CPC, the particle-size magnifier (PSM) is capable of measuring the PNSDs in the size range of 1–3 nm, from which the GRs can be inferred (Vanhanen *et al.*, 2011). The particle-size magnifier does not suffer from low signals but requires relatively stable aerosol populations and accurate calibration for reliable measurements. GR measurements with high time

resolution could be realized with a battery of CPCs (Kangasluoma *et al.*, 2014; Williamson *et al.*, 2018), but this approach has not been widely adopted for growth measurements (Tröstl *et al.*, 2016a). However, it should in principle provide good sensitivity and time resolution (Kangasluoma *et al.*, 2020).

## 3. Measurement of trace vapors, particle-phase composition, hygroscopicity, and volatility

Besides the measurement of the PNSD, chemical information on condensable vapors and nucleation mode particle composition are essential for relating growth measurements to the possible gaseous precursors. Complementary measurements of particle- and gas-phase chemical composition are therefore crucial, especially for model input. Moreover, some studies have shown that, with continuous particle composition measurements during new particle formation, the amount of condensed vapors and hence the GR attributed to them can be estimated (Bzdek *et al.*, 2012, 2014; Mohr *et al.*, 2019; Zheng *et al.*, 2020).

The trace vapor and cluster composition are measured mainly using the atmospheric interface time-of-flight (API-TOF) mass spectrometer (Junninen *et al.*, 2010), which measures the mass-to-charge ratio of charged ions. Naturally charged vapors and clusters can be directly measured with sizes up to around 1 to 2 nm (Sipilä *et al.*, 2016; Jokinen *et al.*, 2018), which is limited mostly by the mass spectrometer transmission. Neutral vapor molecules contributing to new particle growth need to be charged by chemical ionization (CI) before entering the mass spectrometer. Nitrates and their clusters are widely used as reagent ions in laboratory and ambient conditions for their good selectivity of extremely low-volatility vapors such as sulfuric acid and highly oxygenated organics (Jokinen *et al.*, 2012; Ehn *et al.*, 2014). Other reagent ions such as iodides (Lee *et al.*, 2014), bromides (Rissanen *et al.*, 2019), aminium ions (Berndt *et al.*, 2018), and water clusters (Yuan *et al.*, 2017; Krechmer *et al.*, 2018) are also used, with each ionization chemistry optimized for specific types of vapors (Riva *et al.*, 2019). A combination of different ionization chemistry is preferred to cover the broad volatility range of vapors that contribute to particle growth, but such a combination is still rare, especially for ambient studies (Huang *et al.*, 2021). In addition to the CI-API-TOF one, the CI-Orbitrap mass spectrometer, which has a higher mass resolution than the CI-API-TOF spectrometer, has recently proved to be a promising tool to measure neutral vapors and clusters (Riva, Ehn *et al.*, 2019; Riva *et al.*, 2020; Cai, Huang *et al.*, 2022).

Instruments to directly measure nucleation mode particle composition are limited and are mainly scientific instruments used by individual research groups. A more extensive review of these instruments was recently given by Smith *et al.* (2021). Generally, direct and indirect methods to measure the nucleation mode particle chemical composition are scarce, and additional efforts in instrument development would be valuable. In thermal desorption (TD) methods particles are collected on a filter or a filament, from which thermally evaporated species are detected using a mass spectrometer (Smith *et al.*, 2004). In favorable conditions TD methods are

effective down to 10 nm or less (Smith *et al.*, 2004; Lawler *et al.*, 2018; Wagner *et al.*, 2018; Perraud *et al.*, 2020; Li *et al.*, 2021, 2022), while they are in many environments limited by the available particle mass. The nanoaerosol mass spectrometer (Pennington and Johnston, 2012) is similar to the TD methods but uses laser desorption to vaporize the particles and reconstructs the particle composition from the detected elements. Recently a new online TD method was proposed to heat particles in the sampling flow without collecting them on a filter or filament, yet it requires a more detailed characterization of the TD process (Häkkinen *et al.*, 2023; Zhao *et al.*, 2023).

Indirect composition information from the particles can be obtained from their interactions with specific vapors or change with temperature. In a tandem differential mobility analyzer the size classified particles are exposed to either heat or water vapor and based on the change in size indirect information on the composition can be inferred (Sakurai *et al.*, 2005; Biskos *et al.*, 2006; Biskos, Buseck, and Martin, 2009; Lei *et al.*, 2020). Condensation particle counters with different working fluids have been also used to infer information about the composition of nucleation mode particles (Kulmala *et al.*, 2007; Kangasluoma *et al.*, 2014).

#### 4. Instrumental limitations in measuring nanoparticle growth

To measure particle growth, instruments should be able to track the evolution of PNSD with sufficient temporal resolution, size resolution, and low measurement uncertainties. From the perspective of nanoparticle growth measurements, current PNSD measurement techniques are critically challenged in the size range of 1–5 nm and for rapidly changing particle populations. At sizes larger than 5 nm, fluctuations of ambient air masses and the methodology used for GR estimates are the dominating uncertainties. However, below 5 nm diffusional sampling losses, particle detection, and, in the case of mobility spectrometers, particle charging become highly challenging. This results in low measured number concentrations and hence high relative errors of the raw data (counting error) used for the size-distribution inversion and, at the same time, high systematic uncertainty related to unknown charging and detection (Kangasluoma and Kontkanen, 2017; Kangasluoma *et al.*, 2020). Cai *et al.* (2019) demonstrated that the sensitivity of mobility spectrometers with respect to good coverage of the PNSD strongly depends on the overall detection efficiency, detector flow rates, measurement cycles, and DMA resolution. For the sub-10-nm size range Kangasluoma *et al.* (2020) found deviations in the inverted PNSD between different instruments of a factor of up to 10, concluding that these discrepancies are highest when one of the instruments is operating close to its limit of detection in terms of the measured number concentration. A combination of different instruments could lower the uncertainties but is not widely applied (Stolzenburg, Ozon *et al.*, 2022). Kangasluoma and Kontkanen (2017) showed that achieving a lower than 5% counting error in mobility spectrometers would require high particle concentrations ( $> 10^5 \text{ cm}^{-3}$ ). Stolzenburg *et al.* (2023) demonstrated that higher detection flow rates and hence increased counting statistics in a DMPS system could indeed improve the retrieved GRs. In addition,

there are also systematic uncertainties, and the discrepancies between instruments could also originate from particle charging for mobility spectrometers and unknown cutoffs due to an unknown particle composition and charging state for condensation particle counters. This could potentially result in uncertainties up to 5000% for the PSM and 50%–500% for mobility spectrometers (Kangasluoma and Kontkanen, 2017; Kangasluoma *et al.*, 2020). Overall, we conclude that proper uncertainty propagation in PNSD measurements (Sipkens *et al.*, 2023) is often omitted.

Other systematic biases could be, for instance, the role of water in PNSD measurements. Most instruments taking measurements in the size range of 1–10 nm do not dry the sample to maximize the number of counted particles. Therefore, there may be some discrepancies in the measured PNSD between these instruments and, for example, SMPS systems following the Aerosol, Clouds and Trace Gases Research Infrastructure guidelines, in which the relative humidity of the sample flow is regulated to below 40% (Wiedensohler *et al.*, 2012). The drying procedure is applied mainly to avoid aerosol hygroscopic growth during sampling as PNSD measurements at high relative humidity could be problematic due to enhanced water uptake or even condensation on sampling lines.

Overall, specific studies estimating the impact of errors in PNSD measurements on GR estimates are currently missing and need to be evaluated with respect to the GR retrieval method; see Sec. III.B. However, the fact that most instrumentation for PNSD measurements below 5 nm has limits of detection of  $10^2$ – $10^3 \text{ cm}^{-3}$  (Kangasluoma *et al.*, 2020) also prevents nanoparticle growth events with such low number concentrations to be detected accurately. These events are likely to be characterized by low GRs (below  $1 \text{ nm h}^{-1}$ ), as this induces a low survival probability and hence low number concentrations. In contrast, the time resolution of most devices used for PNSD measurements is ranging between 1 and 5 min. If we assume that GR should be resolved down to the scale of 1 nm, this induces an upper limit for GR estimates of  $12$ – $60 \text{ nm h}^{-1}$  for 1–5 min time resolution if we assume that the GR estimate follows the simple definition of Eq. (1).

Besides uncertainties in PNSD, the measurements of condensable vapors also have high systematic uncertainties, which induces uncertainties when vapor concentration derived and measured GRs are compared. There are difficulties to calibrate the charging efficiency of chemical-ionization techniques for the variety of atmospheric compounds. But even if calibration methods exist, they are estimated to have at least 33% systematic uncertainties as in the case of sulfuric acid (Kürten *et al.*, 2012), and these uncertainties are expected to be higher for long-term field measurements. Mass-dependent transmission efficiencies of mass spectrometers might complicate the quantification of condensable vapors over a wide mass range, but methods for determining these transmission losses exist (Heinritzi *et al.*, 2016). In addition, fragmentation of molecules may also influence the measurements (Passananti *et al.*, 2019). Another problem arises from the selective sensitivity of many chemical-ionization techniques toward certain condensable vapors, for instance, organic

molecules with a high or low oxidation state (Riva *et al.*, 2019). This can cause a significant underestimation of low-volatility compounds important for nanoparticle growth (Tröstl *et al.*, 2016a; Stolzenburg *et al.*, 2018). Similar uncertainties occur in mass-spectrometer-based particle-phase measurements, where even more complex effects such as the influence of thermal desorption often need to be considered.

As mentioned, measuring nucleation mode particle composition is challenging. Besides the uncertainties associated with particle collection, evaporation or thermal desorption, ionization, and detection, a major limitation is that the collected nucleation mode particle mass has to exceed the instrumental detection limit. Temporal resolution and size resolution are usually sacrificed to gain sufficient mass in atmospheric measurements (Smith *et al.*, 2010; Li *et al.*, 2021), yet measuring sub-5-nm particles still demands more effort in instrument development (Smith *et al.*, 2021).

## B. Analysis methods applied to estimating nanoparticle growth rates

For a measured NPF event, GR as a function of particle size and time can be estimated from the evolution of the PNSD. In the macroscopic scale, the growth of new particles is reflected by the collective phenomenon of the aerosol size distribution gradually shifting toward a larger size as a function of time. The microscopic information, such as all possible particle and vapor concentrations and the size-dependent evaporation rates of all condensable vapors, is usually unknown, especially for atmospheric observations of NPF. It is furthermore impossible to track the growth trajectory of a single particle from the measured particle-size distribution in the Lagrangian sense. Therefore, GR is usually estimated based on the shift of PNSD toward a large diameter. Alternatively, GR can be retrieved by solving the change of a size-segregated particle number concentration as a function of time. The former approaches to estimate GR are referred to as collective approaches, and the latter are referred to as dynamic approaches.

### 1. Collective approaches: Mode fitting, maximum concentration, and appearance time

The collective approaches calculate the GR from the evolution of the measured PNSD of an aerosol population using  $\Delta d_p / \Delta t$  in Eq. (1). Because of the difficulty in tracking a single particle, either a representative  $d_p$  or a representative  $t$  has to be used for a collective approach (representative diameter and representative time approaches, respectively). However, a shifting size distribution can also be caused by other processes, such as coagulation in addition to condensation growth. That is, the representative  $\Delta d_p$  is not necessarily the increase of particle-size due to condensation growth and the representative  $\Delta t$  is not necessarily the duration of particle growth. As a result, even if the collective approaches use the same formula to calculate the GR as Eq. (1), these approaches directly reflect neither the single-particle GR defined by Eq. (2) nor the GR defined in Eq. (9).

#### a. Mode-fitting method

The mode-fitting method (Hussein *et al.*, 2008) is a representative diameter approach using the temporal evolution of a mode peak. Since an atmospheric aerosol size distribution

is usually characterized by several modes (Whitby, 1978), one to four log-normal distributions are fitted to the entire measured size distribution (Kulmala *et al.*, 2012) and the shift of the peak diameter of the nucleation mode is used to represent the growth of new particles. Some criteria, such as temporal and diameter differences between consecutive peaks, can be applied to automatically validating the fitting results (Paasonen *et al.*, 2018). Alternatively, the peak diameter can be determined simply according to the maximum  $dN/d \log d_p$  for the nucleation mode if it can be clearly distinguished from other modes. With  $\Delta d_p$  as the increase of the peak diameter during  $\Delta t$ , with  $t$  the time for each measured aerosol number size distribution, the value of GR is then retrieved by a linear fit to the  $d_p$  vs  $t$  data, resulting in a  $GR_{\text{mode}}$  according to Eq. (1).

The mode-fitting method characterizes particle growth in the Lagrangian specification.  $GR_{\text{mode}}$  approximates  $GR_{\text{tot}}$ , which is contributed by the condensational and coagulation growth of new particles as in Eq. (2), as the coagulation growth of new particles also increases the peak diameter of the mode (Leppä *et al.*, 2011). The coagulation between two new particles is conventionally named self-coagulation (Lehtinen *et al.*, 2007; Kerminen *et al.*, 2018) or intramodal coagulation (Stolzenburg *et al.*, 2005), neither of which necessarily refer to coagulation of a monodisperse new particle mode but which can include the coagulation of particles of distinct sizes within the same mode. In that sense, self-coagulation is part of the definition of GR according to Eq. (6). The notable contribution of self-coagulation originates from the larger diameter increment per collision compared to vapor-particle association [see Eq. (6)], which scales faster with increasing size than the simultaneous decrease of the association coefficient. Therefore, the effect of self-coagulation increases with particle size (Leppä *et al.*, 2011; Zhao, Li *et al.*, 2018) but is counterbalanced by the typically slowly diminishing number concentration of the growing mode with increasing particle size.

Extramodal coagulation (Stolzenburg *et al.*, 2005), i.e., coagulation scavenging of new particles to preexisting particles of a different mode (sometimes also called intermodal coagulation), is not included in the definition of Eq. (6) but also causes a shift in the peak diameter. This is due to the size dependency of  $\text{CoagS}(d_p)$ , as smaller particles have a larger  $\text{CoagS}(d_p)$  than larger particles, which leads to a net shift of the peak diameter toward larger sizes. Although not associated with particle growth in the sense of Eq. (6), this extramodal coagulation phenomenon increases the measured apparent  $\Delta d_p / \Delta t$  and hence introduces a systematic bias to the analysis method. Like the extramodal coagulation, a possible size dependency of condensation also leads to a shift in the peak diameter.

The influence of self-coagulation and extramodal coagulation on the peak diameter can theoretically be calculated and corrected, which was recommended by Kulmala *et al.* (2012). For each measured aerosol number size distribution at  $t$  and a given  $\Delta t$ , where  $\Delta t$  is the time interval between two measurements, the theoretical peak diameter at  $t + \Delta t$  under the influence of only self-coagulation and extramodal coagulation can be calculated using an approximate analytical method (Stolzenburg *et al.*, 2005; Leppä *et al.*, 2011) or by solving the GDE equation [Eq. (7) or (11)]. In the method

proposed by Stolzenburg *et al.* (2005), the evolution of PNSD during a time bin (usually 3–5 min, determined by the temporal resolution of the instrument) due to self-coagulation and extramodal coagulation is calculated analytically after log-normal mode fitting. The increasing rate of the mode diameter during this time bin is taken as the contribution from self-coagulation and the influence of extramodal coagulation. Subtracting the influence of extramodal coagulation from the measured  $GR_{\text{mode}}$  yields the measured  $GR_{\text{tot}}$ . Further subtracting the contribution of self-coagulation yields the measured  $GR_{\text{cond}}$ . This analytical method based on log-normal mode fitting can be further generalized such that the increase of the peak diameter is calculated numerically. We clarify that this correction method assumes a complete deconvolution between the evolution of PNSD due to coagulation and condensation during each time step, which may introduce uncertainties to the corrected GR, especially for NPF in polluted environments.

The mode-fitting method is applicable to NPF events with a well-defined nucleation mode. For a typical NPF event with a well-defined growth pattern of single modal new particles, the mode-fitting method with corrections can be used to calculate the GR. However, the size distribution of new particles during quasi-steady-state nucleation and growth does not necessarily have a peak, especially in the sub-3-nm size range (McMurry, 1983; Jiang, Zhao *et al.*, 2011). For some continuous NPF events in urban environments, the peaks for the newly formed particles and the grown new particles may merge with each other. This merging also reduces the mode diameter and hence causes an underestimation of  $GR_{\text{tot}}$ . In such cases, it is difficult to use the mode-fitting method to estimate GR for the entire size range of NPF.

#### *b. Maximum concentration and appearance time method*

Instead of tracking  $\Delta d_p(\Delta t)$  for a given  $\Delta t$ , representative time approaches seek  $\Delta t(\Delta d_p)$  for a given  $\Delta d_p$ . The  $d_p$  herein is a preselected particle diameter such as the particle size bin of the instrument. The  $t$  is then a representative moment corresponding to the preselected  $d_p$  rather than the period for particles to grow.

The maximum concentration method takes the moment at which particle number concentration for a given size bin reaches its maximum during an NPF event as the representative  $t$  (Kulmala *et al.*, 2013). The peak position is often estimated by fitting a Gaussian function to the signal in each size channel (Hirsikko *et al.*, 2005). The time shift of the observed moment of peak concentration as a function of particle size is attributed to particle growth.

The appearance time method (Lehtipalo *et al.*, 2014) takes the moment at which particles reach a certain proportion  $m\%$  of the maximum concentration during an NPF event as the representative time  $t_m$ . For instance,  $t_{50}(d_p)$  is the time that the measured concentration of particles with size  $d_p$  reaches its half maximum (50% appearance time method). For  $m$  approaching 100, the method is equivalent to the maximum concentration method, but in general the appearance time method does not require the existence of a peak concentration. For pseudo-steady-state NPF with time-independent

nucleation and GRs, the particle concentration in each size bin reaches a constant value after a certain period.

The maximum concentration method and the appearance time method are Eulerian methods. They do not track the growth of a single particle or a population of particles. The relation between the  $\Delta d_p/\Delta t$  and GR for these methods requires further validation. The validity of the 50% appearance time method has been demonstrated for situations in which the following assumptions are satisfied (He *et al.*, 2021a): (1) the vapor concentration or production rate is constant during the NPF event, (2) the initial particle concentrations are equal to zero, (3) the coagulation between new particles contributes negligibly to particle growth, (4) the evaporation of particles is negligible, and (5) the influence of coagulation loss, transport, and other external sinks of particles is negligible. With these assumptions, the  $\Delta d_p/\Delta t_m$  retrieved using the 50% appearance time method was demonstrated to be approximately equal to  $GR_{\text{cond}}$  with negligible biases (He *et al.*, 2021a). The aforementioned ideal conditions can be satisfied for pseudo-steady-state new particle formation in some chamber experiments. The 50% appearance time method was recommended for chamber studies and its consistency with GDE-based dynamics approaches was reported for chamber results (Dada *et al.*, 2020b).

In the real atmosphere, however, the unavoidable violation of these ideal conditions may introduce systematic biases to the GR retrieved using the appearance time method. Like the mode-fitting method without correction, the appearance time method neglects the fact that the time evolution of the particle concentration at a certain diameter is influenced by more than net condensational growth. Simulations based on aerosol dynamics (Olenius *et al.*, 2014; Kontkanen *et al.*, 2018; Li and McMurry, 2018; R. Cai *et al.*, 2021a) have shown the biases of the appearance time method due to particle evaporation, coagulation, variation of the vapor concentration, and external sinks. According to derivations and simulation results, R. Cai *et al.* (2021a) demonstrated that the influences of extramodal coagulation and external sinks can be readily corrected by subtracting them from the apparent GR calculated by the raw  $\Delta d_p(\Delta t)$ . The influence of self-coagulation on the appearance time needs to be corrected using an approximate formula. The influence of evaporation on the GR is substantial for particles close to the critical size during homogeneous nucleation, whereas the evaporation of volatile vapors during the growth process does not cause a significant bias (R. Cai *et al.*, 2021a).

#### *c. Applicability of collective methods*

In practical applications, the appearance time is typically calculated using the relative PNSD by fitting a sigmoid function to the rising edge of the measured PNSD at each  $d_p$ . Owing to the complexity of the analytical solution for the appearance time (R. Cai *et al.*, 2021a), the sigmoid function is chosen to be a simple function such as  $s = (a - b) / [1 + (t/t_{\text{app}})^c] + b$  (Stolzenburg *et al.*, 2018) or the rising edge of a Gaussian distribution. The value of  $m$  is recommended to be  $> 50\%$  (Lehtipalo *et al.*, 2014) to minimize the influence of growth driven by diffusion in the particle-size space [Eq. (9)] on the inferred GR (Olenius *et al.*, 2018).

However, the measurement uncertainties may be larger than the theoretical bias associated with the value of  $m$ . The appearance time method (and maximum concentration method) are favored by some studies due to their robustness in getting a GR value compared to the mode-fitting method, especially for sub-10-nm particles, as shown in Sec. III.C. They are not affected by the size-dependent systematic biases of measured particle concentrations as long as the signal-to-noise ratio is high enough to fit the sigmoidal rise of the signal. Raw signals proportional to PNSD can also be used to calculate the appearance time (Lehtipalo *et al.*, 2014). Further, signals from different instruments, such as particle concentrations measured using a DMPS and condensable vapor concentrations measured by mass spectrometers, can be used to calculate the appearance time. This can be used to infer the average GR from the vapor size to the smallest detectable particle size (Weber, Marti, and McMurry, 1997; Sihto *et al.*, 2006).

The previously mentioned collective methods are also applicable to the measured size distribution of ions. However, note that the growth of the ion population is also influenced by recombination and charging of the simultaneously growing neutral particles and hence is not necessarily interpretable as a condensational GR in the sense of either Eq. (9) or Eq. (2) (Gonser *et al.*, 2014; Carracedo, Gonzalez *et al.*, 2022).

We emphasize that the GR retrieved using collective approaches is a function of coupled  $d_p$  and  $t$  and calculates  $\text{GR}[d_p(t)]$  (the representative diameter) and  $\text{GR}[t(d_p)]$  (the representative time). The GR is usually analyzed using a linear fit over a certain size range or time span including several representative diameters or times, giving averaged GRs as in Eq. (15). This reduces the influences of random uncertainties on the measured GR and facilitates the comparison between different studies and the simulation of new particle growth. While the GR can be independent of time in a well-controlled chamber study, an atmospheric NPF event is often characterized by changing condensable vapors, clusters, and particles, thereby making the GR dependent on both time and size. Keep in mind that GRs retrieved using collective methods hide these interlinked dependencies of  $t$  and  $d_p$  and are a synergistic result of them.

## 2. Dynamic approaches based on the aerosol general dynamic equation

Approaches based on the population balance of aerosols characterized by the aerosol GDE [Eq. (7)] typically resolve the time and size dependency of the GR simultaneously, which differs from the previously described collective approaches. In practice, Eqs. (11) and (7) give the change of particle number concentration by the formation of particles at this size due to the net condensation growth of these particles into larger sizes, a coagulation sink, and a coagulation source. Both equations can be expanded to also include other possible causes of change of particle number concentration with a given size including dilution, wall loss, primary emission, and other external sources and sinks. When the knowledge about external sources and sinks and known coagulation kernels is included, the evolution of the measured

PNSD can be simulated while excluding the influence of net condensation. The differences between the simulated and measured PNSDs at the next time step is then attributed to net condensation. In that sense, the evolution of the size distribution with time is evaluated for each time step, thereby retrieving the  $\text{GR}_{\text{cond}}(d_p)$  for all sizes as given in Eq. (9).

For  $n$  GDEs corresponding to  $n$  particle sizes, there are  $n + 1$  unknown size-dependent net  $\text{GR}_{\text{cond}}$  characterizing the growth flux into and out of each size interval. Therefore, proper assumptions are needed to reduce the number of variables and solve the net  $\text{GR}_{\text{cond}}$ . The GDE approach in retrieving particle GRs was first applied by McMurry and Wilson (1982), who neglected the effects of coagulation and other sources and sinks and integrated the GDE above a certain diameter  $d_p$  to find the particle GR,

$$\text{GR}(d_p) = \frac{N_{>d_p}(t_2) - N_{>d_p}(t_1)}{(t_2 - t_1)n_{\text{avg}}(d_p)} \quad (16)$$

where  $N_{>d_p}$  is the total number concentration of particles larger than  $d_p$  at a certain moment and  $n_{\text{avg}}(d_p)$  is the average PNSD during the growth interval  $[t_1, t_2]$  at  $d_p$  expressed as  $dN/ddp$ .

In this approach  $\text{GR}(d_p)$  can be calculated from the total particle concentration measurement  $N_{>d_p}$  at two time steps and the average particle concentration is at the threshold size, assuming that there is negligible growth outside of the size range of interest. This simple approach was further developed by Verheggen and Mozurkewich (2002), who first applied a correction for possible dilution and coagulation. They then improved the procedure by fitting the integrated number size distribution expected from the GDE for all sizes with the measured values including the GR as the free parameter (Verheggen and Mozurkewich, 2006). This particle growth and nucleation model was used in several field studies, where it was also further developed (Kanawade, Benson, and Lee, 2012; Young *et al.*, 2013; Kammer *et al.*, 2018). Lehtinen *et al.* (2004) pursued the same approach; however, they reduced the number of free parameters to be fitted by assuming an expected size dependency of the condensational growth ( $\text{GR}_{\text{cond}}$ ) from theoretical condensation at the kinetic limit of a single condensing species. Kuang, McMurry, and McCormick (2009) slightly improved this by including an iterative procedure to determine the size-dependent GR on a fixed interval to eliminate the assumption of negligible growth outside of the region of interest. Moreover, besides a kinetic sulfuric acid condensation term, Kuang, McMurry, and McCormick (2009) included a size-dependent growth enhancement factor accounting for condensation of species other than sulfuric acid.

The approach reported by Pichelstorfer *et al.* (2018) assumed that the net condensation flux out of the largest size interval is negligible, which is practically done by setting the upper limit large size interval to a sufficiently large size. The size-resolved net  $\text{GR}_{\text{cond}}$  is then estimated using methods named TREND and INSIDE, which rely on an aerosol dynamics simulation calculating the expected size distribution at the next time step. The TREND method divides both the measured and simulated PNSDs into a series of size intervals.

Every size interval contains the same number concentration of particles. The net  $GR_{\text{cond}}$  is retrieved from the differences in the count median diameters between measured and simulation results. The INSIDE method evaluates a total concentration of particles larger than a given size. Attributing the difference between the measured and simulated total concentrations to the flux due to net condensation, one can solve the net  $GR_{\text{cond}}$  as a function of the given size. Compared to GDE approaches other than Eq. (16), the methods discussed by Pichelstorfer *et al.* (2018) do not apply a fitting procedure and do not rely on any assumptions about the size dependency of the GR.

Another recent approach was the application of a fixed interval Kalman smoother (Ozon, Seppänen *et al.*, 2021) in order to retrieve the unknown process parameters describing the evolution of the size distribution within the GDEs, i.e., the GR and nucleation rate. Kalman filtering is an iterative procedure that uses the information on the previous state and its covariance to predict the next step via an evolution model. The prediction is then updated by the available measurement refining the *a posteriori* state estimate and its corresponding covariance. Owing to its recursive procedure, the previous state and its uncertainty already include the evolution of all preceding measurements and their corresponding uncertainties. The resulting *a posteriori* estimate therefore improves the previously described GDE approaches, incorporating all preceding knowledge and giving a direct estimate of the resulting uncertainty of the GR at each time step. Kalman filtering has already been used to estimate PNSDs (Viskari *et al.*, 2012), but the GR therein was estimated from measured vapor concentrations. Ozon, Stolzenburg *et al.* (2021) demonstrated that GRs can indeed be reliably estimated from measured PNSDs in chamber experiments, where unknown sources and sinks can be neglected.

### C. Method performance under varying conditions: From rural backgrounds to highly polluted megacities

The accuracy of a given approach to estimate the GR is based on a series of ideal assumptions, as seen in Secs. III.B.1 and III.B.2. These ideal assumptions are violated to different extents for atmospheric NPF events, and the corresponding errors have been investigated via simulations (Olenius *et al.*, 2014; Kontkanen, Olenius *et al.*, 2016; Li and McMurry, 2018; R. Cai *et al.*, 2021a). As a result, the performances of these approaches vary with the atmospheric conditions.

We compare the retrieved GRs of simulated NPF events in clean and polluted atmospheric environments using a sectional aerosol model (Li and Cai, 2020) to evaluate the performance of difference approaches. For NPF events in relatively clean environments such as the rural background, the particle formation rate and coagulation sink are typically low (Dal Maso *et al.*, 2005; Nieminen *et al.*, 2018). In contrast, NPF events in polluted environments such as polluted megacities are reported to occur against high coagulation sink with high new particle formation rates (Iida *et al.*, 2008; Yao *et al.*, 2018; Deng *et al.*, 2020; Kulmala *et al.*, 2021). Compared to rural backgrounds, the coagulation sink for polluted megacities are reported to be 1 order of magnitude higher and the formation rate can be several orders of magnitude higher (Cai and Jiang,

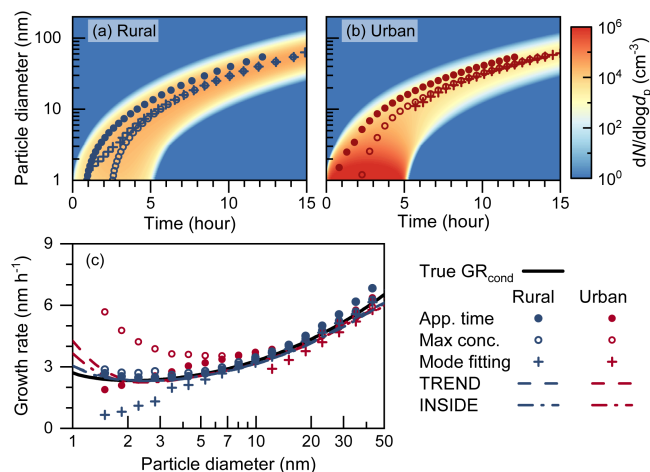


FIG. 4. Method performance for simulated NPF events. Simulated PNSDs are displayed for (a) rural background and (b) urban environments. The  $d_p(t)$  of the mode-fitting method and  $t(d_p)$  are shown for (a) the appearance (app.) time and (b) maximum concentration (conc.) methods. (c) Derived growth rates by different methods and simulation input condensation growth rate plotted against particle diameter.

2017). Coagulation is therefore important for the evolution of new particles in polluted megacities.

As shown in Fig. 4, we tested three collective approaches (the mode-fitting method, the 50% appearance time method, and the maximum concentration method; see Sec. III.B.1) and two GDE-based approaches (the TREND and INSIDE methods; see Sec. III.B.2). The influences of coagulation scavenging and coagulation growth on the mode-fitting method and the appearance time method have been corrected for a simulated urban scenario using the methods given by Stolzenburg *et al.* (2005) and R. Cai *et al.* (2021a), respectively. Such influences are not significant in the rural background scenario. Therefore, the retrieved GRs of the mode-fitting method and the appearance time method shown in Fig. 4(c) are the estimates of the condensation GRs.

The GDE approaches report size- and time-dependent GR and the GR value at  $t(d_p)$  of the appearance time method is presented in Fig. 4(c). The “true” GR is the input of the simulation and is the condensation GR defined in Eq. (2). To facilitate the comparison among different approaches, the true GR is assumed to be size dependent but time independent.

All of the tested approaches report consistent GR for particles larger than 10 nm for the simulated NPF event, and the GDE-based methods go down even to 1.5 nm. For sub-10-nm particles in the rural background, the appearance time method and the maximum concentration method show good estimations of the GR, whereas the mode-fitting method underestimates GR. This underestimation is caused mainly by the formation of new particles, which increases the concentration of particles on the left-hand side of the PNSD peak (Jiang, Zhao *et al.*, 2011), and hence the mode diameter increases slower than the true GR.

For the urban scenario, the corrected appearance time method is consistent with the true GR. The maximum concentration method considerably overestimates GR in the sub-10-nm size range, mainly because the influence of the

high coagulation sink is not corrected. The mode-fitting method cannot retrieve the GR because the PNSD does not have a peak in this range, which is sometimes the case for NPF in polluted megacities.

We clarify that Fig. 4 assumes an ideal condition with negligible vapor dissociation of clusters and a time-independent GR. Vapor dissociation and the temporal variation of the GR may also affect the accuracy of the methods (Olenius *et al.*, 2014; Li and McMurry, 2018; R. Cai *et al.*, 2021a). Further, it shows only the uncertainties due to the systemic biases of the methods. For example, the GR retrieved using the TREND and INSIDE methods agrees well with the true GR because they are based on the GDE equations with the GR as the only unknown variable. For atmospheric measurements and laboratory studies, measurement uncertainties also propagate to the retrieved GR. The GDE methods are expected to be more sensitive to measurement uncertainties because they include many linked equations, and future studies need to target an understanding of these related uncertainties. Averaging the retrieved GR over a size range and a time span (Kuang, Chen, Zhao *et al.*, 2012) helps to reduce the random uncertainties, as in the collective approaches. Approaches based on the Kalman filter integrate the uncertainties of the measurements in the estimation of the GR and therefore yield a more solid error estimate. Furthermore, they can also incorporate a smoothing procedure, which should further increase the stability of the result (Ozon, Stolzenburg *et al.*, 2021).

#### D. Analysis methods for estimating particle survival probabilities

The survival probabilities of growing new particles against coagulation scavenging can be estimated using either the evolution of the measured PNSD or the measured GR and coagulation sink. The estimated survival probabilities using the former and latter approaches are named the measured and theoretical survival probabilities, respectively.

According to the definition in Eq. (12),  $P(d_{p1} \rightarrow d_{p2})$  can be calculated by comparing the total number concentration  $N$  of an aerosol population at  $t_1$  and  $t_2$ . However,  $N$  in Eq. (12) is the decreasing concentration of the same aerosol population formed at  $t_1$ , which cannot be tracked in the measured PNSD. As shown in Fig. 4, an NPF event usually lasts for hours, and it is difficult to distinctly separate the particles formed at a certain moment at  $t_1$  from the particles formed between  $t_1$  and  $t_2$  unless the nucleation rate is negligible after  $t_1$ . Furthermore, for a weak NPF event it is sometimes difficult to separate the growing new particle mode from background particles. As a result, the measured survival probability cannot be accurately calculated using the definition  $N(t_2)/N(t_1)$ . Despite this difference between the measured  $N$  in a certain size range (in the Eulerian specification) and the mode  $N$  in Eq. (12) (in the Lagrangian specification), earlier studies (Weber, Marti, and McMurry, 1997; McMurry *et al.*, 2005) used the former  $N$  as an approximation of the latter to roughly indicate the survival probabilities.

The new particle formation rate  $J$  is also often used to calculate the measured survival probability with  $P(d_{p1} \rightarrow d_{p2}) = J(d_{p2})/J(d_{p1})$  (Kerminen and Kulmala, 2002; Kulmala *et al.*, 2013). This relationship is often conversely used in models to

derive  $J(d_{p2})$  from  $J(d_{p1})$  and  $P$ . However, this approach is valid only for certain types of PNSDs. According to Kerminen and Kulmala (2002),  $J$  in  $J(d_{p2})/J(d_{p1})$  should be the formation rate contributed by the same growing aerosol population corresponding to the mode  $N$  (in the Lagrangian specification) in Eq. (12), and it is derived implicitly based on the monodisperse assumption of the growing mode. Although  $P$  is usually calculated using the formation rate contributed by all the particles (in the Eulerian specification) (Kulmala *et al.*, 2017), Cai, Deng *et al.* (2022) further showed that  $J(d_{p2})/J(d_{p1})$  is also theoretically valid for quasi-steady-state PNSDs, such as those of newly formed particles. However, when using this approach in a wide size range, such as from 1.5 nm to 100 nm, the quasi-steady-state assumption no longer holds and may lead to considerable uncertainty.

Alternatively, Kuang, McMurry, and McCormick (2009) proposed estimating  $P$  using  $P(d_{p1} \rightarrow d_{p2}) = (dN/dd_{p2})/(dN/dd_{p1})$  and derived an analytical formula for  $dN/dd_{p2}$  accounting for size-dependent particle sources, sinks, and GRs. Since  $J = \text{GR } dN/dd_p$ , this approach is equivalent to the  $J(d_{p2})/J(d_{p1})$  given a size-independent GR. Cai, Deng *et al.* (2022) showed that the uncertainties of this approach is associated to the width of the PNSD. If the width of the PNSD in the linear scale maintains at a relatively constant level as particles grow large,  $(dN/dd_{p2})/(dN/dd_{p1})$  and  $J(d_{p2})/J(d_{p1})$  are expected to lead to accurate estimates of  $P$ . However, the PNSD of atmospheric particles tends to be broadened in the linear scale, causing an underestimation in the retrieved  $P$ . An alternative formula  $P(d_{p1} \rightarrow d_{p2}) = (dN/d \log d_{p2})/(dN/d \log d_{p1})$  has correspondingly been proposed, as the variation of width in the logarithmic scale of growing ambient particles is usually smaller than that in the linear scale, and the evolution of a geometric standard deviation can be used for further correction.

The theoretical survival probability can be calculated using Eq. (13) or, in most cases (especially in models), Eq. (14). Equation (14) is theoretically valid with an uncertainty caused by the monodisperse approximation, which is negligible for particles much larger than the nucleation size. However, applying Eq. (14) to measured NPF may cause large uncertainties, which are associated with the inaccurate estimation of GR and CoagS. Good agreement between the measured and theoretical survival probabilities have been reported for particles larger than 3 nm in polluted megacities (Cai, Deng *et al.*, 2022; Tuovinen *et al.*, 2022). However, for sub-3-nm particles in polluted megacities Kulmala *et al.* (2017) reported that the theoretical survival probabilities were orders of magnitudes lower than the measured survival probabilities. This large discrepancy was mainly attributed to the ineffective CoagS of sub-3-nm particles. A later study reported better agreement between the measured and theoretical survival probabilities for 2–6 nm particles within a factor of 2–10 for boreal forests and megacities (Kulmala *et al.*, 2022), but the remaining discrepancies (especially for the boreal forest site) could indicate that the estimates of the survival probability using measured formation rates might still be biased either due to large measurement uncertainties or under the assumptions made in Eq. (14).

To summarize, the measured survival probabilities can be calculated using the measured  $J$ ,  $dN/dd_p$ ,  $dN/d \log d_p$ , or  $N$ . The validity and uncertainties of these approaches is associated with the evolution of PNSDs in different environments. It is important to check the validity of their assumptions before using them to retrieve the measured survival probability or deriving  $J$  of large particles using a theoretical survival probability. The theoretical survival probability can be calculated using the measured GR and CS with Eq. (14), yet its uncertainty in different environments needs to be better clarified in future studies, especially for the sub-3-nm size range.

#### IV. UNDERSTANDING NANOPARTICLE GROWTH: FROM MEASUREMENTS TO PROCESS MODELS

Nanoparticle growth in the sub-25-nm range is closely linked to gas-phase nucleation and is hence often studied alongside these processes. Pioneering research on the activation and subsequent growth of aerosol particles and ions in the presence of a supersaturated vapor was done by J. Aitken and C. T. R. Wilson. Aitken (1889) developed the first aerosol counting device and inferred the first evidence of particle formation in the atmosphere at the end of the 19th century. Wilson (1912) studied the growth of droplets in a supersaturated environment and inferred that atmospheric ions enhance this process, which led to the construction of cloud chambers and which have been widely used in particle physics. It took another half century until the basic kinetics of mass transfer and coagulation were developed by Fuchs (1964) and Fuchs and Sutugin (1971). This led to work of Brock (1972), Heisler, Friedlander, and Husar (1973), and Heisler and Friedlander (1977), who clarified the secondary origin of smog and developed so-called aerosol growth laws, which determined a relationship between the observed GR of the aerosol and the underlying process, for instance, transport-limited or particle-phase reaction limited growth. McMurry, Rader, and Stith (1981) and McMurry and Wilson (1982) continued this work by studying the formation and growth of aerosols in ambient settings such as power plant plumes. However, it took until the 1990s, i.e., 100 years after Aitken's first discovery, that NPF was widely observed in the atmosphere in remote boreal, coastal, and mountaintop sites (Weber *et al.*, 1995; Mäkelä *et al.*, 1997; O'Dowd *et al.*, 1999). At the same time, Clement and Ford (1999a, 1999b) were also able to theoretically describe the growth of aerosol particles with the abundance of low-volatility vapors, especially sulfuric acid. Altogether these pioneering studies led to the emergence of a new field of atmospheric science, which progressively demonstrated the global importance of atmospheric gas-to-particle conversion. This has induced numerous field measurements of atmospheric NPF and growth within the last two decades from highly polluted environments (McMurry *et al.*, 2000; Yao *et al.*, 2018) to remote clean locations such as the polar regions (Jokinen *et al.*, 2018; Baccarini *et al.*, 2020; Beck *et al.*, 2021) or the free troposphere (Weigel *et al.*, 2011; Bianchi *et al.*, 2016, 2021; Zhao *et al.*, 2020). Several reviews have already summarized this variety of ambient observations of NPF (Kulmala, Vehkamäki *et al.*, 2004; Kerminen *et al.*, 2018), but they lack a detailed focus on the process level

understanding of nanoparticle growth where ambient measurements are put into perspective with the underlying concepts of nanoparticle growth and insights gained from laboratory experiments or process modeling. We thus give only an overview of the general characteristics of nanoparticle growth observed in the ambient air and instead focus on the gained physicochemical process level understanding, where we first discuss the importance of collective growth processes, which are often underrepresented in growth studies. We then focus on the pure condensational part on the single-particle level, which is most important in large-scale models.

##### A. Overview of ambient observations of nanoparticle growth

Nanoparticle growth is often observed following the formation of particles by atmospheric nucleation. Most observations focus on so-called regional NPF events, characterized by either steady meteorological conditions or a large spatial extent of the vapor sources, which allow nucleation and growth to occur simultaneously in a large air mass. Such NPF events can then be easily followed by observations at a single site, enabling the analysis of particle growth with the approaches described in Sec. III.B.

New particle formation and subsequent growth also occur on small local scales, from NPF within distinct plumes to smaller scale sources, which can alter the character of simultaneous regional NPF, as we later see. This localized NPF might occur in the vicinity of roads (Pirjola *et al.*, 2006; Kumar *et al.*, 2011), clouds (Weigelt *et al.*, 2009; Wehner *et al.*, 2015), or airports (Hudda and Fruin, 2016), and in combustion plumes, such as those from power plants (McMurry, Rader, and Stith, 1981; Junkermann, Hagemann, and Vogel, 2011; Stevens and Pierce, 2014; Mylläri *et al.*, 2016), biomass burning (Vakkari *et al.*, 2014), ship exhaust (Lack *et al.*, 2009; Jonsson, Westerlund, and Hallquist, 2011), or volcanic eruptions (Boulon, Sellegri, Hervo, and Laj, 2011; Rose *et al.*, 2019). Moreover, a substantial fraction of sub-25-nm particles in urban areas can also be emitted directly from traffic (Kumar *et al.*, 2014), with primary emissions down to particle sizes as small as 1–3 nm (Rönkkö *et al.*, 2017; Olin *et al.*, 2020). Both particles formed through nucleation in the atmosphere and primary emitted particles can subsequently grow to larger sizes (Zimmerman, Petters, and Meskhidze, 2020), but detailed studies on the differences in their growth are still lacking. Altogether such plume-related studies of nanoparticle growth are challenging, as Eulerian measurements at single sites might limit our ability to deduce nanoparticle GRs (Kivekäs *et al.*, 2016). In addition, such plume GRs might be too high to be time resolved for most of the available instrumentation; see Sec. III.A.4.

Hence, focusing on regional NPF, a couple of general characteristics are evident from observations around the globe. Overall, nanoparticle GRs are reported to be mostly within the range of 1–10 nm h<sup>-1</sup> (Manninen *et al.*, 2010; Kerminen *et al.*, 2018; Nieminen *et al.*, 2018), especially the median values for different sites; see Figs. 5 and 7. The limited range of the observed GRs could also originate from the methodology, where clear growing modes have to be identified and the sensitivity and time resolution of the instrumentation used needs to be sufficient for that, as discussed in Sec. III.A.4.

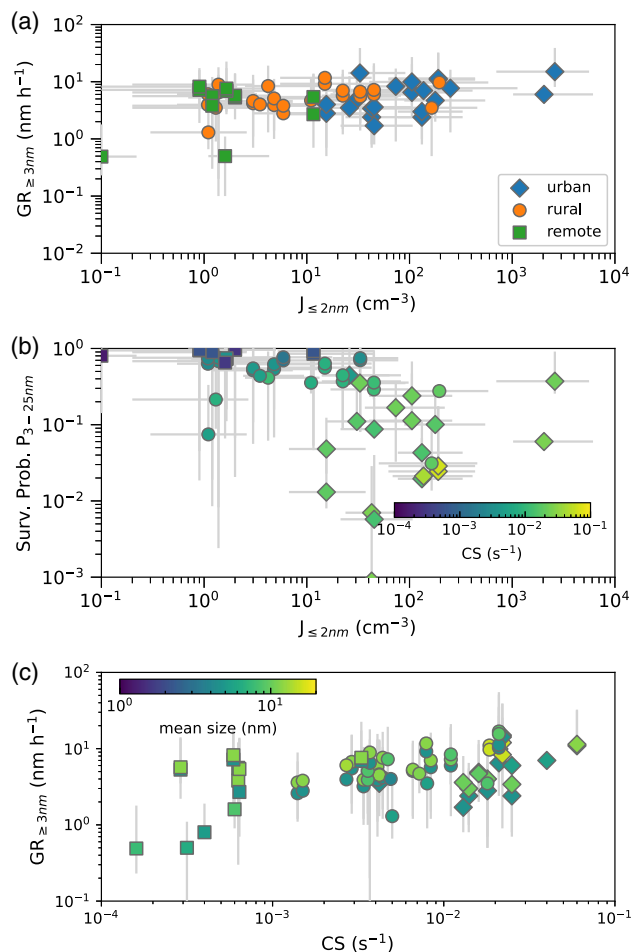


FIG. 5. Cross-study examination of the relationship between (a) GR and particle formation rate, (b) nucleation mode survival probability  $P(3\text{--}25\text{ nm})$  and formation rate, and (c) GR and CS. Data points represent means or medians of the GR,  $J$ , and CS values reported from a single study. We report values only when the median diameter of the GR measurement is  $\geq 3\text{ nm}$  and for measurements where the formation rate size is  $\leq 2\text{ nm}$ . Different size ranges, seasons, and instrumentation and analysis methods used for GR calculations have been separated for the same size, if reported. Error bars show the intrastudy variation of the reported quantities, if reported. Otherwise, a 50% error on the  $J$  and GR values are assumed.

However, slower growth (as low as  $0.1\text{ nm h}^{-1}$ ) is sometimes measured for polar regions (Weller *et al.*, 2015; Baccarini *et al.*, 2020), and faster GRs are observed for several measurements often influenced by strong local emission sources, such as those in heavily polluted and urban environments (Mönkkönen *et al.*, 2005; Iida *et al.*, 2008; Kalafut-Pettibone *et al.*, 2011; Xiao *et al.*, 2015), but also at some rural or coastal sites (O’Dowd *et al.*, 2007; Svenningsson *et al.*, 2008; Vakkari *et al.*, 2011; Sipilä *et al.*, 2016; Kammer *et al.*, 2018). However, high GRs are typically not observed at extended spatial scales, limiting their regional and global influence.

But even if the majority of median ambient observations are within  $1\text{--}10\text{ nm h}^{-1}$ , differences between different locations are apparent. GRs for urban and polluted locations are in

general higher than those for rural and remote sites. Some mountaintop sites can also show higher GRs than other remote sites (Kerminen *et al.*, 2018), but this could be an effect of particle transport (Sellegrì *et al.*, 2019). The comparisons of average GRs often span over different seasons and size ranges, but GRs can significantly vary at a single site during an entire year. Focusing on particle growth at sizes larger than  $10\text{ nm}$ , at many remote and rural midlatitude to high latitude locations, higher GRs are found during summer (Nieminen *et al.*, 2018) in both the Northern (Birmili *et al.*, 2003; Yli-Juuti *et al.*, 2011; Kanawade, Benson, and Lee, 2012) and Southern Hemispheres (Sunı *et al.*, 2008; Vakkari *et al.*, 2011). A summer maximum is also observed for most urban locations, for instance, in European capitals (Hussein *et al.*, 2008; Salma and Németh, 2019) and Chinese megacities (Wang *et al.*, 2013; Qi *et al.*, 2015; Deng *et al.*, 2020). In a recent study the GR at sizes  $> 10\text{ nm}$  was also found to have a summer maximum in a vegetation-free desert zone that is heavily influenced by anthropogenic emissions (Hakala *et al.*, 2019). Therefore, this seasonal variation seems to be influenced by both the enhanced photochemistry and the higher biogenic emissions in the summertime. In contrast, GRs measured at significantly smaller sizes, especially in the sub-3-nm range, exhibit much smaller seasonal variations at all locations (Sunı *et al.*, 2008; Yli-Juuti *et al.*, 2011; Deng *et al.*, 2020). This is also true for measurement sites with a two-season cycle. Rose *et al.* (2015) observed faster GRs for  $7\text{--}20\text{ nm}$  particles during the wet season at a mountaintop station in Bolivia, when air masses arrived from the Amazon Basin, compared to the dry season, but a less pronounced seasonal pattern for GRs in the range of  $1.5\text{ to }3\text{ nm}$ . However, note also that the sub-3-nm size range is the most challenging to resolve, and most common instruments could be significantly limited in detecting both low and high GRs (see Sec. III.A), resulting in fewer observed seasonal variations.

Generally we find a size dependence of GRs across the entire range of regional NPF studies, with GR increasing with an increasing particle size for rural sites (Sunı *et al.*, 2008; Yli-Juuti *et al.*, 2009, 2011; Kulmala *et al.*, 2013; Nieminen *et al.*, 2018; Baalbaki *et al.*, 2021), as well as mountaintops (Rose *et al.*, 2015; Bianchi *et al.*, 2016) and urban or polluted sites (Kuang, Chen, Zhao *et al.*, 2012; Kontkanen, Järvinen *et al.*, 2016; Nieminen *et al.*, 2018; Deng *et al.*, 2020). While such an increase is most apparent in the sub-20-nm size range, there are indications that this feature could extend up to  $100\text{ nm}$  in particle diameter (Paasonen *et al.*, 2018). For sub-3-nm particles, few studies find GRs larger than  $5\text{ nm h}^{-1}$  (Hirsikko *et al.*, 2012; Kuang, Chen, Zhao *et al.*, 2012; Brilke *et al.*, 2020), which is common for GRs above  $10\text{ nm}$  (Manninen *et al.*, 2010; Rose *et al.*, 2015; Nieminen *et al.*, 2018; Yao *et al.*, 2018). Few studies report distinct features in the size dependency of growth other than increasing GR with size: Yu *et al.* (2016) found decreasing GRs with size in the sub-3-nm range for strong NPF event days, and Manninen *et al.* (2010) reported no strictly increasing GRs with size for the sites of Pallas in northern Finland, Mace Head on the coast of Ireland, and the Hohenpeissenberg in Germany. As shown in Sec. III.B.1, this size dependency could also be a result of the used collective GR analysis methods and their interlinked

dependencies on time and size. However, Kuang, Chen, Zhao *et al.* (2012) used a GDE-based method (see Sec. III.B.2) that eliminated this linkage and still found increasing GRs with size.

The regional extent of NPF events is estimated to range from tens to about 1000 km (Wehner *et al.*, 2007; Hussein *et al.*, 2009; Jeong *et al.*, 2010; Wang *et al.*, 2013; Kim *et al.*, 2016; Salma *et al.*, 2016; Vana *et al.*, 2016; Berland *et al.*, 2017; Németh *et al.*, 2018). However, within the same regional NPF event different GRs at different locations can be observed. This indicates that different local vapor sources or altered local atmospheric chemistry can change the growth behavior at different sites, while the occurrence of NPF is determined by regionally favorable conditions. Most studies comparing different sites observe on average higher particle GRs for more polluted conditions than in rural background sites (Wehner *et al.*, 2007; Jeong *et al.*, 2010; Wang *et al.*, 2013; Salma *et al.*, 2016; Bousiotis *et al.*, 2019). However, among different urban (Bousiotis *et al.*, 2019), rural (Crippa and Pryor, 2013), and coastal sites (Berland *et al.*, 2017) some variations of GRs can be found. Furthermore, while there are some studies indicating that the vertical extent of NPF is often confined to the planetary boundary layer (O'Dowd *et al.*, 2009; Crumeyrolle *et al.*, 2010), NPF in the free troposphere (Boulon *et al.*, 2010; Boulon, Sellegri, Hervo, Picard *et al.*, 2011; Rose, Sellegri *et al.*, 2015; Rose *et al.*, 2015; Bianchi *et al.*, 2016; Wang *et al.*, 2016; Williamson *et al.*, 2019) and in the uppermost part of the residual layer (Lampilahti *et al.*, 2021) is also reported. However, comparisons of GRs at higher altitudes with lower level GRs are sparse. Boulon, Sellegri, Hervo, Picard *et al.* (2011) found no difference in GR between growth events occurring only at a high-altitude site when compared to events occurring at both high altitude and mid altitude. Casquero-Vera *et al.* (2020) showed that GRs can be slightly higher at an elevated background site than with the urban GR. Du *et al.* (2021) demonstrated that the particle GR at an altitude of 260 m above a Chinese megacity is significantly reduced compared to the ground level. Across all mentioned studies, the variation of GRs for different locations during the same NPF event is at maximum within a factor of 2 for all regional scales.

The relatively limited variability in the measured values of GRs across different environments on both regional and global scales is a noteworthy feature, considering the fact that there are many atmospheric low-volatility vapors, which can possibly contribute to atmospheric nanoparticle growth. This discrepancy between a lower variation of GRs compared to the variation of total condensable vapors is also observed for individual sites (Kulmala, Cai *et al.*, 2022). As the most important vapor for atmospheric nucleation (Sipilä *et al.*, 2010; Zhang *et al.*, 2012; Gordon *et al.*, 2016), sulfuric acid is often also considered to be an important driver for nanoparticle growth (Jokinen *et al.*, 2018; Sebastian, Kanawade, and Pierce, 2021). Most ambient observations, however, conclude that vapors other than sulfuric acid must participate in growth from early stages onward (Bzdek *et al.*, 2012; Kuang, Chen, Zhao *et al.*, 2012; Kulmala *et al.*, 2013). The most common candidates are low-volatility oxidized organics (Ehn *et al.*, 2014; Bianchi *et al.*, 2019) of either biogenic (Vogel, Schneider *et al.*, 2016; Kammer *et al.*, 2018; Mohr

*et al.*, 2019) or anthropogenic origin (Wang *et al.*, 2015; Guo *et al.*, 2020). However, iodic acid in marine (Sipilä *et al.*, 2016) and arctic environments (Baccarini *et al.*, 2020) contributes to early particle growth. The role of other acids in nucleation mode growth like methanesulfonic acid in the marine boundary layer (Willis *et al.*, 2016; Beck *et al.*, 2021), nitric acid in urban environments (Bzdek *et al.*, 2012; Xu *et al.*, 2019), or carboxylic acids in polluted rural environments (Zhang *et al.*, 2004; Fang *et al.*, 2020) is more debated due to their semivolatile vapor pressures. Additionally, acid condensation is often accompanied by bases such as ammonia (Bzdek *et al.*, 2012; Hodshire *et al.*, 2016; Li *et al.*, 2021) or amines (Smith *et al.*, 2010; Yao *et al.*, 2018; Cai *et al.*, 2022). Ultimately water might play an important role in atmospheric nanoparticle growth, often cocondensing with other species (Verheggen and Mozurkewich, 2002; Stolzenburg *et al.*, 2005). Altogether that variety of vapors potentially influencing nanoparticle growth calls for a more broad application of different techniques to quantify them (Sec. III.A.3), as this is often missing from many of the previously mentioned ambient studies.

The variety of possible contributors to nanoparticle growth, however, is not transformed into a wide range of observed GRs. This is illustrated in Fig. 5, where we show the measured GR above 3 nm from all available studies, which simultaneously reported a new particle formation rate at sizes smaller than 2 nm, i.e., close to the critical size range for atmospheric nucleation (the studies are summarized in Table I). While formation rates span up to 5 orders of magnitude, the GRs are mostly within an order of magnitude, in the range of 1–10 nm h<sup>-1</sup>, as previously mentioned. There is no significant correlation between the observed formation rate and the GR, indicating different major mechanisms promoting formation of stable molecular clusters and their subsequent growth. However, if we approximate the survival probability over the nucleation mode (3–25 nm) as in Eq. (14) with the measured CS at the site during NPF, we obtain some anticorrelation between particle survival and nucleation rate, driven mainly by significant changes in CS across the different sites. Apparently there seems to be a coupling of the sources for particle formation ( $J$ ) and preexisting aerosol loading (CS), which buffers the importance of NPF in the atmospheric system across many different sites and is also found in large-scale models; see Sec. V, Westervelt *et al.* (2013), and Blichner *et al.* (2021). However, and perhaps even more importantly, there is no such link with respect to particle growth. This is in line with individual studies that also did not find any positive correlation between particle GR and CS for single sites (Vakkari *et al.*, 2011; Yli-Juuti *et al.*, 2011). If the sources of CS and GR are not coupled, then higher GRs at the same site efficiently promote particle survival and enhance the atmospheric significance of NPF. However, as the observation methods might be limited when measuring high and low GRs (see Sec. III.A.4), this could also induce a reduced correlation between GR and CS.

## B. Growth as a collective phenomenon

Since the GR retrieved from the measured evolution of PNSDs using a collective method reflects a collective

TABLE I. Overview of growth studies reporting GRs at median sizes  $\geq 3$  nm and formation rates at sizes  $\leq 2$  nm ( $J_{\leq 2}$ ). They are categorized into urban, rural, and remote locations and separated by different seasons, GR methods, size ranges, or used instruments. The variation  $\Delta$ GR is given by the reported standard deviation or 25%–75% quantiles. GR analysis methods are depicted by m.c. for maximum concentration, a.t. for appearance time, mode for mode fitting, GDE for GDE-based approaches, and ch. frac. for the charged fraction method used and presented by Iida *et al.* (2008).

Study	Location	Type	Season	Method	Instrument	Size (nm)	GR (nm h <sup>-1</sup> )	$\Delta$ GR (nm h <sup>-1</sup> )	CS (s <sup>-1</sup> )	$J_{\leq 2}^{\text{nm}}$ (cm <sup>-3</sup> s <sup>-1</sup> )
Yao <i>et al.</i> (2018)	Shanghai, China	Urban	Winter	m.c.	DMPS +NAIS	3–7	6.5	[2.6 13.7]	$2.1 \times 10^{-2}$	106
Xiao <i>et al.</i> (2015)	Shanghai, China	Urban	Winter	m.c.	SMPS	2.39–7	9.9	[7.5 17.1]	$2.1 \times 10^{-2}$	106
Young <i>et al.</i> (2013)	Taichung City, Taiwan	Urban	Summer	GDE	SMPS	7–20	11.4	[1.1 20.7]	$6.0 \times 10^{-2}$	190
Yu <i>et al.</i> (2016)	Nantou County, Taiwan	Rural	Fall	GDE	SMPS	> 10	8.3	[1.1 21.1]	$6.0 \times 10^{-2}$	190
Iida <i>et al.</i> (2008)	Nanjing, China	Urban	All	GDE	SMPS	3–20	7.7	[7.4 8.7]	$1.9 \times 10^{-2}$	195
Manninen <i>et al.</i> (2010)	Tecamac, Mexico	Urban	Spring	ch. frac.	SMPS	3.7–25	15	[6.4 8.5]	$2.2 \times 10^{-2}$	2600
	Pallas, Finland	Remote	All	m.c.	AIS	3–7	5.6	[4.4 6.5]	$6.3 \times 10^{-4}$	1.2
	Mace Head, Ireland	Remote	All	m.c.	AIS	7–20	3.8	[3.5 4.8]	$6.3 \times 10^{-4}$	1.2
	Cabauw, Netherlands	Rural	All	m.c.	AIS	3–7	2.7	[2.0 11.2]	$6.4 \times 10^{-4}$	11.6
	Melpitz, Germany	Rural	All	m.c.	AIS	7–20	5.4	[3.1 8.1]	$6.4 \times 10^{-4}$	11.6
	Hohenpeissenberg, Germany	Rural	All	m.c.	AIS	3–7	5.5	[4.1 9.5]	$2.9 \times 10^{-3}$	33.1
	Jungfraujoch, China	Remote	All	m.c.	AIS	7–20	6.7	[4.8 8.6]	$2.9 \times 10^{-3}$	33.1
	Beijing, China	Urban	Summer	m.c.	DMPS	3–7	14.2	[4.5 7.9]	$8.4 \times 10^{-3}$	22.4
	Po Valley, Italy	Rural	Summer	m.c.	AIS	3–7	6	[5.5 9.2]	$8.4 \times 10^{-3}$	22.4
Wang <i>et al.</i> (2015)	Kent, WA	Rural	All	Mode	SMPS	> 3	3.9	[3.1 6.7]	$4.1 \times 10^{-3}$	3.0
Kontkanen, Järvinen <i>et al.</i> (2016)	Kent, WA	Rural	All	GDE	SMPS	> 3	5.1	[3.9 8.6]	$4.1 \times 10^{-3}$	3.0
Kanawade, Benson, and Lee (2012)	Brookhaven, NY	Rural	Summer	GDE	SMPS	3–10	7.2	[5.3 8.8]	$5.9 \times 10^{-4}$	0.9
Yu <i>et al.</i> (2014)	Kent, WA	Rural	Winter	GDE	SMPS	3–10	3.5	[4.1 9.1]	$5.9 \times 10^{-4}$	0.9
Deng <i>et al.</i> (2020)	Beijing, China	Urban	Winter	Mode	SMPS	7–15	2.4	[3.7 24.7]	$2.2 \times 10^{-2}$	32.9
			Spring	Mode	SMPS	3–7	6	[2.6 12.9]	$1.1 \times 10^{-2}$	45
			Summer	Mode	SMPS	7–15	7.2	[3.8 13.8]	$1.1 \times 10^{-2}$	45
			Winter	Mode	SMPS	3–7	3.9	[2.5 5.3]	$3.6 \times 10^{-3}$	4.8
			Spring	Mode	SMPS	7–15	5.1	[4.1 6.1]	$3.6 \times 10^{-3}$	4.8
			Summer	Mode	SMPS	3–10	1.3	[0.64 2.49]	$5.0 \times 10^{-3}$	1.1
			Winter	Mode	SMPS	3–10	3.5	[2.6 4.7]	$8.0 \times 10^{-3}$	1.3
			Spring	Mode	SMPS	7–15	2.4	[1.6 3.1]	$1.4 \times 10^{-2}$	132
			Summer	Mode	SMPS	3–7	3	[2.0 3.5]	$1.4 \times 10^{-2}$	132
			Fall	Mode	SMPS	7–15	2.4	[1.6 3.1]	$2.5 \times 10^{-2}$	42.8
			Winter	Mode	SMPS	7–15	3.4	[2.7 4.4]	$2.5 \times 10^{-2}$	42.8
			Spring	Mode	SMPS	3–7	2.8	[2.3 3.4]	$1.8 \times 10^{-2}$	15.5
			Summer	Mode	SMPS	7–15	4	[3.3 4.7]	$1.8 \times 10^{-2}$	15.5
			Fall	Mode	SMPS	3–7	1.7	[0.9 2.6]	$1.3 \times 10^{-2}$	45.3
			Winter	Mode	SMPS	7–15	3.6	[2.1 4.4]	$1.3 \times 10^{-2}$	45.3
			Spring	m.c.	SMPS	10–25	4.9	[1.7 8.1]	$1.6 \times 10^{-2}$	30.7
Sebastian, Kanawade, and Pierce (2021)	Hyderabad, India	Urban	Winter	Mode	SMPS	3–25	3.5	[3.0 4.7]	$1.8 \times 10^{-2}$	164
Fang <i>et al.</i> (2020)	Pingyuan, China	Rural	Spring and summer	GDE	SMPS	> 3	8.4	[7.1 10.7]	$1.1 \times 10^{-2}$	4.2
Erupe <i>et al.</i> (2010)	Kent, WA	Rural	Spring and summer	GDE	SMPS	> 3	8.4	[7.1 10.7]	$1.1 \times 10^{-2}$	4.2

(Table continued)

TABLE I. (Continued)

Study	Location	Type	Season	Method	Instrument	Size (nm)	GR ( $\text{nm h}^{-1}$ )	$\Delta\text{GR}$ ( $\text{nm h}^{-1}$ )	CS ( $\text{s}^{-1}$ )	$J_{<2\text{ nm}}$ ( $\text{cm}^{-3} \text{s}^{-1}$ )
Jokinen <i>et al.</i> (2018)	Alboa, Antarctica	Remote	Summer	Mode	DMPS	6–10	0.49	[0.26 1.30]	$1.6 \times 10^{-4}$	0.1
Brean <i>et al.</i> (2020)	Barcelona, Spain	Urban	Summer	a.t.	PSM	1.9–4.5	4.4	[3.4 5.4]	$1.6 \times 10^{-2}$	178
Boulon <i>et al.</i> (2010)	Jungfraujoch, China	Remote	All	Mode	SMPS	4.5–20	4.7	[2.7 6.7]	$1.6 \times 10^{-2}$	178
Rose, Sellegri <i>et al.</i> (2015)	Chacaltaya, Bolivia	Remote	All	m.c.	AIS	3–7	5.3	[1.8 8.8]	$2.9 \times 10^{-4}$	2.0
Kulmala <i>et al.</i> (2013)	Hyytiälä, Finland	Rural	Spring	m.c.	AIS	7–20	5.7	[3.5 7.9]	$2.9 \times 10^{-4}$	2.0
Boulon <i>et al.</i> (2010)	Puy de Dôme, France	Rural	All	a.t.	NAIS	3–7	6.9	[3.9 10.4]	$3.3 \times 10^{-3}$	1.65
Boy <i>et al.</i> (2005)	Rocky Mountains, CO	Rural	Summer	m.c.	AIS	7–20	7.6	[4.9 14.9]	$3.3 \times 10^{-3}$	1.6
Brean <i>et al.</i> (2021)	S. Shetland Islands, Antarctica	Remote	Summer	Mode	DMPS	1–15	2.8	[6.3 6.7]	$1.5 \times 10^{-3}$	5.9
Baalbaki <i>et al.</i> (2021)	Agia Marina, Cyprus	Rural	All	Mode	SMPS	4–10	3.8	[8.8 9.0]	$1.5 \times 10^{-3}$	5.9
Yu <i>et al.</i> (2014)	Ozark Forest, AR	Rural	Summer	a.t.	NAIS	3–7	6.5	[0.4 0.6]	$3.7 \times 10^{-3}$	1.38
Jayarathne <i>et al.</i> (2017)	Beijing, China	Urban	Winter	Mode	SMPS	5–25	8.9		$4.9 \times 10^{-3}$	3.5
Dai <i>et al.</i> (2017)	Nanjing, China	Urban	Fall	m.c.	NAIS	2–10	4		$3.16 \times 10^{-4}$	1.6
Vana <i>et al.</i> (2016)	Järvelja, Estonia	Rural	All	GDE	NAIS	3–7	0.5			
				m.c.		7–25	6.05			

phenomenon due to multiple processes (see Sec. III.B.1), it needs to be reduced to the condensation GR in order to be compared to the contributions from condensable vapors, or vice versa. This could also influence the conclusions from the results presented in Fig. 5, especially the surprisingly small variability in GR with respect to the wide range of possible condensable vapors. Therefore, we now first clarify the role of collective phenomena in atmospheric and laboratory NPF studies and estimate in which settings they are non-negligible.

### 1. Apparent and real growth due to coagulation

The size-dependent coagulation loss of new particles (extramodal coagulation as defined in Sec. III.B.1) does not contribute to the growth of single particles or an aerosol population, yet it shifts the size distribution toward larger diameters. The apparent growth corresponding to this shift has to be corrected before further growth analysis when GR is retrieved by collective methods. For the mode-fitting method, extramodal coagulation is most significant in the sub-10-nm size range (Leppä *et al.*, 2011). In Atlanta (Stolzenburg *et al.*, 2005), Beijing (Yue *et al.*, 2010), and New Delhi (Sarangi, Aggarwal, and Gupta, 2015) the apparent growths due to coagulation scavenging for mode-fitting calculations were 15%, 33%, and 220% of the condensation GR, respectively. For the appearance time method, R. Cai *et al.* (2021a) demonstrated that coagulation scavenging shortens the time of particles to reach the maximum concentration, causing an overestimation of sub-3-nm growth in environments with a high coagulation sink. This apparent growth was thus found to be important for appearance time calculations in urban Beijing (Deng *et al.*, 2021) but can be considered negligible in clean environments or for large particles, similar to the findings for the mode-fitting method. Altogether the apparent growth of new particles poses challenges to particle growth analysis, especially for NPF in polluted environments. However, while correction methods exist (Stolzenburg *et al.*, 2005; Leppä *et al.*, 2011; R. Cai *et al.*, 2021a), their application is limited (Stolzenburg *et al.*, 2005; Deng *et al.*, 2021).

The coagulation among new particles, i.e., self-coagulation, is found to be an important mechanism for new particle growth in some environments, especially those with high nucleation rates and hence high new particle concentrations. Stolzenburg *et al.* (2005) found that, for six NPF events measured in Atlanta, contributions of self-coagulation to GR was on average 30% of the condensation GR contributed by sulfuric acid. This value was reported to be 42% by Yue *et al.* (2010) for the Beijing atmosphere. For an NPF event in New Delhi (Sarangi, Aggarwal, and Gupta, 2015), the self-coagulation contributed  $3.8 \text{ nm h}^{-1}$  to the apparent GR, which was comparable to the contribution of condensation GR of  $3.6 \text{ nm h}^{-1}$ . However, self-coagulation seldom reduces new particle concentration significantly in the planetary boundary layer (Anttila, Kerminen, and Lehtinen, 2010) because the coagulation sink of new particles is mainly contributed by accumulation mode particles (Dal Maso *et al.*, 2002; Cai and Jiang, 2017). Exceptions are situations with a high nucleation rate but low preexisting aerosol concentration, such as in laboratory experiments (Kürten *et al.*, 2018), where self-coagulation has been reported to be a predominating sink of

new particles. The contribution to growth by self-coagulation is at least sometimes acknowledged (Wang *et al.*, 2015), or its induced uncertainty is roughly estimated (Yao *et al.*, 2018). Ultimately in the studies using a GDE-based approach (Sec. III.B.2), both forms of coagulation (self-coagulation and extramodal coagulation) are intrinsically taken into account, thus increasing the confidence in their results (Erupe *et al.*, 2010; Kanawade, Benson, and Lee, 2012; Young *et al.*, 2013; Yu *et al.*, 2014, 2016; Dai *et al.*, 2017).

### 2. Growth driven by diffusion in the particle-size space

The growth driven by diffusion in the particle-size space of an aerosol population is potentially an important mechanism in the initial growth of new particles, though it has rarely been accounted for in particle growth analysis, except for the methods that explicitly solve GDEs in the discrete form; for instance, see the discussion of the Atmospheric Cluster Dynamics Code model by McGrath *et al.* (2012). Besides the collective methods, GDE-based methods such as the TREND method also neglect the diffusion-driven growth term when retrieving the GR from measured PNSDs. Most often GDE-based methods solve for the growth term of the GDE as in Eq. (11), which is simply an approximation of the Fokker-Planck equation. Therefore, the growth term should actually include both the drift- and diffusion-driven terms, and the output of a GDE-based method will not disentangle their contributions. According to Eq. (9), a significant growth by diffusion in the particle-size space requires a strong size-dependent vapor evaporation rate and particle concentration (Kontkanen *et al.*, 2022). Wang, McGraw, and Kuang (2013) suggested the importance of the GR driven by diffusion in particle-size space from volatile species for particles close to the critical size. Olenius *et al.* (2018) further proposed a method using the first- and second-order derivatives of PNSD to characterize the relative importance of diffusion-driven to drift-driven growth terms and showed its applicability using simulated NPF events. Coagulation sink decreases cluster and particle concentrations and increases the concentration gradient of particles in the size space. As a result, the relative importance of growth driven by diffusion in particle-size space is expected to increase with an increasing coagulation sink, as depicted by Olenius *et al.* (2018). Ultimately, even if the effect of growth driven by diffusion in the particle-size space might be important in the sub-3-nm range, there are currently no ambient studies that take it into account when sub-3-nm GR is compared to condensable vapors. Only when a discrete aerosol dynamics model is used for comparison is the effect automatically incorporated into the results of the model (Yao *et al.*, 2018; Kontkanen *et al.*, 2022).

### 3. Other causes of apparent growth: Transport, emissions, and variations in vapor concentration

The collective and GDE-based methods assume a homogeneous system, so the evolution of PNSD is governed by vapor condensation, coagulation, and known losses such as the wall loss. This assumption is valid for controlled laboratory experiments and homogeneous continental NPF events. For example, Wang *et al.* (2013) reported that 52 out of 207 NPF events occurred simultaneously at two sites located 120 km away from each other on the North China Plain, indicating regional NPF events. The criterion introduced by

Dal Maso *et al.* (2005) and Kulmala *et al.* (2012) can help to identify regional NPF events. Besides, the atmospheric residence time of new particles can be used to obtain hints about whether new particles are formed locally (Deng *et al.*, 2021). Nonregional NPF, such as in coastal regions or at high altitudes, is often affected by transport. The change in air mass causes a fast change in vapor concentrations and coagulation sink and hence influences particle growth (Sipilä *et al.*, 2016; Brilke *et al.*, 2020). Further, transport serves as a direct source or sink of new particles. For example, Tröstl *et al.* (2016b) showed that off-site NPF was observed on 55% of days with consistently high sub-25-nm aerosol concentrations and that these particles were observed to further grow on site on subsequent days. Cai *et al.* (2018) proposed a GDE-based method to estimate the influence of transport on the measured PNSDs and proved its importance for NPF events in a valley and on an island.

The influences of primary particle emissions are similar to transport, and they can also be characterized using GDE-based methods (Kontkanen *et al.*, 2020). The influences of transport and emissions unavoidably introduce uncertainties to growth analysis. Further, transport or emissions sometimes predominate the evolution of aerosol size distributions, especially when air masses change. Inhomogeneities in air masses can even result in an apparent shrinkage of the particle population (Hakala *et al.*, 2019). Collective or GDE-based methods may be valid to calculate an apparent GR for such cases, but the apparent GR cannot be interpreted as true particle growth. In addition, daytime atmospheric NPF events are driven mostly by photochemical reactions and are accompanied by significant variations of new particle formation rates and the concentrations of some condensing vapors such as sulfuric acid. An increasing vapor concentration delays the appearance time of particles by increasing the maximum concentration (R. Cai *et al.*, 2021a). Using cluster population simulations, Olenius *et al.* (2014) and Kontkanen *et al.* (2018) showed that the appearance time method can indeed have significant biases when the vapor monomer concentrations change. Further, the predominating nucleation mechanism may vary with the vapor concentration. Gonser *et al.* (2014) and Carracedo, Gonzalez *et al.* (2022) demonstrated that the changing diurnal relative importance of ion-induced nucleation compared to neutral pathways can result in significant differences between the appearance time GR measured from naturally charged particles and from the total particle population, especially below 3 nm.

### C. Mechanistic understanding of condensational growth

Thus far we have laid out several definitions of nanoparticle growth (Sec. II) and we have seen that the experimentally inferred GR often do not correspond directly to pure vapor condensation as it is defined in Eq. (2). While these effects are mostly limited to specific situations and size ranges, they can be significant in polluted conditions (extramodal coagulation, Sec. IV.B.1), in situations with high formation rates (self-coagulation, Sec. IV.B.1), for small sizes (growth driven by diffusion in the particle-size space, Sec. IV.B.2), or when external conditions are varying rapidly (for instance, vapor and air mass changes, Sec. IV.B.3). These aspects should at least be evaluated with respect to their importance in a specific study before conclusions on the physics and chemistry of

vapor condensation are drawn. However, the net condensation growth is still in many cases the predominant cause of the change of the peak diameter in atmospheric conditions, and hence with these difficulties in mind we can still use GR as a quantity to compare to the growth on the single-particle level. In this section, we therefore discuss the current understanding of condensational growth, i.e.,  $GR_{\text{cond}}$ , including effects such as multiphase chemistry, and we can also extend the definition to Eq. (6), including the coagulation of small clusters and particles.

We start by first discussing growth at the kinetic limit of condensation, setting the basis to discuss the nonvolatile condensation of vapors such as sulfuric acid and iodic acid that follows in Sec. IV.C.2. This is then linked to acid-base reactions (Sec. IV.C.3), which can lead to zero evaporation of even the smallest sulfuric acid–base clusters. This has dramatic consequences from a population point of view, as small clusters can become dominant growth agents (discussed in Sec. IV.C.4). We extend our analysis of the current understanding of condensational growth to more volatile vapors, where evaporation becomes important, first to semi-volatile acids (Sec. IV.C.5), second to oxygenated organics (Sec. IV.C.6), and third to their related gas- and particle-phase chemistry (Sec. IV.C.7).

#### 1. Growth at the kinetic collision limit

As pointed out in Sec. II, the growth of a single particle with negligible vapor dissociation results in a easier framework, i.e., Eq. (2), because vapor dissociation rates and hence equilibrium vapor concentration  $N_{\text{eq},i}$  are often much more difficult to assess experimentally. If we examine Eq. (2) with  $N_{\text{eq},i}(d_p) = 0$ , there are three quantities of interest if the GR of a particle of size  $d_p$  needs to be estimated: (1) the vapor molecular size  $d_i$ , (2) the vapor concentration  $N_i$ , and (3) the collision frequency  $\beta(i, p)$ . Owing to the sensitivity of the GR to the collision frequency, growth with no significant evaporation is therefore called growth at the kinetic collision limit.

##### a. Hard-sphere approximation

Vapor uptake was traditionally discussed as a collision of pointlike vapors with larger particles (Fuchs and Sutugin, 1971; Seinfeld and Pandis, 2016), which usually neglects the vapor molecular size in the collision rates (Lehtinen and Kulmala, 2003; Nieminen, Lehtinen, and Kulmala, 2010). To cover kinetic condensation, i.e., association of nonvolatile vapors, in the nucleation mode below 25 nm it is also necessary to account for the vapor size and the diffusion of particles when describing the vapor-particle collision frequency  $\beta(i, p)$ ,

$$\begin{aligned}\beta(i, p) &= 2\pi(d_i + d_p)(D_i + D_p)f(\alpha, \text{Kn}) \\ &= 2\pi(d_i + d_p)(D_i + D_p) \\ &\quad \times \frac{1 + \text{Kn}}{1 + (4/3\alpha + 0.377)\text{Kn} + (4/3\alpha)\text{Kn}^2},\end{aligned}\quad (17)$$

where  $\text{Kn} = 2\lambda/d_p$  is the Knudsen number defining the collision dynamics,  $\lambda$  is the mean free path of the vapor, and  $\alpha$  is the accommodation coefficient (often called the sticking probability) of the collision.  $D_i$  and  $D_p$  are the diffusivities of

the vapor and particle, respectively. Equation (17) uses the transition regime extension of the coagulation kernel obtained from flux-matching theory (Fuchs, 1964; Fuchs and Sutugin, 1971). In that approach, the problem of two colliding entities is solved outside of a so-called limiting sphere with the continuum approach and inside by ballistics arguments, matching the fluxes at the limiting sphere. To include the vapor molecular size correctly, Lehtinen and Kulmala (2003) adopted the Knudsen number and mean free path definition of  $\text{Kn} = 2\lambda/(d_i + d_p)$  and  $\lambda = 3(D_i + D_p)/(c_i^2 + c_p^2)^{1/2}$  including the vapor diffusivity  $D_i$  and mean molecular speed  $c_i^2$ . Nieminen, Lehtinen, and Kulmala (2010) demonstrated how these formulas can be evaluated for sulfuric acid, including hydrated monomer clusters, which requires knowledge of the condensing vapor diffusivity, molecular mass, and density, with the density usually approximated from bulk properties. Note that temperature plays only a minor role in kinetically limited growth, as the collision frequencies are rather insensitive to temperature over typical tropospheric temperature ranges. The usage of the transformation  $d_i = (6/\pi \cdot m_i/\rho_i)^{1/3}$  in the collision frequency is usually called the hard-sphere collision rate, where the vapor size is deduced from bulk properties and a spherical molecule assumption.

However, the hard-sphere assumption has clear limitations. For example, the vapor molecular size inferred from a spherical bulk property assumption cannot reproduce the vapor molecule diffusivity using the Stokes-Einstein relation for spherical particles, as shown for sulfuric acid by Hanson and Eisele (2000). Moreover, electrical mobility equivalent diameters differ from mass- and bulk-density-related equivalent diameters for sub-3-nm clusters (Larriba *et al.*, 2011). But most importantly the hard-sphere collisions entirely neglect attractive intermolecular forces between the two educts of a collision (Fuchs, 1964; Ouyang, Gopalakrishnan, and Hogan, 2012), which can lead to significantly higher collision cross sections, and hence higher condensation rates. For atmospherically relevant condensational growth, the following intermolecular forces might be important: (1) between an electrically charged molecule and an oppositely charged particle, (2) between a charged molecule and a neutral particle or vice versa, and (3) finally between neutral molecules and neutral particles through Van der Waals forces, which include permanent dipole–permanent dipole bonds, permanent dipole-induced dipole interactions, and London dispersion forces (London, 1937).

#### b. Intermolecular forces

The collision rates including intermolecular forces are usually described via an enhancement factor compared to the hard-sphere collision frequencies, which is typically distinct for the continuum and free-molecular regime (Ouyang, Gopalakrishnan, and Hogan, 2012). For the continuum regime, Fuchs (1964) connected the enhancement factor  $\eta_C$  to the interaction potential  $\phi(x)$  expressed relative to the distance  $x$  between the two centers of the colliding entities,

$$\beta(i, p) = 2\pi(d_i + d_p)(D_i + D_p)\eta_C, \quad (18)$$

$$\eta_C = \frac{2}{d_i + d_p} \left[ \int_{(d_i+d_p)/2}^{\infty} \exp\left(\frac{\phi(x)}{k_B T} x^{-2} dx\right) \right]^{-1}.$$

For the free-molecular regime, the derivation of the enhancement factor is based on kinetic arguments, and different approaches exist in order to link the enhancement factor  $\eta_{\text{FM}}$  to the interaction potential. Following conservation of energy and momentum, Fuchs and Sutugin (1965) gave a relation between the impact parameter  $b$  and the minimum distance  $x_{\text{min}}$ ,

$$b = x_{\text{min}} \sqrt{1 + \frac{2|\phi(x_{\text{min}})|}{\mu v_{\text{rel}}^2}}. \quad (19)$$

If a real value for the minimum distance with  $x_{\text{min}} > (d_i + d_p)/2$  can be found for a given set of the impact parameter  $b$ , the contact potential  $\phi$ , the relative velocity of the colliding entities  $v_{\text{rel}}$ , and the reduced mass  $\mu$ , then no collision occurs. However, if Eq. (19) yields only an imaginary solution or a real value with  $x_{\text{min}} \leq (d_i + d_p)/2$ , a collision takes place. The smallest value of  $b$  for which a noncollision is still found is therefore the critical impact parameter  $b_{\text{crit}}$ , which can be related to the free-molecular enhancement factor by comparing it to the pure geometrical collision cross section,

$$\beta(i, p) = \frac{\pi}{4} (d_i + d_p)^2 \left( \frac{8k_B T}{\pi \mu} \right)^{1/2} \eta_{\text{FM}}, \quad (20)$$

$$\eta_{\text{FM}} = 4b_{\text{crit}}^2 / (d_i + d_p)^2.$$

Fuchs and Sutugin (1965) assumed that the mean relative speed  $v_{\text{rel}} = \sqrt{3k_B T/\mu}$  holds for all collisions, reducing the problem to a simple minimization of the right-hand side of Eq. (19). Ouyang, Gopalakrishnan, and Hogan (2012) improved this by proposing a procedure to also include the Maxwell-Boltzmann distribution of speeds for both colliding entities. Other approaches in retrieving  $\eta_{\text{FM}}$  were given by Marlow (1980) and Sceats (1989). Ouyang, Gopalakrishnan, and Hogan (2012) pointed out that the aforementioned approaches differ in the free-molecular regime and that the flux-matching theory of Fuchs (1964) for the transition regime  $0.1 < \text{Kn} < 10$  might break down in the presence of strong contact potentials.

For Coulomb interactions, the free-molecular and continuum regime enhancement factors can be readily calculated if both particle and vapor are charged (Allen, 1992; Matsoukas, 1997). If one of the colliding entities is neutral, image charge needs to be considered and it leads to a more complicated contact potential (Fuchs, 1963; Adachi, Kousaka, and Okuyama, 1985). Hoppel and Frick (1986) refined this approach by also taking so-called three-body trapping, where the approaching ion might still collide with a gas molecule inside the limiting sphere, into account. López-Yglesias and Flagan (2013) further developed the Hoppel and Frick approach by including nonconductive particles and a non-negligible ion size. Gopalakrishnan and Hogan (2012) and Ouyang, Gopalakrishnan, and Hogan (2012) examined Coulomb interactions with the so-called mean first passage time method (Gopalakrishnan and Hogan, 2011), which is not based on flux-matching theory. In addition to the image-charge effect, the interaction between polar molecules and

charged particles is often relevant for the atmosphere. See Nadykto and Yu (2003) and Lushnikov and Kulmala (2004) for such calculations of the permanent dipole-charge interaction and the corresponding enhancement factors.

Last, Hamaker (1937) developed a theory to describe Van der Waals potentials, which can be converted to describe the collision enhancement factors in collisions of neutral molecules and neutral particles due to dipole-dipole interactions. Detailed derivations of the enhancement factors given by Fuchs and Sutugin (1965), Sceats (1989), and Ouyang, Gopalakrishnan, and Hogan (2012) indicated that the material-dependent Hamaker constant in the Van der Waals potential remains the free parameter of the theory. When these adjustments for ion-ion recombination, ion-dipole, and dipole-dipole interactions are included, the collision kernel frequency can be described from the free-molecular to the transition regime. In the case of a nonvolatile vapor, this collision frequency together with the vapor concentration determines the particle GR [Eq. (2)], which in that case is called growth at the kinetic limit.

Figure 6(a) examines the different contributions to the collision rate between an unhydrated sulfuric acid molecule and a growing aerosol particle for the size range of interest in this review (1–25 nm). In this range, the transition regime correction is almost negligible, which can be seen in the differences at larger diameters for both hard-sphere cases and between the solution of Sceats (1989), which includes a transition regime correction, and the approach taken by Fuchs and Sutugin (1965), where we plotted only the free-molecular collision kernel. Deviation at the smaller sizes for the two approaches including the Van der Waals forces arises entirely from the different relation of the same Hamaker constant ( $A = 5.2 \times 10^{-20}$  J) (Stolzenburg *et al.*, 2020) to the free-molecular enhancement factor  $\eta_{\text{FM}}$ . The ion-particle and vapor-charged particle interactions are calculated following López-Yglesias and Flagan (2013) and Nadykto and Yu (2003), respectively. For the latter we summed the effects of the Van der Waals forces and the dipole-charge interaction. Figure 6(b) shows the resulting GR at a concentration of  $10^7 \text{ cm}^{-3}$  sulfuric acid. The hard-sphere GR directly illustrates the important characteristic of growth at the kinetic collision limit, as postulated also in the growth laws by Brock (1972) and McMurry and Wilson (1982). As the size dependency of GR is controlled by the collision kernel [Eq. (17)],  $\text{GR}(d_p)$  is roughly constant with diameter in the free-molecular regime with  $d_p < 50$  nm but with  $d_i \ll d_p$ , i.e., in the range where the vapor molecular size is negligible ( $> 3$  nm) (Nieminen, Lehtinen, and Kulmala, 2010). In the continuum regime ( $d_p > 1 \mu\text{m}$ ), kinetic collision-limited GRs are then proportional to  $1/d_p$ . Apart from that basic diameter dependence, we see in Fig. 6(b) that intermolecular forces induce increasing GR with decreasing diameter in the free-molecular regime on top of the effect of a non-negligible vapor size. The strongest effect would be expected for ion-particle collisions due to the collision physics [Fig. 6(a)], but ion growth is typically contributing much less to the total GR due to a lower abundance of condensable ions compared to neutral vapors for most parts of the atmosphere. Therefore, polar vapor-neutral particle interaction is decisive for growth

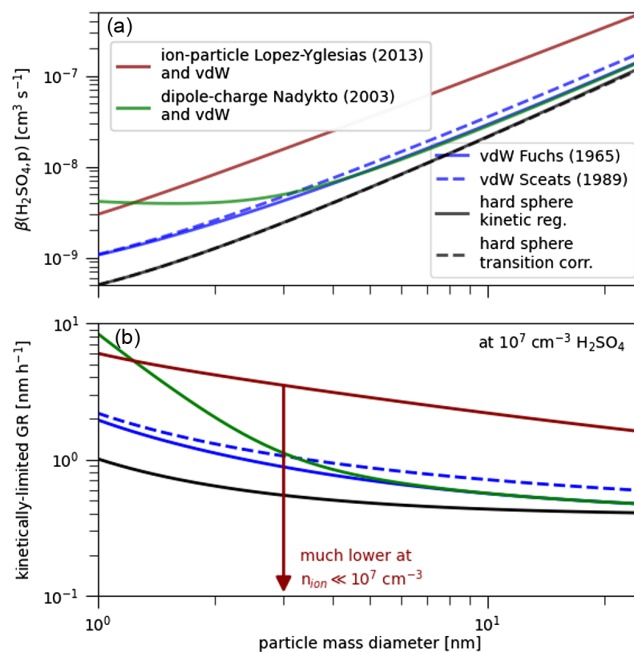


FIG. 6. (a) Collision kernel for dry  $\text{H}_2\text{SO}_4$ -particle collisions vs particle diameter for different collision physics. The baseline is the hard-sphere kernel where the collision cross section is purely geometrical, with the vapor and particle diameters inferred from the bulk density of sulfuric acid ( $1830 \text{ kg m}^{-3}$ ). It is shown for both the free-molecular regime only and the transition regime correction using flux-matching theory. Additionally, the free-molecular collision kernels including different intermolecular forces are included. Van der Waals forces using the description of Sceats (1989) and the approach of Fuchs and Sutugin (1965) and additional dipole-charge interactions in the case of a charged growing particle (Nadykto and Yu, 2003) or image-charge interaction in the case of a charged vapor molecule (López-Yglesias and Flagan, 2013). (b) Resulting size dependency for a kinetically limited GR using Eq. (2) assuming a nonvolatile vapor concentration of  $10^7 \text{ cm}^{-3}$ . Note that for the ion-particle case, such high charged vapor concentrations are typically not achieved in the lower atmosphere.

at the kinetic collision limit, as we now demonstrate for sulfuric acid.

## 2. Nonvolatile acids: Sulfuric and iodic acid

### a. Sulfuric acid

We first focus our review of vapor condensation on sulfuric acid ( $\text{H}_2\text{SO}_4$ ), which is one of the most important species in atmospheric nucleation (Dunne *et al.*, 2016) and hence is also suspected to significantly contribute to nanoparticle growth. With the help of other stabilizing species such as water, ammonia, and amines, sulfuric acid is often considered to be essentially nonvolatile for particle growth (Marti *et al.*, 1997), i.e., to have a negligible vapor pressure, meaning that evaporation rates from particles can be assumed to be zero. As we later see, this assumption might not be entirely valid for all atmospheric conditions.

Owing to the nonvolatility assumption, many studies have estimated the contribution of sulfuric acid to atmospheric nanoparticle growth using Eq. (2) from measured gas-phase

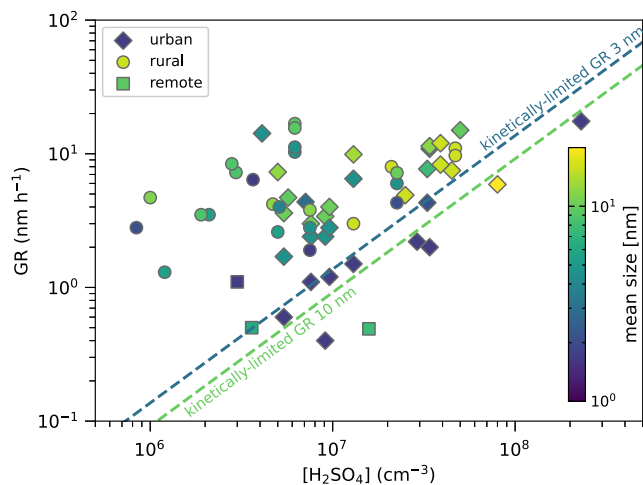


FIG. 7. Cross-study examination on the effect of  $\text{H}_2\text{SO}_4$  on particle growth. Preferentially, study median values for sulfuric acid and GRs are used when available; otherwise, study means are shown. The color code shows the geometric mean diameter of the size range for which the GR is measured. Dashed lines show the kinetic limit of sulfuric acid condensation for 3 and 10 nm according to Stolzenburg *et al.* (2020).

concentrations with  $N_{\text{eq},i} = 0$  (Boy *et al.*, 2005; Fiedler *et al.*, 2005; Yue *et al.*, 2010; Kuang, Chen, Zhao *et al.*, 2012; Jokinen *et al.*, 2018; Yao *et al.*, 2018) or estimates of gas-phase sulfuric acid (Yli-Juuti *et al.*, 2009, 2011; Young *et al.*, 2013; Vakkari *et al.*, 2015; Xiao *et al.*, 2015; Kontkanen, Järvinen *et al.*, 2016; Salma and Németh, 2019) using so-called proxy calculations (Petäjä *et al.*, 2009; Mikkonen *et al.*, 2011; Lu *et al.*, 2019; Dada *et al.*, 2020a). Some studies back-calculate the amount of sulfuric acid required to explain the observed GRs and compare this to gas-phase measurements or estimates (Weller *et al.*, 2015). Bzdek *et al.* (2012) and Bzdek, Horan *et al.* (2013) estimated the contribution of sulfuric acid based on particle-phase composition measurements assuming irreversible kinetic condensation. By comparing the particle-phase increase of sulfur of 20 nm particles to the measured gas-phase concentration of  $\text{H}_2\text{SO}_4$  during NPF, Pennington *et al.* (2013) could even conclude that sulfuric acid growth proceeds kinetically limited. However, the correlation between ambient sulfuric acid and GR measurements is weak, as shown in Fig. 7, which is in line with individual studies also finding no significant correlation between measured and estimated sulfuric acid and GR (Birmili *et al.*, 2003; Yli-Juuti *et al.*, 2011; Salma and Németh, 2019). This strongly suggests that sulfuric acid almost never dominates atmospheric nanoparticle growth alone. This is especially true for GRs at sizes larger than 5–10 nm, where only Stolzenburg *et al.* (2005) and Jokinen *et al.* (2018) measured enough gas-phase sulfuric acid to explain the observed growth. Most studies find sulfuric acid contributions to growth of < 10%–50% for sizes larger than 3 nm (Birmili *et al.*, 2003; Boy *et al.*, 2005; Fiedler *et al.*, 2005; Riipinen *et al.*, 2011; Vakkari *et al.*, 2011; Bzdek *et al.*, 2012; Mohr *et al.*, 2019; Deng *et al.*, 2020). Only in the sub-3-nm range, can sulfuric acid explain the growth entirely in a Chinese megacity (Xiao *et al.*, 2015; Yao *et al.*, 2018; Deng *et al.*, 2020). This can also

be seen in Fig. 7, where only urban observations with small median diameters of the GR measurement are close to the predicted kinetically limited GR using the collision kernels outlined in Sec. IV.C.1.

However, with respect to our analysis on kinetic condensation, note that several such estimates of the sulfuric acid contribution to the measured GR do not take into account the effect of vapor molecular size (Fiedler *et al.*, 2005; Mönkkönen *et al.*, 2005; Pennington *et al.*, 2013; Weller *et al.*, 2015), and most do not consider the enhancement due to Van der Waals forces, which has been taken into account only in recent studies by Deng *et al.* (2020), Baccarini *et al.* (2020), and Beck *et al.* (2021). Moreover, as the studies where growth can be solely attributed to sulfuric acid alone are sparse, there are no ambient observations that provide support for kinetic condensation of sulfuric acid and negligible evaporation rates.

In contrast, laboratory experiments at the CERN Cosmics Leaving Outdoor Droplets (CLOUD) experiment (Kirby *et al.*, 2011) investigated the validity of Eq. (2) with  $N_{\text{eq},i} = 0$  with respect to sulfuric acid in the sub-10-nm range (Lehtipalo *et al.*, 2016; Stolzenburg *et al.*, 2020). Stolzenburg *et al.* (2020) found that the growth of particles larger than 2 nm was indeed kinetically limited and provided an indirect measurement of the zero evaporation rates. Moreover, they measured a Van der Waals enhancement factor of 2.3–1.5 for monomer condensation on particles between 2 and 10 nm linked with a Hamaker constant of  $A = 5.2 \times 10^{-20}$  J. A similar enhancement factor of  $\eta_{\text{FM}} = 2.2$  in the free-molecular limit was also found for quantum chemical calculations of sulfuric acid monomer-monomer collisions (Halonen *et al.*, 2019) and for the growth of sulfuric acid–amine particles (Lehtipalo *et al.*, 2016). In addition, studies comparing measured nucleation rates with discrete aerosol dynamics models also found agreement including a Van der Waals free-molecular regime enhancement factor of 2 to 3 (Kürten, 2019). Measurements of the coagulation rates of larger particles and the size distribution of smog-chamber data have deduced a similar Hamaker constant for sulfuric acid particles (McMurry, 1980; Chan and Mozurkewich, 2001).

Laboratory experiments have also revealed the effect of charge on the collision rate in the sulfuric acid case. For pure sulfuric acid condensation the growth of charged particles proceeds faster due to the polar vapor-charged particle interaction (Lehtipalo *et al.*, 2016; Stolzenburg *et al.*, 2020). Charged sulfuric-acid-containing ions can also contribute significantly to the total GR, when absolute sulfuric acid concentrations are low. This is relevant in the upper troposphere (Svensmark *et al.*, 2017), where the ion fraction is high and hence the contribution via the faster ion-particle collision kernel is higher; see Fig. 6. However, for atmospheric measurements a faster GR for the ion population than for the neutral particles is not observed (Yli-Juuti *et al.*, 2011; Kulmala *et al.*, 2013), but this could be masked due to ion-ion recombination and ion attachment during the growth (Gonser *et al.*, 2014). Moreover, for ambient measurements detailed comparisons of charged and neutral GRs are lacking in the sub-3-nm range, where the charge enhancement is most important (Stolzenburg *et al.*, 2020).

### b. Iodic acid

Besides sulfuric acid, another possible candidate for atmospheric nucleation and growth is nonvolatile iodine compounds (Kulmala, 2003). Iodine species originating from biotic or abiotic emissions of inorganic iodine species [molecular iodine ( $I_2$ ) or hypoiodous acid (HOI)] or iodicarbons (mainly  $CH_3I$  and  $CH_2I_2$ ) have long been identified as precursors of coastal new particle formation (Hoffmann, O'Dowd, and Seinfeld, 2001; O'Dowd *et al.*, 2002; McFiggans *et al.*, 2004). Iodine species might be an important contributor to nanoparticle growth, as they are found in marine, polar, coastal, and even urban aerosols and clusters (Allan *et al.*, 2015; Sipilä *et al.*, 2016; Yu *et al.*, 2019; Shi *et al.*, 2021). Particle-phase measurements indicate the presence of a variety of iodine containing compounds in larger-sized aerosols (Jimenez *et al.*, 2003; Saunders and Plane, 2005), so the exact mechanism of iodine-related particle formation is strongly debated. O'Dowd *et al.* (2002), Jimenez *et al.* (2003), Saunders and Plane (2005), Saunders *et al.* (2010), and Gómez Martín *et al.* (2020) speculated on OIO and higher iodine oxides ( $I_2O_n$ ) as the drivers of the formation and growth of iodine-containing particles. However, Sipilä *et al.* (2016), Baccharini *et al.* (2020), and Beck *et al.* (2021) recently provided evidence from ambient measurements that iodic acid ( $HIO_3$ ) might be the key component initializing iodine particle formation. This was supported by the laboratory experiments of He *et al.* (2021b), who showed that two iodine oxoacids [iodous acid ( $HIO_2$ ) and iodic acid ( $HIO_3$ )] are responsible for iodine particle nucleation, while the growth is predominantly contributed by  $HIO_3$ . However, the formation mechanisms of gas-phase iodine oxoacids are still under debate: He *et al.* (2021b) observed the formation of  $HIO_2$  and  $HIO_3$  in the absence of known  $HO_x$  sources and proposed possible formation pathways involving reactions of iodine atoms and oxides with water and ozone (such as  $I + H_2O + O_3 \rightarrow HIO_3 + OH$  and  $I_2O_2 + H_2O \rightarrow HIO_2 + HOI$ ), whereas Gómez Martín *et al.* (2020) concluded that gas-phase formations of  $HIO_3$  might be too slow to explain iodine-related particle growth. While the experiments of Gómez Martín *et al.* (2020) were carried out with vapor concentrations at several orders of magnitude higher than ambient environments, the results of He *et al.* (2021b) were retrieved at similar-to-ambient vapor concentrations and could predict recent field observations (Sipilä *et al.*, 2016; Baccharini *et al.*, 2020; Beck *et al.*, 2021). A detailed formation pathway of  $HIO_3$  from IOIO intermediates (in the presence of ozone and water only) was recently given by Finkenzeller *et al.* (2023) and is in good agreement with experiments and field observations. He *et al.* (2021b) also measured small amounts of  $I_2O_5$  and  $I_2O_4$  in molecular clusters; however, they explained their occurrence by charged cluster dehydration reactions induced by the mass spectrometer, in a manner similar to Sipilä *et al.* (2016). This dehydration reaction may also occur in the particle phase, as predicted by Kumar, Saiz-Lopez, and Francisco (2018). For particles between 1.8 and 10 nm He *et al.* (2021b) suggested that  $HIO_3$  primarily drives particle growth. They found that  $HIO_3$  was the main particle-phase component measured in the growing particles and could demonstrate a closure between gas- and particle-phase  $HIO_3$ . The dominant role of  $HIO_3$  in

particle growth to CCN sizes was observed by Baccharini *et al.* (2020) in the Central Arctic, who used Eq. (2) with  $N_{eq,i} = 0$  in order to estimate the irreversible GR from iodic acid condensation and found good agreement with the measured GR for several NPF events. As iodic acid is a polar molecule, collision enhancements due to Van der Waals forces and ion-vapor interactions were considered by Baccharini *et al.* (2020), but they assumed the same Hamaker constant as for sulfuric acid, as a direct measurement is currently still missing. He *et al.* (2021a, 2021b) further quantified the collision rates of neutral iodic acid molecules with charged clusters and found reasonable agreement with the so-called surface charge capture theory (Kummerlöwe and Beyer, 2005). Overall He *et al.* (2021a, 2021b) concluded that the ion-induced nucleation pathway of  $HIO_3$  proceeds at the kinetic limit. Hence, it is also reasonable to assume that the growth of neutral particles above the initial cluster sizes proceeds in a kinetically limited fashion, as charge is typically needed only for the stabilization of the initial clusters, as seen in the sulfuric acid system.

### c. Hygroscopicity effects

Besides both being polar molecules, there are substantial differences between sulfuric and iodic acid when it comes to their hygroscopic behavior. While sulfuric acid is highly hygroscopic (Biskos, Buseck, and Martin, 2009; Kim *et al.*, 2016; Lei *et al.*, 2020), hygroscopic growth factors for iodine species are significantly lower (Jimenez *et al.*, 2003; Murray *et al.*, 2012). Nevertheless, water plays a decisive role in iodine chemistry, which needs to be considered when more complex iodine growth mechanisms for situations with high and low relative humidity are discussed (Saunders *et al.*, 2010). On the other hand, when growth by sulfuric acid is studied, the effects of water and relative humidity need to be directly taken into account, as hygroscopic growth always accompanies sulfuric acid uptake. The distribution of  $(H_2SO_4)-(H_2O)_n$  clusters was studied theoretically with classical thermodynamics (Wexler and Clegg, 2002) and with quantum chemistry models (Kurtén *et al.*, 2007; Temelso *et al.*, 2012). The latter show significant hydration ( $n = 1-2$ ) of sulfuric acid monomers at moderate relative humidity (RH) between 20% and 80% and temperatures from 220 to 300 K. Henschel *et al.* (2014) extended those calculations to larger molecular clusters of sulfuric acid. Detailed investigations on the role of water in growth are lacking and, as pointed out in Sec. III.A, there is often a discrepancy between GRs reported above 10 nm (from dry size-distribution measurements) and below 10 nm (mostly from wet size-distribution measurements). Skrabalova *et al.* (2014) did not find a consistent enhancement of the GR in flow tube experiments but found that it varies with the sulfuric acid concentration used. Stolzenburg *et al.* (2020) showed that water already plays an important role in sulfuric acid growth at  $RH < 40\%$ , which is the threshold value for most size-distribution measurements. Verheggen and Mozurkewich (2002) developed a theoretical description of combined sulfuric acid and water uptake and concluded from this combined estimate that their approximated sulfuric acid concentrations were significantly overestimated. However, the aqueous phase of the growing

particles can still be extremely important for most heterogeneous or multiphase particle-phase reactions. This is especially true in the context of acid-base interactions, where the dissolution of the condensing compounds into molecular ions and the subsequent salt formation alter the chemical equilibria between the gas and particle phases, as discussed in Sec. IV.C.3.

### 3. Acid-base interactions: Sulfuric acid with ammonia and amines

Highly linked to sulfuric acid is the role of acid-base interactions in atmospheric nanoparticle growth. Nitrogen-containing bases such as ammonia and amines are abundant at many different locations. For example, ammonia levels often reach ppb levels in the continental boundary layer (Backes *et al.*, 2016). Globally, ammonia and amines are produced mainly in agricultural processes from livestock (Schade and Crutzen, 1995; Sintermann *et al.*, 2014) and fertilizers (Erisman *et al.*, 2008), and their emissions are expected to further rise on a global scale in the future (Galloway *et al.*, 2004).

#### a. Equilibrium thermodynamics

Acid-base interactions are a fundamental part of aerosol particle-phase chemistry (Clegg, Brimblecombe, and Wexler, 1998; Finlayson-Pitts and Pitts, 2000). Typically, aerosol acid-base chemistry is treated in the framework of equilibrium thermodynamics, where equilibrium is assumed between the gas and particle phases (Seinfeld and Pandis, 2016). Thermodynamic equilibria are also calculated for subsequent reactions of acids and bases inside the aerosol aqueous phase, i.e., dissociation and salt formation. The formation of effectively nonvolatile ammonium sulfate and semivolatile ammonium nitrate salts leads to reduced evaporation rates of both acids (sulfuric acid and nitric acid) and bases (ammonia). While sulfuric acid is almost nonvolatile by itself (Marti *et al.*, 1997; Stolzenburg *et al.*, 2020), the acid-base effect is especially important for reactive uptake of volatile or semivolatile species such as ammonia or nitric acid. Many equilibrium thermodynamic models exist to predict the composition of inorganic aerosols under different temperature, relative humidity, and precursor concentrations (Nenes, Pandis, and Pilinis, 1998; Wexler and Clegg, 2002). Semeniuk and Dastoor (2020) provided a recent overview of equilibrium thermodynamic aerosol models and Pye *et al.* (2020) put some of them into the context of available measurements. A review on aerosol phase-transition chemistry was given by Martin (2000). For the most atmospherically relevant inorganic system of H<sub>2</sub>O, H<sub>2</sub>SO<sub>4</sub>, HNO<sub>3</sub>, and NH<sub>3</sub>, thermodynamic equilibrium models predict that neutralization of sulfuric acid by ammonia occurs predominantly until a molar ratio  $n_{\text{NH}_3}/n_{\text{H}_2\text{SO}_4} = 2$  is achieved and all sulfur is contained as ammonium sulfate. Only if ammonia is in excess after full neutralization of sulfuric acid can nitric acid together with ammonia condense to the particle phase (Finlayson-Pitts and Pitts, 2000).

Underlying all models is the equilibrium assumption (Mai *et al.*, 2015), which, at least for the atmospheric bases, is often justified, as the relevant timescales for equilibration of bases

are much smaller than the timescales of kinetic condensation of acids due to the higher vapor pressures and diffusivities. This is especially true for sulfuric acid, the dominant acid for the nucleation mode (Wexler and Seinfeld, 1990; Yli-Juuti *et al.*, 2013). Besides this significant difference in equilibration timescales, equilibrium thermodynamics predict the gas-particle-phase partitioning to scale with preexisting aerosol mass, which favors accumulation or coarse mode uptake. However, condensation in the nucleation mode is a dynamic process in which pure equilibrium considerations might not be sufficient.

#### b. Ammonia

Progressing from the smallest molecular clusters onward, bases can enhance particle nucleation rates from acids by several orders of magnitude (Kirkby *et al.*, 2011; Chen *et al.*, 2012; Almeida *et al.*, 2013; Jen, McMurry, and Hanson, 2014; Kürten *et al.*, 2014; Glasoe *et al.*, 2015). This acid-base stabilization is effectively reducing the evaporation rates of sulfuric acid and hence also increases particle GRs. Lehtipalo *et al.* (2016) demonstrated that for sub-2-nm particles the presence of ppt-level ammonia is lowering sulfuric acid evaporation rates such that sulfuric acid condensation can be regarded as an irreversible process. This is in line with a model describing acid-base growth using the equilibrium assumption for ammonia but condensation kinetics for acids (Yli-Juuti *et al.*, 2013), where mass fractions below 10% for ammonia are found in sub-25-nm nucleation mode particles. In addition, Smith *et al.* (2010) and Pennington *et al.* (2013) did not find more than 20% ammonia in mass fraction in 10–30 nm-sized freshly nucleated particles. Apart from the low mass contribution of ammonia due to its minor molecular mass, two studies exposing sulfuric acid particles to ammonia vapors found a negligible (25%–75% RH) (Zhang *et al.*, 2009) or minor (5% RH) (Biskos, Buseck, and Martin, 2009) diameter increase due to neutralization by ammonia, which was speculated to originate from the replacement of water by ammonia in the acidic particles, reducing the net growth effect due to base addition.

Apart from water replacement by ammonia, Pennington *et al.* (2013) also found a molar ammonia-to-sulfate ratio under 2 for nucleation mode particles, indicating that the growing particles are not fully neutralized, as predicted from thermodynamic equilibria considerations when ammonia is in excess of sulfuric acid. Studies focusing on molecular cluster growth came to the same conclusion, namely, that full neutralization of sulfuric acid is not achieved in the initial steps of NPF (Kirkby *et al.*, 2011; Froyd and Lovejoy, 2012; Bzdek, DePalma *et al.*, 2013; Schobesberger *et al.*, 2013) and that neutralization starts to slowly increase only from 2 nm on (Schobesberger *et al.*, 2013). This suggests that classical thermodynamic equilibrium assumptions are not valid in the cluster-particle transition regime below 10 nm, but that NH<sub>3</sub> exhibits an energy barrier for additions to a H<sub>2</sub>SO<sub>4</sub> cluster.

These observations are supported by quantum chemical calculations predicting that, in H<sub>2</sub>SO<sub>4</sub>-NH<sub>3</sub>-driven particle formation, there are thermodynamic energy barriers and most stable clusters (up to clusters with four to five acid and four to five base molecules) have close to a one-to-one ratio of H<sub>2</sub>SO<sub>4</sub>

and  $\text{NH}_3$  molecules (Olenius *et al.*, 2013, 2017; Myllys, Kubečka *et al.*, 2019). Quantum chemical calculations also suggest that  $\text{H}_2\text{SO}_4\text{-NH}_3$  clusters contain fewer water molecules than pure  $\text{H}_2\text{SO}_4$  clusters (Henschel *et al.*, 2014), which can be explained by the “neutralizing” effect of  $\text{NH}_3$ . However, based on these calculations, clusters with an equal number of  $\text{H}_2\text{SO}_4$  and  $\text{NH}_3$  molecules acquire more water than those with one excess molecule of  $\text{H}_2\text{SO}_4$ , while according to classical thermodynamics these clusters contain little to no water (Henschel *et al.*, 2014).

### c. Amines

Compared to ammonia, amines are stronger bases (Qiu and Zhang, 2013), but emissions are 2 to 3 and ambient concentrations mostly 1 to 2 orders of magnitudes smaller (Schade and Crutzen, 1995; Ge, Wexler, and Clegg, 2011). Amines [specifically dimethylamine ( $\text{C}_2\text{H}_7\text{N}$ )] can enhance sulfuric acid NPF rates by 4 to 5 orders of magnitude compared to the system of sulfuric acid plus ammonia (Almeida *et al.*, 2013). Therefore, it might be the key component for new particle formation in heavily polluted environments (Yao *et al.*, 2018; Xiao *et al.*, 2021) but can also contribute to NPF in clean environments such as Antarctica (Brean *et al.*, 2021).

Kürten *et al.* (2014) showed that the growth in the sulfuric acid–dimethylamine system proceeds again at an acid–base molar ratio of 1 : 1 for the initial clusters. This is also supported by quantum chemical calculations (Myllys, Kubečka *et al.*, 2019) and cluster kinetics simulations using the quantum chemical data that showed that the initial growth occurs by additions of a cluster involving one  $\text{H}_2\text{SO}_4$ , one DMA, and any number of water molecules (Olenius *et al.*, 2017). Observations suggested that the acid–base molar ratio starts to increase for clusters larger than seven acid and six base molecules (Almeida *et al.*, 2013), indicating a higher degree of acid neutralization at larger sizes. However, Ahlm *et al.* (2016) showed that full neutralization, i.e., complete aminium sulfate formation in the particle phase, is not achieved up to sizes from 10 to 30 nm, which is similar to sulfuric acid and ammonia and unlike thermodynamic equilibrium predictions.

Jen, McMurry, and Hanson (2014), Glasoe *et al.* (2015), and Yu, McGraw, and Lee (2012) investigated the effects of alkyl amines other than dimethylamine and found that with increasing basicity from  $\text{NH}_3$  to methylamine to dimethylamine or trimethylamine the enhancement of the nucleation rate increases. Cluster kinetics simulations using quantum chemical data support these observations (Olenius *et al.*, 2017). The conclusions about growth, however, remain ambiguous: owing to the larger mass of amines compared to ammonia, the acid–base growth could also proceed at a significantly faster GR than pure sulfuric acid or sulfuric acid plus ammonia. This was found by Yu, McGraw, and Lee (2012); however, Glasoe *et al.* (2015) reported the opposite for lower and more atmospherically relevant dimethylamine concentrations. Wang *et al.* (2010, 2011) also found a significant uptake of amines in tandem-DMA experiments, where sulfuric acid particles were exposed to trimethylamine vapor with growth factors of 1.1–1.2 for particles in the 4–20 nm range. In addition, Smith *et al.* (2010) reported evidence of a significant contribution of different amines to

10–30 nm particle composition, and increasing importance in urban environments. Last, several studies have investigated the interplay between amines and ammonia in cluster formation and growth, finding evidence for base displacement and enhancing effects in the presence of several bases, where the dominance of dimethylamine and trimethylamine over ammonia decreases with increasing particle size (Bzdek, DePalma, and Johnston, 2017; Myllys, Chee *et al.*, 2019), but the exact contribution (especially to growth) remains unquantified.

### 4. Contribution of clusters to particle growth

Besides their direct condensational contribution to growth, amines can also enhance the amount of condensable molecular clusters in the atmosphere. In addition to vapor condensation, the coagulation between a molecular cluster and a particle or cluster may sometimes enhance particle growth and is therefore included in our definition of single-particle growth in Eq. (6). To achieve a GR comparable to that contributed by nonvolatile vapors, cluster concentrations need to be high. As a result, clusters formed with nucleation rate well below the kinetic limit, for instance, via sulfuric acid and ammonia nucleation, are not expected to contribute significantly to the growth (Stolzenburg *et al.*, 2020).

In contrast, the initial cluster formation of sulfuric acid and dimethylamine already proceeds at the kinetic collision limit (Kürten *et al.*, 2014; Kürten, 2019). This means that the presence of dimethylamine (> 20 ppt) reduces the evaporation rates of sulfuric acid particles to a negligible value from the monomer onward, and hence nanoparticle growth will also be entirely kinetically limited. Lehtipalo *et al.* (2016) showed in laboratory measurements that cluster–cluster collisions are therefore a significant driver of growth in the presence of dimethylamine and sulfuric acid. In such systems significant amounts of condensable material are contained in the first molecular clusters “hidden” from the vapor measurement but contributing to growth, as shown by discrete and discrete-sectional aerosol dynamics models (Kontkanen, Olenius *et al.*, 2016; Li and McMurry, 2018; Kontkanen *et al.*, 2022). This results in GRs above the potential kinetic collision limit of vapor monomer condensation. Sulfuric acid–amine nucleation is reported to be a governing NPF mechanism in megacities (Yao *et al.*, 2018; Cai *et al.*, 2022), and hence cluster growth is expected to be most important in polluted environments. However, although sulfuric acid–amine clusters evaporate negligibly compared to their formation and GRs (Kürten *et al.*, 2018), the clusters are quickly scavenged in the presence of the high coagulation sink in polluted environments. For example, sulfuric acid dimer concentrations in urban Beijing are 1 order of magnitude lower than concentrations of monomers (R. Cai *et al.*, 2021b; Yan *et al.*, 2021), and hence the dimers contribute little to the particle growth. Lehtipalo *et al.* (2016) and Yao *et al.* (2018) compared observed particle GRs to GRs derived from one-component cluster kinetics simulations while assuming no evaporation. In the chamber experiment, simulated sub-3-nm particle GRs matched well with the observed ones when a collision enhancement factor of 2.3 is assumed (Lehtipalo *et al.*, 2016). In the polluted atmosphere, however, the median

GR for sub-3-nm particles was lower than that based on model simulations (Yao *et al.*, 2018).

Apart from the sulfuric acid–amine system, He *et al.* (2021b) found that at  $-10^{\circ}\text{C}$  the growth of iodine oxoacid particles exceeds the kinetic limit for  $\text{HIO}_3$  particles due to the contribution from  $\text{HIO}_3$  clusters. Studies utilizing cluster population simulations also show a high contribution of cluster-cluster collisions to particle growth at high vapor saturation ratios (Kontkanen, Olenius *et al.*, 2016; Kontkanen *et al.*, 2018).

Summarizing these findings, we conclude that, for non-volatile vapor condensation, a significant contribution from clusters to particle growth requires both negligible cluster evaporation and low sink so that the cluster concentrations are sufficiently high compared to vapor concentrations. Besides laboratory environments (Lehtipalo *et al.*, 2016), such a mechanism may be important in clean and cold environments such as coastal regions (Sipilä *et al.*, 2016) and the upper troposphere, where the evaporation of semistable clusters are suppressed. Baccarini *et al.* (2020) reported that during NPF events over high Arctic pack ice the concentrations of iodic acid dimers and trimers are of the same order of magnitude as monomers; hence, contributions from iodic cluster to GR are anticipated. For the scenario in which condensation is dominated by semivolatile vapors, clustering might be weaker; however, the clusters are expected to have lower vapor pressures than the monomers, which could enhance their importance in growth. Peroxy radicals ( $\text{RO}_2$ ) during the autoxidation of VOCs can rapidly form dimers upon collision with each other (ROOR) (Ehn *et al.*, 2014) and the volatility of these dimers is lower than that of the corresponding monomers (Kirkby *et al.*, 2016; Stolzenburg *et al.*, 2018). Considering that organics containing  $\leq 10$  carbon atoms may not be of extremely low volatility (Kurtén *et al.*, 2016), the dimers are important during the initial growth of clusters (Lehtipalo *et al.*, 2018). However, the formation of these dimers in polluted environments with high  $\text{NO}_x$  concentrations is suppressed as the termination reactions with  $\text{NO}_x$  compete with the autoxidation process, resulting in less dimer but more organic nitrate monomer formation (Yan *et al.*, 2020, 2021; Li *et al.*, 2022).

## 5. Other acids: Nitric acid, methanesulfonic acid, and organic acids

### a. Nitric acid

Besides the importance of available bases in nanoparticle growth, acids other than sulfuric acid need to be considered. However, most atmospheric acids have significantly higher vapor pressures than sulfuric acid, and hence their role in initial nanoparticle growth has not been clearly identified. Nitric acid is often several orders of magnitude more abundant than sulfuric acid. Nitric acid and ammonia are thought to be semivolatile with respect to particulate ammonium nitrate (Takahama *et al.*, 2004). This means that its equilibration timescale is short, and gas-particle equilibrium is rapidly reached when ammonia or nitric acid concentrations or temperature change. However, it is the excess concentration  $N_i - N_{\text{eq},i}(d_p)$  that is the driving force of condensation and, if high supersaturation with respect to ammonium nitrate is

achieved rapidly, this can induce ammonia and nitric acid condensation in the smallest aerosol particles, overcoming the Kelvin barrier (Wang *et al.*, 2020b). The activation of nanometer-sized particles to growth by ammonium nitrate can be captured by a monodisperse thermodynamic model as well as a nano-Köhler theory (Kulmala, Kerminen *et al.*, 2004), based on the thermodynamic equilibrium among nitric acid, ammonia, and ammonium sulfate seed particles (Wang *et al.*, 2020b). In the case of high concentrations of nitric acid and ammonia, which are sometimes found in the polluted troposphere, this process might be extremely rapid, causing GRs of up to several hundred  $\text{nm h}^{-1}$ . However, such high GRs are typically not observed. Localized emissions and temperature changes in urban turbulence might cause this high supersaturation to promote particle growth through the critical sub-10-nm range, which explains the occurrence of NPF in polluted megacities (Kulmala *et al.*, 2017; Wang *et al.*, 2020b; Marten *et al.*, 2022), but it could be masked by typical averaging GR analysis methods and the limited temporal resolution (several minutes) of aerosol size spectrometers. However, note that significant amounts of ammonium nitrate are typically not found in nucleation mode particle composition measurements in polluted megacities (Li *et al.*, 2021). Wang *et al.* (2020b) further showed in chamber experiments that ammonium nitrate can even lead to the nucleation of new particles at low temperatures, such as in the upper troposphere. The possible role of nitric acid and ammonia in particle growth at elevated altitudes hence needs to be studied in the future.

### b. Methanesulfonic acid

In contrast to nitric acid, which by itself has a high vapor pressure, the vapor pressure of methanesulfonic acid [(MSA);  $\text{CH}_4\text{O}_3\text{S}$ ] is not well quantified (Hodshire *et al.*, 2019). MSA is measured in significant quantities in marine and coastal regions, as it is produced by the oxidation of dimethylsulfide [(DMS);  $\text{C}_2\text{H}_6\text{S}$ ] (Shen *et al.*, 2022), which is typically released by phytoplankton (Keller, 1989; Lana *et al.*, 2011). DMS is also a precursor of  $\text{SO}_2$  and hence  $\text{H}_2\text{SO}_4$ , but oxidation of DMS is the only known source of gaseous MSA in the atmosphere. The particulate  $\text{MSA}/\text{nns-SO}_4^{2-}$  (non-sea-salt-sulfate) ratio is hence often used to characterize the sources of particulate sulfate.

MSA is found in the particle phase in polar environments (Kerminen *et al.*, 1997), over the open ocean (Huang *et al.*, 2017), in the maritime free troposphere (Froyd *et al.*, 2009), at urban sites with an influence of maritime air masses (Gaston *et al.*, 2010), at coastal sites in the Mediterranean (Bardouki *et al.*, 2003; Mansour *et al.*, 2020), and at midlatitudes (Ovadnevaite *et al.*, 2014). Ayers and Gras (1991) hypothesized that MSA can promote particle growth to CCN sizes due to a strong correlation in the annual CCN and particulate methanesulfonate (MSA) cycles. Heintzenberg and Leck (1994) found a correlation of fine particle number concentrations with particulate MSA concentrations. Dall’Osto *et al.* (2018) and Beck *et al.* (2021) found high gaseous MSA concentrations occurring during new particle formation. Brean *et al.* (2021) explained the observed GRs in Antarctica and over the open ocean by a combination of sulfuric acid, iodic

acid, and MSA, but the MSA contribution is minor. In contrast, Beck *et al.* (2021) concluded that MSA has played a significant role in new particle growth in the Svalbard archipelago in the Arctic Ocean. This is similar to the discoveries of Willis *et al.* (2016), who found high particulate MSA of 80 nm particles during particle growth events in northern Canada, speculating that MSA could also be a major driver of the growth of small particles. In air masses transported rapidly from the open ocean to Hyytiälä, Finland, Lawler *et al.* (2018) observed MSA in both Aitken-mode particles and the gas phase during some of the NPF events. In contrast, Berresheim *et al.* (2002) found an anticorrelation of ambient RH and particulate MSA, concluding that MSA quickly equilibrates with preexisting aerosol; i.e., MSA would be semivolatile and not able to condense onto the smallest particles.

Kerminen *et al.* (1997) found higher MSA/nns-SO<sub>4</sub><sup>2-</sup> ratios (0.15–0.4) for Aitken-mode measurements than for typical accumulation mode particles (0–0.1) (Kreidenweis *et al.*, 1991; Chen *et al.*, 2012). In addition, Willis *et al.* (2016) found a higher MSA/nns-SO<sub>4</sub><sup>2-</sup> ratio (0.15) during the particle growth period, and both results potentially indicate that MSA is a stronger driver of growth than sulfuric acid. However, Hoppel (1987) and Kreidenweis *et al.* (1991) had previously pointed out that this ratio depends on the branching between DMS oxidation to MSA and SO<sub>2</sub> and furthermore is influenced by long-range transport of anthropogenic sulfates, aqueous-phase-promoted production of sulfates (Chen *et al.*, 2012), or high relative humidity and NO<sub>x</sub> levels promoting the formation of MSA (Van Rooy *et al.*, 2021). Furthermore, measurements of that ratio are typically dominated by the bulk aerosol and hence not indicative of any significant nucleation mode uptake.

Altogether these observations point toward an important role of MSA in newly formed aerosol particle growth in marine regions. This was hypothesized by Hoppel (1987), who estimated the vapor pressure of MSA and concluded that typical gaseous MSA concentrations might reach supersaturation to condense onto small particles while not being high enough to induce significant nucleation. Rosati *et al.* (2021) directly studied the growth of new particles from DMS oxidation in the presence of trace amounts of ammonia and found a dominant contribution of MSA in the particle phase, with MSA/SO<sub>4</sub><sup>2-</sup> ratios well above 1. This is also in line with recent laboratory studies that suggest that the presence of bases could be crucial in promoting nucleation of MSA, especially amines such as trimethylamine or dimethylamine (Dawson *et al.*, 2012; Chen *et al.*, 2016). Furthermore, the MSA-base systems are highly sensitive to relative humidity (Chen *et al.*, 2016). High RH promotes nucleation of all MSA-base combinations but increases particle growth only for MSA-methylamine and MSA-NH<sub>3</sub>, whereas MSA-dimethylamine and MSA-trimethylamine growth was not affected. Furthermore, while the MSA-methylamine system reached the highest formation rates, they found the highest GR for MSA-dimethylamine and MSA-trimethylamine systems and speculated that this might be due to their higher molecular mass, higher hygroscopicity, and lower formation rates rapidly consuming all condensable material. The behavior of

MSA-methylamine and MSA-dimethylamine systems is also different than the case of sulfuric acid, which is explained by structural effects and steric hindrance in initial cluster growth of the MSA-DMA system, which outweighs the higher basicity (Shen *et al.*, 2020). Particle-phase composition measurements down to 5 nm for MSA-methylamine and MSA-methylamine-ammonia flow tube experiments (similar to those for sulfuric acid) confirmed a higher acidity of smaller particles, and full neutralization reached only above 10 nm (Perraud *et al.*, 2020). These measurements also confirmed the dominant role of methylamine in the MSA system, finding a much higher molar ratio of methylamine to ammonia in the particle phase than in the gas phase.

### *c. Small organic acids*

Like MSA, organic acids are speculated to have rather semivolatile vapor pressures (Zhang and Wexler, 2002; Donahue *et al.*, 2011). Like nitric acid, organic acids are globally abundant in the atmosphere and range from simple and low molecular weight monocarboxylic alkanic acids to dicarboxylic acids, aromatic acids, and higher molecular weight acids such as pinic, cis-pinonic acid, and 3-methyl-1,2,3-butanetricarboxylic acid, which are monoterpene oxidation products. Monocarboxylic acids such as formic acid (HCOOH) and acetic acid (CH<sub>3</sub>COOH) form a significant portion of atmospheric nonmethane hydrocarbons (Khare *et al.*, 1999) and, besides primary emissions from biomass burning, biofuels, fossil fuels, soil, and vegetation, they are formed predominantly from isoprene oxidation; i.e., they often have a biogenic origin (Paulot *et al.*, 2011). Longer chain alkanic acids can also have marine biogeochemical sources (Tervahattu, Juhanoja, and Kupiainen, 2002) or can be emitted from tree waxes (Beri and Lemon, 1970). Dicarboxylic acids, with the most abundant oxalic acid (C<sub>2</sub>H<sub>2</sub>O<sub>4</sub>), malonic acid (C<sub>3</sub>H<sub>4</sub>O<sub>4</sub>), and succinic acid (C<sub>4</sub>H<sub>6</sub>O<sub>4</sub>), have sources similar to monoacids (Kawamura and Bikkina, 2016) and are found in large quantities in polluted environments (Ho *et al.*, 2007). Aromatic acids are also often related to anthropogenic emissions and the photochemical degradation of aromatic hydrocarbons (Forstner, Flagan, and Seinfeld, 1997; Suh *et al.*, 2003), while the often-studied pinic and cis-pinonic acids originate from monoterpene oxidation and are hence attributed to biogenic VOC emissions (Yu *et al.*, 1999).

Organic acids could contribute to atmospheric nucleation via acid-base interactions (Xu and Zhang, 2013; Lin *et al.*, 2019) or could even enhance sulfuric acid–(ammonia)–water nucleation through strong double hydrogen bonding in the initial clusters (Nadykto and Yu, 2007; Zhao *et al.*, 2009; Elm, Myllys, and Kurtén, 2017). Quantum chemical simulations suggest that the presence of perfluorocarboxylic acids provides additional cluster formation routes in H<sub>2</sub>SO<sub>4</sub>–DMA nucleation resulting in higher nucleation rates through faster initial cluster growth, and such clusters have actually been found in megacities during NPF (Lu *et al.*, 2020). Laboratory experiments have verified the enhancement of sulfuric acid nucleation for aromatic acids (Zhang *et al.*, 2004) and have also demonstrated the effect in a MSA–methylamine–oxalic acid system (Arquero, Benny Gerber, and Finlayson-Pitts,

2017). Recent ambient measurements demonstrated that in the presence of diacids even higher nucleation rates than those in the sulfuric acid–amine system are found in rural polluted environments (Fang *et al.*, 2020). While ambient observations of the contribution of small organic acids to nucleation are limited, even more important might be the contribution of low molecular weight acids to nanoparticle growth (Zhang *et al.*, 2012). However, Zhang and Wexler (2002) speculated that, due to the observed anticorrelation of the strength of the Kelvin barrier and the overall vapor pressure, most organic molecules will not have a low enough vapor pressure to overcome the Kelvin barrier and participate in 1 to 2 nm particle growth. This is in line with the observations of Zhang *et al.* (2009), who found no organic acids in grown particles of a few nanometers in laboratory experiments. However, Zhang *et al.* (2009) also showed that the addition of a single cis-pinonic acid molecule to the smallest sulfuric acid clusters can contribute to nucleation through double-hydrogen-bond stabilization. Therefore, while organic acids influence small cluster stability and can possibly also enhance dipole-dipole interactions for further sulfuric acid–water addition, they do not seem to contribute directly to growth without further heterogeneous reactions in the particle phase, effectively lowering the volatility of these compounds (Zhang and Wexler, 2002). Like the aforementioned acids, acid-base chemistry could be such a driver of growth by small organic acids (Barsanti, McMurry, and Smith, 2009), but other mechanisms such as polymerization (Zhang and Wexler, 2002; Limbeck, Kulmala, and Puxbaum, 2003) and reactions with particulate sulfuric acid (Zhang and Wexler, 2002) have also been debated, although they are thought to be more important for larger particles (Riipinen *et al.*, 2012; Yli-Juuti *et al.*, 2013).

Low molecular weight organic acids are found in ambient particle-phase measurements, especially in sub-50-nm samples (Laitinen *et al.*, 2011). Smith *et al.* (2008, 2010) measured significant fractions of low molecular weight organic acids in growing 10–30 nm particles in Tecamac, Mexico, and Hyytiälä, Finland. Smith *et al.* (2010) simultaneously reported significant signals from amines and elevated hygroscopic growth factors, which were interpreted as a strong indication of organic acid-aminium salt formation during new particle growth, explaining 47% of the observed GR in Tecamac and 23% of the observed GR in Hyytiälä. In contrast to this, a process model based on thermodynamic equilibrium assumptions as well as condensation kinetics revealed that the vapor pressure of such organic acids must be much lower than typically observed in order to explain the contribution to growth via salt formation for conditions at Hyytiälä (Yli-Juuti *et al.*, 2013). This study also found a steep dependence of the organic acid partitioning on the available amine, ammonia, and humidity, indicating that organic salt formation could be more important in polluted and humid environments. Overall, Yli-Juuti *et al.* (2013) suggested that there must be other mechanistic pathways in order to explain the widespread observations that organics play a major role in atmospheric nanoparticle growth, which was also the conclusion of Lawler *et al.* (2018), who performed measurements similar to those of Smith *et al.* (2010) in Hyytiälä and again found a high fraction of organic acids, but also an increased

contribution of terpenoid oxidation products. The latter oxygenated organic molecules (OOMs) are suspected to contribute via reversible condensation, similar to sulfuric acid. However, the wide variety of oxidation products and the range of several orders of magnitude of possible vapor pressures of these compounds calls for a different theoretical framework of reversible condensation than in the kinetically limited growth scheme presented in Sec. IV.C.1. We address this in Sec. IV.C.6.

## 6. Reversible condensation of oxidized organics: Semivolatile partitioning and low-volatility growth

Gas-phase oxidation of VOCs produces a variety of oxygenated organics that can possibly condense onto particles. VOCs can have biogenic and anthropogenic sources and are abundant in the atmosphere (Kansal, 2009). Isoprene and other terpenes are the most dominant nonmethane organic compound globally (Guenther *et al.*, 2012), but locally anthropogenic sources and biomass burning can also be significant (Van Marle *et al.*, 2017; Hoesly *et al.*, 2018). Oxidation of VOCs can be induced by atmospheric oxidants such as O<sub>3</sub>, OH, and NO<sub>x</sub>. We focus here on VOC oxidation products and their properties and possible contribution to nanoparticle growth, while we later show that the formation chemistry affects the growth potential significantly.

### a. Kinetic condensation versus thermodynamic equilibrium

VOC oxidation products have long been known to contribute to secondary organic aerosol (SOA) mass formation (Jimenez *et al.*, 2003; Hallquist *et al.*, 2009). However, as previously pointed out, the Kelvin barrier for most organic species potentially suppresses their condensation onto nucleation mode particles (Zhang and Wexler, 2002). This means that for many organic compounds the driving force of condensation  $N_i - N_{i,\text{eq}}$  will be close to zero, requiring an application of Eq. (2) in order to describe reversible condensation onto nucleation mode particles. In contrast, SOA formation in smog-chamber experiments and some models is treated under partitioning theory, which is based on the work from Pankow (1994) and Odum *et al.* (1996) and assumes thermodynamic equilibrium between the gas and particle phases, where species can also be found in the particle phase at subsaturation. The partitioning mass fraction found in the particle phase  $F_i = C_{i,p}/C_{i,t}$  of an organic compound  $i$  with total mass concentration  $C_i = C_{i,p} + C_{i,g}$  can be described by

$$F_i = \left(1 + \frac{C_i^*}{C_{\text{OA}}}\right)^{-1}, \quad \text{with } C_{\text{OA}} = \sum_i F_i C_{i,t}. \quad (21)$$

$C_{\text{OA}}$  is the total organic aerosol (OA) mass concentration and  $C_i^*$  is the effective saturation mass concentration of the compound, which can be related to its vapor pressure and particle-phase activity and can be used like the equilibrium constant (Donahue *et al.*, 2006). Equation (21) was originally designed for organic aerosols only but can be extended to inorganic-organic mixtures if it is assumed that they form the same phase (Kulmala, Kerminen *et al.*, 2004; Yli-Juuti *et al.*, 2013; Mohr *et al.*, 2019). The direct consequence of the

partitioning relation in Eq. (21) is that, for a species with saturation mass concentration  $C_i^*$ , any additional increase in the total organic mass loading  $C_{OA}$  will lead to an increase of species  $i$  in the particle phase. In other words, 50% of the mass of compound  $i$  resides in the particle phase and 50% in the gas phase whenever the total aerosol mass loading  $C_{OA}$  is identical to the effective saturation mass concentration  $C_i^*$  of that compound. Furthermore, for  $C_i^* \ll C_{OA}$  the compound will reside almost entirely in the particle phase. This leads to the conclusion that at high organic aerosol mass loading more volatile products can reside in the particle phase.

Several chamber experiments have elucidated the role of different VOCs in SOA production and measured the SOA yield  $Y$ , i.e., the fraction of formed SOA mass divided by the amount of reacted precursor concentration  $Y = \Delta C_{OA} / \Delta \text{VOC}$  (Hallquist *et al.*, 2009). However, distributing aerosol mass onto the aerosol size distribution via partitioning theory neglects the dynamics of the condensation process and assumes instantaneous equilibrium. As the volatility of organic molecules in the atmosphere span several orders of magnitude, their condensation behavior also changes. As pointed out by Riipinen *et al.* (2011) and Zhang, Pandis, and Seinfeld (2012), dynamic organic condensation can be viewed within two effective limits, the “kinetic” regime, where everything condenses irreversibly and the thermodynamic properties are neglected, and the “thermodynamic” or “quasiequilibrium” regime, where an equilibrium between the gas and particle phases is quickly reached, but apparent growth can be observed due to a shifting equilibrium driving more compounds into the particle phase. Ideally, organic condensation is treated within a hybrid approach, using either limit when appropriate and incorporating the proper transition behavior (Riipinen *et al.*, 2011).

In the previous analogy kinetic condensation of a single vapor species is identical to growth at the kinetic collision limit as discussed in Sec. IV.C.1, with the same consequence for a  $1/d_p$  dependence of the GR in the continuum regime and an independence of  $d_p$  for GRs in the free-molecular regime at sizes smaller than  $< 3$  nm. Conversely, thermodynamic growth of semivolatile vapors is driven by the shift of equilibrium between the gas and particle phases, which may be due to the change of semivolatile vapor concentrations. Organic aerosol partitioning is described using the equilibrium thermodynamics that was outlined in Eq. (21) and hence scales with the preexisting aerosol mass distribution. Hence, when a new equilibrium is obtained through a slow change of the semivolatile vapor concentration, such thermodynamic condensation GRs will scale with  $d_p$  for all particle sizes, favoring the largest particles, as demonstrated by Zhang, Pandis, and Seinfeld (2012).

Note that the exact vapor pressures of most organic compounds in the atmosphere remain unknown, and hence their condensation regime in the previously discussed sense cannot be specified straightaway. Pierce *et al.* (2011) estimated that equilibrium vapor pressures need to be as low as  $10^{-8}$  to  $10^{-7}$  Pa to be consistent with growth observations and particle evaporation measurements starting at 3 nm. This was at the time in contrast to measured vapor pressures of typical monoterpene oxidation products (Cappa and Jimenez, 2010).

However, Ehn *et al.* (2014) later reported a mechanism called autoxidation, which can lead to rapid oxygenation of monoterpenes through several steps of intramolecular H migration and subsequent  $O_2$  addition of peroxy radicals ( $RO_2$ ) formed during the initial oxidation of VOCs. This process can also be observed for VOCs of anthropogenic origin (Rissanen, 2021). In both cases, the resulting highly oxygenated organic molecules (HOMs) are defined as oxygenated organics including more than six oxygen atoms and originating from gas-phase autoxidation (Bianchi *et al.*, 2019). These compounds potentially have low enough vapor pressures for condensation from monomer sizes onward due to their high degree of functionalization. It was demonstrated by laboratory experiments that such HOMs can nucleate in the absence of sulfuric acid (Kirkby *et al.*, 2016). The pure biogenic nucleation mechanisms were also later found to be relevant in the atmosphere (Bianchi *et al.*, 2016; Rose *et al.*, 2018). Tröstl *et al.* (2016a) finally showed that HOMs from  $\alpha$ -pinene ozonolysis can indeed condense onto molecular clusters and grow particles at GRs similar to that of the atmosphere. However, assuming kinetic condensation ( $N_{eq,i} = 0$ ) of all measured HOMs according to Eq. (2) using average HOM characteristics, they obtained reasonable agreement for GRs below 3 nm but could not explain the observed increased GR at larger particle sizes. The effect of accelerating GRs with size was also observed in many ambient studies, as previously discussed (Kuang, Chen, Zhao *et al.*, 2012; Kulmala *et al.*, 2013), and was attributed to the Kelvin effect hindering organic condensation onto small particles. A framework using Eq. (2) including the Kelvin term [Eq. (3)] and solution effects [Eq. (4)] is therefore required to obtain the correct size dependence of particle GRs. However, this implies knowledge of the volatility (i.e., the vapor pressure) of large varieties of organic compounds.

#### b. Volatility basis set

Organic vapor pressures are often estimated from bulk properties (Donahue *et al.*, 2011) or identified from functional groups of known molecular structures (Pankow and Asher, 2008). Only recent attempts have measured the volatility of nanosized condensed-phase products with extremely low volatility directly via thermal desorption from collecting filters (Mohr *et al.*, 2019; Ye *et al.*, 2019; Wang *et al.*, 2020a; Ylisirniö *et al.*, 2021), mostly confirming the extremely low volatility of several HOM compounds formed via autoxidation of the VOCs. However, a direct measurement of the volatility of all compounds found in the gas phase is usually not feasible, and parametrizations according to the carbon, oxygen, and nitrogen numbers of a specific molecule are usually used in order to infer its volatility (Tröstl *et al.*, 2016a; Stolzenburg *et al.*, 2018; Mohr *et al.*, 2019; Yan *et al.*, 2020). Wang *et al.* (2020a) demonstrated that these volatility parametrizations depend on the origin of the organic molecules, and that multigeneration oxidation can also lead to compounds of low volatility (Garmash *et al.*, 2020), which, however, have a different functionalization than HOMs. Moreover, Stolzenburg *et al.* (2018) also showed that reversible condensation at reduced temperatures is heavily influenced by less oxygenated compounds. Therefore, the strict

definition of HOMs given by Bianchi *et al.* (2019) is too narrow to describe the organic's contribution to reversible nucleation mode growth. However, owing to the broad range of OOMs as potential contributors to nucleation mode growth, sub-25-nm aerosol particles will be composed of a mixture of thousands of compounds, similar to bulk SOAs (Goldstein and Galbally, 2007). Grouping of organic molecules according to their vapor pressures is therefore often used to facilitate organic growth characteristics. A prominent approach is the volatility basis set (VBS) (Donahue *et al.*, 2006, 2011), which was developed to describe organic partitioning by grouping organics according to their volatility (expressed as saturation mass concentrations) into bins separated by 1 order of magnitude in  $C^*$  at 300 K.

Using a VBS and a simple differentiation between semi-volatile and low-volatility organics, with the former condensing only on larger particles, Brean *et al.* (2020) showed that growth both below and above 5 nm can be explained by kinetic condensation of measured sulfuric acid and organics in a major European city. However, their study concluded that the uncertainties in this approach are large and likely lead to overestimation of the role of semivolatile organic compounds (SVOCs), as a detailed treatment of the vapor pressures according to Eq. (2) is neglected. Tröstl *et al.* (2016a) used a more sophisticated approach, with a dynamic condensation model based on the VBS to represent the condensation behavior of HOMs with different volatilities, which was recently summarized by Stolzenburg, Wang *et al.* (2022). The VBS facilitates the solution chemistry of the organic mixture, which is an essential part of the condensation dynamics, as we need to assume that different organics are soluble within each other. This results in reduced vapor pressures according to Raoult's law [Eq. (4)]. The approach of Tröstl *et al.* (2016a) put the grouping of the measured HOMs into a one-dimensional VBS and solved the resulting set of coupled ordinary differential equations based on Eq. (5) for the bins of the VBS,

$$\text{GR}_i = \beta(i, p) \frac{d_i^3}{3d_p^2} \times \left( N_i - \underbrace{\gamma_{\text{act},i}^m}_{\text{Raoult term}} \frac{N_{i,p} M_i}{\sum_i N_{i,p} M_i} \exp\left(\underbrace{\frac{4\sigma_i M_i}{RT\rho_i d_p}}_{\text{Kelvin term}}\right) N_{i,\text{eq},0} \right). \quad (22)$$

In Eq. (22)  $N_{i,\text{eq},0}$  is the pure-component saturation vapor concentration over a flat surface, which together with a Kelvin term and a Raoult term [including the particle-phase mass-based activity coefficient  $\gamma_{\text{act},i}^m$ , which is similar to Eq. (4) but formulated with mass concentrations] gives the equilibrium vapor pressure of the individual bins  $i$ . As the GR of each bin is linked to the change of particle-phase concentration  $dN_{i,p}/dt$  and the total change of particle-phase mass concentration  $\sum_i N_{i,p} M_i$ , the differential equations are coupled and numerical solutions need to be calculated.

Using a volatility-based growth model, Tröstl *et al.* (2016a) demonstrated that the increasing GR with size for  $\alpha$ -pinene

ozonolysis is a result of the volatility distribution of the HOMs. Therefore, this together with diurnal vapor concentrations changes can explain the widespread observation of increasing GR with size; see Sec. IV.A. Stolzenburg *et al.* (2018) included the temperature dependence of OOM volatility in the same growth model as Tröstl *et al.* (2016a) and demonstrated that  $\alpha$ -pinene ozonolysis and subsequent autoxidation is efficiently providing low enough volatility compounds to drive particle growth from  $-25^\circ\text{C}$  to  $+25^\circ\text{C}$ . Moreover, that study clarified the important role of low-volatility compounds ( $C^0 = 10^{-3} - 10^{-1} \mu\text{g m}^{-3}$  and  $N_{\text{eq},0,i} = 2 \times 10^6 - 2 \times 10^8 \text{ cm}^{-3}$ , with  $M_i = 300 \text{ u}$ ), which were largely underestimated by Tröstl *et al.* (2016a). Mohr *et al.* (2019) extended the approach of Tröstl *et al.* (2016a) within a modeling framework that, in addition to the VBS description of organic growth, included inorganic aerosol composition (Yli-Juuti *et al.*, 2013). They showed good agreement between the growth measured in springtime in Hyytiälä and the growth model prediction. Note also that Mohr *et al.* (2019) used a different chemical-ionization technique for the measurement of the OOMs (see Sec. III.A.3) in order to access the low-volatility compound (LVOC) range in more detail than Tröstl *et al.* (2016a) did.

The volatility-based growth model by Tröstl *et al.* (2016a) and especially the approach from Mohr *et al.* (2019) including inorganics and water are similar to the nano-Köhler theory that was postulated earlier (Kulmala, Kerminen *et al.*, 2004). In nano-Köhler theory, organic growth is described as the activation of nanometer-sized inorganic clusters by condensation of an organic vapor completely soluble in the inorganic compound and water mixture (Kulmala, Kerminen *et al.*, 2004). A thermodynamic equilibrium among the clusters, the organic vapor, and water is assumed, in a manner analogous to traditional Köhler theory, describing the equilibrium between cloud condensation nuclei and water. When the equilibrium saturation ratio of the organic vapor is plotted as a function of the cluster size, a curve with a peak resulting from the combination of Kelvin and Raoult effects is obtained, similar to traditional Köhler curves (Kulmala, Kerminen *et al.*, 2004; Kontkanen *et al.*, 2018). When the saturation ratio of the organic vapor exceeds the peak value of the curve, the clusters start to grow spontaneously by condensation of organic vapor. The nano-Köhler theory has been applied to describe the particle growth by condensation of organic vapors in earlier aerosol dynamics models (Korhonen, Lehtinen, and Kulmala, 2004). However, it is unclear whether the simple theory can correctly describe the initial particle growth in real atmospheric systems, in which there is neither a single seed nor a single condensing vapor, but rather a distribution of clusters that interact with each other and with larger particles and that may not be in thermodynamic equilibrium (Kontkanen *et al.*, 2018). Kontkanen *et al.* (2018) simulated the growth of a cluster population by sulfuric acid and an organic vapor and observed nano-Köhler-type behavior, when the saturation ratio of the organic vapor and the ratio between organic vapor and sulfuric acid concentrations were in a suitable range. Consistent with Tröstl *et al.* (2016a), they found that GRs derived from simulations using the appearance time method started to increase close to the size at which the

organic vapor started to dominate the growth. However, they found that nano-Köhler theory was unable to exactly predict the size at which the organic vapor started to condense on the clusters.

But even if the description of reversible OOM condensation via the VBS (including Kelvin and Raoult effects) is significantly facilitated and has shown its potential in describing ambient observations of growth, an ambiguity remains when the results from Tröstl *et al.* (2016a) are compared to earlier smog-chamber experiments. The organic mass yields observed at atmospherically relevant conditions by Tröstl *et al.* (2016a) are much higher than the SOA mass yields derived from  $\alpha$ -pinene ozonolysis experiments in smog chambers (Presto and Donahue, 2006). Specifically, the high yields of extremely low-volatility compounds found by Tröstl *et al.* (2016a) were not observed in SOA formation experiments, leading to the conclusion that most atmospheric organics cannot overcome the Kelvin barrier for participation in initial growth. Chuang and Donahue (2017) explored these differences and attributed them partly to the dynamic behavior of condensation compared to instantaneous partitioning, which is typically not taken into account when classical SOA mass yields are derived. Altogether this indicates the need for a dynamic approach when describing organic condensation in the sub-25-nm range and shows the limitations of partitioning theory.

## 7. Gas- and particle-phase chemistry influencing oxygenated-organic-molecule-driven growth

### a. Gas-phase chemistry

Chuang and Donahue (2017) explored the role of gas- and particle-phase chemistry in the observed differences between smog-chamber experiments and the results from the CERN CLOUD experiment. Smog-chamber measurements are often characterized by a boosted oxidation chemistry, which interferes with the autoxidation reactions of the  $\text{RO}_2$  radicals (Chuang and Donahue, 2017). This highlights the importance of the gas-phase chemistry when describing sub-25-nm growth. Several SOA formation studies showed that the presence of  $\text{NO}_x$  significantly influences SOA yields from monoterpenes due to the interference of  $\text{NO}_x$  in the  $\text{RO}_2$  chemistry (Presto, Hartz, and Donahue, 2005; Wildt *et al.*, 2014; Zhao *et al.*, 2018). Following the work of Tröstl *et al.* (2016a), Yan *et al.* (2020) found that the autoxidation termination via  $\text{NO}_x$  in  $\alpha$ -pinene ozonolysis competes with the formation of HOMs via  $\text{RO}_2 + \text{HO}_2$  termination reactions. This increases the yield of HOMs with nitrate groups, which generally have a higher volatility, influencing early growth compared to no- $\text{NO}_x$  conditions and suppressing condensation onto small particles ( $< 5$  nm) (Yan *et al.*, 2020). This is in line with the finding that sulfuric acid can counterbalance reduced SOA yields in the presence of  $\text{NO}_x$  because the initial organic growth suppression is compensated by sulfuric acid growth (Zhao *et al.*, 2018). Similar observations have been made in highly polluted urban atmospheres, where the presence of  $\text{NO}_x$  and therefore the higher abundance of higher volatility HOMs could be the cause for a higher influence of sulfuric acid on growth below 3 nm (Yan *et al.*, 2021). This has been partly confirmed by observations during

the COVID-19 lockdown period in 2020, where significantly decreased  $\text{NO}_x$  emissions induced faster particle growth in Chinese megacities (X. Shen *et al.*, 2021; Tang *et al.*, 2021; Yan *et al.*, 2022). An increase in SOA formation was also found in South-Central Europe during the lockdown periods, where  $\text{NO}_x$  was reduced (Ciarelli *et al.*, 2021), but analysis of particle GRs at two sites did not indicate an increase in GR compared to previous years (J. Shen *et al.*, 2021).

Apart from the influence of  $\text{NO}_x$ , interferences from different organics can significantly alter gas-phase chemistry, resulting in different particle growth patterns. Isoprene has been determined to interfere with NPF related to monoterpene oxidation with high isoprene levels typically suppressing the particle formation rates (Kiendler-Scharr *et al.*, 2009). The presence of isoprene has thus been attributed to the observation of less frequent new particle formation than expected in the Eastern U.S. (Kanawade *et al.*, 2011; Yu *et al.*, 2014; Lee *et al.*, 2016) and the Amazon Basin (Martin *et al.*, 2010). Lee *et al.* (2016) explicitly showed that it is the absence of new particle growth in an isoprene rich environment that hinders the occurrence of NPF events. McFiggans *et al.* (2019) attributed the suppression of the produced SOA mass in the presence of monoterpenes and isoprene to two sources: (1) scavenging of peroxy radicals (OH) by isoprene and hence reduced monoterpene oxidation rates, as previously suggested by Kiendler-Scharr *et al.* (2009), and (2) an increased rate of  $\text{RO}_2 + \text{RO}_2$  reactions between  $\alpha$ -pinene and isoprene oxidation products. Heinritzi *et al.* (2020) explicitly studied NPF at atmospherically relevant levels of precursors and oxidants and showed that the suppression through the increased production of  $\text{C}_{15}$  dimers compared to  $\text{C}_{20}$  dimers in  $\text{RO}_2 + \text{RO}_2$  termination reactions is responsible for the suppression of nucleation rates and early GRs. The  $\text{C}_{15}$  products have higher volatilities, which hinders their condensation onto the smallest particles. For low temperatures, the increased fraction of  $\text{C}_{15}$  compounds in the presence of isoprene is also observed in particle-phase composition measurements (Caudillo *et al.*, 2021). Furthermore, the OH scavenging as a possible reason for isoprene suppression could be excluded by showing that increased OH levels yield a further suppression of NPF at atmospherically relevant concentration ranges (Heinritzi *et al.*, 2020). This again demonstrates that smog-chamber experiments with boosted chemistry might not be representative for real atmospheric conditions. However, the conclusion by McFiggans *et al.* (2019), namely, that atmospherically relevant molecules such as CO or other  $\text{RO}_2$  radicals from different VOCs will influence the final volatility distribution of the organic mix, remains highly relevant. This is especially important since especially anthropogenic VOC emissions show large varieties with many compounds capable of contributing to secondary organic aerosol formation not resulting from combustion-related processes (McDonald *et al.*, 2018; Shah *et al.*, 2020). A recent study by Voliotis *et al.* (2021) explored the changes in volatility of SOA when anthropogenic and biogenic VOCs were simultaneously oxidized. The suppression of high molecular weight compounds and the identification of a variety of unique-to-the-mixture compounds underline the need for a volatility description of particle growth, which includes the chemistry describing the interference of different

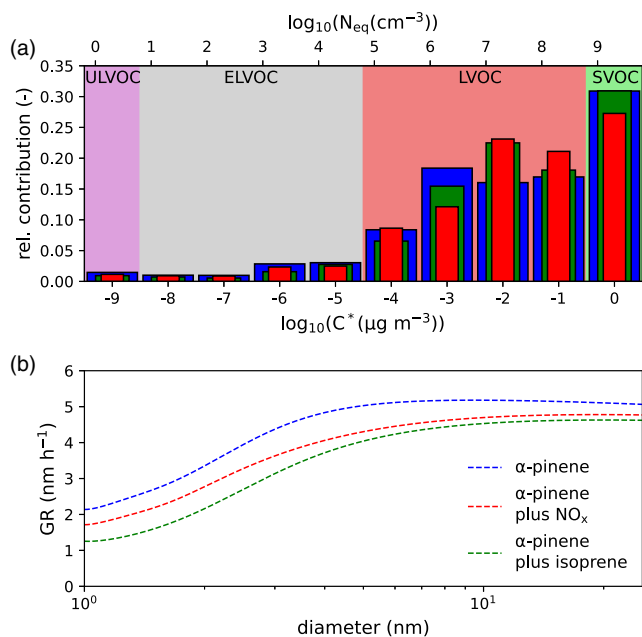


FIG. 8. (a) Idealized volatility distribution at 300 K for pure  $\alpha$ -pinene ozonolysis (blue bars),  $\alpha$ -pinene ozonolysis including  $\text{NO}_x$  (red bars), and  $\alpha$ -pinene ozonolysis in the presence of isoprene (green bars). Data are similar to results from the CERN CLOUD experiment (Stolzenburg *et al.*, 2018; Heinritzi *et al.*, 2020; Yan *et al.*, 2020) and are scaled to the total OOM concentration. (b) The resulting GR assuming a total OOM concentration of  $10^8 \text{ cm}^{-3}$  using a growth model solving the set of coupled differential equations given in Eq. (22).

VOC oxidation products. Figure 8(a) shows three different one-dimensional VBS distributions for  $\alpha$ -pinene ozonolysis experiments carried out at atmospherically relevant oxidation and precursor levels, demonstrating the effects of isoprene and  $\text{NO}_x$  on the volatility of gas-phase OOMs. Owing to the presence of  $\text{NO}_x$  or isoprene, the fraction of ultralow-volatility compounds (potential nucleator molecules) (Simon *et al.*, 2020) and extremely low-volatility compounds (ELVOCs) is reduced, while LVOCs with  $C^* > 10^{-2} \mu\text{g cm}^{-3}$  are found in higher fractions. Figure 8(b) shows modeled size-dependent particle GRs using the same framework as Tröstl *et al.* (2016a), indicating that the shift in the volatility distribution due to the presence of isoprene or  $\text{NO}_x$  results, in particular, in slower initial particle GRs. Similar determinations of the full volatility distribution (i.e., good sensitivity coverage across the entire volatility range) are required in a wide variety of atmospheric settings, different VOC-oxidant combinations, and VOC mixtures to narrow down the differing interplay of atmospheric organics with respect to particle growth.

#### b. Particle-phase reactions

While gas-phase chemistry involving different organics and  $\text{NO}_x$  can suppress new particle growth, particle-phase chemistry effectively lowering the volatility of particle-phase compounds can potentially enhance particle GRs from OOM. This could be another possible explanation for the differences between smog-chamber and similar-to-atmosphere experiments discussed in Sec. IV.C.6 (Chuang and Donahue,

2017). Analysis of SOA composition reveals strong particle-phase yields of oligomers (Kalberer *et al.*, 2004; Tolocka *et al.*, 2004) and organosulfates (Riva *et al.*, 2016; Vogel *et al.*, 2016), which are typically not observed in the gas phase. Particle-phase accretion reactions can effectively lower the volatility of a compound by increasing its molecular weight or changing its functionalization (Vesterinen *et al.*, 2007). Wang *et al.* (2010) showed that oligomerization and alkylammonium sulphate formation takes place in nanoparticles upon exposure to volatile vapors such as glyoxal and dimethylamine, resulting in significant particle growth under suitable conditions. Apsokardu and Johnston (2018) and Heitto *et al.* (2022) explored the influence of such oligomerization reactions on nucleation mode aerosol growth within modeling schemes and found significantly increased GRs when oligomerization is included. Apsokardu and Johnston (2018) demonstrated that the necessary reaction rates for such oligomerization reactions to explain SOA formation experiments are in line with condensed-phase organic chemistry. However, Vesterinen *et al.* (2007) speculated that the particle-phase reaction rates needed to explain ambient growth observations would be higher. Moreover, Apsokardu and Johnston (2018) concluded that such particle-phase accretion reactions would contribute mainly to the growth of particles larger than 20 nm, where SVOCs responsible for volatility lowering particle-phase reactions can be found in significant amounts in the condensed phase. In contrast, acid-catalyzed oligomerization reactions could potentially grow even smaller particles (Xu *et al.*, 2014). Epoxides originating in large yields from isoprene oxidation can oligomerize in the presence of acids such as sulfuric acid (Xu *et al.*, 2014), which would be typical for nanoparticle growth where freshly formed sulfuric acid particles are grown by organics (Kulmala *et al.*, 2013). The sulfuric acid–OOM interplay has also been investigated within SOA formation experiments, indicating that particle acidity or aerosol sulfate can promote the formation of organosulfates and other particle-phase chemistry, especially related to isoprene SOA formation (Surratt *et al.*, 2007; Xu *et al.*, 2015; Riva *et al.*, 2016). Recent measurements in Beijing have revealed the presence of organosulfates in ultrafine particles (Li *et al.*, 2021). However, it remains unresolved whether the particle-phase production of such compounds are important drivers of sub-25-nm growth. In that sense, we conclude that the particle-phase chemistry of nucleation mode aerosols remains highly uncertain.

## V. LARGE-SCALE MODELING OF NANOPARTICLE GROWTH: THE CURRENT STATE

### A. Representation of growth in large-scale models

In this section we review the most common approaches for representing sub-25-nm nanoparticle growth in atmospheric three-dimensional models that contain a description of aerosol number size-distribution evolution. These models can be used for assessing the role of atmospheric aerosol particles in the climate system (Makkonen *et al.*, 2009; Yu, McGraw, and Lee, 2012), as well as their contribution to air quality and health (Jung *et al.*, 2010; Julin *et al.*, 2018). The level of interaction of the aerosol size distribution with the other

components of the atmosphere and the Earth system as a whole varies considerably between the different modeling approaches from chemical transport models (Spracklen *et al.*, 2006; D’Andrea *et al.*, 2013; Dunne *et al.*, 2016; Julin *et al.*, 2018) to atmospheric global climate models (Makkonen *et al.*, 2012a) all the way to the fully coupled Earth system models (ESMs) (Seland *et al.*, 2020; Blichner *et al.*, 2021; Döschner *et al.*, 2022). The basic approach of representing nanoparticle growth in all these models can be generally summarized as follows: the amount of condensable vapor is calculated based on their chemical production and then distributed to the simulated size distribution during the model time step based on assumptions about volatility, kinetics, and other vapor properties. The way that the nanoparticle growth is represented in large-scale models thus depends on (1) how the particle number size distribution and its dynamics (including any nucleation rate parametrization) are described in the model, (2) which condensable vapors are considered within the model, and (3) what is assumed about the properties of these vapors and the chemistry producing them.

### 1. Representation of the particle number size distribution and aerosol dynamics

In terms of the numerical representation of the aerosol size-distribution function, there is large variability between different three-dimensional regional and global scale models, depending on which research questions the models have been designed to answer (from prescribed, entirely noninteractive aerosol fields to sectional approaches with a large number of size bins whose evolution and interactions with each other and the surrounding atmosphere are calculated within each time step of the model). Since prescribed aerosol fields do not contain an explicit description of nanoparticle growth (or condensation in general), we focus here on the main types of interactive schemes used in atmospheric models, namely, modal (Makkonen *et al.*, 2014; Scott *et al.*, 2015) and sectional schemes (Spracklen *et al.*, 2006; Westervelt, Pierce, and Adams, 2014; Julin *et al.*, 2018) and their various hybrids (Blichner *et al.*, 2021).

Sectional models represent the particle-size distribution by dividing the size range into a number of bins and keeping track of the number of particles within each bin. The advantage of this approach is that it does not presuppose any shape to the size distribution, while the disadvantage is that the number of bins required is large and these schemes are typically computationally heavy. Modal schemes, on the other hand, are inspired by the shape of the empirical size distribution (Whitby, 1978) and represent the distribution by some number of log-normal modes. These schemes can thus get away with many fewer modes and lower computational costs but also presuppose the shape of the distribution. On top of the purely sectional or modal schemes, there are also various hybrids of these two used in global and regional modeling approaches, which use a detailed sectional scheme to describe the small end of the size distribution coupled to a modal scheme for describing the part of the size distribution with most of the aerosol mass (Lee, Pierce, and Adams, 2013; Blichner *et al.*, 2021). Approaches that combine a modal scheme with lookup tables outputted from detailed sectional models (Makkonen

*et al.*, 2014; Kirkevåg *et al.*, 2018) or, for instance, use cluster kinetic codes for NPF and early growth (Baranizadeh *et al.*, 2016) can also be considered hybrids aiming to balance the benefits of the computational speed of modal schemes without sacrificing too much of the necessary detail for describing the dynamics of the smallest nanoparticles.

In general the aerosol dynamics schemes applied within climate models have low size resolution (bins or modes) below 20 nm. For example, reproducing a nucleation event with an individual nucleation mode below 10 nm in diameter would suffer from numerical deterioration in describing the flux of particles toward Aitken-mode sizes. Global models, therefore, typically do not explicitly model the first steps of particle growth, but rather parametrize the formation of particles at 3 or 5 nm from the nucleation rate (Spracklen *et al.*, 2006; Bergman *et al.*, 2022) or extrapolate the size distribution to 1 nm (Westervelt, Pierce, and Adams, 2014). Two widely applied formation parametrizations are Kerminen and Kulmala (2002) and Lehtinen *et al.* (2007); see Eq. (14). However, such parametrizations typically reduce the description of nanoparticle growth to condensational growth of a single particle only, i.e., Eq. (2). Moreover, their applicability to extend to larger sizes, particularly to the Aitken mode (Makkonen *et al.*, 2014), is limited by changes in sinks and condensable vapor concentrations during growth, the importance of collisions among the growing nanoparticle population, and the common assumption of a steady state of the growing population; see also Lee, Pierce, and Adams (2013) and Olenius and Riipinen (2017). Recently there have been efforts to improve the description of early growth to account for more details in nucleation and subsequent growth. Blichner *et al.* (2021) implemented a sectional model for early growth below Aitken-mode size to complement the modal OsloAero aerosol module in NorESM. The new approach uses the work of Lehtinen *et al.* (2007) to convert nucleation rates to 5 nm formation rates, after which a five-bin sectional scheme is used between 5 and 23.6 nm. Given the assumptions made in the common parametrizations for scaling nucleation rates up to larger sizes, the diameter at which the nucleated particles are entered to the evolving particle-size distribution is of central importance for the description of sub-25-nm particle growth. Another key aspect determining sub-25-nm growth in global and regional models is the identities and properties of condensable vapors, along with the mechanism through which they are distributed to the particle-size distribution.

### 2. Condensable vapors considered for growth processes

The impact of NPF on CCN depends on the interplay between growth and coagulation loss [Eq. (13)] (Blichner *et al.*, 2021). As we saw in Sec. IV.C, vapor condensation dominates this growth, although in some conditions the growth by cluster collisions might also be important for the smallest particles (typically sub-3-nm size); see Sec. IV.C.4 (Olenius and Riipinen, 2017).

The vapor mixture contributing to particle growth is highly dependent on the environment, but the most important vapor compounds for sub-25-nm growth are sulfuric acid, various secondary organic species, nitric acid, ammonia, amines, and

water. However, iodic acid and MSA can contribute in specific environments; see Sec. IV.C. There is a large variation in the complexity of the chemical schemes of the models, and hence the vapors considered. The exception is growth by sulfuric acid, which is considered in practically all large-scale models that represent atmospheric nucleation (Spracklen *et al.*, 2006; Pierce and Adams, 2009; Jung *et al.*, 2010; D'Andrea *et al.*, 2013; Scott *et al.*, 2015; Baranizadeh *et al.*, 2016; Dunne *et al.*, 2016). Most current models consider the sub-25-nm particle growth as a combination of practically nonvolatile, noninteracting and pointlike sulfuric acid (potentially also including simplified treatment of acid-base chemistry with ammonia and amines), and secondary organic species, with slightly differing assumptions on the volatility of the organic compounds and on whether organic compounds are able to contribute to growth even at the smallest (typically < 3 nm) particle sizes. In general predictions of growth for sulfuric acid seem to agree relatively well among the different models. We therefore focus on growth by organic vapors in the rest of this section.

Owing to the complexity of the atmospheric organic mixture and their chemical production pathways (Secs. IV.C.6 and IV.C.7), their treatment varies considerably among models. First, modeling chemistry in large-scale models is a balancing act between comprehensiveness and computational cost. Adding complex chemistry includes adding a large number of tracers, and this greatly increases the computational cost of running the model. Most large-scale models therefore use highly simplified chemistry schemes, often with fixed, precalculated oxidant fields (OH, O<sub>3</sub>, and NO<sub>3</sub>). Using fixed oxidant fields essentially means that there is no change in the available oxidants based on meteorological conditions (for instance, cloudy versus clear sky), and also that changes in emissions of organics cannot influence the oxidant concentrations and in turn the oxidation pathways in the model. Second, the SOA precursors are usually lumped together in one tracer for monoterpenes, one for isoprene, etc. [see Makkonen *et al.* (2014), Scott *et al.* (2014), Tilmes *et al.* (2019), and Sporre *et al.* (2020)], although some models do separate between additional properties such as endocyclic and other monoterpenes (Jokinen *et al.*, 2015). This means that most chemical schemes require one reaction rate and one SOA yield for each precursor tracer with each oxidant, even though this tracer may in reality be the sum of compounds with slightly different properties. Third, the number of individual oxidation products from VOC oxidation is far too large to be represented in a large-scale model. To tackle this issue, various approaches to grouping the oxidation products are deployed. In the following, we go through some of these from the more complex to the most simplified variants.

Representing the organic mixture with a set of effective volatilities (the VBS approach; see Sec. IV.C.6) has become a common way of describing the evolution of the atmospheric organic compounds with varying levels of complexity (Donahue *et al.*, 2006; Pandis *et al.*, 2013; Patoulias *et al.*, 2015, 2018; Liu *et al.*, 2021). These representations vary from using a fixed yield for each volatility bin from the oxidation of VOCs (Patoulias *et al.*, 2018; Tilmes *et al.*, 2019) to those who represent aging or fragmentation in the gas phase (Yu, 2011; Shrivastava *et al.*, 2015; Hodzic *et al.*, 2016). Some models

include the impact of NO<sub>x</sub> concentrations on the yields (Patoulias *et al.*, 2018), while most ESMs operate with simple fixed yields for each oxidant and precursor (Makkonen *et al.*, 2012b; Westervelt, Pierce, and Adams, 2014; Dunne *et al.*, 2016; Kirkevåg *et al.*, 2018). While VBS schemes are becoming more popular, most global models still deploy simpler schemes. A popular approach is a two-product scheme, where the entire range of volatilities are reduced to two tracers with different volatilities and/or properties (Riipinen *et al.*, 2011; Kirkevåg *et al.*, 2018; Van Noije *et al.*, 2021). Some large-scale models also skip modeling the atmospheric formation of SOAs but instead treat it in a “pseudoprimary” manner, with a fixed global SOA yield from the emitted precursors (Makkonen *et al.*, 2009; Scott *et al.*, 2014; Westervelt, Pierce, and Adams, 2014). SOA can contribute to early growth even in these schemes, depending on how the mass is distributed over the aerosol surface area.

The treatment of the condensation is in general done by assuming (1) that the organics condense essentially as nonvolatile and condense kinetically to the particle surface area (see Sec. IV.C), (2) some version of thermodynamic absorptive partitioning theory to the existing OA mass (Odum *et al.*, 1996; Van Noije *et al.*, 2021), or (3) a combination of (1) and (2) (Yu, 2011; Sengupta *et al.*, 2021), for instance, with a two-product model with one tracer for each approach (Van Noije *et al.*, 2021). Other approaches include representing volatility by prescribing which sizes the organics can condense onto and the fraction that should go to each size range (Makkonen *et al.*, 2009; D'Andrea *et al.*, 2013; Blichner *et al.*, 2021). Certain implementations of organic condensation have omitted partitioning to the nucleation mode altogether (O'Donnell, Tsigaridis, and Feichter (2011)) and can show even a decrease of Aitken-mode or CCN number concentration due to SOA formation (Armeth *et al.*, 2010; Sporre *et al.*, 2020). In AeroCom phase II, 13 out of 31 global models applied a parametrization where SOAs are effectively modeled as a primary source of 19.1 Tg a<sup>-1</sup> (Tsigaridis *et al.*, 2014), but these models include various approaches to distribute OAs into the aerosol population. With increased details on SOA formation, 14 out of 31 AeroCom II models simulated reversible partitioning of SOA formation (Tsigaridis *et al.*, 2014). Hodzic *et al.* (2020) compared organics in eight models, and of these four have some form of a VBS scheme and two also have a nonvolatile tracer (GC12-REF and GC12-DYN) (Bey *et al.*, 2001). The other four models treat SOAs as pseudoprimary and nonvolatile with a fixed yield mass from the emissions.

Overall the variability in the setup of SOA modeling and how it contributes to early growth reflect a lack of theoretical understanding of the processes involved (Shrivastava *et al.*, 2015, 2017) and a field in fast development. The sensitivities these models will exhibit to organics in general and their contributions to early growth will depend heavily on how the model is set up, the assumptions about volatility, which processes these contribute to, etc.

## B. Importance of nanoparticle growth in global and regional scale atmospheric predictions

There are few regional or global scale model studies that have a specific focus on sub-25-nm particle growth. Typically,

in relevant sensitivity experiments the models are perturbed by changing either the nucleation rate (the parametrization or relevant coefficients) (Spracklen *et al.*, 2006; Makkonen *et al.*, 2009; Reddington *et al.*, 2011; Fountoukis *et al.*, 2012; Dunne *et al.*, 2016; Julin *et al.*, 2018) or the amount and properties of condensable vapors (emission or partitioning properties) (Spracklen *et al.*, 2006; Makkonen *et al.*, 2012a; D’Andrea *et al.*, 2013; Dunne *et al.*, 2016; Sporre *et al.*, 2020), and not specifically the early growth *per se*. Besides affecting sub-25-nm particle growth, modulating SO<sub>2</sub>, ammonia, or monoterpene emissions impacts the aerosol population throughout the size distribution, as well as nucleation rates and atmospheric chemistry in general. Hence, it is difficult to provide estimates of model sensitivity to early growth specifically without changing other important parameters affecting the predicted aerosol numbers. We can, however, examine aerosol particles and CCN originating from nucleation, which should be sensitive to nucleation and subsequent growth in a given model setup. Furthermore, there are studies that evaluate the predicted particle growth against observations and discuss it in detail as an important part of predicting aerosol number size distributions (Spracklen *et al.*, 2006; Fountoukis *et al.*, 2012; Makkonen *et al.*, 2012a, 2014; D’Andrea *et al.*, 2013; Westervelt *et al.*, 2013; Scott *et al.*, 2015; Dunne *et al.*, 2016; Patoulias *et al.*, 2018; Patoulias and Pandis, 2022). The conclusions from these studies highlight the importance of including the condensation of secondary organic species to sub-CCN-sized particles, in addition to sulfuric acid, to capture the important features of aerosol size distributions (Spracklen *et al.*, 2006; Fountoukis *et al.*, 2012; D’Andrea *et al.*, 2013; Westervelt *et al.*, 2013; Makkonen *et al.*, 2014; Tröstl *et al.*, 2016a; Patoulias *et al.*, 2018). On the other hand, the results tend to suggest that the details of the sub-3-nm particle growth are of minor importance in capturing the expected CCN concentrations (Spracklen *et al.*, 2006; D’Andrea *et al.*, 2013; Lee, Pierce, and Adams, 2013; Dunne *et al.*, 2016).

Table II summarizes results from 12 global and regional modeling studies focusing on the effects of nucleation on particle number concentrations (*total* is denoted as  $N_{\text{tot}}$  but usually indicates a lower limit of 3 nm, larger than 10 nm is denoted as  $N_{10}$ , and 100 nm is denoted as  $N_{100}$ ) and CCN at 0.2% supersaturation, which can be considered to be roughly comparable to  $N_{100}$ . While not representing a comprehensive review of all relevant studies [see also Yu and Luo (2009), Riipinen *et al.* (2011), D’Andrea *et al.* (2013), Posner and Pandis (2015), Scott *et al.* (2015), Gordon *et al.* (2016), Patoulias *et al.* (2018), Blichner, Sporre, and Berntsen (2021), Blichner *et al.* (2021), and Patoulias and Pandis (2022)], the studies presented in Table II have been chosen based on their level of intercomparability in terms of the model experiment setup, nucleation mechanisms investigated, and output variables reported. These experiments focus primarily on examining the sensitivity of CCN to the nucleation rate itself, not on sub-CCN GRs. Nevertheless, models vary in their description of early growth and provide a substantial range in estimates of survival rate of nucleated particles to CCN size. While the exact fraction depends on the model setup and details of the analysis, studies to date report that up to about half of CCN-sized particles originate from NPF in current conditions, with

a large variation in the estimates depending on the region and exact model setup (Makkonen *et al.*, 2009; Merikanto *et al.*, 2009; Westervelt, Pierce, and Adams, 2014; Dunne *et al.*, 2016). Considering the full picture in Table II, the fraction of CCN originating from NPF does seem to depend on the vapors contributing to the early growth of particles: the studies assuming that only sulfuric acid contributes to this growth tend to predict a considerably lower fraction (on average about 5%) of  $N_{100}$  or CCN (0.2%) to originate from NPF as compared with the studies allowing organics to grow the newly formed particles. For studies using PMCAMx-UF that do not include organics in early growth, for example, the influence of nucleation on  $N_{\text{tot}}$  is large (above 250%), while the impact seems to disappear before the particles reach CCN sizes, with impacts on  $N_{100}$  of below or equal to 15% [and even  $-4\%$  in the work of Ahlm *et al.* (2013)].

Some of the aforementioned studies did, however, investigate the performance of the applied models in terms of reproducing observed sub-25-nm nanoparticle GRs and discussed the sensitivity of the results to assumptions about the growth. Makkonen *et al.* (2009) demonstrated that the addition of organic condensation increased the NPF contribution to CCN (0.2%) from about 10% to about 53%, under the condition that all monoterpene oxidation products were allowed to condense on the newly formed particles. Fountoukis *et al.* (2012) concluded that their regional model setup omitting the condensation of organics onto ultrafine particles resulted in an underestimation of nucleation mode GRs in the European domain, hence likely resulting in underpredictions of  $N_{100}$ . This work was later followed up on by Patoulias *et al.* (2018), who implemented condensation of organic vapors on the ultrafine aerosol fraction and reported a 50%–120% increase in the  $N_{100}$  concentration mainly in Central and Northern Europe, while the sub-10-nm particle concentration decreased by 10%–30%. The further consideration of a fraction of the organics to be extremely low in volatility and contribute to the nucleation mode growth did not make a large difference in the predicted number concentrations (Patoulias and Pandis, 2022). Westervelt *et al.* (2013) concluded that their global model setup with nonvolatile secondary organics from monoterpenes reproduced the particle GRs observed in Hyytiälä (boreal), Pittsburgh (urban), and Atlanta (urban), highlighting the importance of the contribution of organics to nanoparticle growth, which is in line with D’Andrea *et al.* (2013) and Scott *et al.* (2015). Makkonen *et al.* (2014) revised the scheme with entirely nonvolatile organics to a scheme for the NorESM model where 50% of the monoterpene oxidation products were assumed to be able to contribute to sub-23-nm growth, and reported a somewhat underpredicted particle growth for Hyytiälä. The inclusion of organic vapors in growing ultrafine aerosol particles resulted in up to a 10%–20% increase in CCN-sized particles.

Keeping in mind that the overall sensitivity of the CCN budget to NPF is around 50%, the sensitivity to processes in early growth is important but modest. This is probably due to the buffering effects in the size-distribution dynamics: while the increased condensable material enhances the growth, it can also enhance the CS and result in more numerous particles, yet with a smaller final size; see Sec. IV.A and Blichner *et al.*

TABLE II. Global and regional modeling studies on the role NPF as a source of particles and CCN (if available, defined at 0.2% supersaturation). In nucleation mechanisms (nucl. mech.), ACT refers to semiempirical “activation” nucleation within the boundary layer, BHN indicates binary homogeneous nucleation by sulfuric acid and water, TER refers to ternary homogeneous nucleation mechanisms with or without (denoted by n) a semiempirical scaling factor of  $10^{-6}$ – $10^{-5}$ , ACT + org indicates a semiempirical activation mechanism also involving low-volatility organics (Paasonen *et al.*, 2010), CLOUD inorg + org stands for a mechanism based on observations from the CLOUD chamber (Dunne *et al.*, 2016), and NONUC refers to control runs that do not incorporate any nucleation mechanisms. In addition, MT refers to monoterpenes and IP indicates isoprene. For the change in CCN or potential cloud forming particles ( $N_{100}$  or  $N_{70}$ ) a dagger indicates that the study looked into the difference in  $N_{100}$  ( $\Delta N_{100}$ ), an asterisk indicates that the study investigated the difference in  $N_{70}$  ( $\Delta N_{70}$ ), and no label indicates that changes in CCN concentrations ( $\Delta$ CCN) at a certain supersaturation were explicitly calculated.

Reference	Model	Nucl. mech.	Vapors for early growth	SOA yield for early growth	$\Delta N_{\text{tot}}$ or $\Delta N_3$	$\Delta N_{10}$	$\Delta N_{100}$ , $\Delta N_{70}$ , or $\Delta$ CCN	Region
Spracklen <i>et al.</i> (2006)	GLOMAP	ACT + BHN vs BHN or NONUC	H <sub>2</sub> SO <sub>4</sub> + MT ox. prod.	13% of MT emissions	420%–2300%			Hyttälä spring
Spracklen <i>et al.</i> , 2008	GLOMAP	ACT + BHN vs NONUC	H <sub>2</sub> SO <sub>4</sub> + MT ox. prod.	13% of MT emissions			3%–20%	Global
Merikanto <i>et al.</i> (2009)	GLOMAP	ACT + BHN vs NONUC	H <sub>2</sub> SO <sub>4</sub> + MT ox. prod.	13% of MT emissions			31%–49%	Global
Wang and Penner (2009)	IMPACT/CCSM3	BHN + ACT vs BHN	H <sub>2</sub> SO <sub>4</sub>	None			5%	Global
Pierce and Adams (2009)	GISS-2-prime	TERn vs NONUC	H <sub>2</sub> SO <sub>4</sub> + SOA	19 Tg of kinetic SOAs		430%	44%	Global
Makkonen <i>et al.</i> (2009)	ECHAM	ACT + BHN vs BHN	H <sub>2</sub> SO <sub>4</sub>	64 Tg of kinetic SOAs		400%	64%	Global
				None		115%	10%	Medians of nine stations
				7.5% of MT emissions		192%	10%	
Jung <i>et al.</i> (2010)	PMCAMx-UF	TER vs NONUC	H <sub>2</sub> SO <sub>4</sub>	15% of MT emissions		298%	53%	
Fountoukis <i>et al.</i> (2012)	PMCAMx-UF	TER vs NONUC	H <sub>2</sub> SO <sub>4</sub>	None	250%	75%	15% <sup>†</sup>	Eastern U.S.
Ahlm <i>et al.</i> (2013)	PMCAMx-UF	TER vs NONUC	H <sub>2</sub> SO <sub>4</sub>	None	300%	110%	0.5% <sup>†</sup>	Europe
Makkonen <i>et al.</i> (2014)	NorESM	BHN + ACT vs NONUC	H <sub>2</sub> SO <sub>4</sub> + MT ox. prod.	7.5% of MT emissions	280%	80%	–4% <sup>†</sup>	Europe in 2030
				7.5% of MT emissions	48%			Global
Westervelt, Pierce, and Adams (2014)	GEOS-Chem	BHN + ACT + org vs NONUC	H <sub>2</sub> SO <sub>4</sub> + MT ox. prod.	7.5% of MT emissions	56%			
				10% of MT emissions		140%	66%	Global
				10% of MT emissions		190%	78%	
				10% of MT emissions		48%	56%	
Dunne <i>et al.</i> (2016)	GLOMAP	CLOUD inorg + org vs NONUC	H <sub>2</sub> SO <sub>4</sub> + MT and IP ox. prod.	13% of MT emissions	71%		43%*	Global

(2021). Some studies have paid special attention to sub-10- or even sub-3-nm particle growth with a general conclusion of smaller sensitivity to the exact GRs and vapors contributing to the growth at these small sizes (Spracklen *et al.*, 2006; Lee, Pierce, and Adams, 2013; Dunne *et al.*, 2016). This is similar to the relatively small impact of considering ELVOC contributions to the particle growth (Makkonen *et al.*, 2009, 2014; Patoulias and Pandis, 2022). However, the effect of ELVOC can show significant differences in different models (Sporre *et al.*, 2020). Tröstl *et al.* (2016a) found that locally the sensitivity to including organics in the earliest growth (1.7–3 nm) can be up to  $\pm 50\%$ , though in most areas it is smaller than 10%. We conclude that while most models predict that the sensitivity to organic growth is less than half of the total sensitivity to NPF, the sensitivity varies significantly between different models and simulation setups [testing the effect of different SOA yields, different SOA precursors, or vapors of different volatility; see Sporre *et al.* (2020)], implying that future work on the sensitivity of organic growth in ESMs is still of the utmost importance.

Keep in mind that there generally could be further sensitivity of the CCN predictions to the treatment of organic species, for example, in the conditions of the preindustrial atmosphere (Carslaw *et al.*, 2013). Moreover, the influence of other modeled processes and aerosol properties on the importance of NPF and particle growth should be assessed. Williamson *et al.* (2019) suggested that a too efficient wet deposition in climate models reduces the possible impact of upper tropospheric nucleation and growth on boundary layer clouds, resulting in an underestimate of the influence of upper tropospheric NPF and subsequent growth to the CCN budget. Furthermore, organic growth might not be the only important growth agent besides sulfuric acid, but other vapors such as nitric acid, MSA, and  $\text{HIO}_3$  need to be investigated in the future. Finally, it is also not resolved under which conditions NPF and subsequent growth actually increase CCN activation in clouds, as several modeling studies suggest that NPF may both increase and suppress cloud droplet activation (Roldin *et al.*, 2019; Blichner, Sporre, and Berntsen, 2021).

### C. Testing the sensitivity to early growth in Earth system models

As summarized, the majority of the past large-scale modeling studies did not focus on the role of sub-25-nm particle growth *per se*, but instead looked at the fraction of particles from NPF under various assumptions on the growth. Furthermore, the majority of the studies listed in Table II and reviewed in Sec. V.A are conducted using chemical transport models instead of coupled climate model setups. The latter would ideally be required to investigate how changes in nanoparticle growth reflect on, for instance, cloud droplet number concentrations or radiative forcing estimates. Finally, the varying model setups and output parameters in the studies in Table II make direct comparisons of past investigations challenging. Only a few of these studies (Makkonen *et al.*, 2009; D'Andrea *et al.*, 2013; Scott *et al.*, 2015; Patoulias *et al.*, 2018) presented results from systematically varying only the factors influencing nanoparticle growth. We therefore conduct a set of dedicated simulations with three global models contributing to the Coupled Model Intercomparison

Project 6 (CMIP6), and therefore being representative of a wide range of atmospheric models that include detailed aerosol microphysics: NorESM, ECHAM, and TM5, where the first two are ESMs and TM5 is the atmospheric chemistry module of an ESM (EC-Earth). For the purpose of this review, we do simulations with fixed sea surface temperature and sea ice, and thus not fully coupled climate simulations. For the interpretation of the model results, we have conducted simulations that are as similar as possible to all models and that output the same variables (CCN at varying supersaturations,  $N_{10}$ , and  $N_{100}$ ) for comparison with each other.

## 1. Model descriptions

### a. NorESM (OsloAero and OsloAeroSec)

Two versions of the aerosol scheme in NorESM are included here: OsloAero (Kirkevåg *et al.*, 2018; Seland *et al.*, 2020) and OsloAeroSec (Blichner *et al.*, 2021). We first describe what they have in common: Both versions have SOA formation only from biogenic sources. Emissions of biogenic volatile organic compounds (BVOCs) are calculated using MEGAN2.1 (Guenther *et al.*, 2012) and are categorized into two tracers, monoterpene and isoprene. Oxidation is subsequently calculated for reactions with OH,  $\text{O}_3$ , and  $\text{NO}_3$ ; see Karset *et al.* (2018) for details. Each of these reactions has a certain yield of condensable organics: 5% for isoprene and 15% for monoterpenes. Both model versions treat organics as essentially nonvolatile but include a treatment of volatility by two tracers that participate in the growth of particles in different size ranges and processes. The first, called low volatile, is produced only through monoterpenes reacting with ozone and can participate in nucleation and early growth. The second, named semivolatile, is produced through all the other reactions and can condense only onto particles of larger sizes. OsloAero parametrizes all particle growth below 23.6 nm based on Lehtinen *et al.* (2007) and lets only the low volatile tracer participate in the growth below this diameter. OsloAeroSec, on the other hand, combines the original OsloAero scheme (which is similar to a modal scheme) with a sectional scheme for the smallest particles that are not modeled explicitly in OsloAero. Additional differences to the original scheme include a nucleation scheme updated from that of Paasonen *et al.* (2010) to that of Riccobono *et al.* (2014).

### b. TM5

In TM5, the SOA has been added to the original M7 model (Vignati, Wilson, and Stier, 2004) in four soluble modes (nucleation, Aitken, accumulation, and coarse) and the insoluble Aitken mode. The SOA is produced from its gas precursors isoprene and monoterpene, of which natural emissions are derived from MEGANv2.1 (Guenther *et al.*, 2012; Sindelarova *et al.*, 2014), and biomass-burning emissions are from the inventory provided by Van Marle *et al.* (2017). The two precursors can be oxidized by OH and  $\text{O}_3$  to form ELVOC and SVOC. The ELVOC is considered to first participate in new particle formation processes that include four parametrized phases of the formation of 5 nm particles. The formation rate of 1 nm particles  $J_{\text{BHN}(1)}$  was first calculated with the binary homogeneous water–sulfuric acid

nucleation method (Vehkamäki *et al.*, 2002) based on which the formation rate of 1.7 nm particles  $J_{\text{BHN}(1.7)}$  was calculated with the condensation of ELVOC and  $\text{H}_2\text{SO}_4$  (Kerminen and Kulmala, 2002). After that an additional formation rate of 1.7 nm particles  $J_{\text{RICCO}(1.7)}$  associated with ELVOC and  $\text{H}_2\text{SO}_4$  (Riccobono *et al.*, 2014) was added to  $J_{\text{BHN}(1.7)}$ . Finally, the formation rate of 5 nm particles based on  $J_{\text{RICCO}(1.7)} + J_{\text{BHN}(1.7)}$  was calculated again by Kerminen and Kulmala (2002) with ELVOC and  $\text{H}_2\text{SO}_4$  as condensing vapors.

The remaining ELVOC after the nucleation processes then condenses onto existing aerosol particles in all soluble modes and the insoluble Aitken mode, and the mass distribution follows the kinetic approach (Spracklen *et al.*, 2010). The SVOC does not participate in new particle formation processes and thus completely condenses onto three larger soluble modes (Aitken, accumulation, and coarse) and the insoluble Aitken mode with the equilibrium approach (Pankow, 1994). All of these condensation processes occur within one time step (1 h), so the transport of ELVOC and SVOC is not calculated in the model. More details were described by Bergman *et al.* (2022).

### c. ECHAM

Like TM5, ECHAM describes an aerosol population with M7 microphysics (Vignati, Wilson, and Stier, 2004). SOA formation is described by nonreversible condensation of BVOC oxidation products: ELVOCs and SVOCs are formed via OH and  $\text{O}_3$  oxidation of monoterpenes and isoprene, as described by Jokinen *et al.* (2015). Only ELVOCs can contribute to aerosol growth in the nucleation mode ( $< 10$  nm) via kinetic condensation or an increasing GR in early growth parametrization (Kerminen and Kulmala, 2002) that is applied between 2 and 3 nm in ECHAM. Here we apply nucleation mechanisms developed by Vehkamäki *et al.* (2002) and Paasonen *et al.* (2010).

## 2. Model results

To test the sensitivity of the models to early growth by organics, we run the following simulations:

- *CTRL (all models)*.—The default version of the model with the inclusion of organics in nanoparticle growth as previously described.
- *NoOrgLeh (OsloAero and OsloAeroSec)*.—No organics in the Lehtinen parametrization, i.e., in the growth below 23.6 nm (OsloAero) and below 5 nm (OsloAeroSec).
- *NoOrg10 (OsloAeroSec, TM5, and ECHAM)*.—No organics in growth of particles smaller than approximately 10 nm (nucleation mode).
- *NoOrg25 (OsloAeroSec)*.—No organics in growth of particles smaller than approximately 25 nm (nucleation mode).
- *NoOrg39 (OsloAeroSec)*.—No organics in the sectional scheme (below 39.6 nm).
- *NoOrgAit (TM5)*.—No organics on Aitken-mode particles.

The simulations are not the same for all of the different models, due to their constraints from their setups. All

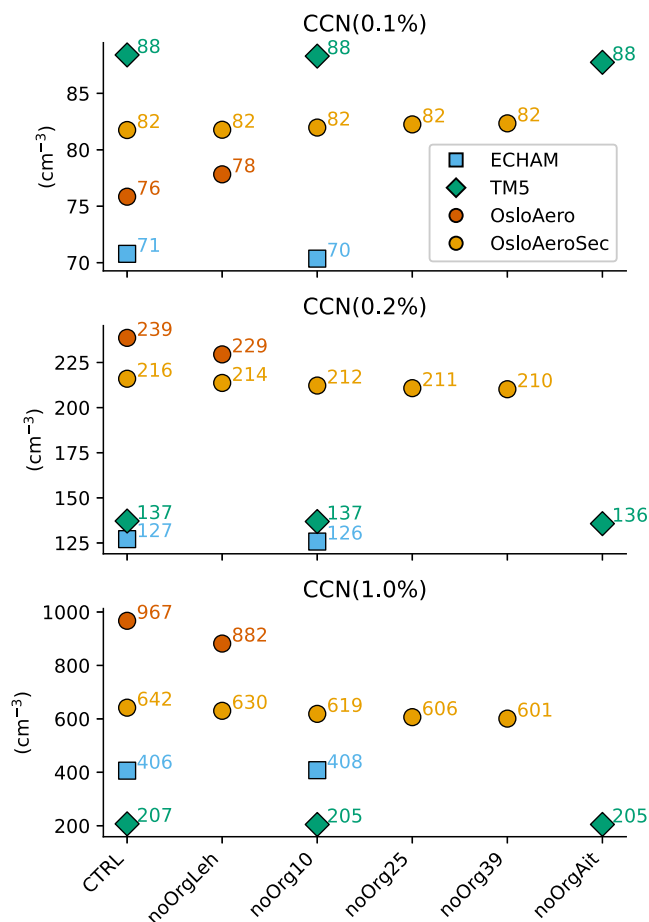


FIG. 9. Global average concentrations of CCN at 0.1%, 0.2%, and 1.0% supersaturation in simulations with different treatments of organics in the early growth of particles for models NorESM, TM5, and ECHAM. Results are global averages for values below 850 hPa and are weighted by the pressure difference in each grid box. Note that ECHAM results are calculated from mixing ratio [1/kg (air)] to concentration (1/cm<sup>3</sup>) by assuming a standard temperature (273.15 K) since the actual temperature was not available as an output.

simulations were conducted for a full year in 2009 (NorESM and TM5) and 2010 (ECHAM) and used elements of meteorology from ERA-Interim reanalysis data (European Centre for Medium-Range Weather Forecast) and emissions corresponding to historical simulations for CMIP6.

In general the models show medium sensitivity in global CCN to the treatment of nucleation mode growth but vary considerably among each other (more than a factor of 5 for CCN at 1.0% supersaturation). Figure 9 shows the globally averaged CCN at 0.1%, 0.2%, and 1.0% supersaturations and how it changes in the different runs. For supersaturation 0.2%, all models show a decrease in CCN with reduced influence of organics in early growth. However, the change is below 5% in all cases, with OsloAero showing the largest change. On the other hand, for 0.1% the two NorESM models (OsloAero and OsloAeroSec) show a slight increase (not visible for OsloAeroSec). This is due to the fact that the reduced number of new particles forming leads to higher growth for the larger particles, thus making it easier for them to activate at low

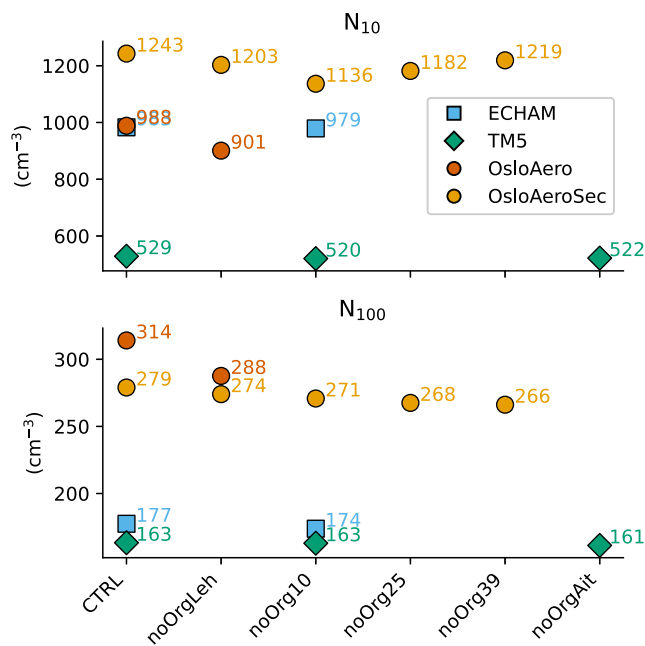


FIG. 10. Global average concentrations of  $N_{10}$  and  $N_{100}$  in simulations with different treatments of organics in the early growth of particles for models NorESM, TM5, and ECHAM. The results are global averages for results below 850 hPa and are weighted by the pressure difference in each grid box. Note that for TM5 and ECHAM,  $N_{10}$  is estimated as the sum of the Aitken modes and above and  $N_{100}$  is estimated as the sum of the accumulation modes and above.

supersaturations; see Blichner, Sporre, and Berntsen (2021) for a thorough discussion. TM5 shows essentially no change for the lowest supersaturations, while ECHAM shows a slight reduction. Last, for a supersaturation of 1.0% (bottom panel in Fig. 9) TM5, OsloAero, and OsloAeroSec show decreases in CCN with a decreased contribution of organics in growth (up to 10%), which is consistent with reductions in Aitken and accumulation mode particles from NPF. On the other hand, ECHAM has a slight increase, which may be due to an increase in Aitken-mode particles and an increase in median diameter of the accumulation mode in ECHAM (likely due to more available condensable vapors to grow the particles). Note, however, that the regional increase in Aitken-mode particles may be related to particles staying longer in the nucleation mode and thus forming in regions with longer lifetimes. Another notable point is that we do not see the same effect in TM5, despite both having the same aerosol scheme (M7).

For particle number concentration (Fig. 10), the panel for  $N_{100}$  looks similar to that for CCN at 0.2% supersaturation, as expected. For  $N_{10}$ , OsloAero shows an approximately 10% decrease when organics are neglected in early growth, while the changes in TM5 and ECHAM are negligible. OsloAeroSec has a weaker decrease in  $N_{10}$  than OsloAero and also shows some nonlinearities with decreased organics in early growth (toward the right). These nonlinearities likely are related to different treatments of loss rates in the different size ranges, and therefore changes in particle lifetime.

Despite the global averages showing a weak response in CCN to removal of organics in early growth, the local effects

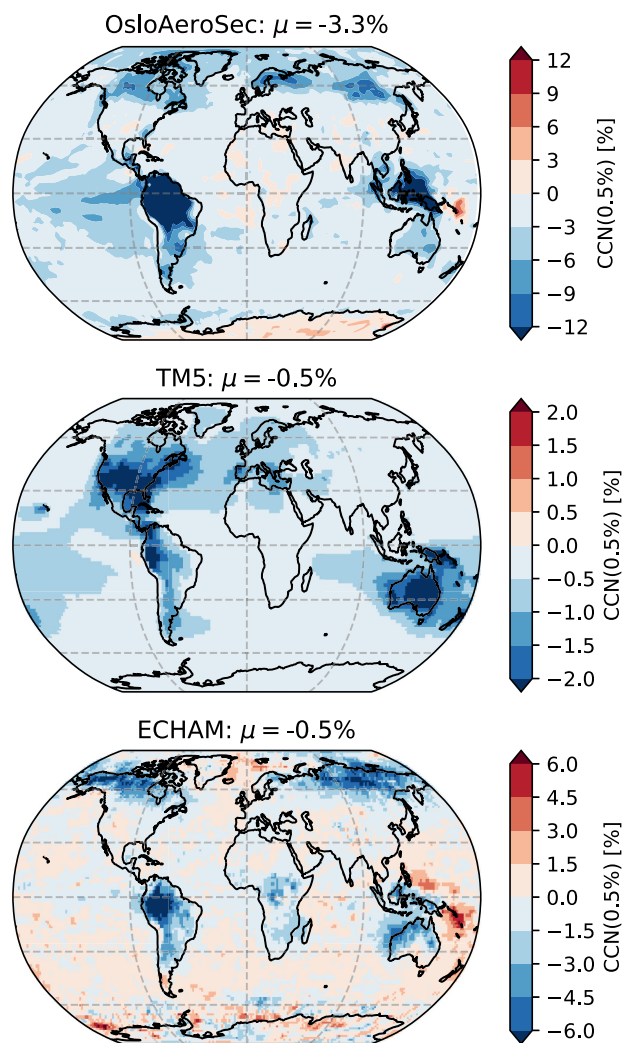


FIG. 11. Relative change in CCN at 0.5% supersaturation when organics are excluded from growth below 10 nm in NorESM, TM5, and ECHAM. The results are for averages below 850 hPa and are weighted by the pressure difference in each grid box.

are in some cases stronger. This is illustrated in Fig. 11, which shows the map of relative changes in CCN concentrations at 0.5% supersaturation in OsloAeroSec, TM5, and ECHAM when organics are removed from growth below 10 nm. For OsloAeroSec local changes can be well beyond 10%, and for ECHAM they are up to approximately 5%. For TM5, however, the change rarely exceeds approximately 3%. Note also the difference in spatial patterns in the response. The largest negative responses in OsloAeroSec and ECHAM are over the boreal forest zone and in typical tropical rain forest zones. On the other hand, TM5 has little response over the boreal forests, and more over Australia and the U.S. It is also noticeable that ECHAM has a weak positive response over most ocean regions, thus compensating for some of the negative responses in the global average.

These results demonstrating the relatively modest sensitivity to nanoparticle growth seem to be in line with previous studies applying somewhat comparable simulation experiments (Makkonen *et al.*, 2009; D'Andrea *et al.*, 2015; Scott *et al.*, 2015; Patoulias *et al.*, 2018; Patoulias and Pandis,

2022). However, as in the case of Tröstl *et al.* (2016a), the local effects can be considerable. Moreover, the modest average sensitivity results mostly from the low sensitivity over the open oceans, where organics are expected to have a minor impact on growth, but other species such as MSA and HIO<sub>3</sub> could potentially contribute but are not typically accounted for in current models. Last, the differences between OsloAero and OsloAeroSec also reveal that the CCN concentrations are sensitive to the dynamic treatment of nucleation mode growth [up to 25% differences in CCN(1.0%)], which is the major difference between these two simulations (Blichner *et al.*, 2021). This indicates that future conceptual work might be necessary to improve model predictions for growth.

## VI. CONCLUSION AND OUTLOOK

### A. Summary

In this review, we analyzed advances in the research on atmospheric sub-25-nm nanoparticle growth over the last two decades. During that time a rapidly increasing number of studies have observed ambient NPF around the globe. The general characteristics of particle growth in regional NPF events can be summarized as follows (Sec. IV.A): The bulk of site-specific median GR observations are within the range of 1–10 nm h<sup>-1</sup>, but with apparent local and temporal differences for larger GRs (> 3 nm) and with faster growth in polluted environments and during the summer (for most midlatitude locations). In contrast, less seasonal variation for the smallest particles (< 3 nm) is observed, where GRs rarely exceed 5 nm h<sup>-1</sup>, which is in line with the overall tendency of increasing GR with increasing size. The limited variation in global GRs is a noteworthy observation because there is a wide range of low-volatility vapors that can contribute to growth. This points toward a still limited mechanistic understanding of the growth processes and potential shortcomings of the methodology used, thereby preventing theoretical mass closure for the gas-to-particle conversion of aerosol growth. First, accurate particle-size-distribution measurements in the sub-10-nm range are highly challenging (Sec. III.A.4). Second, gas- and particle-phase chemical composition measurements are sparse and subject to high uncertainty (Sec. III.A.4). And third, we pointed out that different definitions of the particle GR exist, one with respect to the growth of a single particle and one with respect to the growth of a particle population (Sec. II). This results in ambiguities among the different methods used to derive GRs (Sec. III) and how they are used within experimental studies (Sec. IV) or in large-scale models (Sec. V). Specifically, coagulation- or stochastic-population dynamics can result in significant differences between the analytical methods for GR derivation from experimental data and the GR formulation in models. The former mostly obtain population average GRs that can be corrected for coagulation and only implicitly include stochastic effects (Sec. III.B). The latter often use single-particle GRs derived from vapor concentrations, and the population dynamics are only calculated within highly simplified modal schemes (Sec. V.A). Despite these methodological challenges, the aerosol community has achieved significant advances in

exploring the different nanoparticle growth mechanisms; the main results are summarized in Fig. 12. This review shows that sulfuric acid, which is thought to be the globally dominant agent in particle nucleation, contributes on only a minor level to the subsequent growth, with its contribution decreasing with particle size and from polluted to cleaner environments. Growth from sulfuric acid can be described using a kinetic process (above 2 nm), where the gaseous sulfuric acid condenses upon collision and the evaporation of sulfuric acid from particles is negligible. This means that the particle GR is determined solely by the vapor-particle collision rate (Sec. IV.C.1). The same is also highly likely for iodic acid, which was recently identified as the most important iodine species contributing to growth in the marine boundary layer and/or polar regions. However, even for these simple systems of individual acids contributing to nanoparticle growth, several challenges remain: The role of water needs to be elucidated (Sec. IV.C.2), especially when acid-base interactions are present (Sec. IV.C.3). The stabilizing nature of strong bases (such as dimethylamine) can result in a purely kinetic process of cluster formation from the smallest cluster onward. This can lead to high concentrations of small molecular clusters subsequently contributing to the growth by coagulation (Sec. IV.C.4), but difficult to detect quantitatively, complicating the closure between observed gas-phase acids and GRs.

Other more volatile acids such as MSA, nitric acid, and small organic (di)acids are expected to contribute to growth as inferred from laboratory studies, theoretical calculations, or particle-phase composition measurements (Sec. IV.C.5). However, they are rarely measured directly in the gas phase, even if they are often several orders of magnitude more abundant than sulfuric acid. These species almost certainly require an interplay with atmospheric bases and water via the formation of salts in the particle phase to essentially lower their evaporation rates and enable net condensation of both the acids and bases onto nucleation mode aerosols. But while the presence of organic and inorganic salts in ambient particle-phase samples was measured at a variety of locations, the mechanistic understanding of the contributions of MSA, nitric acid, and small organic acids to atmospheric nanoparticle growth remains elusive. This is due to our incomplete understanding of particulate phase acid-base neutralization, its dependency on the aerosol water content, the solution chemistry, and the unknown vapor pressures of both the acids and the formed salts.

The most dominant contributor to continental boundary layer aerosol growth are OOMs (Sec. IV.C.6). This is indicated by the higher summertime GRs (due to higher organic precursor emissions) and the widely observed increasing GRs with size (due to the multicomponent Kelvin effect enabling consecutively less oxygenated, and hence more volatile, OOMs to condense on less curved particle surfaces). The overwhelming variety of OOMs formed in the atmosphere, however, is still a challenge for both their experimental detection and their growth modeling. While the complexity is now often reduced along the volatility axis by lumping compounds together and focusing on the degree of oxygenation (Donahue *et al.*, 2011), the vapor pressures assigned to individual organic compounds are still subject to uncertainties

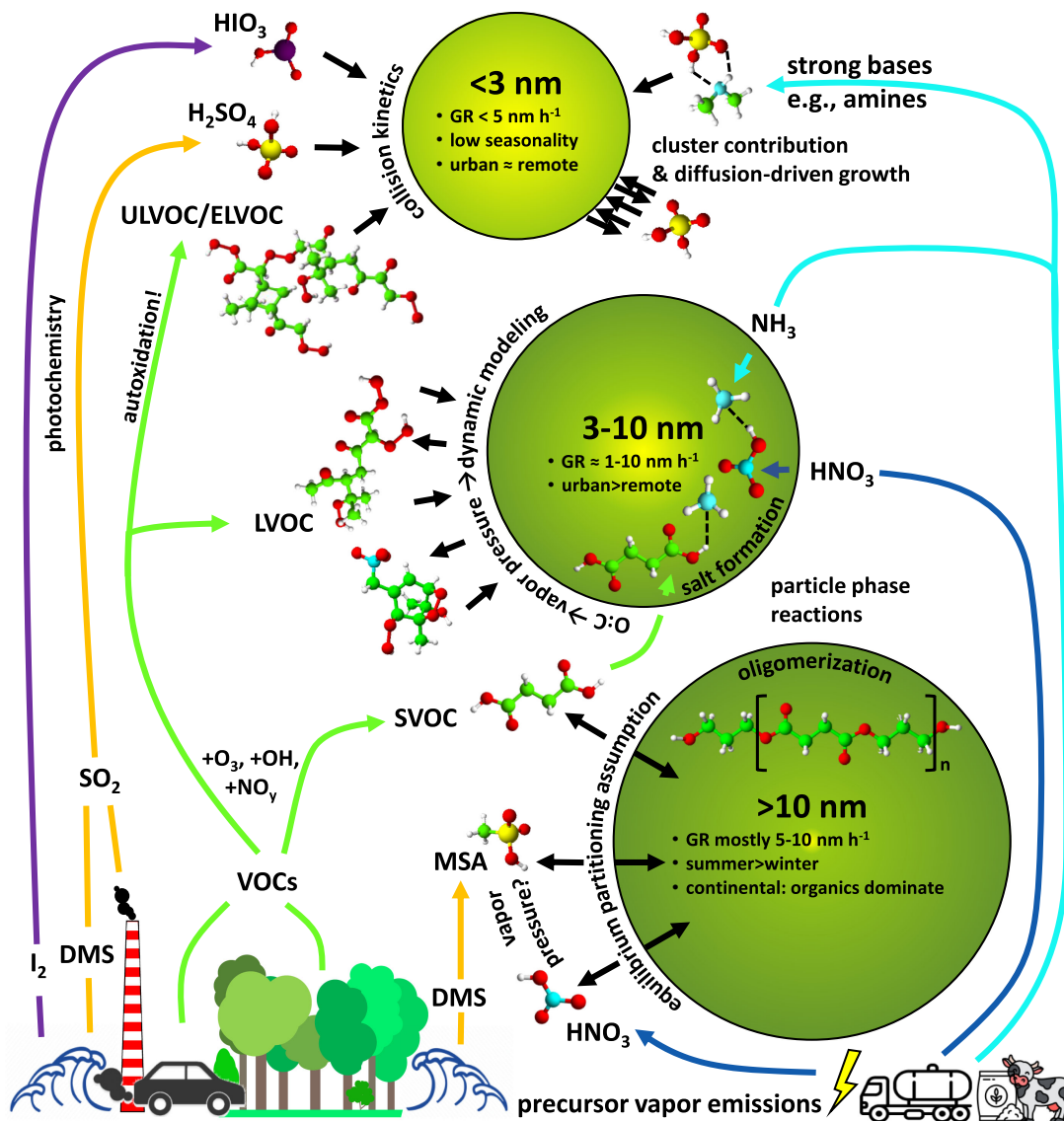


FIG. 12. Summary over the most important atmospheric nanoparticle growth contributors (from sources to trace vapors) and involved processes. The anthroposphere, the biosphere, and the marine environment emit volatile gases into the atmosphere, which can lead to the formation of different vapors contributing to growth. At the smallest sizes ( $< 3\text{ nm}$ ), the amount of potential contributing vapors is limited to ultralow-volatility compounds. Collision kinetics, cluster condensation, and stochastic effects become observable within these nonreversible vapor accommodation processes. At larger sizes ( $3\text{--}10\text{ nm}$ ), the condensing vapors often already exhibit significant reevaporation, as a larger variety of higher vapor pressure compounds can overcome the Kelvin barrier. They are difficult to estimate, especially the wide variety of organics. Particle-phase processes start to be more important but could be even more decisive at larger sizes ( $> 10\text{ nm}$ ). At that size semivolatile vapors start to contribute to growth, while their gas-particle phase transition is often modeled only within the equilibrium assumption due to its simplicity. However, note that all processes relevant for smaller sizes typically still occur for larger particles, and the exact transitions between these regimes are not sharp and potentially depend on the environment where the growth is studied.

of at least one but potentially even several orders of magnitude. Moreover, our understanding of the gas-phase chemistry leading to OOM formation is still far too limited. Our knowledge of individual oxidation pathways from a single precursor-oxidant system has significantly improved for some of the most dominant atmospheric VOCs through the discovery of atmospheric autoxidation as a driver for HOM formation and the importance of multigeneration OH attacks for aromatic precursors (Sec. IV.C.7). However, the interplay of different organics and oxidants, in particular, has recently

been investigated in more detail and could be decisive for the resulting GRs due to its strong influence on the volatility distribution of the produced OOMs. In addition, particle-phase chemistry of these compounds remains poorly explored but almost certainly occurs frequently in nanoparticles, resulting in substantial oligomerization of the organic compounds and eventually also in organosulfate formation or acid-catalyzed reactions.

The large variety of complex physicochemical processes resulting in nanoparticle growth can evidently not be

represented in large-scale models, both due to limited understanding (as previously discussed) and because computational costs need to be limited. First, we showed that most large-scale models use highly simplified representations of the aerosol size distribution with growth at the smallest sizes often parametrized with survival schemes (Sec. V.A), leading to the aforementioned ambiguities resulting from the different definitions of a GR (Sec. II). Second, the large variety of different growth agents is not represented in models, which, besides purely kinetic condensation of sulfuric acid, mostly treat only the condensation of organics (Sec. V.A). For the latter, yields of OOM tracer compounds are often calculated from pre-calculated oxidant fields and some lumped surrogate precursors. More recent model approaches also group the OOMs along the volatility axis, as suggested by the experimental results, but with various degrees of complexity and with many using only two OOM products. Condensation of organics is then treated within models as purely kinetic, with a partitioning approach, or using a hybrid of the two methods, with the partitioning approach typically underestimating the organic contribution to nucleation mode growth. Our analysis of the literature revealed that studies directly investigating the model sensitivity to growth processes or perform comparisons between modeled and observed GRs are limited (Sec. V.B). Most models look into the effects of either the incorporation of NPF *per se* or the overall presence of condensable organics. Nevertheless, these studies show a significant sensitivity of the number of CCN (around 50%) to NPF and the presence of organics (up to half of the sensitivity to NPF). To further test the sensitivity of modern ESM we conducted a sensitivity test on the role of OOMs in growth with four representative models (Sec. V.C). We found significant intermodel variation on global CCN numbers, which, for two models, could be attributed to the representation of the aerosol size-distribution dynamics, highlighting the importance of removing ambiguities from GR definitions. The global CCN averages showed only a modest sensitivity on the incorporated organic condensation scheme, which, however, had some significant local influence.

## B. Recommendations for future growth studies

### 1. Experimental requirements

The first fundamental requirement for atmospheric growth studies that yield additional insights compared to the current body of knowledge is the deployment of instrumentation providing high-quality size-distribution data, preferably covering the size range 1.5–1000 nm. As seen in the review of the currently available instrumentation (Sec. III.A), recent advances have particularly improved our ability to measure the size distribution below 10 nm. The usage of such instrumentation in future growth studies is therefore highly encouraged. In particular, electrical mobility spectrometers with diethylene glycol-based detectors for sub-3-nm size-distribution measurements should be deployed more widely, as they achieve stable size classifications and can potentially provide the highest size and time resolution of sub-10-nm size-distribution instruments. Future instrumental setups for particle growth measurements should put more emphasis on

the role of water. However, as drying procedures might cause significant particle loss in the sub-10-nm range, resulting in a lower instrumental sensitivity, the role of water might need to be investigated indirectly, for instance, via dedicated aerosol liquid water content measurements.

Linked to the aerosol hygroscopicity is the knowledge of the gas- and particle-phase chemical composition. To advance our understanding of nanoparticle growth in the atmosphere, we need more insight into the responsible mechanisms, and this calls for complementary measurements, i.e., simultaneous quantification of condensable vapor concentrations, nucleation mode particle composition and dynamics (such as coagulation and nucleation rates, sink values, and their linkage), or at least ambient parameters such as air mass origin, temperature, and relative humidity. The baseline contribution of sulfuric acid should always be estimated, especially as the usage of sophisticated proxy methods can provide good estimates if verified for a specific location (Dada *et al.*, 2020a). Direct measurements are preferable and can also facilitate simultaneous measurements of condensable organics. Here, however, the emphasis should be put on ELVOC and LVOC (and to some extent also SVOC) detection when nanoparticle growth is studied, which means that the nitrate chemical-ionization scheme might be limited and that other approaches covering that volatility range should be deployed more widely. We also see a serious need to reduce systematic uncertainties in (E)LVOC compound detection, which requires higher resolving power at high sensitivities for compound identification and subsequent careful calibration of their charging efficiencies for absolute quantification. Apart from condensable OOMs, more focus should be put on the measurement of possible other agents in nanoparticle growth such as small organic acids, nitric acid, MSA, and HIO<sub>3</sub>, which also might require the application of complementary ionization schemes. In addition, the gas-phase measurements need to be further supported by measurements of the particle-phase chemical composition, where the instrumentation has to be further optimized for enhanced sensitivity to the low particulate mass in the nucleation mode.

With the full size distribution ranging from 1.5 to 1000 nm measured in a consistent way together with condensable vapor concentrations or other relevant ambient parameters, future studies should always try to extend measurement periods, going toward long-term observations (Kulmala, 2018). If long-term measurements are not feasible, enough NPF events need to be collected to provide sufficient statistics to estimate the variance in GR and related measurements and to put case studies into the perspective of the general characteristics at that measurement site. Therefore, every study should mention the underlying statistics in terms of median and 25th to 75th quantiles (more indicative than mean and standard deviations, which could be biased high by a few rapid growth events). If data related to the growth measurements are available, for instance, condensable vapor concentrations, formation rate, CS, or ambient parameters, they should be evaluated over the same time intervals where growth was measured and also reported with median and corresponding quantiles. Note that this might result in different time intervals for different GR size intervals (although they are not necessarily needed for the formation rate) if an integrative GR measurement approach is

chosen. In that case, the GR should be size resolved as much as possible, but if a high precision, as expected with GDE-based analysis techniques, is not feasible, the size dependency should at least be reported to some extent. Many studies have focused on the intervals of 1.5–3, 3–7, and 7–15/25 nm in order to identify possible size-dependent trends in the GRs, which is useful for study comparability.

Our review has shown that GR analysis, especially for sub-5-nm particles, should if GDE-based methods are not at hand rely mainly on the appearance time or maximum concentration methods instead of modal GRs; see Sec. III. Intercomparison between different methods is recommended when GRs of particles larger than 5 nm are calculated in ambient NPF events. We also recommend using the total particle number size distribution for sizes smaller than 3–5 nm as the basis for GR analyses, not ion distributions, as the complex interaction schemes between ions and particles can lead to ion GRs that are not representative of the growth of the total particle population in the sub-3-nm range (Gonser *et al.*, 2014; Carracedo, Gonzalez *et al.*, 2022). In the same sense, we suggest the application of methods disentangling the contributions of coagulation suggested by R. Cai *et al.* (2021a), especially for heavily polluted environments with a high coagulation sink. Comparisons to GDE-based GR analysis methods would also be highly beneficial. Careful estimates of the uncertainties in GR measurements should at least be reported (Dada *et al.*, 2020b; Ozon, Stolzenburg *et al.*, 2021). In addition, considerations of the effects of coagulation scavenging, self-coagulation, or growth driven by diffusion in the particle-size space on the measured GRs should be included. In the same sense, studies should also include a discussion of the meteorology and air mass history to put the observed growth into a spatial perspective and avoid bias due to effects caused by air mass changes.

Ideally an increasing amount of high-quality growth studies should induce future work on chamber experiments, where growth processes can be studied under controlled conditions. The experimental recommendations for such studies are equal to the aforementioned ambient measurements and protocols for successful chamber experiments were recently detailed (Dada *et al.*, 2020b). Here we point out that chamber experiments should refrain from boosted oxidation chemistry and should represent ambient boundary conditions such as sink rates as closely as possible. There are significant differences between smog-chamber and similar-to-ambient laboratory experiments (Chuang and Donahue, 2017), which need to be addressed when results from chambers are transformed into model input. However, when only growth processes  $> 3$  nm are studied, experiments most likely do not need to reach the purity levels of chamber experiments exploring nucleation mechanisms.

## 2. Recommendations for model setup

The varying model and simulation setups (for instance, outputting particle numbers versus CCN, or studying contribution of NPF versus direct sensitivity to growth or inclusion of SOAs in the model) continue to make direct comparison of the different studies challenging. Hence, no unambiguous protocols for conducting such simulations exist

but would be desirable for yielding robust conclusions about the role of NPF and nanoparticle growth in CCN budgets in the atmosphere. A baseline for all NPF-related large-scale modeling studies should be comparisons of runs with and without nucleation. With respect to nanoparticle growth, we acknowledge that its representation is seldom the primary goal of any atmospheric model. However, it is recommended to test any new model application with a focus on size-resolved aerosol concentrations and their impacts on CCN against field observations of GRs; see Fountoukis *et al.* (2012), Westervelt *et al.* (2013), and Makkonen *et al.* (2014). Keeping in mind that definitions of growth in models and experiments often differ (Sec. II) and modal model schemes do not provide a direct output of GR, at least comparisons of size-segregated number concentrations  $N_{10}$ ,  $N_{50}$ , and  $N_{100}$  with field observations should be evaluated. Furthermore, it is favorable to support such evaluation by comparisons of formation rates, CS and CoagS. The increasing wealth of global observations of aerosol particle number size distributions provides an opportunity for such studies.

To facilitate the previously outlined comparisons of different models with respect to nanoparticle growth, it would be ideal for model studies to agree within their typical output. Therefore, we recommend to report at least  $N_{10}$  (or Aitken mode and above),  $N_{100}$  (or accumulation mode and above), and GR contributions from different components (sulfuric acid, organics, etc.) if they are used as inputs in particle survival calculations. If the model is able to quantify CCN concentrations, at least two supersaturation levels should be reported (0.2% and 1.0%).

We have observed that the aerosol dynamics in the sub-25-nm range can be influenced by a variety of processes other than condensational growth (Secs. IV.B and IV.C). Sectional modeling approaches might be better at capturing such dynamics, as they are based on the GDE [Eq. (11)]. This is in contrast to the fact that many models still use the simple promotion of particles through a size range using an analytical survival probability formula [for instance, Eq. (14)], which was initially designed for small sizes (less than 3 nm) under controlled conditions and might not be applicable within the entire nucleation mode. However, even at the smallest sizes, its application might be biased, as the input GR calculated from condensational growth accounts for neither cluster dynamics (Sec. IV.C.4) nor growth driven by diffusion in the particle-size space (Sec. IV.B.2). Ideally studies should systematically assess the strength of the potential errors introduced by the simplifications mentioned in this review (Sec. V.A). Comparisons against not only measurements but also accurate aerosol dynamics models could be beneficial here.

Apart from population dynamics, the condensable vapors included in any atmospheric model bear significant importance for representing nanoparticle growth. Carslaw, Lee *et al.* (2013) found that for uncertainties in  $N_{50}$  processes that control the availability of gas-phase nucleating vapors matter more than nucleation rates in themselves. Besides sulfuric acid, organics seem to be especially important in the continental atmosphere, and their inclusion is an important component for correctly predicting nanoparticle growth and CCN (Sec. V). Detailed sensitivity tests of the included

growth processes (as in Sec. V.C) are preferred for all future studies explicitly targeting at estimates of the role of NPF in the climate system because growth and nucleation are equally important for it (Sec. V.B). This also holds for potentially important additional vapors that should be included in future model development, such as nitric acid, MSA, and  $\text{HIO}_3$ . Ultimately progress through detailed molecular-level studies (including aerosol process models) on the detailed properties (such as saturation vapor pressures, mixture thermodynamics, and multiphase chemistry) of condensable vapors (Sec. IV.C) should eventually translate into methodological large-scale model studies that target specific processes (like nanoparticle growth).

Finally, model developments should also be evaluated in past and/or future emission scenarios, where the effects may be substantially different. Earlier studies have already shown that changes to NPF parametrizations play out much differently in preindustrial or future emission scenarios than in present-day simulations (Gordon *et al.*, 2016, 2017). We recommend at least running preindustrial simulations because they impact the estimated effective anthropogenic radiative forcing and because future scenarios usually include reductions in aerosol emissions, and the effects would likely go in the same direction.

### C. Future work

With the recommendations for both experimental studies and models in place, we will be able to reduce the ambiguities arising from the different definitions in nanoparticle growth in the future. From the experiment side, future work should focus here on the improvements of our measurement techniques toward lower detection limits and higher temporal resolution, as high-quality size distributions can promote the application of GDE-based analysis methods that can resolve many problems associated with the collective methods (Sec. III.B). At the same time, for most of these GDE-based methods dedicated studies on the sensitivity toward fluctuating particle number concentrations need to be further investigated. From the modeling perspective, future work remains on evaluating whether parametrizations for sub-3-nm growth that account for cluster dynamics and growth driven by diffusion in the particle-size space are needed to better describe the population effects on particle growth. Generally the concept of particle survival laid out in Sec. II.B is challenged by our observations under highly polluted conditions (Kulmala *et al.*, 2017) and might require new theoretical concepts for both experimentalists and modelers. In that sense, keep in mind that models can be sensitive only to processes that are included in the models. New critical analysis of the model sensitivity results presented here is therefore warranted, as novel findings with robust observational evidence and theoretical interpretations emerge.

Large-scale models have only recently started to incorporate more detailed organic condensation schemes, with dynamic condensation approaches coupled to a variety of organic volatilities such as the VBS approach (Donahue *et al.*, 2011). We have also seen that organic gas- and particle-phase chemistry have a large influence on the resulting atmospheric

organic volatility distribution, and hence their condensation behavior (Sec. IV.C.7). Future experimental work needs to find good representations of organic chemistry within such volatility schemes and compare them to ambient organic growth observations in different environments. Organic mass closure in growth processes is far from being achieved, and future measurements need to address this with novel approaches to measure gas-phase organics and particle-phase composition.

The complex particle-phase interactions in the sub-25-nm range need to be investigated in the future by dedicated experiments and process models, which search for limitations or promoting effects in multiphase particle growth. In addition, it needs to be determined whether these compounds are important drivers of growth on a global scale or whether they really are only locally important. This calls for ambient studies at locations difficult to access (the open oceans, the free troposphere, or highly dynamic urban settings), which might be feasible only by novel instrumentation or analysis approaches. On the other hand, models need to judge whether such growth processes are relevant for the size of a model grid box. Care should be taken when considering processes relevant only on smaller scales, which can, however, still be non-negligible (Williamson *et al.*, 2019). Given the global importance of oceans and marine clouds, particularly the investigation of the potential global importance of MSA and iodic acid on the aerosol number, size-distribution dynamics is recommended here.

An important application of detailed understanding of the molecular-scale growth processes (Sec. IV.C) is to also develop the simplest possible ways to represent it without losing the necessary precision required to answer the question at hand. Aerosol process models, in particular, could support the large-scale models in that respect and should be further developed to best represent our experimental findings. Here more work on the quantum chemistry of cluster formation and stability is vital for bringing experiments and process models into better agreement. While such studies are critical for model development and evaluation, there is also the continuous need to use the new and improved large-scale models to target the “big questions” such models are particularly well designed to answer. Such questions could include the magnitudes of feedback within the Earth system (associated, for instance, with biosphere-atmosphere interactions or ocean-atmosphere interactions), impacts of future air quality and climate policies, or links among large-scale circulation, aerosols, and clouds. In such studies nanoparticle growth is only one process in a chain of processes and (while often important) not necessarily the main determining factor (see Table II), in which case some constrained uncertainty is acceptable in return for a reduced computational burden.

To address these big questions from an experimental point of view, a broader coverage on growth measurements on a global scale is urgently required. This could confirm the hypothesis of GR values being limited mostly within  $1\text{--}10\text{ nm h}^{-1}$ , which we laid out in Sec. IV.A and which has only recently begun to be investigated (Kulmala, Cai *et al.*, 2022; Kulmala *et al.*, 2023). This calls for future work on the sensitivity of our GR methods toward fast and low growth to

verify that the limited observations are not an artifact of the underlying methodology. However, the models currently seem to have medium sensitivities to the growth descriptions used when globally averaged parameters such as CCN concentrations are investigated (Sec. V.C). Both the experimental and global modeling data therefore suggest that the atmospheric system is highly buffered against high particle survival probabilities. However, the reason for this has not been entirely revealed and, while models attribute it to the correlation of the sources for particle formation and sink, ambient observations do not find that correlation for the GR and CS, but instead only for  $J$  and CS (Sec. IV.A). On the one hand, that buffering might not even be attributed to the particle survival, but rather to limited overall condensable mass (total organics, for example), to grow the newly formed particles large (from 50 to 150 nm) during their lifetime (on the order of a week for accumulation mode). With higher particle survival in the nucleation mode, that limited condensable mass along their atmospheric trajectory is split up among more particles, resulting in a lower final size. With the CCN ability being a steep function of size, this directly results in a buffering toward high particle survival probabilities. On the other hand, the significant changes in CCN numbers when different aerosol dynamics schemes are included in the same model (Blichner *et al.*, 2021) still point toward the fact that part of that buffering is also due to oversimplifications in the growth description.

While models could still have significant conceptual shortcomings, as previously discussed, experimental observations are highly incomplete. As outlined in Sec. VI.B, studies with a full coverage of the size distribution, condensable vapor measurements, and insights into nucleation mode particle composition are sparse. In addition to the open oceans and the free troposphere (calling for more ship- or aircraft-based studies), large areas of continents are also still underrepresented in experimental studies, for instance, Latin America, Africa, Siberia, and Southeast Asia. Their diverse vegetation systems might induce different growth patterns than corresponding regions on other continents, which are more closely studied. Here fair collaborations aiming for capacity building of local researchers in these regions should be promoted, which also increases the future need for development of low-cost instrumentation for measuring nanoparticle growth with the previously outlined precision. The availability of low-cost equipment could further promote studies that cover larger areas simultaneously, investigating local differences in particle growth and the regional extent of growth processes. The latter could then also ideally be investigated through novel approaches using satellite data.

Altogether we saw that future work on nanoparticle growth still needs to address highly challenging research questions. As of now there is no complete and detailed picture on how atmospheric particles are growing from molecular cluster sizes through the decisive cluster-particle transition regime below 25 nm. Both the physics of condensation and population dynamics and the multiphase chemistry including the gas and particle phase need to be resolved in depth in the future in order to define the importance of nanoparticle growth in the atmospheric system. Laboratory studies, ambient measurements, and the theoretical and large-scale modeling

communities should work more closely together in the future toward resolving the growth of ambient new particles, and this review has set the basis for these developments.

## LIST OF SYMBOLS AND ABBREVIATIONS

NPF	new particle formation
CCN	cloud condensation nuclei
GR (nm h <sup>-1</sup> )	growth rate
PNSD (cm <sup>-3</sup> )	particle number size distribution
VOC	volatile organic compound
SVOC	semivolatile organic compound
LVOC	low-volatility organic compound
ELVOC	extremely low-volatility organic compound
CS (s <sup>-1</sup> )	condensation sink
DMA	differential mobility analyzer
CPC	condensation particle counter
SMPS	scanning mobility particle sizer
DMPS	differential mobility particle sizer
NAIS	neutral cluster and air ion spectrometer
AIS	air ion spectrometer
CI-API-TOF-MS	chemical-ionization atmospheric pressure interface time-of-flight mass spectrometer
GDE	general dynamic equation
SOA	secondary organic aerosol
MSA	methanesulfonic acid (CH <sub>3</sub> SO <sub>3</sub> H)
DMS	dimethylsulfide (C <sub>2</sub> H <sub>6</sub> S)
nns-SO <sub>4</sub> <sup>2-</sup>	non-sea-salt sulfate
HOM	highly oxygenated organic molecule
OOM	oxygenated organic molecule
BVOC	biogenic volatile organic compound
ESM	Earth system model
VBS	volatility basis set
$d_p$ (nm)	particle (mass) diameter
$d_i$ (nm)	condensable vapor (mass) diameter
GR <sub>tot</sub> (nm h <sup>-1</sup> )	total GR of a single particle or particle population caused by condensation and coagulation
GR <sub>cond</sub> (nm h <sup>-1</sup> )	GR caused by condensation
GR <sub>Coag</sub> (nm h <sup>-1</sup> )	GR caused by coagulation
GR <sub>drift</sub> (nm h <sup>-1</sup> )	GR caused by deterministic drift in particle-size space
GR <sub>diffusion</sub> (nm h <sup>-1</sup> )	GR caused by stochastic diffusion in particle-size space
$N_{i/k/p}$ (cm <sup>-3</sup> )	number concentration of vapor $i$ , molecular cluster containing $k$ monomers or particles $p$

$T$ (K)	temperature	$C_{i,p/g/t}$ ( $\mu\text{g m}^{-3}$ )	mass concentration of vapor $i$ in the particle phase or gas phase or total gas plus particle phase
RH (%)	relative humidity	$C_i^*$ ( $\mu\text{g m}^{-3}$ )	effective saturation mass concentration
$R$ ( $\text{J K}^{-1} \text{mol}^{-1}$ )	ideal gas constant	$C_{\text{OA}}$ ( $\mu\text{g m}^{-3}$ )	total organic aerosol mass concentration (particle phase)
$k_B$ ( $\text{J K}^{-1}$ )	Boltzmann constant		
$\beta(i, p)$ ( $\text{cm}^3 \text{s}^{-1}$ )	vapor $i$ particle $p$ collision rate coefficient		
$N_{\text{eq},i}$ ( $\text{cm}^{-3}$ )	effective condensable vapor saturation number concentration		
$N_{\text{eq},0,i}$ ( $\text{cm}^{-3}$ )	condensable vapor saturation number concentration for flat surfaces and pure substances		
$\sigma_i$ ( $\text{N m}^{-1}$ )	surface tension of vapor $i$		
$M_i$ ( $\text{g mol}^{-1}$ or g)	molecular mass of vapor $i$		
$\rho_i$ ( $\text{g cm}^{-3}$ )	density of vapor $i$		
$\gamma_{\text{act},i}$	activity coefficient of vapor $i$ in the particle phase based on mole fractions		
$\gamma_{\text{act},i}^m$	activity coefficient of vapor $i$ in the particle phase based on mass fractions		
$\gamma_k$ ( $\text{s}^{-1}$ )	evaporation rate of cluster containing $k$ monomers		
CoagSrc ( $\text{cm}^{-3} \text{s}^{-1}$ )	coagulation source, i.e., rate of particles produced by coagulation of smaller entities		
CoagS ( $\text{s}^{-1}$ )	coagulation sink, i.e., rate of particles lost by coagulation with other entities		
$n(v)$ ( $\mu\text{m}^{-3} \text{cm}^{-3}$ )	particle number volume distribution		
$P(d_{p1} \rightarrow d_{p2})$	particle survival probability against coagulation scavenging between diameters $d_{p1}$ and $d_{p2}$		
$J$ ( $\text{cm}^{-3} \text{s}^{-1}$ )	new particle formation (nucleation) rate		
CS ( $\text{s}^{-1}$ )	condensation sink for condensable vapors		
Kn	Knudsen number defining the collision dynamics between vapor and particle		
$f(\alpha, \text{Kn})$	Fuchs-Sutugin transition regime correction factor		
$D_{i/p}$ ( $\text{cm}^2 \text{s}^{-1}$ )	diffusion coefficient of vapor $i$ or particle $p$		
$c_{i,p}$ ( $\text{m s}^{-1}$ )	mean thermal velocity of vapor $i$ or particle $p$		
$\eta_{\text{C/FM}}$	collision enhancement factor for the continuum or free-molecular regimes		
A	Hamaker constant describing collision enhancement due to Van der Waals forces		

## ACKNOWLEDGMENTS

We thank Rima Baalbaki, Xu-Cheng He, and Mingyi Wang for the useful discussions. We acknowledge funding through the following projects: ACCC Flagship, funded by the Academy of Finland Grant No. 337549, academy professorship funded by the Academy of Finland (Grant No. 302958), Academy of Finland Projects No. 325656, No. 332547, No. 316114, No. 346370, and No. 356134, Russian mega grant project “Megapolis—Heat and pollution island: Interdisciplinary hydroclimatic, geochemical and ecological analysis” Application Reference No. 2020-220-08-5835, “Quantifying carbon sink, CarbonSink+ and their interaction with air quality,” INAR project funded by the Jane and Aatos Erkkö Foundation, University of Helsinki Three-Year Grant No. 75284132, the Knut and Alice Wallenberg Foundation (Wallenberg Academy Fellowship AtmoRemove Project No. 2015.0162), European Research Council (ERC) projects ATM-GTP (Project No. 742206) and INTEGRATE (Project No. 865799) and the European Union’s Horizon 2020 research and innovation program projects FORCeS (Project No. 821205) and CRiceS (Project No. 101003826), Marie Skłodowska-Curie Grant Agreement No. 895875 (“NPF-PANDA”), and the Vienna Science and Technology Fund (WWTF) through Project No. VRG22-003.

D. S. and R. C. contributed equally to this work. D. S., R. C., and S. M. B. performed the newly introduced analyses and created the figures. All authors drafted and commented upon the manuscript.

## REFERENCES

- Aalto, Pasi, *et al.*, 2001, “Physical characterization of aerosol particles during nucleation events,” *Tellus B* **53**, 344–358.
- Ackerman, Andrew S., Owen B. Toon, Jonathan P. Taylor, Doug W. Johnson, Peter V. Hobbs, and Ronald J. Ferek, 2000, “Effects of aerosols on cloud albedo: Evaluation of Twomey’s parameterization of cloud susceptibility using measurements of ship tracks,” *J. Atmos. Sci.* **57**, 2684–2695.
- Adachi, M., Y. Kousaka, and K. Okuyama, 1985, “Unipolar and bipolar diffusion charging of ultrafine aerosol particles,” *J. Aerosol Sci.* **16**, 109–123.
- Ahlm, L., J. Julin, C. Fountoukis, S. N. Pandis, and I. Riipinen, 2013, “Particle number concentrations over Europe in 2030: The role of emissions and new particle formation,” *Atmos. Chem. Phys.* **13**, 10271–10283.

- Ahlm, L., *et al.*, 2016, “Modeling the thermodynamics and kinetics of sulfuric acid-dimethylamine-water nanoparticle growth in the CLOUD chamber,” *Aerosol Sci. Technol.* **50**, 1017–1032.
- Aitken, John, 1889, “I.—On the number of dust particles in the atmosphere,” *Trans. R. Soc. Edinburgh* **35**, 1–19.
- Albrecht, B. A., 1989, “Aerosols, cloud microphysics, and fractional cloudiness,” *Science* **245**, 1227–1230.
- Allan, J. D., *et al.*, 2015, “Iodine observed in new particle formation events in the Arctic atmosphere during ACCACIA,” *Atmos. Chem. Phys.* **15**, 5599–5609.
- Allen, J. E., 1992, “Probe theory—The orbital motion approach,” *Phys. Scr.* **45**, 497–503.
- Almeida, J., *et al.*, 2013, “Molecular understanding of sulphuric acid–amine particle nucleation in the atmosphere,” *Nature (London)* **502**, 359–363.
- Andreae, M. O., and D. Rosenfeld, 2008, “Aerosol-cloud-precipitation interactions. Part 1. The nature and sources of cloud-active aerosols,” *Earth-Sci. Rev.* **89**, 13–41.
- Anttila, Tatu, Veli-Matti Kerminen, and Kari E. J. Lehtinen, 2010, “Parameterizing the formation rate of new particles: The effect of nuclei self-coagulation,” *J. Aerosol Sci.* **41**, 621–636.
- Apokardu, M. J., and M. V. Johnston, 2018, “Nanoparticle growth by particle-phase chemistry,” *Atmos. Chem. Phys.* **18**, 1895–1907.
- Apte, Joshua S., Michael Brauer, Aaron J. Cohen, Majid Ezzati, and C. Arden Pope, 2018, “Ambient PM<sub>2.5</sub> reduces global and regional life expectancy,” *Environ. Sci. Technol. Lett.* **5**, 546–551.
- Arneth, A., *et al.*, 2010, “Terrestrial biogeochemical feedbacks in the climate system,” *Nat. Geosci.* **3**, 525–532.
- Arquero, Kristine D., R. Benny Gerber, and Barbara J. Finlayson-Pitts, 2017, “The role of oxalic acid in new particle formation from methanesulfonic acid, methylamine, and water,” *Environ. Sci. Technol.* **51**, 2124–2130.
- Ayers, G. P., and J. L. Gras, 1991, “Seasonal relationship between cloud condensation nuclei and aerosol methanesulphonate in marine air,” *Nature (London)* **353**, 834–835.
- Baalbaki, R., *et al.*, 2021, “Towards understanding the characteristics of new particle formation in the eastern Mediterranean,” *Atmos. Chem. Phys.* **21**, 9223–9251.
- Baccarini, Andrea, *et al.*, 2020, “Frequent new particle formation over the high Arctic pack ice by enhanced iodine emissions,” *Nat. Commun.* **11**, 4924.
- Backes, Anna, Armin Aulinger, Johannes Bieser, Volker Matthias, and Markus Quante, 2016, “Ammonia emissions in Europe, part I: Development of a dynamical ammonia emission inventory,” *Atmos. Environ.* **131**, 55–66.
- Baranzadeh, E., *et al.*, 2016, “Implementation of state-of-the-art ternary new-particle formation scheme to the regional chemical transport model PMCAMx-UF in Europe,” *Geosci. Model Dev.* **9**, 2741–2754.
- Bardouki, H., H. Berresheim, M. Vrekoussis, J. Sciare, G. Kouvarakis, K. Oikonomou, J. Schneider, and N. Mihalopoulos, 2003, “Gaseous (DMS, MSA, SO<sub>2</sub>, H<sub>2</sub>SO<sub>4</sub> and DMSO) and particulate (sulfate and methanesulfonate) sulfur species over the northeastern coast of Crete,” *Atmos. Chem. Phys.* **3**, 1871–1886.
- Barsanti, K. C., P. H. McMurry, and J. N. Smith, 2009, “The potential contribution of organic salts to new particle growth,” *Atmos. Chem. Phys.* **9**, 2949–2957.
- Beck, Lisa J., *et al.*, 2021, “Differing mechanisms of new particle formation at two arctic sites,” *Geophys. Res. Lett.* **48**, e2020GL091334.
- Bellouin, N., *et al.*, 2020, “Bounding global aerosol radiative forcing of climate change,” *Rev. Geophys.* **58**, e2019RG000660.
- Bergman, T., R. Makkonen, R. Schrödner, E. Swietlicki, V. T. J. Phillips, P. Le Sager, and T. van Noije, 2022, “Description and evaluation of a secondary organic aerosol and new particle formation scheme within TM5-MP v1.2,” *Geosci. Model Dev.* **15**, 683–713.
- Beri, R. M., and H. W. Lemon, 1970, “Chemical examination of the wax from needles of black spruce (*Picea mariana*) and balsam fir (*Abies balsamea*),” *Can. J. Chem.* **48**, 67–69.
- Berland, K., *et al.*, 2017, “Spatial extent of new particle formation events over the Mediterranean Basin from multiple ground-based and airborne measurements,” *Atmos. Chem. Phys.* **17**, 9567–9583.
- Berndt, Torsten, Wiebke Scholz, Bernhard Mentler, Lukas Fischer, Hartmut Herrmann, Markku Kulmala, and Armin Hansel, 2018, “Accretion product formation from self- and cross-reactions of RO<sub>2</sub> radicals in the atmosphere,” *Angew. Chem., Int. Ed.* **57**, 3820–3824.
- Berresheim, H., T. Elste, H. G. Tremmel, A. G. Allen, H.-C. Hansson, K. Rosman, M. Dal Maso, J. M. Mäkelä, M. Kulmala, and C. D. O’Dowd, 2002, “Gas-aerosol relationships of H<sub>2</sub>SO<sub>4</sub>, MSA, and OH: Observations in the coastal marine boundary layer at Mace Head, Ireland,” *J. Geophys. Res. Atmos.* **107**, PAR 5-1–PAR 5-12.
- Bey, Isabelle, Daniel J. Jacob, Robert M. Yantosca, Jennifer A. Logan, Brendan D. Field, Arlene M. Fiore, Qinbin Li, Hongyue Y. Liu, Loretta J. Mickley, and Martin G. Schultz, 2001, “Global modeling of tropospheric chemistry with assimilated meteorology: Model description and evaluation,” *J. Geophys. Res. Atmos.* **106**, 23073–23095.
- Bianchi, F., *et al.*, 2016, “New particle formation in the free troposphere: A question of chemistry and timing,” *Science* **352**, 1109–1112.
- Bianchi, F., *et al.*, 2021, “Biogenic particles formed in the Himalaya as an important source of free tropospheric aerosols,” *Nat. Geosci.* **14**, 4–9.
- Bianchi, Federico, *et al.*, 2019, “Highly oxygenated organic molecules (hom) from gas-phase autoxidation involving peroxy radicals: A key contributor to atmospheric aerosol,” *Chem. Rev.* **119**, 3472–3509.
- Birmili, W., H. Berresheim, C. Plass-Dülmer, T. Elste, S. Gilge, A. Wiedensohler, and U. Uhrner, 2003, “The Hohenpeissenberg aerosol formation experiment (HAFEX): A long-term study including size-resolved aerosol, H<sub>2</sub>SO<sub>4</sub>, OH, and monoterpenes measurements,” *Atmos. Chem. Phys.* **3**, 361–376.
- Biskos, G., P. R. Buseck, and S. T. Martin, 2009, “Hygroscopic growth of nucleation-mode acidic sulfate particles,” *J. Aerosol Sci.* **40**, 338–347.
- Biskos, G., D. Paulsen, L. M. Russell, P. R. Buseck, and S. T. Martin, 2006, “Prompt deliquescence and efflorescence of aerosol nanoparticles,” *Atmos. Chem. Phys.* **6**, 4633–4642.
- Blichner, S. M., M. K. Sporre, and T. K. Berntsen, 2021, “Reduced effective radiative forcing from cloud-aerosol interactions (ERFaci) with improved treatment of early aerosol growth in an Earth system model,” *Atmos. Chem. Phys.* **21**, 17243–17265.
- Blichner, S. M., M. K. Sporre, R. Makkonen, and T. K. Berntsen, 2021, “Implementing a sectional scheme for early aerosol growth from new particle formation in the Norwegian Earth system model v2: Comparison to observations and climate impacts,” *Geosci. Model Dev.* **14**, 3335–3359.
- Boucher, O., *et al.*, 2013, “Clouds and aerosols,” in *Climate Change 2013: The Physical Science Basis. Contribution of Working Group I to the Fifth Assessment Report of the Intergovernmental Panel on Climate Change*, edited by T. F. Stocker, D. Qin, G.-K. Plattner,

- M. Tignor, S. K. Allen, J. Boschung, A. Nauels, Y. Xia, V. Bex, and P. M. Midgale (IPCC) (Cambridge University Press, Cambridge, England).
- Boulon, J., K. Sellegri, M. Hervo, D. Picard, J.-M. Pichon, P. Fréville, and P. Laj, 2011, “Investigation of nucleation events vertical extent: A long term study at two different altitude sites,” *Atmos. Chem. Phys.* **11**, 5625–5639.
- Boulon, J., *et al.*, 2010, “New particle formation and ultrafine charged aerosol climatology at a high altitude site in the Alps (Jungfraujoch, 3580 m a.s.l., Switzerland),” *Atmos. Chem. Phys.* **10**, 9333–9349.
- Boulon, Julien, Karine Sellegri, Maxime Hervo, and Paolo Laj, 2011, “Observations of nucleation of new particles in a volcanic plume,” *Proc. Natl. Acad. Sci. U.S.A.* **108**, 12223–12226.
- Bousiotis, D., M. Dall’Osto, D. C. S. Beddows, F. D. Pope, and R. M. Harrison, 2019, “Analysis of new particle formation (NPF) events at nearby rural, urban background and urban roadside sites,” *Atmos. Chem. Phys.* **19**, 5679–5694.
- Boy, M., *et al.*, 2005, “Sulphuric acid closure and contribution to nucleation mode particle growth,” *Atmos. Chem. Phys.* **5**, 863–878.
- Brean, J., D. C. S. Beddows, Z. Shi, B. Temime-Roussel, N. Marchand, X. Querol, A. Alastuey, M. C. Minguillón, and R. M. Harrison, 2020, “Molecular insights into new particle formation in Barcelona, Spain,” *Atmos. Chem. Phys.* **20**, 10029–10045.
- Brean, James, Manuel Dall’Osto, Rafel Simó, Zongbo Shi, David C. S. Beddows, and Roy M. Harrison, 2021, “Open ocean and coastal new particle formation from sulfuric acid and amines around the Antarctic Peninsula,” *Nat. Geosci.* **14**, 383–388.
- Brilke, S., N. Fölker, T. Müller, K. Kandler, X. Gong, J. Peischl, B. Weinzierl, and P. M. Winkler, 2020, “New particle formation and sub–10 nm size distribution measurements during the A-LIFE field experiment in Paphos, Cyprus,” *Atmos. Chem. Phys.* **20**, 5645–5656.
- Brock, J. R., 1972, “Condensational growth of atmospheric aerosols,” *J. Colloid Interface Sci.* **39**, 32–36.
- Bulatovic, I., A. L. Igel, C. Leck, J. Heintzenberg, I. Riipinen, and A. M. L. Ekman, 2021, “The importance of Aitken mode aerosol particles for cloud sustenance in the summertime high Arctic—A simulation study supported by observational data,” *Atmos. Chem. Phys.* **21**, 3871–3897.
- Bzdek, Bryan R., Joseph W. DePalma, and Murray V. Johnston, 2017, “Mechanisms of atmospherically relevant cluster growth,” *Acc. Chem. Res.* **50**, 1965–1975.
- Bzdek, Bryan R., Joseph W. DePalma, Douglas P. Ridge, Julia Laskin, and Murray V. Johnston, 2013, “Fragmentation energetics of clusters relevant to atmospheric new particle formation,” *J. Am. Chem. Soc.* **135**, 3276–3285.
- Bzdek, Bryan R., Andrew J. Horan, M. Ross Pennington, Joseph W. DePalma, Jun Zhao, Coty N. Jen, David R. Hanson, James N. Smith, Peter H. McMurry, and Murray V. Johnston, 2013, “Quantitative and time-resolved nanoparticle composition measurements during new particle formation,” *Faraday Discuss.* **165**, 25–43.
- Bzdek, Bryan R., Andrew J. Horan, M. Ross Pennington, Nathan J. Janecek, Jaemeen Baek, Charles O. Stanier, and Murray V. Johnston, 2014, “Silicon is a frequent component of atmospheric nanoparticles,” *Environ. Sci. Technol.* **48**, 11137–11145.
- Bzdek, Bryan R., Christopher A. Zordan, M. Ross Pennington, George W. Luther, and Murray V. Johnston, 2012, “Quantitative assessment of the sulfuric acid contribution to new particle growth,” *Environ. Sci. Technol.* **46**, 4365–4373.
- Cai, M., *et al.*, 2021, “The important roles of surface tension and growth rate in the contribution of new particle formation (NPF) to cloud condensation nuclei (CCN) number concentration: Evidence from field measurements in southern China,” *Atmos. Chem. Phys.* **21**, 8575–8592.
- Cai, R., C. Deng, D. Stolzenburg, C. Li, J. Guo, V.-M. Kerminen, J. Jiang, M. Kulmala, and J. Kangasluoma, 2022, “Survival probability of new atmospheric particles: Closure between theory and measurements from 1.4 to 100 nm,” *Atmos. Chem. Phys.* **22**, 14571–14587.
- Cai, R., and J. Jiang, 2017, “A new balance formula to estimate new particle formation rate: Reevaluating the effect of coagulation scavenging,” *Atmos. Chem. Phys.* **17**, 12659–12675.
- Cai, R., *et al.*, 2018, “Estimating the influence of transport on aerosol size distributions during new particle formation events,” *Atmos. Chem. Phys.* **18**, 16587–16599.
- Cai, R., *et al.*, 2021a, “Impacts of coagulation on the appearance time method for new particle growth rate evaluation and their corrections,” *Atmos. Chem. Phys.* **21**, 2287–2304.
- Cai, R., *et al.*, 2021b, “Sulfuric acid–amine nucleation in urban Beijing,” *Atmos. Chem. Phys.* **21**, 2457–2468.
- Cai, Runlong, Michel Attoui, Jingkun Jiang, Frans Korhonen, Jiming Hao, Tuukka Petäjä, and Juha Kangasluoma, 2018, “Characterization of a high-resolution supercritical differential mobility analyzer at reduced flow rates,” *Aerosol Sci. Technol.* **52**, 1332–1343.
- Cai, Runlong, Da-Ren Chen, Jiming Hao, and Jingkun Jiang, 2017, “A miniature cylindrical differential mobility analyzer for sub–3 nm particle sizing,” *J. Aerosol Sci.* **106**, 111–119.
- Cai, Runlong, Wei Huang, Melissa Meder, Frederic Bourgain, Konstantin Aizikov, Matthieu Riva, Federico Bianchi, and Mikael Ehn, 2022, “Improving the sensitivity of Fourier transform mass spectrometer (Orbitrap) for online measurements of atmospheric vapors,” *Anal. Chem.* **94**, 15746–15753.
- Cai, Runlong, Jingkun Jiang, Sander Mirme, and Juha Kangasluoma, 2019, “Parameters governing the performance of electrical mobility spectrometers for measuring sub–3 nm particles,” *J. Aerosol Sci.* **127**, 102–115.
- Cai, Runlong, *et al.*, 2022, “The missing base molecules in atmospheric acid–base nucleation,” *Natl. Sci. Rev.* **9**, nwac137.
- Cappa, C. D., and J. L. Jimenez, 2010, “Quantitative estimates of the volatility of ambient organic aerosol,” *Atmos. Chem. Phys.* **10**, 5409–5424.
- Carracedo, Gonzalez, L., K. Lehtipalo, L. R. Ahonen, N. Sarnela, S. Holm, J. Kangasluoma, M. Kulmala, P. M. Winkler, and D. Stolzenburg, 2022, “On the relation between apparent ion and total particle growth rates in the boreal forest and related chamber experiments,” *Atmos. Chem. Phys.* **22**, 13153–13166.
- Carshaw, K. S., *et al.*, 2013, “Large contribution of natural aerosols to uncertainty in indirect forcing,” *Nature (London)* **503**, 67–71.
- Carshaw, Kenneth S., Lindsay A. Lee, Carly L. Reddington, Graham W. Mann, and Kirsty J. Pringle, 2013, “The magnitude and sources of uncertainty in global aerosol,” *Faraday Discuss.* **165**, 495–512.
- Casquero-Vera, J. A., H. Lyamani, L. Dada, S. Hakala, P. Paasonen, R. Román, R. Fraile, T. Petäjä, F. J. Olmo-Reyes, and L. Alados-Arboledas, 2020, “New particle formation at urban and high-altitude remote sites in the south-eastern Iberian Peninsula,” *Atmos. Chem. Phys.* **20**, 14253–14271.
- Caudillo, L., *et al.*, 2021, “Chemical composition of nanoparticles from  $\alpha$ -pinene nucleation and the influence of isoprene and relative humidity at low temperature,” *Atmos. Chem. Phys.* **21**, 17099–17114.
- Chan, Tak Wai, and Michael Mozurkewich, 2001, “Measurement of the coagulation rate constant for sulfuric acid particles as a function

- of particle size using tandem differential mobility analysis,” *J. Aerosol Sci.* **32**, 321–339.
- Charlson, R. J., S. E. Schwartz, J. M. Hales, R. D. Cess, J. A. Coakley, J. E. Hansen, and D. J. Hofmann, 1992, “Climate forcing by anthropogenic aerosols,” *Science* **255**, 423–430.
- Chen, Haihan, Mychel E. Varner, R. Benny Gerber, and Barbara J. Finlayson-Pitts, 2016, “Reactions of methanesulfonic acid with amines and ammonia as a source of new particles in air,” *J. Phys. Chem. B* **120**, 1526–1536.
- Chen, Modi, *et al.*, 2012, “Acid-base chemical reaction model for nucleation rates in the polluted atmospheric boundary layer,” *Proc. Natl. Acad. Sci. U.S.A.* **109**, 18713–18718.
- Chuang, W. K., and N. M. Donahue, 2017, “Dynamic consideration of smog chamber experiments,” *Atmos. Chem. Phys.* **17**, 10019–10036.
- Ciarelli, Giancarlo, Jianhui Jiang, Imad El Haddad, Alessandro Bigi, Sebnem Aksoyoglu, André S. H. Prévôt, Angela Marinoni, Jiali Shen, Chao Yan, and Federico Bianchi, 2021, “Modeling the effect of reduced traffic due to COVID-19 measures on air quality using a chemical transport model: Impacts on the Po Valley and the Swiss Plateau regions,” *Environ. Sci. Atmos.* **1**, 228–240.
- Clegg, Simon L., Peter Brimblecombe, and Anthony S. Wexler, 1998, “Thermodynamic model of the system  $\text{H}^+ \text{-NH}_4^+ \text{-SO}_4^{2-} \text{-NO}_3^- \text{-H}_2\text{O}$  at tropospheric temperatures,” *J. Phys. Chem. A* **102**, 2137–2154.
- Clement, Charles F., and Ian J. Ford, 1999a, “Gas-to-particle conversion in the atmosphere: I. Evidence from empirical atmospheric aerosols,” *Atmos. Environ.* **33**, 475–487.
- Clement, Charles F., and Ian J. Ford, 1999b, “Gas-to-particle conversion in the atmosphere: II. Analytical models of nucleation bursts,” *Atmos. Environ.* **33**, 489–499.
- Clement, Charles F., Kari E. J. Lehtinen, and Markku Kulmala, 2004, “Size diffusion for the growth of newly nucleated aerosol,” *J. Aerosol Sci.* **35**, 1439–1451.
- Covert, David S., Alfred Wiedensohler, Pasi Aalto, Jost Heintzenberg, Peter H. McMurry, and Caroline Leck, 1996, “Aerosol number size distributions from 3 to 500 nm diameter in the Arctic marine boundary layer during summer and autumn,” *Tellus B* **48**, 197–212.
- Crippa, P., and S. C. Pryor, 2013, “Spatial and temporal scales of new particle formation events in eastern North America,” *Atmos. Environ.* **75**, 257–264.
- Crumeyrolle, S., H. E. Manninen, K. Sellegri, G. Roberts, L. Gomes, M. Kulmala, R. Weigel, P. Laj, and A. Schwarzenboeck, 2010, “New particle formation events measured on board the ATR-42 aircraft during the EUCAARI campaign,” *Atmos. Chem. Phys.* **10**, 6721–6735.
- Dada, L., *et al.*, 2020a, “Sources and sinks driving sulfuric acid concentrations in contrasting environments: Implications on proxy calculations,” *Atmos. Chem. Phys.* **20**, 11747–11766.
- Dada, Lubna, *et al.*, 2020b, “Formation and growth of sub-3-nm aerosol particles in experimental chambers,” *Nat. Protoc.* **15**, 1013–1040.
- Dai, Liang, *et al.*, 2017, “Regional and local new particle formation events observed in the Yangtze River Delta region, China,” *J. Geophys. Res. Atmos.* **122**, 2389–2402.
- Dall’Osto, M., R. Simo, Roy M. Harrison, D. C. S. Beddows, A. Saiz-Lopez, R. Lange, H. Skov, J. K. Nøjgaard, I. E. Nielsen, and A. Massling, 2018, “Abiotic and biotic sources influencing spring new particle formation in North East Greenland,” *Atmos. Environ.* **190**, 126–134.
- Dal Maso, M., M. Kulmala, K. E. J. Lehtinen, J. M. Mäkelä, P. Aalto, and C. D. O’Dowd, 2002, “Condensation and coagulation sinks and formation of nucleation mode particles in coastal and boreal forest boundary layers,” *J. Geophys. Res. Atmos.* **107**, PAR 2-1–PAR 2-10.
- Dal Maso, Miikka, Markku Kulmala, Ilona Riipinen, Robert Wagner, Tareq Hussein, Pasi P. Aalto, and Kari E. J. Lehtinen, 2005, “Formation and growth of fresh atmospheric aerosols: Eight years of aerosol size distribution data from SMEAR II, Hyytiälä, Finland,” *Boreal Environ. Res.* **10**, 323–336, <https://www.borenv.net/BER/archive/pdfs/ber10/ber10-323.pdf>.
- D’Andrea, S. D., J. C. Acosta Navarro, S. C. Farina, C. E. Scott, A. Rap, D. K. Farmer, D. V. Spracklen, I. Riipinen, and J. R. Pierce, 2015, “Aerosol size distribution and radiative forcing response to anthropogenically driven historical changes in biogenic secondary organic aerosol formation,” *Atmos. Chem. Phys.* **15**, 2247–2268.
- D’Andrea, S. D., S. A. K. Häkkinen, D. M. Westervelt, C. Kuang, E. J. T. Levin, V. P. Kanawade, W. R. Leitch, D. V. Spracklen, I. Riipinen, and J. R. Pierce, 2013, “Understanding global secondary organic aerosol amount and size-resolved condensational behavior,” *Atmos. Chem. Phys.* **13**, 11519–11534.
- Dawson, Matthew L., Mychel E. Varner, Véronique Perraud, Michael J. Ezell, R. Benny Gerber, and Barbara J. Finlayson-Pitts, 2012, “Simplified mechanism for new particle formation from methanesulfonic acid, amines, and water via experiments and *ab initio* calculations,” *Proc. Natl. Acad. Sci. U.S.A.* **109**, 18719–18724.
- Deng, Chenjuan, Runlong Cai, Chao Yan, Jun Zheng, and Jingkun Jiang, 2021, “Formation and growth of sub-3 nm particles in megacities: Impact of background aerosols,” *Faraday Discuss.* **226**, 348–363.
- Deng, Chenjuan, *et al.*, 2020, “Seasonal characteristics of new particle formation and growth in urban Beijing,” *Environ. Sci. Technol.* **54**, 8547–8557.
- Donahue, N. M., S. A. Epstein, S. N. Pandis, and A. L. Robinson, 2011, “A two-dimensional volatility basis set: 1. Organic-aerosol mixing thermodynamics,” *Atmos. Chem. Phys.* **11**, 3303–3318.
- Donahue, N. M., A. L. Robinson, C. O. Stanier, and S. N. Pandis, 2006, “Coupled partitioning, dilution, and chemical aging of semivolatile organics,” *Environ. Sci. Technol.* **40**, 2635–2643.
- Döschner, R., *et al.*, 2022, “The EC-Earth3 Earth system model for the Coupled Model Intercomparison Project 6,” *Geosci. Model Dev.* **15**, 2973–3020.
- Du, Wei, *et al.*, 2021, “A 3D study on the amplification of regional haze and particle growth by local emissions,” *npj Clim. Atmos. Sci.* **4**, 4.
- Dunne, Eimear M., *et al.*, 2016, “Global atmospheric particle formation from CERN CLOUD measurements,” *Science* **354**, 1119–1124.
- Ehn, M., *et al.*, 2014, “A large source of low-volatility secondary organic aerosol,” *Nature (London)* **506**, 476–479.
- Elm, Jonas, Nanna Myllys, and Theo Kurtén, 2017, “What is required for highly oxidized molecules to form clusters with sulfuric acid?,” *J. Phys. Chem. A* **121**, 4578–4587.
- Erismann, Jan Willem, Mark A. Sutton, James Galloway, Zbigniew Klimont, and Wilfried Winiwarter, 2008, “How a century of ammonia synthesis changed the world,” *Nat. Geosci.* **1**, 636–639.
- Erupe, Mark E., *et al.*, 2010, “Correlation of aerosol nucleation rate with sulfuric acid and ammonia in Kent, Ohio: An atmospheric observation,” *J. Geophys. Res. Atmos.* **115**.
- Fang, Xin, *et al.*, 2020, “Observational evidence for the involvement of dicarboxylic acids in particle nucleation,” *Environ. Sci. Technol. Lett.* **7**, 388–394.
- Fanourgakis, G. S., *et al.*, 2019, “Evaluation of global simulations of aerosol particle and cloud condensation nuclei number, with

- implications for cloud droplet formation,” *Atmos. Chem. Phys.* **19**, 8591–8617.
- Fiedler, V., *et al.*, 2005, “The contribution of sulphuric acid to atmospheric particle formation and growth: A comparison between boundary layers in Northern and Central Europe,” *Atmos. Chem. Phys.* **5**, 1773–1785.
- Finkenzeller, Henning, *et al.*, 2023, “The gas-phase formation mechanism of iodic acid as an atmospheric aerosol source,” *Nat. Chem.* **15**, 129–135.
- Finlayson-Pitts, B. J., and J. N. Pitts, 2000, *Chemistry of the Upper and Lower Atmosphere*, 2nd ed. (Academic Press, San Diego).
- Flagan, Richard C., Shih Chen Wang, Fangdong Yin, John H. Seinfeld, Georg Reischl, Wolfgang Winklmayr, and Rudolf Karch, 1991, “Electrical mobility measurements of fine-particle formation during chamber studies of atmospheric photochemical reactions,” *Environ. Sci. Technol.* **25**, 883–890.
- Forstner, Hali J. L., Richard C. Flagan, and John H. Seinfeld, 1997, “Secondary organic aerosol from the photooxidation of aromatic hydrocarbons: Molecular composition,” *Environ. Sci. Technol.* **31**, 1345–1358.
- Fountoukis, C., I. Riipinen, H. A. C. van der Gon, P. E. Charalampidis, C. Pilinis, A. Wiedensohler, C. O’Dowd, J. P. Putaud, M. Moerman, and S. N. Pandis, 2012, “Simulating ultrafine particle formation in Europe using a regional CTM: Contribution of primary emissions versus secondary formation to aerosol number concentrations,” *Atmos. Chem. Phys.* **12**, 8663–8677.
- Froyd, K. D., D. M. Murphy, T. J. Sanford, D. S. Thomson, J. C. Wilson, L. Pfister, and L. Lait, 2009, “Aerosol composition of the tropical upper troposphere,” *Atmos. Chem. Phys.* **9**, 4363–4385.
- Froyd, Karl D., and Edward R. Lovejoy, 2012, “Bond energies and structures of ammonia–sulfuric acid positive cluster ions,” *J. Phys. Chem. A* **116**, 5886–5899.
- Fu, Yueyun, Mo Xue, Runlong Cai, Juha Kangasluoma, and Jingkun Jiang, 2019, “Theoretical and experimental analysis of the core sampling method: Reducing diffusional losses in aerosol sampling line,” *Aerosol Sci. Technol.* **53**, 793–801.
- Fuchs, N. A., 1963, “On the stationary charge distribution on aerosol particles in a bipolar ionic atmosphere,” *Geofis. Pura Appl.* **56**, 185–193.
- Fuchs, N. A., 1964, in *The Mechanics of Aerosols*, revised ed., edited by C. N. Davies (MacMillan, New York).
- Fuchs, N. A., and A. G. Sutugin, 1965, “Coagulation rate of highly dispersed aerosols,” *J. Colloid Sci.* **20**, 492–500.
- Fuchs, N. A., and A. G. Sutugin, 1971, “High dispersed aerosols,” in *Topics in Current Aerosol Research (Part 2)*, edited by G. M. Hidy and J. R. Brock (Pergamon, New York), pp. 1–200.
- Galloway, J. N., *et al.*, 2004, “Nitrogen cycles: Past, present, and future,” *Biogeochemistry* **70**, 153–226.
- Garmash, O., *et al.*, 2020, “Multi-generation OH oxidation as a source for highly oxygenated organic molecules from aromatics,” *Atmos. Chem. Phys.* **20**, 515–537.
- Gaston, Cassandra J., Kerri A. Pratt, Xueying Qin, and Kimberly A. Prather, 2010, “Real-time detection and mixing state of methanesulfonate in single particles at an inland urban location during a phytoplankton bloom,” *Environ. Sci. Technol.* **44**, 1566–1572.
- Ge, Xinlei, Anthony S. Wexler, and Simon L. Clegg, 2011, “Atmospheric amines—Part I. A review,” *Atmos. Environ.* **45**, 524–546.
- Gelbard, Fred, and John H. Seinfeld, 1979, “The general dynamic equation for aerosols. Theory and application to aerosol formation and growth,” *J. Colloid Interface Sci.* **68**, 363–382.
- Gelbard, Fred, Yoram Tambour, and John H. Seinfeld, 1980, “Sectional representations for simulating aerosol dynamics,” *J. Colloid Interface Sci.* **76**, 541–556.
- Glase, W. A., K. Volz, B. Panta, N. Freshour, R. Bachman, D. R. Hanson, P. H. McMurry, and C. Jen, 2015, “Sulfuric acid nucleation: An experimental study of the effect of seven bases,” *J. Geophys. Res. Atmos.* **120**, 1933–1950.
- Goldstein, Allen H., and Ian E. Galbally, 2007, “Known and unexplored organic constituents in the Earth’s atmosphere,” *Environ. Sci. Technol.* **41**, 1514–1521.
- Gómez Martín, Juan Carlos, Thomas R. Lewis, Mark A. Blitz, John M. C. Plane, Manoj Kumar, Joseph S. Francisco, and Alfonso Saiz-Lopez, 2020, “A gas-to-particle conversion mechanism helps to explain atmospheric particle formation through clustering of iodine oxides,” *Nat. Commun.* **11**, 4521.
- Gonser, S. G., F. Klein, W. Birmili, J. Größ, M. Kulmala, H. E. Manninen, A. Wiedensohler, and A. Held, 2014, “Ion-particle interactions during particle formation and growth at a coniferous forest site in central Europe,” *Atmos. Chem. Phys.* **14**, 10547–10563.
- Goodrich, F. C., 1964, “Nucleation rates and the kinetics of particle growth II. The birth and death process,” *Proc. R. Soc. A* **277**, 167–182.
- Gopalakrishnan, Ranganathan, and Christopher J. Hogan, 2011, “Determination of the transition regime collision kernel from mean first passage times,” *Aerosol Sci. Technol.* **45**, 1499–1509.
- Gopalakrishnan, Ranganathan, and Christopher J. Hogan, 2012, “Coulomb-influenced collisions in aerosols and dusty plasmas,” *Phys. Rev. E* **85**, 026410.
- Gordon, Hamish, *et al.*, 2016, “Reduced anthropogenic aerosol radiative forcing caused by biogenic new particle formation,” *Proc. Natl. Acad. Sci. U.S.A.* **113**, 12053–12058.
- Gordon, Hamish, *et al.*, 2017, “Causes and importance of new particle formation in the present-day and preindustrial atmospheres,” *J. Geophys. Res. Atmos.* **122**, 8739–8760.
- Guenther, A. B., X. Jiang, C. L. Heald, T. Sakulyanontvittaya, T. Duhl, L. K. Emmons, and X. Wang, 2012, “The model of emissions of gases and aerosols from nature version 2.1 (MEGAN2.1): An extended and updated framework for modeling biogenic emissions,” *Geosci. Model Dev.* **5**, 1471–1492.
- Guo, Song, *et al.*, 2014, “Elucidating severe urban haze formation in China,” *Proc. Natl. Acad. Sci. U.S.A.* **111**, 17373–17378.
- Guo, Song, *et al.*, 2020, “Remarkable nucleation and growth of ultrafine particles from vehicular exhaust,” *Proc. Natl. Acad. Sci. U.S.A.* **117**, 3427–3432.
- Hakala, S., *et al.*, 2019, “New particle formation, growth and apparent shrinkage at a rural background site in western Saudi Arabia,” *Atmos. Chem. Phys.* **19**, 10537–10555.
- Häkkinen, E., J. Zhao, F. Graeffe, N. Fauré, J. Krechmer, D. Worsnop, H. Timonen, M. Ehn, and J. Kangasluoma, 2023, “Online measurement of highly oxygenated compounds from organic aerosol,” *Atmos. Meas. Tech.* **16**, 1705–1721.
- Hallquist, M., *et al.*, 2009, “The formation, properties and impact of secondary organic aerosol: Current and emerging issues,” *Atmos. Chem. Phys.* **9**, 5155–5236.
- Halonen, R., E. Zapadinsky, T. Kurtén, H. Vehkamäki, and B. Reischl, 2019, “Rate enhancement in collisions of sulfuric acid molecules due to long-range intermolecular forces,” *Atmos. Chem. Phys.* **19**, 13355–13366.
- Hamaker, H. C., 1937, “The London–van der Waals attraction between spherical particles,” *Physica (Amsterdam)* **4**, 1058–1072.

- Hanson, D. R., and F. Eisele, 2000, "Diffusion of  $\text{H}_2\text{SO}_4$  in humidified nitrogen: Hydrated  $\text{H}_2\text{SO}_4$ ," *J. Phys. Chem. A* **104**, 1715–1719.
- Haywood, J. M., and K. P. Shine, 1995, "The effect of anthropogenic sulfate and soot aerosol on the clear sky planetary radiation budget," *Geophys. Res. Lett.* **22**, 603–606.
- He, Xu-Cheng, *et al.*, 2021a, "Determination of the collision rate coefficient between charged iodine acid clusters and iodine acid using the appearance time method," *Aerosol Sci. Technol.* **55**, 231–242.
- He, Xu-Cheng, *et al.*, 2021b, "Role of iodine oxoacids in atmospheric aerosol nucleation," *Science* **371**, 589–595.
- Heinritzi, M., M. Simon, G. Steiner, A. C. Wagner, A. Kürten, A. Hansel, and J. Curtius, 2016, "Characterization of the mass-dependent transmission efficiency of a CIMS," *Atmos. Meas. Tech.* **9**, 1449–1460.
- Heinritzi, M., *et al.*, 2020, "Molecular understanding of the suppression of new-particle formation by isoprene," *Atmos. Chem. Phys.* **20**, 11809–11821.
- Heintzenberg, Jost, and Caroline Leck, 1994, "Seasonal variation of the atmospheric aerosol near the top of the marine boundary layer over Spitsbergen related to the Arctic sulphur cycle," *Tellus B* **46**, 52–67.
- Heisler, S. L., and S. K. Friedlander, 1977, "Gas-to-particle conversion in photochemical smog: Aerosol growth laws and mechanisms for organics," *Atmos. Environ.* **11**, 157–168.
- Heisler, S. L., S. K. Friedlander, and R. B. Husar, 1973, "The relationship of smog aerosol size and chemical element distributions to source characteristics," *Atmos. Environ.* **7**, 633–649.
- Heitto, A., K. Lehtinen, T. Petäjä, F. Lopez-Hilfiker, J. A. Thornton, M. Kulmala, and T. Yli-Juuti, 2022, "Effects of oligomerization and decomposition on the nanoparticle growth: A model study," *Atmos. Chem. Phys.* **22**, 155–171.
- Henschel, Henning, Juan C Acosta Navarro, Taina Yli-Juuti, Oona Kupiainen-Määttä, Tinja Olenius, Ismael K. Ortega, Simon L. Clegg, Theo Kurtén, Ilona Riipinen, and Hanna Vehkamäki, 2014, "Hydration of atmospherically relevant molecular clusters: Computational chemistry and classical thermodynamics," *J. Phys. Chem. A* **118**, 2599–2611.
- Hirsikko, A., *et al.*, 2012, "Characterisation of sub-micron particle number concentrations and formation events in the western Bushveld Igneous Complex, South Africa," *Atmos. Chem. Phys.* **12**, 3951–3967.
- Hirsikko, Anne, Lauri Laakso, Urmas Hórrak, Pasi P. Aalto, Veli-Matti Kerminen, and Markku Kulmala, 2005, "Annual and size dependent variation of growth rates and ion concentrations in boreal forest," *Boreal Environ. Res.* **10**, 357–369, <https://www.borenav.net/BER/archive/pdfs/ber10/ber10-357.pdf>.
- Ho, K. F., J. J. Cao, S. C. Lee, Kimitaka Kawamura, R. J. Zhang, Judith C. Chow, and John G. Watson, 2007, "Dicarboxylic acids, ketocarboxylic acids, and dicarbonyls in the urban atmosphere of China," *J. Geophys. Res. Atmos.* **112**.
- Hodshire, A. L., *et al.*, 2016, "Multiple new-particle growth pathways observed at the US DOE Southern Great Plains field site," *Atmos. Chem. Phys.* **16**, 9321–9348.
- Hodshire, Anna L., Pedro Campuzano-Jost, John K. Kodros, Betty Croft, Benjamin A. Nault, Jason C. Schroder, Jose L. Jimenez, and Jeffrey R. Pierce, 2019, "The potential role of methanesulfonic acid (MSA) in aerosol formation and growth and the associated radiative forcings," *Atmos. Chem. Phys.* **19**, 3137–3160.
- Hodzic, A., P. S. Kasibhatla, D. S. Jo, C. D. Cappa, J. L. Jimenez, S. Madronich, and R. J. Park, 2016, "Rethinking the global secondary organic aerosol (SOA) budget: Stronger production, faster removal, shorter lifetime," *Atmos. Chem. Phys.* **16**, 7917–7941.
- Hodzic, A., *et al.*, 2020, "Characterization of organic aerosol across the global remote troposphere: A comparison of ATom measurements and global chemistry models," *Atmos. Chem. Phys.* **20**, 4607–4635.
- Hoesly, R. M., *et al.*, 2018, "Historical (1750–2014) anthropogenic emissions of reactive gases and aerosols from the Community Emissions Data System (CEDS)," *Geosci. Model Dev.* **11**, 369–408.
- Hoffmann, Thorsten, Colin D. O'Dowd, and John H. Seinfeld, 2001, "Iodine oxide homogeneous nucleation: An explanation for coastal new particle production," *Geophys. Res. Lett.* **28**, 1949–1952.
- Holten, V., and M. E. H. van Dongen, 2009, "Comparison between solutions of the general dynamic equation and the kinetic equation for nucleation and droplet growth," *J. Chem. Phys.* **130**, 14102.
- Hoppel, W. A., 1987, "Nucleation in the MSA-water vapor system," *Atmos. Environ.* **21**, 2703–2709.
- Hoppel, William A., and Glendon M. Frick, 1986, "Ion-aerosol attachment coefficients and the steady-state charge distribution on aerosols in a bipolar ion environment," *Aerosol Sci. Technol.* **5**, 1–21.
- Huang, Shan, Laurent Poulain, Dominik van Pinxteren, Manuela van Pinxteren, Zhijun Wu, Hartmut Herrmann, and Alfred Wiedensohler, 2017, "Latitudinal and seasonal distribution of particulate MSA over the Atlantic using a validated quantification method with HR-ToF-AMS," *Environ. Sci. Technol.* **51**, 418–426.
- Huang, W., H. Li, N. Sarnela, L. Heikkinen, Y. J. Tham, J. Mikkilä, S. J. Thomas, N. M. Donahue, M. Kulmala, and F. Bianchi, 2021, "Measurement report: Molecular composition and volatility of gaseous organic compounds in a boreal forest—From volatile organic compounds to highly oxygenated organic molecules," *Atmos. Chem. Phys.* **21**, 8961–8977.
- Hudda, N., and S. A. Fruin, 2016, "International airport impacts to air quality: Size and related properties of large increases in ultrafine particle number concentrations," *Environ. Sci. Technol.* **50**, 3362–3370.
- Hussein, T., H. Junninen, P. Tunved, A. Kristensson, M. Dal Maso, I. Riipinen, P. P. Aalto, H.-C. Hansson, E. Swietlicki, and M. Kulmala, 2009, "Time span and spatial scale of regional new particle formation events over Finland and southern Sweden," *Atmos. Chem. Phys.* **9**, 4699–4716.
- Hussein, Tareq, Jyrki Martikainen, Heikki Junninen, Larisa Sogacheva, Robert Wagner, Miikka Dal Maso, Ilona Riipinen, Pasi P. Aalto, and Markku Kulmala, 2008, "Observation of regional new particle formation in the urban atmosphere," *Tellus B* **60**, 509–521.
- Iida, Kenjiro, Mark R. Stolzenburg, Peter H. McMurry, and James N. Smith, 2008, "Estimating nanoparticle growth rates from size-dependent charged fractions: Analysis of new particle formation events in Mexico City," *J. Geophys. Res. Atmos.* **113**.
- Jayarathne, R., B. Pushpawela, C. He, H. Li, J. Gao, F. Chai, and L. Morawska, 2017, "Observations of particles at their formation sizes in Beijing, China," *Atmos. Chem. Phys.* **17**, 8825–8835.
- Jen, Coty N., Peter H. McMurry, and David R. Hanson, 2014, "Stabilization of sulfuric acid dimers by ammonia, methylamine, dimethylamine, and trimethylamine," *J. Geophys. Res. Atmos.* **119**, 7502–7514.
- Jeong, C.-H., G. J. Evans, M. L. McGuire, R. Y.-W. Chang, J. P. D. Abbatt, K. Zeromskiene, M. Mozurkewich, S.-M. Li, and W. R. Leitch, 2010, "Particle formation and growth at five rural and urban sites," *Atmos. Chem. Phys.* **10**, 7979–7995.
- Jiang, Jingkun, Modi Chen, Chongai Kuang, Michel Attoui, and Peter H. McMurry, 2011, "Electrical mobility spectrometer using a diethylene glycol condensation particle counter for measurement of

- aerosol size distributions down to 1 nm,” *Aerosol Sci. Technol.* **45**, 510–521.
- Jiang, Jingkun, Jun Zhao, Modi Chen, Fred L. Eisele, Jacob Scheckman, Brent J. Williams, Chongai Kuang, and Peter H. McMurry, 2011, “First measurements of neutral atmospheric cluster and 1–2 nm particle number size distributions during nucleation events,” *Aerosol Sci. Technol.* **45**, ii–v.
- Jimenez, Jose L., Roya Bahreini, David R Cocker III, Hong Zhuang, Varuntida Varutbangkul, Richard C. Flagan, John H. Seinfeld, Colin D. O’Dowd, and Thorsten Hoffmann, 2003, “New particle formation from photooxidation of diiodomethane (CH<sub>2</sub>I<sub>2</sub>),” *J. Geophys. Res. Atmos.* **108**, 4318.
- Jokinen, T., M. Sipilä, H. Junninen, M. Ehn, G. Lönn, J. Hakala, T. Petäjä, R. L. Mauldin III, M. Kulmala, and D. R. Worsnop, 2012, “Atmospheric sulphuric acid and neutral cluster measurements using CI-API-TOF,” *Atmos. Chem. Phys.* **12**, 4117–4125.
- Jokinen, T., M. Sipilä, J. Kontkanen, V. Vakkari, P. Tisler, E. Duplissy, and H. Junninen, 2018, “Ion-induced sulfuric acid–ammonia nucleation drives particle formation in coastal Antarctica,” *Sci. Adv.* **4**, eaat9744.
- Jokinen, Tuija, *et al.*, 2015, “Production of extremely low volatile organic compounds from biogenic emissions: Measured yields and atmospheric implications,” *Proc. Natl. Acad. Sci. U.S.A.* **112**, 7123–7128.
- Jonsson, Åsa M., Jonathan Westerlund, and Mattias Hallquist, 2011, “Size-resolved particle emission factors for individual ships,” *Geophys. Res. Lett.* **38**.
- Julin, Jan, Benjamin N. Murphy, David Patoulias, Christos Fountoukis, Tinja Olenius, Spyros N. Pandis, and Ilona Riipinen, 2018, “Impacts of future European emission reductions on aerosol particle number concentrations accounting for effects of ammonia, amines, and organic species,” *Environ. Sci. Technol.* **52**, 692–700.
- Jung, JaeGun, Christos Fountoukis, Peter J. Adams, and Spyros N. Pandis, 2010, “Simulation of *in situ* ultrafine particle formation in the eastern United States using PMCAMx-UF,” *J. Geophys. Res. Atmos.* **115**.
- Junkermann, W., R. Hagemann, and B. Vogel, 2011, “Nucleation in the Karlsruhe plume during the COPS/TRACKS-Lagrange experiment,” *Q. J. R. Meteorol. Soc.* **137**, 267–274.
- Junninen, H., *et al.*, 2010, “A high-resolution mass spectrometer to measure atmospheric ion composition,” *Atmos. Meas. Tech.* **3**, 1039–1053.
- Kalafut-Pettibone, A. J., J. Wang, W. E. Eichinger, A. Clarke, S. A. Vay, D. R. Blake, and C. O. Stanier, 2011, “Size-resolved aerosol emission factors and new particle formation/growth activity occurring in Mexico City during the MILAGRO 2006 Campaign,” *Atmos. Chem. Phys.* **11**, 8861–8881.
- Kalberer, M., *et al.*, 2004, “Identification of polymers as major components of atmospheric organic aerosols,” *Science* **303**, 1659–1662.
- Kammer, J., E. Perraudin, P.-M. Flaud, E. Lamaud, J. M. Bonnefond, and E. Villenave, 2018, “Observation of nighttime new particle formation over the French Landes forest,” *Sci. Total Environ.* **621**, 1084–1092.
- Kanawade, V. P., B. T. Jobson, A. B. Guenther, M. E. Erupe, S. N. Pressley, S. N. Tripathi, and S.-H. Lee, 2011, “Isoprene suppression of new particle formation in a mixed deciduous forest,” *Atmos. Chem. Phys.* **11**, 6013–6027.
- Kanawade, Vijay P., David R. Benson, and Shan-Hu Lee, 2012, “Statistical analysis of 4-year observations of aerosol sizes in a semi-rural continental environment,” *Atmos. Environ.* **59**, 30–38.
- Kangasluoma, J., and J. Kontkanen, 2017, “On the sources of uncertainty in the sub–3 nm particle concentration measurement,” *J. Aerosol Sci.* **112**, 34–51.
- Kangasluoma, J., C. Kuang, D. Wimmer, M. P. Rissanen, K. Lehtipalo, M. Ehn, D. R. Worsnop, J. Wang, M. Kulmala, and T. Petäjä, 2014, “Sub–3 nm particle size and composition dependent response of a nano-CPC battery,” *Atmos. Meas. Tech.* **7**, 689–700.
- Kangasluoma, J., *et al.*, 2016, “Operation of the Airmodus A11 Nano Condensation Nucleus Counter at various inlet pressures and various operation temperatures, and design of a new inlet system,” *Atmos. Meas. Tech.* **9**, 2977–2988.
- Kangasluoma, J., *et al.*, 2018, “Laboratory verification of a new high flow differential mobility particle sizer, and field measurements in Hyytiälä,” *J. Aerosol Sci.* **124**, 1–9.
- Kangasluoma, J., *et al.*, 2020, “Overview of measurements and current instrumentation for 1–10 nm aerosol particle number size distributions,” *J. Aerosol Sci.* **148**, 105584.
- Kansal, Ankur, 2009, “Sources and reactivity of NMHCs and VOCs in the atmosphere: A review,” *J. Hazard. Mater.* **166**, 17–26.
- Karset, I. H. H., T. K. Berntsen, T. Storelvmo, K. Alterskjær, A. Grini, D. Olivieri, A. Kirkevåg, Ø. Seland, T. Iversen, and M. Schulz, 2018, “Strong impacts on aerosol indirect effects from historical oxidant changes,” *Atmos. Chem. Phys.* **18**, 7669–7690.
- Kawamura, Kimitaka, and Srinivas Bikkina, 2016, “A review of dicarboxylic acids and related compounds in atmospheric aerosols: Molecular distributions, sources and transformation,” *Atmos. Res.* **170**, 140–160.
- Keller, Maureen D., 1989, “Dimethyl sulfide production and marine phytoplankton: The importance of species composition and cell size,” *Biol. Oceanogr.* **6**, 375–382, <https://www.tandfonline.com/doi/abs/10.1080/01965581.1988.10749540>.
- Kerminen, V.-M., and M. Kulmala, 2002, “Analytical formulae connecting the ‘real’ and the ‘apparent’ nucleation rate and the nuclei number concentration for atmospheric nucleation events,” *J. Aerosol Sci.* **33**, 609–622.
- Kerminen, V.-M., *et al.*, 2012, “Cloud condensation nuclei production associated with atmospheric nucleation: A synthesis based on existing literature and new results,” *Atmos. Chem. Phys.* **12**, 12037–12059.
- Kerminen, Veli-Matti, Minna Aurela, Risto E. Hillamo, and Aki Virkkula, 1997, “Formation of particulate MSA: Deductions from size distribution measurements in the Finnish Arctic,” *Tellus B* **49**, 159–171.
- Kerminen, Veli-Matti, Xuemeng Chen, Ville Vakkari, Tuukka Petäjä, Markku Kulmala, and Federico Bianchi, 2018, “Atmospheric new particle formation and growth: Review of field observations,” *Environ. Res. Lett.* **13**, 103003.
- Kerminen, Veli-Matti, and Anthony S. Wexler, 1995, “Growth laws for atmospheric aerosol particles: An examination of the bimodality of the accumulation mode,” *Atmos. Environ.* **29**, 3263–3275.
- Khare, Puja, N. Kumar, K. M. Kumari, and S. S. Srivastava, 1999, “Atmospheric formic and acetic acids: An overview,” *Rev. Geo-phys.* **37**, 227–248.
- Kiendler-Scharr, Astrid, Jürgen Wildt, Miikka Dal Maso, Thorsten Hohaus, Einhard Kleist, Thomas F. Mentel, Ralf Tillmann, Ricarda Uerlings, Uli Schurr, and Andreas Wahner, 2009, “New particle formation in forests inhibited by isoprene emissions,” *Nature (London)* **461**, 381.
- Kim, Yumi, Sang-Woo Kim, Soon-Chang Yoon, Jin-Soo Park, Jae-Hyun Lim, Jihyung Hong, Han-Cheol Lim, Jegyu Ryu, Chul-Kyu Lee, and Bok-Haeng Heo, 2016, “Characteristics of formation and

- growth of atmospheric nanoparticles observed at four regional background sites in Korea,” *Atmos. Res.* **168**, 80–91.
- Kirkby, Jasper, *et al.*, 2011, “Role of sulphuric acid, ammonia and galactic cosmic rays in atmospheric aerosol nucleation,” *Nature (London)* **476**, 429–433.
- Kirkby, Jasper, *et al.*, 2016, “Ion-induced nucleation of pure biogenic particles,” *Nature (London)* **533**, 521–526.
- Kirkevåg, A., *et al.*, 2018, “A production-tagged aerosol module for Earth system models, OsloAero5.3—Extensions and updates for CAM5.3-Oslo,” *Geosci. Model Dev.* **11**, 3945–3982.
- Kivekäs, Niku, Jimmie Carpmann, Pontus Roldin, Johannes Leppä, Ewan O’Connor, Adam Kristensson, and Eija Asmi, 2016, “Coupling an aerosol box model with one-dimensional flow: A tool for understanding observations of new particle formation events,” *Tellus B* **68**, 29706.
- Kong, W., S. Amanatidis, H. Mai, C. Kim, B. C. Schulze, Y. Huang, G. S. Lewis, S. V. Hering, J. H. Seinfeld, and R. C. Flagan, 2021, “The nano-scanning electrical mobility spectrometer (nSEMS) and its application to size distribution measurements of 1.5–25 nm particles,” *Atmos. Meas. Tech.* **14**, 5429–5445.
- Kontkanen, J., E. Järvinen, H. E. Manninen, K. Lehtipalo, J. Kangasluoma, S. Decesari, G. P. Gobbi, A. Laaksonen, T. Petäjä, and M. Kulmala, 2016, “High concentrations of sub-3 nm clusters and frequent new particle formation observed in the Po Valley, Italy, during the PEGASOS 2012 campaign,” *Atmos. Chem. Phys.* **16**, 1919–1935.
- Kontkanen, J., T. Olenius, K. Lehtipalo, H. Vehkamäki, M. Kulmala, and K. E. J. Lehtinen, 2016, “Growth of atmospheric clusters involving cluster-cluster collisions: Comparison of different growth rate methods,” *Atmos. Chem. Phys.* **16**, 5545–5560.
- Kontkanen, J., *et al.*, 2020, “Size-resolved particle number emissions in Beijing determined from measured particle size distributions,” *Atmos. Chem. Phys.* **20**, 11329–11348.
- Kontkanen, Jenni, Tinja Olenius, Markku Kulmala, and Ilona Riipinen, 2018, “Exploring the potential of nano-Köhler theory to describe the growth of atmospheric molecular clusters by organic vapors using cluster kinetics simulations,” *Atmos. Chem. Phys.* **18**, 13733–13754.
- Kontkanen, Jenni, Dominik Stolzenburg, Tinja Olenius, Chao Yan, Lubna Dada, Lauri Ahonen, Mario Simon, Katrianne Lehtipalo, and Ilona Riipinen, 2022, “What controls the observed size-dependency of the growth rates of sub-10 nm atmospheric particles?,” *Environ. Sci. Atmos.* **2**, 449–468.
- Korhonen, H., K. E. J. Lehtinen, and M. Kulmala, 2004, “Multi-component aerosol dynamics model UHMA: Model development and validation,” *Atmos. Chem. Phys.* **4**, 757–771.
- Korhonen, Hannele, Veli-Matti Kerminen, Harri Kokkola, and Kari E. J. Lehtinen, 2014, “Estimating atmospheric nucleation rates from size distribution measurements: Analytical equations for the case of size dependent growth rates,” *J. Aerosol Sci.* **69**, 13–20.
- Krechmer, Jordan, *et al.*, 2018, “Evaluation of a new reagent-ion source and focusing ion–molecule reactor for use in proton-transfer-reaction mass spectrometry,” *Anal. Chem.* **90**, 12011–12018.
- Kreidenweis, S. M., J. E. Penner, F. Yin, and J. H. Seinfeld, 1991, “The effects of dimethylsulfide upon marine aerosol concentrations,” *Atmos. Environ. A* **25**, 2501–2511.
- Kuang, C., M. Chen, J. Zhao, J. Smith, P. H. McMurry, and J. Wang, 2012, “Size and time-resolved growth rate measurements of 1 to 5 nm freshly formed atmospheric nuclei,” *Atmos. Chem. Phys.* **12**, 3573–3589.
- Kuang, C., P. H. McMurry, and A. V. McCormick, 2009, “Determination of cloud condensation nuclei production from measured new particle formation events,” *Geophys. Res. Lett.* **36**.
- Kuang, C., I. Riipinen, S.-L. Sihto, M. Kulmala, A. V. McCormick, and P. H. McMurry, 2010, “An improved criterion for new particle formation in diverse atmospheric environments,” *Atmos. Chem. Phys.* **10**, 8469–8480.
- Kuang, Chongai, Modi Chen, Peter H. McMurry, and Jian Wang, 2012, “Modification of laminar flow ultrafine condensation particle counters for the enhanced detection of 1 nm condensation nuclei,” *Aerosol Sci. Technol.* **46**, 309–315.
- Kulmala, M., M. Dal Maso, J. M. Mäkelä, L. Pirjola, M. Väkevä, P. Aalto, P. Miikkulainen, K. Hämeri, and C. D. O’Dowd, 2001, “On the formation, growth and composition of nucleation mode particles,” *Tellus B* **53**, 479–490.
- Kulmala, M., V.-M. Kerminen, T. Petäjä, A. J. Ding, and L. Wang, 2017, “Atmospheric gas-to-particle conversion: Why NPF events are observed in megacities?,” *Faraday Discuss.* **200**, 271–288.
- Kulmala, M., L. Laakso, K. E. J. Lehtinen, I. Riipinen, M. Dal Maso, T. Anttila, V.-M. Kerminen, U. Hörrak, M. Vana, and H. Tammet, 2004, “Initial steps of aerosol growth,” *Atmos. Chem. Phys.* **4**, 2553–2560.
- Kulmala, M., H. Vehkamäki, T. Petäjä, M. Dal Maso, A. Lauri, V.-M. Kerminen, W. Birmili, and P. H. McMurry, 2004, “Formation and growth rates of ultrafine atmospheric particles: A review of observations,” *J. Aerosol Sci.* **35**, 143–176.
- Kulmala, M., *et al.*, 2023, “Direct link between the characteristics of atmospheric new particle formation and Continental Biosphere-Atmosphere-Cloud-Climate (COBACC) feedback loop,” *Boreal Environ. Res.* **28**, 1–13, <https://www.borenav.net/BER/archive/pdfs/ber28/ber28-001-013.pdf>.
- Kulmala, Markku, 2003, “How particles nucleate and grow,” *Science* **302**, 1000–1001.
- Kulmala, Markku, 2018, “Build a global Earth observatory,” *Nature (London)* **553**, 21–23.
- Kulmala, Markku, Runlong Cai, Dominik Stolzenburg, Ying Zhou, Lubna Dada, Yishuo Guo, Chao Yan, Tuukka Petäjä, Jingkun Jiang, and Veli-Matti Kerminen, 2022, “The contribution of new particle formation and subsequent growth to haze formation,” *Environ. Sci. Atmos.* **2**, 352–361.
- Kulmala, Markku, Veli-Matti Kerminen, Tatu Anttila, Ari Laaksonen, and Colin D. O’Dowd, 2004, “Organic aerosol formation via sulphate cluster activation,” *J. Geophys. Res. Atmos.* **109**.
- Kulmala, Markku, Ari Laaksonen, Robert J. Charlson, and Pekka Korhonen, 1997, “Clouds without supersaturation,” *Nature (London)* **388**, 336–337.
- Kulmala, Markku, Anne Toivonen, Jyrki M. Mäkelä, and Ari Laaksonen, 1998, “Analysis of the growth of nucleation mode particles observed in boreal forest,” *Tellus B* **50**, 449–462.
- Kulmala, Markku, *et al.*, 2007, “The condensation particle counter battery (CPCB): A new tool to investigate the activation properties of nanoparticles,” *J. Aerosol Sci.* **38**, 289–304.
- Kulmala, Markku, *et al.*, 2012, “Measurement of the nucleation of atmospheric aerosol particles,” *Nat. Protoc.* **7**, 1651–1667.
- Kulmala, Markku, *et al.*, 2013, “Direct observations of atmospheric aerosol nucleation,” *Science* **339**, 943–946.
- Kulmala, Markku, *et al.*, 2021, “Is reducing new particle formation a plausible solution to mitigate particulate air pollution in Beijing and other Chinese megacities?,” *Faraday Discuss.* **226**, 334–347.

- Kulmala, Markku, *et al.*, 2022, “Towards a concentration closure of sub-6 nm aerosol particles and sub-3 nm atmospheric clusters,” *J. Aerosol Sci.* **159**, 105878.
- Kumar, Manoj, Alfonso Saiz-Lopez, and Joseph S. Francisco, 2018, “Single-molecule catalysis revealed: Elucidating the mechanistic framework for the formation and growth of atmospheric iodine oxide aerosols in gas-phase and aqueous surface environments,” *J. Am. Chem. Soc.* **140**, 14704–14716.
- Kumar, Prashant, Matthias Ketzel, Sotiris Vardoulakis, Liisa Pirjola, and Rex Britter, 2011, “Dynamics and dispersion modeling of nanoparticles from road traffic in the urban atmospheric environment—A review,” *J. Aerosol Sci.* **42**, 580–603.
- Kumar, Prashant, Lidia Morawska, Wolfram Birmili, Pauli Paasonen, Min Hu, Markku Kulmala, Roy M. Harrison, Leslie Norford, and Rex Britter, 2014, “Ultrafine particles in cities,” *Environ. Int.* **66**, 1–10.
- Kummerlöwe, Grit, and Martin K. Beyer, 2005, “Rate estimates for collisions of ionic clusters with neutral reactant molecules,” *Int. J. Mass Spectrom.* **244**, 84–90.
- Kurtén, Theo, Madis Noppel, Hanna Vehkamäki, Martta Salonen, and Markku Kulmala, 2007, “Quantum chemical studies of hydrate formation of  $\text{H}_2\text{SO}_4$  and  $\text{HSO}_4^-$ ,” *Boreal Environ. Res.* **12**, 431–453, <https://www.borenv.net/BER/archive/pdfs/ber12/ber12-431.pdf>.
- Kurtén, Theo, Kirsi Tiusanen, Pontus Roldin, Matti Rissanen, Jan-Niclas Luy, Michael Boy, Mikael Ehn, and Neil Donahue, 2016, “Alpha-pinene autooxidation products may not have extremely low saturation vapor pressures despite high O:C ratios,” *J. Phys. Chem. A* **120**, 2569–2582.
- Kürten, A., 2019, “New particle formation from sulfuric acid and ammonia: nucleation and growth model based on thermodynamics derived from CLOUD measurements for a wide range of conditions,” *Atmos. Chem. Phys.* **19**, 5033–5050.
- Kürten, A., *et al.*, 2018, “New particle formation in the sulfuric acid–dimethylamine–water system: Reevaluation of CLOUD chamber measurements and comparison to an aerosol nucleation and growth model,” *Atmos. Chem. Phys.* **18**, 845–863.
- Kürten, Andreas, Linda Rondo, Sebastian Ehrhart, and Joachim Curtius, 2012, “Calibration of a chemical ionization mass spectrometer for the measurement of gaseous sulfuric acid,” *J. Phys. Chem. A* **116**, 6375–6386.
- Kürten, Andreas, *et al.*, 2014, “Neutral molecular cluster formation of sulfuric acid–dimethylamine observed in real time under atmospheric conditions,” *Proc. Natl. Acad. Sci. U.S.A.* **111**, 15019–15024.
- Kwon, Hyouk-Soo, Min Hyung Ryu, and Christopher Carlsten, 2020, “Ultrafine particles: Unique physicochemical properties relevant to health and disease,” *Exp. Mol. Med.* **52**, 318–328.
- Lack, Daniel A., *et al.*, 2009, “Particulate emissions from commercial shipping: Chemical, physical, and optical properties,” *J. Geophys. Res. Atmos.* **114**.
- Laitinen, Totti, Mikael Ehn, Heikki Junninen, José Ruiz-Jimenez, Jevgeni Parshintsev, Kari Hartonen, Marja-Liisa Riekkola, Douglas R. Worsnop, and Markku Kulmala, 2011, “Characterization of organic compounds in 10- to 50-nm aerosol particles in boreal forest with laser desorption-ionization aerosol mass spectrometer and comparison with other techniques,” *Atmos. Environ.* **45**, 3711–3719.
- Lampilahti, J., *et al.*, 2021, “Zeppelin-led study on the onset of new particle formation in the planetary boundary layer,” *Atmos. Chem. Phys.* **21**, 12649–12663.
- Lana, A., *et al.*, 2011, “An updated climatology of surface dimethylsulfide concentrations and emission fluxes in the global ocean,” *Global Biogeochem. Cycles* **25**.
- Larriba, Carlos, Christopher J Hogan Jr., Michel Attoui, Rafael Borrajo, Juan Fernandez Garcia, and Juan Fernandez de la Mora, 2011, “The mobility-volume relationship below 3.0 nm examined by tandem mobility-mass measurement,” *Aerosol Sci. Technol.* **45**, 453–467.
- Lawler, Michael J., Matti P. Rissanen, Mikael Ehn, R. Lee Mauldin III, Nina Sarnela, Mikko Sipilä, and James N. Smith, 2018, “Evidence for diverse biogeochemical drivers of boreal forest new particle formation,” *Geophys. Res. Lett.* **45**, 2038–2046.
- Lee, Ben H., Felipe D. Lopez-Hilfiker, Claudia Mohr, Theo Kurtén, Douglas R. Worsnop, and Joel A. Thornton, 2014, “An iodide-adduct high-resolution time-of-flight chemical-ionization mass spectrometer: Application to atmospheric inorganic and organic compounds,” *Environ. Sci. Technol.* **48**, 6309–6317.
- Lee, Shan-Hu, *et al.*, 2016, “Isoprene suppression of new particle formation: Potential mechanisms and implications,” *J. Geophys. Res. Atmos.* **121**, 14,614–14,635.
- Lee, Y. H., J. R. Pierce, and P. J. Adams, 2013, “Representation of nucleation mode microphysics in a global aerosol model with sectional microphysics,” *Geosci. Model Dev.* **6**, 1221–1232.
- Lehtinen, K. E. J., and M. Kulmala, 2003, “A model for particle formation and growth in the atmosphere with molecular resolution in size,” *Atmos. Chem. Phys.* **3**, 251–257.
- Lehtinen, K. E. J., Ü. Rannik, T. Petäjä, M. Kulmala, and P. Hari, 2004, “Nucleation rate and vapor concentration estimations using a least squares aerosol dynamics method,” *J. Geophys. Res. Atmos.* **109**.
- Lehtinen, Kari E. J., Miikka Dal Maso, Markku Kulmala, and Veli-Matti Kerminen, 2007, “Estimating nucleation rates from apparent particle formation rates and vice versa: Revised formulation of the Kerminen-Kulmala equation,” *J. Aerosol Sci.* **38**, 988–994.
- Lehtipalo, K., *et al.*, 2014, “Methods for determining particle size distribution and growth rates between 1 and 3 nm using the particle size magnifier,” *Boreal Environ. Res.* **19**, 215–236, <https://helda.helsinki.fi/server/api/core/bitstreams/5c523985-2078-4d2e-85b5-23789b8b4559/content>.
- Lehtipalo, Katrianne, *et al.*, 2016, “The effect of acid-base clustering and ions on the growth of atmospheric nano-particles,” *Nat. Commun.* **7**, 11594.
- Lehtipalo, Katrianne, *et al.*, 2018, “Multicomponent new particle formation from sulfuric acid, ammonia, and biogenic vapors,” *Sci. Adv.* **4**, eaau5363.
- Lei, T., *et al.*, 2020, “Nano-hygroscopicity tandem differential mobility analyzer (nano-HTDMA) for investigating hygroscopic properties of sub-10 nm aerosol nanoparticles,” *Atmos. Meas. Tech.* **13**, 5551–5567.
- Lelieveld, J., J. S. Evans, M. Fnais, D. Giannadaki, and A. Pozzer, 2015, “The contribution of outdoor air pollution sources to premature mortality on a global scale,” *Nature (London)* **525**, 367.
- Leppä, J., T. Anttila, V.-M. Kerminen, M. Kulmala, and K. E. J. Lehtinen, 2011, “Atmospheric new particle formation: Real and apparent growth of neutral and charged particles,” *Atmos. Chem. Phys.* **11**, 4939–4955.
- Li, Chenxi, and Runlong Cai, 2020, “Tutorial: The discrete-sectional method to simulate an evolving aerosol,” *J. Aerosol Sci.* **150**, 105615.
- Li, Chenxi, and Peter H. McMurry, 2018, “Errors in nanoparticle growth rates inferred from measurements in chemically reacting aerosol systems,” *Atmos. Chem. Phys.* **18**, 8979–8993.

- Li, Xiaoxiao, Yuyang Li, Michael J. Lawler, Jiming Hao, James N. Smith, and Jingkun Jiang, 2021, “Composition of ultrafine particles in urban Beijing: Measurement using a thermal desorption chemical ionization mass spectrometer,” *Environ. Sci. Technol.* **55**, 2859–2868.
- Li, Xiaoxiao, *et al.*, 2022, “Insufficient condensable organic vapors lead to slow growth of new particles in an urban environment,” *Environ. Sci. Technol.* **56**, 9936–9946.
- Limbeck, Andreas, Markku Kulmala, and Hans Puxbaum, 2003, “Secondary organic aerosol formation in the atmosphere via heterogeneous reaction of gaseous isoprene on acidic particles,” *Geophys. Res. Lett.* **30**.
- Lin, Y., Y. Ji, Y. Li, J. Secrest, W. Xu, F. Xu, Y. Wang, T. An, and R. Zhang, 2019, “Interaction between succinic acid and sulfuric acid–base clusters,” *Atmos. Chem. Phys.* **19**, 8003–8019.
- Liu, Y., X. Dong, M. Wang, L. K. Emmons, Y. Liu, Y. Liang, X. Li, and M. Shrivastava, 2021, “Analysis of secondary organic aerosol simulation bias in the Community Earth System Model (CESM2.1),” *Atmos. Chem. Phys.* **21**, 8003–8021.
- London, F., 1937, “The general theory of molecular forces,” *Trans. Faraday Soc.* **33**, 8b–26.
- López-Yglesias, Xerxes, and Richard C. Flagan, 2013, “Ion–aerosol flux coefficients and the steady-state charge distribution of aerosols in a bipolar ion environment,” *Aerosol Sci. Technol.* **47**, 688–704.
- Lowe, S. J., D. G. Partridge, J. F. Davies, K. R. Wilson, D. Topping, and I. Riipinen, 2019, “Key drivers of cloud response to surface-active organics,” *Nat. Commun.* **10**, 5214.
- Lu, Y., *et al.*, 2019, “A proxy for atmospheric daytime gaseous sulfuric acid concentration in urban Beijing,” *Atmos. Chem. Phys.* **19**, 1971–1983.
- Lu, Yiqun, Ling Liu, An Ning, Gan Yang, Yiliang Liu, Theo Kurtén, Hanna Vehkamäki, Xiuhui Zhang, and Lin Wang, 2020, “Atmospheric sulfuric acid–dimethylamine nucleation enhanced by trifluoroacetic acid,” *Geophys. Res. Lett.* **47**, e2019GL085627.
- Lushnikov, A. A., and M. Kulmala, 2004, “Charging of aerosol particles in the near free-molecule regime,” *Eur. Phys. J. D* **29**, 345–355.
- Mai, Huajun, Manabu Shiraiwa, Richard C. Flagan, and John H. Seinfeld, 2015, “Under what conditions can equilibrium gas-particle partitioning be expected to hold in the atmosphere?,” *Environ. Sci. Technol.* **49**, 11485–11491.
- Mäkelä, J. M., P. Aalto, V. Jokinen, T. Pohja, A. Nissinen, S. Palmroth, T. Markkanen, K. Seitsonen, H. Lihavainen, and M. Kulmala, 1997, “Observations of ultrafine aerosol particle formation and growth in boreal forest,” *Geophys. Res. Lett.* **24**, 1219–1222.
- Makkonen, R., A. Asmi, V.-M. Kerminen, M. Boy, A. Arneth, A. Guenther, and M. Kulmala, 2012a, “BVOC–aerosol–climate interactions in the global aerosol–climate model ECHAM5.5–HAM2,” *Atmos. Chem. Phys.* **12**, 10077–10096.
- Makkonen, R., A. Asmi, V.-M. Kerminen, M. Boy, A. Arneth, P. Hari, and M. Kulmala, 2012b, “Air pollution control and decreasing new particle formation lead to strong climate warming,” *Atmos. Chem. Phys.* **12**, 1515–1524.
- Makkonen, R., Ø. Seland, A. Kirkevåg, T. Iversen, and J. E. Kristjansson, 2014, “Evaluation of aerosol number concentrations in NorESM with improved nucleation parameterization,” *Atmos. Chem. Phys.* **14**, 5127–5152.
- Makkonen, R., *et al.*, 2009, “Sensitivity of aerosol concentrations and cloud properties to nucleation and secondary organic distribution in ECHAM5–HAM global circulation model,” *Atmos. Chem. Phys.* **9**, 1747–1766.
- Manninen, H. E., *et al.*, 2009, “Long-term field measurements of charged and neutral clusters using Neutral Cluster and Air Ion Spectrometer (NAIS),” *Boreal Environ. Res.* **14**, 591–605, <https://www.borenav.net/BER/archive/pdfs/ber14/ber14-591.pdf>.
- Manninen, H. E., *et al.*, 2010, “EUCAARI ion spectrometer measurements at 12 European sites—Analysis of new particle formation events,” *Atmos. Chem. Phys.* **10**, 7907–7927.
- Mansour, Karam, *et al.*, 2020, “Particulate methanesulfonic acid over the central Mediterranean Sea: Source region identification and relationship with phytoplankton activity,” *Atmos. Res.* **237**, 104837.
- Marlow, William H., 1980, “Derivation of aerosol collision rates for singular attractive contact potentials,” *J. Chem. Phys.* **73**, 6284–6287.
- Marten, Ruby, *et al.*, 2022, “Survival of newly formed particles in haze conditions,” *Environ. Sci. Atmos.* **2**, 491–499.
- Marti, James J., Anne Jefferson, Xiao Ping Cai, Chad Richert, Peter H. McMurry, and Fred Eisele, 1997, “H<sub>2</sub>SO<sub>4</sub> vapor pressure of sulfuric acid and ammonium sulfate solutions,” *J. Geophys. Res. Atmos.* **102**, 3725–3735.
- Martin, Scot T., 2000, “Phase transitions of aqueous atmospheric particles,” *Chem. Rev.* **100**, 3403–3454.
- Martin, Scot T., *et al.*, 2010, “Sources and properties of Amazonian aerosol particles,” *Rev. Geophys.* **48**.
- Masson-Delmotte, V., *et al.* (IPCC), 2023, Eds., *Climate Change 2021: The Physical Science Basis. Contribution of Working Group I to the Sixth Assessment Report of the Intergovernmental Panel on Climate Change* (Cambridge University Press, Cambridge, England).
- Matsoukas, Themis, 1997, “The coagulation rate of charged aerosols in ionized gases,” *J. Colloid Interface Sci.* **187**, 474–483.
- Mauritsen, T., *et al.*, 2011, “An Arctic CCN-limited cloud–aerosol regime,” *Atmos. Chem. Phys.* **11**, 165–173.
- McDonald, Brian C., *et al.*, 2018, “Volatile chemical products emerging as largest petrochemical source of urban organic emissions,” *Science* **359**, 760–764.
- McFiggans, G., *et al.*, 2004, “Direct evidence for coastal iodine particles from Laminaria macroalgae—Linkage to emissions of molecular iodine,” *Atmos. Chem. Phys.* **4**, 701–713.
- McFiggans, G., *et al.*, 2006, “The effect of physical and chemical aerosol properties on warm cloud droplet activation,” *Atmos. Chem. Phys.* **6**, 2593–2649.
- McFiggans, Gordon, *et al.*, 2019, “Secondary organic aerosol reduced by mixture of atmospheric vapours,” *Nature (London)* **565**, 587–593.
- McGrath, M. J., T. Olenius, I. K. Ortega, V. Loukonen, P. Paasonen, T. Kurtén, M. Kulmala, and H. Vehkamäki, 2012, “Atmospheric Cluster Dynamics Code: A flexible method for solution of the birth–death equations,” *Atmos. Chem. Phys.* **12**, 2345–2355.
- McMurry, P. H., 1983, “New particle formation in the presence of an aerosol: Rates, time scales, and sub–0.01 micrometer size distributions,” *J. Colloid Interface Sci.* **95**, 72–80.
- McMurry, P. H., and S. K. Friedlander, 1979, “New particle formation in the presence of an aerosol,” *Atmos. Environ.* **13**, 1635–1651.
- McMurry, P. H., D. J. Rader, and J. L. Stith, 1981, “Studies of aerosol formation in power plant plumes—I. Growth laws for secondary aerosols in power plant plumes: Implications for chemical conversion mechanisms,” *Atmos. Environ.* **15**, 2315–2327.
- McMurry, P. H., and J. C. Wilson, 1982, “Growth laws for the formation of secondary ambient aerosols: Implications for chemical conversion mechanisms,” *Atmos. Environ.* **16**, 121–134.

- McMurry, P. H., *et al.*, 2005, “A criterion for new particle formation in the sulfur-rich Atlanta atmosphere,” *J. Geophys. Res. Atmos.* **110**.
- McMurry, Peter H., 1980, “Photochemical aerosol formation from SO<sub>2</sub>: A theoretical analysis of smog chamber data,” *J. Colloid Interface Sci.* **78**, 513–527.
- McMurry, Peter H., Keung Shan Woo, Rodney Weber, Da-Ren Chen, and David Y. H. Pui, 2000, “Size distributions of 3–10 nm atmospheric particles: Implications for nucleation mechanisms,” *Phil. Trans. R. Soc. A* **358**, 2625–2642.
- Merikanto, J., D. V. Spracklen, G. W. Mann, S. J. Pickering, and K. S. Carslaw, 2009, “Impact of nucleation on global CCN,” *Atmos. Chem. Phys.* **9**, 8601–8616.
- Mikkonen, S., *et al.*, 2011, “A statistical proxy for sulphuric acid concentration,” *Atmos. Chem. Phys.* **11**, 11319–11334.
- Mirme, Aadu, Eduard Tamm, Genrik Mordas, Marko Vana, Janek Uin, Sander Mirme, T. Bernotas, Lauri Laakso, Anne Hirsikko, and Markku Kulmala, 2007, “A wide-range multi-channel air ion spectrometer,” *Boreal Environ. Res.* **12**, 247–264, <https://www.borenav.net/BER/archive/pdfs/ber12/ber12-247.pdf>.
- Mohr, Claudia, *et al.*, 2019, “Molecular identification of organic vapors driving atmospheric nanoparticle growth,” *Nat. Commun.* **10**, 4442.
- Mönkkönen, P., I. K. Koponen, K. E. J. Lehtinen, K. Hämeri, R. Uma, and M. Kulmala, 2005, “Measurements in a highly polluted Asian mega city: Observations of aerosol number size distribution, modal parameters and nucleation events,” *Atmos. Chem. Phys.* **5**, 57–66.
- Murray, B. J., *et al.*, 2012, “Glass formation and unusual hygroscopic growth of iodine acid solution droplets with relevance for iodine mediated particle formation in the marine boundary layer,” *Atmos. Chem. Phys.* **12**, 8575–8587.
- Myhre, Gunnar, 2009, “Consistency between satellite-derived and modeled estimates of the direct aerosol effect,” *Science* **325**, 187–190.
- Mylläri, F., *et al.*, 2016, “New particle formation in the fresh flue-gas plume from a coal-fired power plant: Effect of flue-gas cleaning,” *Atmos. Chem. Phys.* **16**, 7485–7496.
- Myllys, N., J. Kubečka, V. Besel, D. Alfaouri, T. Olenius, J. N. Smith, and M. Passananti, 2019, “Role of base strength, cluster structure and charge in sulfuric-acid-driven particle formation,” *Atmos. Chem. Phys.* **19**, 9753–9768.
- Myllys, Nanna, Sabrina Chee, Tinja Olenius, Michael Lawler, and James Smith, 2019, “Molecular-level understanding of synergistic effects in sulfuric acid-amine-ammonia mixed clusters,” *J. Phys. Chem. A* **123**, 2420–2425.
- Nadykto, Alexey B., and Fangqun Yu, 2003, “Uptake of neutral polar vapor molecules by charged clusters/particles: Enhancement due to dipole-charge interaction,” *J. Geophys. Res. Atmos.* **108**, 4717.
- Nadykto, Alexey B., and Fangqun Yu, 2007, “Strong hydrogen bonding between atmospheric nucleation precursors and common organics,” *Chem. Phys. Lett.* **435**, 14–18.
- Németh, Zoltán, Bernadette Rosati, Naděžda Zíková, Imre Salma, László Bozó, Carmen Dameto de España, Jaroslav Schwarz, Vladimír Ždímal, and Anna Wonaschütz, 2018, “Comparison of atmospheric new particle formation events in three Central European cities,” *Atmos. Environ.* **178**, 191–197.
- Nenes, Athanasios, Spyros N. Pandis, and Christodoulos Pilinis, 1998, “ISORROPIA: A new thermodynamic equilibrium model for multiphase multicomponent inorganic aerosols,” *Aquat. Geochem.* **4**, 123–152.
- Nieminen, T., K. E. J. Lehtinen, and M. Kulmala, 2010, “Sub-10 nm particle growth by vapor condensation—Effects of vapor molecule size and particle thermal speed,” *Atmos. Chem. Phys.* **10**, 9773–9779.
- Nieminen, T., *et al.*, 2018, “Global analysis of continental boundary layer new particle formation based on long-term measurements,” *Atmos. Chem. Phys.* **18**, 14737–14756.
- O’Donnell, D., K. Tsigaridis, and J. Feichter, 2011, “Estimating the direct and indirect effects of secondary organic aerosols using ECHAM5-HAM,” *Atmos. Chem. Phys.* **11**, 8635–8659.
- O’Dowd, C. D., Y. J. Yoon, W. Junkerman, P. Aalto, M. Kulmala, H. Lihavainen, and Y. Viisanen, 2007, “Airborne measurements of nucleation mode particles I: Coastal nucleation and growth rates,” *Atmos. Chem. Phys.* **7**, 1491–1501.
- O’Dowd, C. D., Y. J. Yoon, W. Junkermann, P. Aalto, M. Kulmala, H. Lihavainen, and Y. Viisanen, 2009, “Airborne measurements of nucleation mode particles II: Boreal forest nucleation events,” *Atmos. Chem. Phys.* **9**, 937–944.
- O’Dowd, Colin, *et al.*, 1999, “On the photochemical production of new particles in the coastal boundary layer,” *Geophys. Res. Lett.* **26**, 1707–1710.
- O’Dowd, Colin D., Jose L. Jimenez, Roya Bahreini, Richard C. Flagan, John H. Seinfeld, Kaarle Hämeri, Liisa Pirjola, Markku Kulmala, S. Gerard Jennings, and Thorsten Hoffmann, 2002, “Marine aerosol formation from biogenic iodine emissions,” *Nature (London)* **417**, 632–636.
- Odum, Jay R., Thorsten Hoffmann, Frank Bowman, Don Collins, Richard C. Flagan, and John H. Seinfeld, 1996, “Gas/particle partitioning and secondary organic aerosol yields,” *Environ. Sci. Technol.* **30**, 2580–2585.
- Olenius, T., O. Kupiainen-Maatta, I. K. Ortega, T. Kurtén, and H. Vehkamäki, 2013, “Free energy barrier in the growth of sulfuric acid–ammonia and sulfuric acid–dimethylamine clusters,” *J. Chem. Phys.* **139**, 84312.
- Olenius, Tinja, Roope Halonen, Theo Kurtén, Henning Henschel, Oona Kupiainen-Määttä, Ismael K. Ortega, Coty N. Jen, Hanna Vehkamäki, and Ilona Riipinen, 2017, “New particle formation from sulfuric acid and amines: Comparison of monomethylamine, dimethylamine, and trimethylamine,” *J. Geophys. Res. Atmos.* **122**, 7103–7118.
- Olenius, Tinja, Lukas Pichelstorfer, Dominik Stolzenburg, Paul M. Winkler, Kari E. J. Lehtinen, and Ilona Riipinen, 2018, “Robust metric for quantifying the importance of stochastic effects on nanoparticle growth,” *Sci. Rep.* **8**, 14160.
- Olenius, Tinja, and Ilona Riipinen, 2017, “Molecular-resolution simulations of new particle formation: Evaluation of common assumptions made in describing nucleation in aerosol dynamics models,” *Aerosol Sci. Technol.* **51**, 397–408.
- Olenius, Tinja, Ilona Riipinen, Katrianne Lehtipalo, and Hanna Vehkamäki, 2014, “Growth rates of atmospheric molecular clusters based on appearance times and collision-evaporation fluxes: Growth by monomers,” *J. Aerosol Sci.* **78**, 55–70.
- Olin, M., H. Kuuluvainen, M. Aurela, J. Kalliokoski, N. Kuitinen, M. Isotalo, H. J. Timonen, J. V. Niemi, T. Rönkkö, and M. Dal Maso, 2020, “Traffic-originated nanocluster emission exceeds H<sub>2</sub>SO<sub>4</sub>-driven photochemical new particle formation in an urban area,” *Atmos. Chem. Phys.* **20**, 1–13.
- Ortega, I. K., O. Kupiainen, T. Kurtén, T. Olenius, O. Wilkman, M. J. McGrath, V. Loukonen, and H. Vehkamäki, 2012, “From quantum chemical formation free energies to evaporation rates,” *Atmos. Chem. Phys.* **12**, 225–235.
- Ouyang, Hui, Ranganathan Gopalakrishnan, and Christopher J. Hogan, 2012, “Nanoparticle collisions in the gas phase in the presence of singular contact potentials,” *J. Chem. Phys.* **137**, 64316.

- Ovadnevaite, Jurgita, Darius Ceburnis, Stephan Leinert, Manuel Dall'Osto, Manjula Canagaratna, Simon O'Doherty, Harald Berresheim, and Colin O'Dowd, 2014, "Submicron NE Atlantic marine aerosol chemical composition and abundance: Seasonal trends and air mass categorization," *J. Geophys. Res. Atmos.* **119**, 11,850–11,863.
- Ozon, Matthew, Aku Seppänen, Jari P. Kaipio, and Kari E. J. Lehtinen, 2021, "Retrieval of process rate parameters in the general dynamic equation for aerosols using Bayesian state estimation: BAYROSOL1.0," *Geosci. Model Dev.* **14**, 3715–3739.
- Ozon, Matthew, Dominik Stolzenburg, Lubna Dada, Aku Seppänen, and Kari E. J. Lehtinen, 2021, "Aerosol formation and growth rates from chamber experiments using Kalman smoothing," *Atmos. Chem. Phys.* **21**, 12595–12611.
- Paasonen, P., M. Peltola, J. Kontkanen, H. Junninen, V.-M. Kerminen, and M. Kulmala, 2018, "Comprehensive analysis of particle growth rates from nucleation mode to cloud condensation nuclei in boreal forest," *Atmos. Chem. Phys.* **18**, 12085–12103.
- Paasonen, P., *et al.*, 2010, "On the roles of sulphuric acid and low-volatility organic vapours in the initial steps of atmospheric new particle formation," *Atmos. Chem. Phys.* **10**, 11223–11242.
- Pandis, Spyros N., Neil M. Donahue, Benjamin N. Murphy, Ilona Riipinen, Christos Fountoukis, Eleni Karnezzi, David Patoulias, and Ksakousti Skyllakou, 2013, "Introductory lecture: Atmospheric organic aerosols: Insights from the combination of measurements and chemical transport models," *Faraday Discuss.* **165**, 9–24.
- Pankow, J. F., and W. E. Asher, 2008, "SIMPOL.1: A simple group contribution method for predicting vapor pressures and enthalpies of vaporization of multifunctional organic compounds," *Atmos. Chem. Phys.* **8**, 2773–2796.
- Pankow, James F., 1994, "An absorption model of the gas/aerosol partitioning involved in the formation of secondary organic aerosol," *Atmos. Environ.* **28**, 189–193.
- Passananti, Monica, Evgeni Zapadinsky, Tommaso Zanca, Juha Kangasluoma, Nanna Mylly, Matti P. Rissanen, Theo Kurtén, Mikael Ehn, Michel Attoui, and Hanna Vehkamäki, 2019, "How well can we predict cluster fragmentation inside a mass spectrometer?," *Chem. Commun. (Cambridge)* **55**, 5946–5949.
- Patoulias, D., C. Fountoukis, I. Riipinen, A. Asmi, M. Kulmala, and S. N. Pandis, 2018, "Simulation of the size-composition distribution of atmospheric nanoparticles over Europe," *Atmos. Chem. Phys.* **18**, 13639–13654.
- Patoulias, D., C. Fountoukis, I. Riipinen, and S. N. Pandis, 2015, "The role of organic condensation on ultrafine particle growth during nucleation events," *Atmos. Chem. Phys.* **15**, 6337–6350.
- Patoulias, D., and S. N. Pandis, 2022, "Simulation of the effects of low volatility organic compounds on aerosol number concentrations in Europe," *Atmos. Chem. Phys.* **22**, 1689–1706.
- Paulot, F., *et al.*, 2011, "Importance of secondary sources in the atmospheric budgets of formic and acetic acids," *Atmos. Chem. Phys.* **11**, 1989–2013.
- Pedata, Paola, Tobias Stoeger, Ralf Zimmermann, Annette Peters, Günter Oberdörster, and Andrea D'Anna, 2015, "Are we forgetting the smallest, sub 10 nm combustion generated particles?," *Part. Fibre Toxicol.* **12**, 34.
- Peng, J. F., *et al.*, 2014, "Submicron aerosols at thirteen diversified sites in China: Size distribution, new particle formation and corresponding contribution to cloud condensation nuclei production," *Atmos. Chem. Phys.* **14**, 10249–10265.
- Pennington, M. R., B. R. Bzdek, J. W. DePalma, J. N. Smith, A.-M. Kortelainen, L. Hildebrandt Ruiz, T. Petäjä, M. Kulmala, D. R. Worsnop, and M. V. Johnston, 2013, "Identification and quantification of particle growth channels during new particle formation," *Atmos. Chem. Phys.* **13**, 10215–10225.
- Pennington, M. R., and Murray V. Johnston, 2012, "Trapping charged nanoparticles in the nano aerosol mass spectrometer (NAMS)," *Int. J. Mass Spectrom.* **311**, 64–71.
- Perraud, Véronique, Xiaoxiao Li, Jingkun Jiang, Barbara J. Finlayson-Pitts, and James N. Smith, 2020, "Size-resolved chemical composition of sub-20 nm particles from methanesulfonic acid reactions with methylamine and ammonia," *ACS Earth Space Chem.* **4**, 1182–1194.
- Petäjä, T., R. L. Mauldin III, E. Kosciuch, J. McGrath, T. Nieminen, P. Paasonen, M. Boy, A. Adamov, T. Kotiaho, and M. Kulmala, 2009, "Sulfuric acid and OH concentrations in a boreal forest site," *Atmos. Chem. Phys.* **9**, 7435–7448.
- Petters, M. D., and S. M. Kreidenweis, 2007, "A single parameter representation of hygroscopic growth and cloud condensation nucleus activity," *Atmos. Chem. Phys.* **7**, 1961–1971.
- Pichelstorfer, L., D. Stolzenburg, J. Ortega, T. Karl, H. Kokkola, A. Laakso, K. E. J. Lehtinen, J. N. Smith, P. H. McMurry, and P. M. Winkler, 2018, "Resolving nanoparticle growth mechanisms from size- and time-dependent growth rate analysis," *Atmos. Chem. Phys.* **18**, 1307–1323.
- Pierce, J. R., and P. J. Adams, 2007, "Efficiency of cloud condensation nuclei formation from ultrafine particles," *Atmos. Chem. Phys.* **7**, 1367–1379.
- Pierce, J. R., and P. J. Adams, 2009, "Uncertainty in global CCN concentrations from uncertain aerosol nucleation and primary emission rates," *Atmos. Chem. Phys.* **9**, 1339–1356.
- Pierce, J. R., I. Riipinen, M. Kulmala, M. Ehn, T. Petäjä, H. Junninen, D. R. Worsnop, and N. M. Donahue, 2011, "Quantification of the volatility of secondary organic compounds in ultrafine particles during nucleation events," *Atmos. Chem. Phys.* **11**, 9019–9036.
- Pirjola, L., *et al.*, 2006, "Dispersion of particles and trace gases nearby a city highway: Mobile laboratory measurements in Finland," *Atmos. Environ.* **40**, 867–879.
- Posner, Laura N., and Spyros N. Pandis, 2015, "Sources of ultrafine particles in the eastern United States," *Atmos. Environ.* **111**, 103–112.
- Presto, Albert A., and Neil M. Donahue, 2006, "Investigation of  $\alpha$ -pinene + ozone secondary organic aerosol formation at low total aerosol mass," *Environ. Sci. Technol.* **40**, 3536–3543.
- Presto, Albert A., Kara E. Huff Hartz, and Neil M. Donahue, 2005, "Secondary organic aerosol production from terpene ozonolysis. 2. Effect of NO<sub>x</sub> concentration," *Environ. Sci. Technol.* **39**, 7046–7054.
- Pye, H. O. T., *et al.*, 2020, "The acidity of atmospheric particles and clouds," *Atmos. Chem. Phys.* **20**, 4809–4888.
- Qi, X. M., *et al.*, 2015, "Aerosol size distribution and new particle formation in the western Yangtze River Delta of China: 2 years of measurements at the SORPES station," *Atmos. Chem. Phys.* **15**, 12445–12464.
- Qiu, Chong, and Renyi Zhang, 2013, "Multiphase chemistry of atmospheric amines," *Phys. Chem. Chem. Phys.* **15**, 5738–5752.
- Quaas, J., *et al.*, 2020, "Constraining the Twomey effect from satellite observations: Issues and perspectives," *Atmos. Chem. Phys.* **20**, 15079–15099.
- Raoult, F. M., 1886, "Loi générale des tensions de vapeur des dissolvants," *C.R. Hebd. Seances Acad. Sci.* **104**, 1430–1433.
- Reddington, C. L., *et al.*, 2011, "Primary versus secondary contributions to particle number concentrations in the European boundary layer," *Atmos. Chem. Phys.* **11**, 12007–12036.

- Riccobono, Francesco, *et al.*, 2014, “Oxidation products of biogenic emissions contribute to nucleation of atmospheric particles,” *Science* **344**, 717–721.
- Riipinen, I., *et al.*, 2011, “Organic condensation: A vital link connecting aerosol formation to cloud condensation nuclei (CCN) concentrations,” *Atmos. Chem. Phys.* **11**, 3865–3878.
- Riipinen, Ilona, Taina Yli-Juuti, Jeffrey R. Pierce, Tuukka Petäjä, Douglas R. Worsnop, Markku Kulmala, and Neil M. Donahue, 2012, “The contribution of organics to atmospheric nanoparticle growth,” *Nat. Geosci.* **5**, 453–458.
- Rissanen, M. P., J. Mikkilä, S. Iyer, and J. Hakala, 2019, “Multi-scheme chemical ionization inlet (MION) for fast switching of reagent ion chemistry in atmospheric pressure chemical ionization mass spectrometry (CIMS) applications,” *Atmos. Meas. Tech.* **12**, 6635–6646.
- Rissanen, Matti, 2021, “Anthropogenic volatile organic compound (AVOC) autoxidation as a source of highly oxygenated organic molecules (HOM),” *J. Phys. Chem. A* **125**, 9027–9039.
- Riva, M., M. Brüggemann, D. Li, S. Perrier, C. George, H. Herrmann, and T. Berndt, 2020, “Capability of CI-orbitrap for gas-phase analysis in atmospheric chemistry: A comparison with the CI-API-TOF technique,” *Anal. Chem.* **92**, 8142–8150.
- Riva, M., M. Ehn, D. Li, S. Tomaz, F. Bourgain, S. Perrier, and C. George, 2019, “CI-Orbitrap: An analytical instrument to study atmospheric reactive organic species,” *Anal. Chem.* **91**, 9419–9423.
- Riva, M., *et al.*, 2019, “Evaluating the performance of five different chemical ionization techniques for detecting gaseous oxygenated organic species,” *Atmos. Meas. Tech.* **12**, 2403–2421.
- Riva, Matthieu, *et al.*, 2016, “Chemical characterization of secondary organic aerosol from oxidation of isoprene hydroxyhydroperoxides,” *Environ. Sci. Technol.* **50**, 9889–9899.
- Roldin, Pontus, *et al.*, 2019, “The role of highly oxygenated organic molecules in the boreal aerosol-cloud-climate system,” *Nat. Commun.* **10**, 4370.
- Rönkkö, Topi, *et al.*, 2017, “Traffic is a major source of atmospheric nanocluster aerosol,” *Proc. Natl. Acad. Sci. U.S.A.* **114**, 7549–7554.
- Rosati, Bernadette, *et al.*, 2021, “New particle formation and growth from dimethyl sulfide oxidation by hydroxyl radicals,” *ACS Earth Space Chem.* **5**, 801–811.
- Rose, C., B. Foucart, D. Picard, A. Colomb, J.-M. Metzger, P. Tulet, and K. Sellegri, 2019, “New particle formation in the volcanic eruption plume of the Piton de la Fournaise: Specific features from a long-term dataset,” *Atmos. Chem. Phys.* **19**, 13243–13265.
- Rose, C., K. Sellegri, E. Freney, R. Dupuy, A. Colomb, J.-M. Pichon, M. Ribeiro, T. Bourianne, F. Burnet, and A. Schwarzenboeck, 2015, “Airborne measurements of new particle formation in the free troposphere above the Mediterranean Sea during the HYMEX campaign,” *Atmos. Chem. Phys.* **15**, 10203–10218.
- Rose, C., *et al.*, 2015, “Frequent nucleation events at the high altitude station of Chacaltaya (5240 m a.s.l.), Bolivia,” *Atmos. Environ.* **102**, 18–29.
- Rose, Clémence, *et al.*, 2018, “Observations of biogenic ion-induced cluster formation in the atmosphere,” *Sci. Adv.* **4**, 10.1126/sciadv.aar5218.
- Sakurai, Hiromu, Melissa A. Fink, Peter H. McMurry, Lee Mauldin, Katharine F. Moore, James N. Smith, and Fred L. Eisele, 2005, “Hygroscopicity and volatility of 4–10 nm particles during summertime atmospheric nucleation events in urban Atlanta,” *J. Geophys. Res. Atmos.* **110**.
- Salma, I., Z. Nemeth, V.-M. Kerminen, P. Aalto, T. Nieminen, T. Weidinger, Á. Molnár, K. Imre, and M. Kulmala, 2016, “Regional effect on urban atmospheric nucleation,” *Atmos. Chem. Phys.* **16**, 8715–8728.
- Salma, I., and Z. Németh, 2019, “Dynamic and timing properties of new aerosol particle formation and consecutive growth events,” *Atmos. Chem. Phys.* **19**, 5835–5852.
- Sarangi, Bighnaraj, Shankar G. Aggarwal, and Prabhat K. Gupta, 2015, “A simplified approach to calculate particle growth rate due to self-coagulation, scavenging and condensation using SMPS measurements during a particle growth event in New Delhi,” *Aerosol Air Qual. Res.* **15**, 166–179.
- Saunders, R. W., R. Kumar, J. C. Gómez Martín, A. S. Mahajan, B. J. Murray, and J. M. C. Plane, 2010, “Studies of the formation and growth of aerosol from molecular iodine precursor,” *Z. Phys. Chem. (Wiesbaden)* **224**, 1095–1117.
- Saunders, Russell W., and John M. C. Plane, 2005, “Formation pathways and composition of iodine oxide ultra-fine particles,” *Environ. Chem.* **2**, 299–303.
- Sceats, Mark G., 1989, “Brownian coagulation in aerosols—The role of long range forces,” *J. Colloid Interface Sci.* **129**, 105–112.
- Schade, Gunnar W., and Paul J. Crutzen, 1995, “Emission of aliphatic amines from animal husbandry and their reactions: Potential source of N<sub>2</sub>O and HCN,” *J. Atmos. Chem.* **22**, 319–346.
- Schobesberger, Siegfried, *et al.*, 2013, “Molecular understanding of atmospheric particle formation from sulfuric acid and large oxidized organic molecules,” *Proc. Natl. Acad. Sci. U.S.A.* **110**, 17223–17228.
- Scott, C. E., *et al.*, 2014, “The direct and indirect radiative effects of biogenic secondary organic aerosol,” *Atmos. Chem. Phys.* **14**, 447–470.
- Scott, C. E., *et al.*, 2015, “Impact of gas-to-particle partitioning approaches on the simulated radiative effects of biogenic secondary organic aerosol,” *Atmos. Chem. Phys.* **15**, 12989–13001.
- Sebastian, Mathew, Vijay P. Kanawade, and Jeffrey R. Pierce, 2021, “Observation of sub-3 nm particles and new particle formation at an urban location in India,” *Atmos. Environ.* **256**, 118460.
- Seinfeld, J., and S. Pandis, 2016, *Atmospheric Chemistry and Physics: From Air Pollution to Climate Change*, 3rd ed. (Wiley, New York).
- Seland, Ø., *et al.*, 2020, “Overview of the Norwegian Earth System Model (NorESM2) and key climate response of CMIP6 DECK, historical, and scenario simulations,” *Geosci. Model Dev.* **13**, 6165–6200.
- Sellegri, Karine, Clemence Rose, Angela Marinoni, Angelo Lupi, Alfred Wiedensohler, Marcos Andrade, Paolo Bonasoni, and Paolo Laj, 2019, “New particle formation: A review of ground-based observations at mountain research stations,” *Atmos.-Ocean* **10**, 493.
- Semeniuk, Kirill, and Ashu Dastoor, 2020, “Current state of atmospheric aerosol thermodynamics and mass transfer modeling: A review,” *Atmos.-Ocean* **11**, 156.
- Sengupta, K., K. Pringle, J. S. Johnson, C. Reddington, J. Browse, C. E. Scott, and K. Carslaw, 2021, “A global model perturbed parameter ensemble study of secondary organic aerosol formation,” *Atmos. Chem. Phys.* **21**, 2693–2723.
- Shah, Rishabh U., Matthew M. Coggon, Georgios I. Gkatzelis, Brian C. McDonald, Antonios Tasoglou, Heinz Huber, Jessica Gilman, Carsten Warneke, Allen L. Robinson, and Albert A. Presto, 2020, “Urban oxidation flow reactor measurements reveal significant secondary organic aerosol contributions from volatile emissions of emerging importance,” *Environ. Sci. Technol.* **54**, 714–725.

- Shen, Jiali, *et al.*, 2021, “Emerging investigator series: COVID-19 lockdown effects on aerosol particle size distributions in northern Italy,” *Environ. Sci. Atmos.* **1**, 214–227.
- Shen, Jiali, *et al.*, 2022, “High gas-phase methanesulfonic acid production in the OH-initiated oxidation of dimethyl sulfide at low temperatures,” *Environ. Sci. Technol.* **56**, 13931–13944.
- Shen, Jiewen, Jonas Elm, Hong-Bin Xie, Jingwen Chen, Junfeng Niu, and Hanna Vehkamäki, 2020, “Structural effects of amines in enhancing methanesulfonic acid-driven new particle formation,” *Environ. Sci. Technol.* **54**, 13498–13508.
- Shen, X., J. Sun, F. Yu, Y. Wang, J. Zhong, Y. Zhang, X. Hu, C. Xia, S. Zhang, and X. Zhang, 2021, “Enhancement of nanoparticle formation and growth during the COVID-19 lockdown period in urban Beijing,” *Atmos. Chem. Phys.* **21**, 7039–7052.
- Shi, Xiaodi, Xinghua Qiu, Qi Chen, Shiyi Chen, Min Hu, Yinon Rudich, and Tong Zhu, 2021, “Organic iodine compounds in fine particulate matter from a continental urban region: Insights into secondary formation in the atmosphere,” *Environ. Sci. Technol.* **55**, 1508–1514.
- Shrivastava, Manish, *et al.*, 2015, “Global transformation and fate of SOA: Implications of low-volatility SOA and gas-phase fragmentation reactions,” *J. Geophys. Res. Atmos.* **120**, 4169–4195.
- Shrivastava, Manish, *et al.*, 2017, “Recent advances in understanding secondary organic aerosol: Implications for global climate forcing,” *Rev. Geophys.* **55**, 509–559.
- Sihto, S.-L., *et al.*, 2006, “Atmospheric sulphuric acid and aerosol formation: Implications from atmospheric measurements for nucleation and early growth mechanisms,” *Atmos. Chem. Phys.* **6**, 4079–4091.
- Sihto, S.-L., *et al.*, 2011, “Seasonal variation of CCN concentrations and aerosol activation properties in boreal forest,” *Atmos. Chem. Phys.* **11**, 13269–13285.
- Simon, M., *et al.*, 2020, “Molecular understanding of new-particle formation from  $\alpha$ -pinene between  $-50$  and  $+25$  °C,” *Atmos. Chem. Phys.* **20**, 9183–9207.
- Sindelarova, K., C. Granier, I. Bouarar, A. Guenther, S. Tilmes, T. Stavrou, J.-F. Müller, U. Kuhn, P. Stefani, and W. Knorr, 2014, “Global data set of biogenic VOC emissions calculated by the MEGAN model over the last 30 years,” *Atmos. Chem. Phys.* **14**, 9317–9341.
- Sintermann, J., S. Schallhart, M. Kajos, M. Jocher, A. Bracher, A. Mürner, D. Johnson, A. Neftel, and T. Ruuskanen, 2014, “Trimethylamine emissions in animal husbandry,” *Biogeosciences* **11**, 5073–5085.
- Sipilä, Mikko, *et al.*, 2010, “The role of sulfuric acid in atmospheric nucleation,” *Science* **327**, 1243–1246.
- Sipilä, Mikko, *et al.*, 2016, “Molecular-scale evidence of aerosol particle formation via sequential addition of  $\text{HIO}_3$ ,” *Nature (London)* **537**, 532.
- Sipkens, Timothy A., Joel C. Corbin, Samuel J. Grauer, and Gregory J. Smallwood, 2023, “Tutorial: Guide to error propagation for particle counting measurements,” *J. Aerosol Sci.* **167**, 106091.
- Skrabalova, L., D. Brus, T. Anttila, V. Zdimal, and H. Lihavainen, 2014, “Growth of sulphuric acid nanoparticles under wet and dry conditions,” *Atmos. Chem. Phys.* **14**, 6461–6475.
- Smith, J. N., M. J. Dunn, T. M. VanReken, K. Iida, M. R. Stolzenburg, P. H. McMurry, and L. G. Huey, 2008, “Chemical composition of atmospheric nanoparticles formed from nucleation in Tecamac, Mexico: Evidence for an important role for organic species in nanoparticle growth,” *Geophys. Res. Lett.* **35**.
- Smith, J. N., K. F. Moore, P. H. McMurry, and F. L. Eisele, 2004, “Atmospheric measurements of sub-20 nm diameter particle chemical composition by thermal desorption chemical ionization mass spectrometry,” *Aerosol Sci. Technol.* **38**, 100–110.
- Smith, James N., Kelley C. Barsanti, Hans R. Friedli, Mikael Ehn, Markku Kulmala, Donald R. Collins, Jacob H. Scheckman, Brent J. Williams, and Peter H. McMurry, 2010, “Observations of aminium salts in atmospheric nanoparticles and possible climatic implications,” *Proc. Natl. Acad. Sci. U.S.A.* **107**, 6634–6639.
- Smith, James N., Danielle C. Draper, Sabrina Chee, Michelia Dam, Hayley Glicker, Deanna Myers, Adam E. Thomas, Michael J. Lawler, and Nanna Myllys, 2021, “Atmospheric clusters to nanoparticles: Recent progress and challenges in closing the gap in chemical composition,” *J. Aerosol Sci.* **153**, 105733.
- Sporre, M. K., S. M. Blichner, R. Schrödner, I. H. H. Karset, T. K. Berntsen, T. van Noije, T. Bergman, D. O’Donnell, and R. Makkonen, 2020, “Large difference in aerosol radiative effects from BVOC-SOA treatment in three Earth system models,” *Atmos. Chem. Phys.* **20**, 8953–8973.
- Spracklen, D. V., K. S. Carslaw, M. Kulmala, V.-M. Kerminen, G. W. Mann, and S.-L. Sihto, 2006, “The contribution of boundary layer nucleation events to total particle concentrations on regional and global scales,” *Atmos. Chem. Phys.* **6**, 5631–5648.
- Spracklen, D. V., *et al.*, 2008, “Contribution of particle formation to global cloud condensation nuclei concentrations,” *Geophys. Res. Lett.* **35**, L06808.
- Spracklen, D. V., *et al.*, 2010, “Explaining global surface aerosol number concentrations in terms of primary emissions and particle formation,” *Atmos. Chem. Phys.* **10**, 4775–4793.
- Stevens, R. G., and J. R. Pierce, 2014, “The contribution of plume-scale nucleation to global and regional aerosol and CCN concentrations: Evaluation and sensitivity to emissions changes,” *Atmos. Chem. Phys.* **14**, 13661–13679.
- Stolzenburg, D., T. Laurila, P. Aalto, J. Vanhanen, T. Petäjä, and J. Kangasluoma, 2023, “Improved counting statistics of an ultrafine DMPS system,” *Atmos. Meas. Tech.* **16**, 2471–2483.
- Stolzenburg, D., G. Steiner, and P. M. Winkler, 2017, “A DMA-train for precision measurement of sub-10 nm aerosol dynamics,” *Atmos. Meas. Tech.* **10**, 1639–1651.
- Stolzenburg, D., M. Wang, M. Schervish, and N. M. Donahue, 2022, “Tutorial: Dynamic organic growth modeling with a volatility basis set,” *J. Aerosol Sci.* **166**, 106063.
- Stolzenburg, D., *et al.*, 2020, “Enhanced growth rate of atmospheric particles from sulfuric acid,” *Atmos. Chem. Phys.* **20**, 7359–7372.
- Stolzenburg, Dominik, Matthew Ozon, Markku Kulmala, Kari E. J. Lehtinen, Katrianne Lehtipalo, and Juha Kangasluoma, 2022, “Combining instrument inversions for sub-10 nm aerosol number size-distribution measurements,” *J. Aerosol Sci.* **159**, 105862.
- Stolzenburg, Dominik, *et al.*, 2018, “Rapid growth of organic aerosol nanoparticles over a wide tropospheric temperature range,” *Proc. Natl. Acad. Sci. U.S.A.* **115**, 9122–9127.
- Stolzenburg, Mark R., Peter H. McMurry, Hiromu Sakurai, James N. Smith, R. Lee Mauldin III, Fred L. Eisele, and Charles F. Clement, 2005, “Growth rates of freshly nucleated atmospheric particles in Atlanta,” *J. Geophys. Res. Atmos.* **110**.
- Suh, Inseon, Renyi Zhang, Luisa T. Molina, and Mario J. Molina, 2003, “Oxidation mechanism of aromatic peroxy and bicyclic radicals from OH-toluene reactions,” *J. Am. Chem. Soc.* **125**, 12655–12665.
- Suni, T., *et al.*, 2008, “Formation and characteristics of ions and charged aerosol particles in a native Australian Eucalypt forest,” *Atmos. Chem. Phys.* **8**, 129–139.
- Surratt, Jason D., Michael Lewandowski, John H. Offenberg, Mohammed Jaoui, Tadeusz E. Kleindienst, Edward O. Edney,

- and John H. Seinfeld, 2007, “Effect of acidity on secondary organic aerosol formation from isoprene,” *Environ. Sci. Technol.* **41**, 5363–5369.
- Svenningsson, B., *et al.*, 2008, “Aerosol particle formation events and analysis of high growth rates observed above a subarctic wetland-forest mosaic,” *Tellus B* **60**, 353–364.
- Svensmark, H., M. B. Enghoff, N. J. Shaviv, and J. Svensmark, 2017, “Increased ionization supports growth of aerosols into cloud condensation nuclei,” *Nat. Commun.* **8**, 2199.
- Takahama, Satoshi, Ann E. Wittig, Dimitris V. Vayenas, Cliff I. Davidson, and Spyros N. Pandis, 2004, “Modeling the diurnal variation of nitrate during the Pittsburgh Air Quality Study,” *J. Geophys. Res. Atmos.* **109**.
- Tammet, H., 2006, “Continuous scanning of the mobility and size distribution of charged clusters and nanometer particles in atmospheric air and the balanced scanning mobility analyzer BSMA,” *Atmos. Res.* **82**, 523–535.
- Tang, Lizi, Dongjie Shang, Xin Fang, Zhijun Wu, Yanting Qiu, Shiyi Chen, Xin Li, Limin Zeng, Song Guo, and Min Hu, 2021, “More significant impacts from new particle formation on haze formation during COVID-19 lockdown,” *Geophys. Res. Lett.* **48**, e2020GL091591.
- Temelso, Berhane, Thomas E. Morrell, Robert M. Shields, Marco A. Allodi, Elena K. Wood, Karl N. Kirschner, Thomas C. Castonguay, Kaye A. Archer, and George C. Shields, 2012, “Quantum mechanical study of sulfuric acid hydration: Atmospheric implications,” *J. Phys. Chem. A* **116**, 2209–2224.
- Tervahattu, Heikki, Jyrki Juhanoja, and Kaarle Kupiainen, 2002, “Identification of an organic coating on marine aerosol particles by TOF-SIMS,” *J. Geophys. Res. Atmos.* **107**, ACH 18-1–ACH 18-7.
- Tilmes, S., *et al.*, 2019, “Climate forcing and trends of organic aerosols in the Community Earth System Model (CESM2),” *J. Adv. Model. Earth Syst.* **11**, 4323–4351.
- Tolocka, Michael P., Myoseon Jang, Joy M. Ginter, Frederick J. Cox, Richard M. Kamens, and Murray V. Johnston, 2004, “Formation of oligomers in secondary organic aerosol,” *Environ. Sci. Technol.* **38**, 1428–1434.
- Tröstl, Jasmin, *et al.*, 2016a, “The role of low-volatility organic compounds in initial particle growth in the atmosphere,” *Nature (London)* **533**, 527–531.
- Tröstl, Jasmin, *et al.*, 2016b, “Contribution of new particle formation to the total aerosol concentration at the high-altitude site Jungfraujoch (3580 m asl, Switzerland),” *J. Geophys. Res. Atmos.* **121**, 11,692–11,711.
- Tsigaridis, K., *et al.*, 2014, “The AeroCom evaluation and inter-comparison of organic aerosol in global models,” *Atmos. Chem. Phys.* **14**, 10845–10895.
- Tuovinen, S., R. Cai, V.-M. Kerminen, J. Jiang, C. Yan, M. Kulmala, and J. Kontkanen, 2022, “Survival probabilities of atmospheric particles: Comparison based on theory, cluster population simulations, and observations in Beijing,” *Atmos. Chem. Phys.* **22**, 15071–15091.
- Twomey, S., 1974, “Pollution and the planetary albedo,” *Atmos. Environ.* **8**, 1251–1256.
- Vakkari, V., H. Laakso, M. Kulmala, A. Laaksonen, D. Mabaso, M. Molefe, N. Kgabi, and L. Laakso, 2011, “New particle formation events in semi-clean South African savannah,” *Atmos. Chem. Phys.* **11**, 3333–3346.
- Vakkari, Ville, *et al.*, 2014, “Rapid changes in biomass burning aerosols by atmospheric oxidation,” *Geophys. Res. Lett.* **41**, 2644–2651.
- Vakkari, Ville, *et al.*, 2015, “Reevaluating the contribution of sulfuric acid and the origin of organic compounds in atmospheric nanoparticle growth,” *Geophys. Res. Lett.* **42**, 10,486–10,493.
- Vana, M., K. Komsaare, U. Hörrak, S. Mirme, T. Nieminen, J. Kontkanen, H. E. Manninen, T. Petäjä, Steffen M. Noe, and M. Kulmala, 2016, “Characteristics of new particle formation at three SMEAR stations,” *Boreal Environ. Res.* **21**, 345–362, <https://helda.helsinki.fi/server/api/core/bitstreams/75665bb7-3bcb-48d6-b93a-eb72928cf696/content>.
- Vanhanen, J., J. Mikkilä, K. Lehtipalo, M. Sipilä, H. E. Manninen, E. Siivola, T. Petäjä, and M. Kulmala, 2011, “Particle size magnifier for nano-CN detection,” *Aerosol Sci. Technol.* **45**, 533–542.
- van Marle, M. J. E., *et al.*, 2017, “Historic global biomass burning emissions for CMIP6 (BB4 CMIP) based on merging satellite observations with proxies and fire models (1750–2015),” *Geosci. Model Dev.* **10**, 3329–3357.
- van Noije, T., *et al.*, 2021, “EC-Earth3-AerChem: A global climate model with interactive aerosols and atmospheric chemistry participating in CMIP6,” *Geosci. Model Dev.* **14**, 5637–5668.
- Van Rooy, Paul, Ryan Drover, Tanner Cress, Cara Michael, Kathleen L Purvis-Roberts, Philip J. Silva, Matthew J. Nee, and David Cocker, 2021, “Methanesulfonic acid and sulfuric acid aerosol formed through oxidation of reduced sulfur compounds in a humid environment,” *Atmos. Environ.* **261**, 118504.
- Vehkamäki, H., M. Kulmala, I. Napari, K. E. J. Lehtinen, C. Timmreck, M. Noppel, and A. Laaksonen, 2002, “An improved parameterization for sulfuric acid–water nucleation rates for tropospheric and stratospheric conditions,” *J. Geophys. Res. Atmos.* **107**, AAC 3-1–AAC 3-10.
- Vehkamäki, Hanna, and Ilona Riipinen, 2012, “Thermodynamics and kinetics of atmospheric aerosol particle formation and growth,” *Chem. Soc. Rev.* **41**, 5160–5173.
- Verheggen, B., and M. Mozurkewich, 2006, “An inverse modeling procedure to determine particle growth and nucleation rates from measured aerosol size distributions,” *Atmos. Chem. Phys.* **6**, 2927–2942.
- Verheggen, Bart, and Michael Mozurkewich, 2002, “Determination of nucleation and growth rates from observation of a SO<sub>2</sub> induced atmospheric nucleation event,” *J. Geophys. Res. Atmos.* **107**, AAC 5-1–AAC 5-12.
- Vesterinen, M., K. E. J. Lehtinen, M. Kulmala, and A. Laaksonen, 2007, “Effect of particle phase oligomer formation on aerosol growth,” *Atmos. Environ.* **41**, 1768–1776.
- Vignati, Elisabetta, Julian Wilson, and Philip Stier, 2004, “M7: An efficient size-resolved aerosol microphysics module for large-scale aerosol transport models,” *J. Geophys. Res. Atmos.* **109**.
- Viskari, T., E. Asmi, P. Kolmonen, H. Vuollekoski, T. Petäjä, and H. Järvinen, 2012, “Estimation of aerosol particle number distributions with Kalman filtering—Part 1: Theory, general aspects and statistical validity,” *Atmos. Chem. Phys.* **12**, 11767–11779.
- Vogel, Alexander L., Johannes Schneider, Christina Müller-Tautges, Thomas Klimach, and Thorsten Hoffmann, 2016, “Aerosol chemistry resolved by mass spectrometry: Insights into particle growth after ambient new particle formation,” *Environ. Sci. Technol.* **50**, 10814–10822.
- Vogel, Alexander L., *et al.*, 2016, “Aerosol chemistry resolved by mass spectrometry: Linking field measurements of cloud condensation nuclei activity to organic aerosol composition,” *Environ. Sci. Technol.* **50**, 10823–10832.
- Voliotis, A., Y. Wang, Y. Shao, M. Du, T. J. Bannan, C. J. Percival, S. N. Pandis, M. R. Alfarra, and G. McFiggans, 2021, “Exploring the composition and volatility of secondary organic aerosols in

- mixed anthropogenic and biogenic precursor systems,” *Atmos. Chem. Phys.* **21**, 14251–14273.
- Wagner, A. C., *et al.*, 2018, “Size resolved online chemical analysis of nano aerosol particles: A thermal desorption differential mobility analyzer coupled to a chemical ionization time of flight mass spectrometer,” *Atmos. Meas. Tech.* **11**, 5489–5506.
- Wagner, R., *et al.*, 2017, “The role of ions in new particle formation in the CLOUD chamber,” *Atmos. Chem. Phys.* **17**, 15181–15197.
- Wang, J., R. L. McGraw, and C. Kuang, 2013, “Growth of atmospheric nano-particles by heterogeneous nucleation of organic vapor,” *Atmos. Chem. Phys.* **13**, 6523–6531.
- Wang, Jian, *et al.*, 2016, “Amazon boundary layer aerosol concentration sustained by vertical transport during rainfall,” *Nature (London)* **539**, 416–419.
- Wang, Lin, Alexei F. Khalizov, Jun Zheng, Wen Xu, Yan Ma, Vinita Lal, and Renyi Zhang, 2010, “Atmospheric nanoparticles formed from heterogeneous reactions of organics,” *Nat. Geosci.* **3**, 238–242.
- Wang, Lin, Wen Xu, Alexei F. Khalizov, Jun Zheng, Chong Qiu, and Renyi Zhang, 2011, “Laboratory investigation on the role of organics in atmospheric nanoparticle growth,” *J. Phys. Chem. A* **115**, 8940–8947.
- Wang, M., *et al.*, 2020a, “Photo-oxidation of aromatic hydrocarbons produces low-volatility organic compounds,” *Environ. Sci. Technol.* **54**, 7911–7921.
- Wang, M., *et al.*, 2020b, “Rapid growth of new atmospheric particles by nitric acid and ammonia condensation,” *Nature (London)* **581**, 184–189.
- Wang, M., and J. E. Penner, 2009, “Aerosol indirect forcing in a global model with particle nucleation,” *Atmos. Chem. Phys.* **9**, 239–260.
- Wang, Shih Chen, and Richard C. Flagan, 1990, “Scanning electrical mobility spectrometer,” *Aerosol Sci. Technol.* **13**, 230–240.
- Wang, Z. B., M. Hu, X. Y. Pei, R. Y. Zhang, P. Paasonen, J. Zheng, D. L. Yue, Z. J. Wu, M. Boy, and A. Wiedensohler, 2015, “Connection of organics to atmospheric new particle formation and growth at an urban site of Beijing,” *Atmos. Environ.* **103**, 7–17.
- Wang, Z. B., M. Hu, J. Y. Sun, Z. J. Wu, D. L. Yue, X. J. Shen, Y. M. Zhang, X. Y. Pei, Y. F. Cheng, and A. Wiedensohler, 2013, “Characteristics of regional new particle formation in urban and regional background environments in the North China Plain,” *Atmos. Chem. Phys.* **13**, 12495–12506.
- Weber, R. J., J. J. Marti, and P. H. McMurry, 1997, “Measurements of new particle formation and ultrafine particle growth rates at a clean continental site,” *J. Geophys. Res. Atmos.* **102**, 4375–4385.
- Weber, R. J., P. H. McMurry, F. L. Eisele, and D. J. Tanner, 1995, “Measurement of expected nucleation precursor species and 3–500-nm diameter particles at Mauna Loa Observatory, Hawaii,” *J. Atmos. Sci.* **52**, 2242–2257.
- Wehner, B., F. Werner, F. Ditas, R. A. Shaw, M. Kulmala, and H. Siebert, 2015, “Observations of new particle formation in enhanced UV irradiance zones near cumulus clouds,” *Atmos. Chem. Phys.* **15**, 11701–11711.
- Wehner, Birgit, Holger Siebert, Frank Stratmann, Thomas Tuch, Alfred Wiedensohler, Tuukka Petäjä, Miikka Dal Maso, and Markku Kulmala, 2007, “Horizontal homogeneity and vertical extent of new particle formation events,” *Tellus B* **59**, 362–371.
- Weigel, R., *et al.*, 2011, “*In situ* observations of new particle formation in the tropical upper troposphere: The role of clouds and the nucleation mechanism,” *Atmos. Chem. Phys.* **11**, 9983–10010.
- Weigelt, A., M. Hermann, P. F. J. van Velthoven, C. A. M. Brenninkmeijer, G. Schlaf, A. Zahn, and A. Wiedensohler, 2009, “Influence of clouds on aerosol particle number concentrations in the upper troposphere,” *J. Geophys. Res. Atmos.* **114**.
- Weller, R., K. Schmidt, K. Teinilä, and R. Hillamo, 2015, “Natural new particle formation at the coastal Antarctic site Neumayer,” *Atmos. Chem. Phys.* **15**, 11399–11410.
- Westervelt, D. M., J. R. Pierce, and P. J. Adams, 2014, “Analysis of feedbacks between nucleation rate, survival probability and cloud condensation nuclei formation,” *Atmos. Chem. Phys.* **14**, 5577–5597.
- Westervelt, D. M., J. R. Pierce, I. Riipinen, W. Trivitayanurak, A. Hamed, M. Kulmala, A. Laaksonen, S. Decesari, and P. J. Adams, 2013, “Formation and growth of nucleated particles into cloud condensation nuclei: Model-measurement comparison,” *Atmos. Chem. Phys.* **13**, 7645–7663.
- Wexler, Anthony S., and Simon L. Clegg, 2002, “Atmospheric aerosol models for systems including the ions  $H^+$ ,  $NH_4^+$ ,  $Na^+$ ,  $SO_4^{2-}$ ,  $NO_3^-$ ,  $Cl^-$ ,  $Br^-$ , and  $H_2O$ ,” *J. Geophys. Res. Atmos.* **107**, ACH 14-1–ACH 14-14.
- Wexler, Anthony S., and John H. Seinfeld, 1990, “The distribution of ammonium salts among a size and composition dispersed aerosol,” *Atmos. Environ. A* **24**, 1231–1246.
- Whitby, Kenneth T., 1978, “The physical characteristics of sulfur aerosols,” *Atmos. Environ.* **12**, 135–159.
- Wiedensohler, A., *et al.*, 2012, “Mobility particle size spectrometers: Harmonization of technical standards and data structure to facilitate high quality long-term observations of atmospheric particle number size distributions,” *Atmos. Meas. Tech.* **5**, 657–685.
- Wildt, J., *et al.*, 2014, “Suppression of new particle formation from monoterpene oxidation by  $NO_x$ ,” *Atmos. Chem. Phys.* **14**, 2789–2804.
- Williamson, C., A. Kupc, J. Wilson, D. W. Gesler, J. M. Reeves, F. Erdesz, R. McLaughlin, and C. A. Brock, 2018, “Fast time response measurements of particle size distributions in the 3–60 nm size range with the nucleation mode aerosol size spectrometer,” *Atmos. Meas. Tech.* **11**, 3491–3509.
- Williamson, Christina J., *et al.*, 2019, “A large source of cloud condensation nuclei from new particle formation in the tropics,” *Nature (London)* **574**, 399–403.
- Willis, M. D., *et al.*, 2016, “Growth of nucleation mode particles in the summertime Arctic: A case study,” *Atmos. Chem. Phys.* **16**, 7663–7679.
- Wilson, C. T. R., 1912, “On an expansion apparatus for making visible the tracks of ionising particles in gases and some results obtained by its use,” *Proc. R. Soc. A* **87**, 277–292.
- Wimmer, D., *et al.*, 2013, “Performance of diethylene glycol-based particle counters in the sub-3 nm size range,” *Atmos. Meas. Tech.* **6**, 1793–1804.
- Wyslouzil, Barbara E., and Gerald Wilemski, 1995, “Binary nucleation kinetics. II. Numerical solution of the birth-death equations,” *J. Chem. Phys.* **103**, 1137–1151.
- Xiao, M., *et al.*, 2021, “The driving factors of new particle formation and growth in the polluted boundary layer,” *Atmos. Chem. Phys.* **21**, 14275–14291.
- Xiao, S., *et al.*, 2015, “Strong atmospheric new particle formation in winter in urban Shanghai, China,” *Atmos. Chem. Phys.* **15**, 1769–1781.
- Xu, Lu, *et al.*, 2015, “Effects of anthropogenic emissions on aerosol formation from isoprene and monoterpenes in the southeastern United States,” *Proc. Natl. Acad. Sci. U.S.A.* **112**, 37–42.
- Xu, Weiqi, *et al.*, 2019, “Changes in aerosol chemistry from 2014 to 2016 in winter in Beijing: Insights from high-resolution aerosol mass spectrometry,” *J. Geophys. Res. Atmos.* **124**, 1132–1147.

- Xu, Wen, Mario Gomez-Hernandez, Song Guo, Jeremiah Secrest, Wilmarie Marrero-Ortiz, Annie L. Zhang, and Renyi Zhang, 2014, “Acid-catalyzed reactions of epoxides for atmospheric nanoparticle growth,” *J. Am. Chem. Soc.* **136**, 15477–15480.
- Xu, Wen, and Renyi Zhang, 2013, “A theoretical study of hydrated molecular clusters of amines and dicarboxylic acids,” *J. Chem. Phys.* **139**, 64312.
- Yan, C., *et al.*, 2020, “Size-dependent influence of NO<sub>x</sub> on the growth rates of organic aerosol particles,” *Sci. Adv.* **6**, eaay4945.
- Yan, C., *et al.*, 2022, “The effect of COVID-19 restrictions on atmospheric new particle formation in Beijing,” *Atmos. Chem. Phys.* **22**, 12207–12220.
- Yan, Chao, *et al.*, 2021, “The synergistic role of sulfuric acid, bases, and oxidized organics governing new-particle formation in Beijing,” *Geophys. Res. Lett.* **48**, e2020GL091944.
- Yao, Lei, *et al.*, 2018, “Atmospheric new particle formation from sulfuric acid and amines in a Chinese megacity,” *Science* **361**, 278–281.
- Ye, Q., *et al.*, 2019, “Molecular composition and volatility of nucleated particles from  $\alpha$ -pinene oxidation between  $-50^{\circ}\text{C}$  and  $+25^{\circ}\text{C}$ ,” *Environ. Sci. Technol.* **53**, 12357–12365.
- Yli-Juuti, T., K. Barsanti, L. Hildebrandt Ruiz, A.-J. Kieloaho, U. Makkonen, T. Petäjä, T. Ruuskanen, M. Kulmala, and I. Riipinen, 2013, “Model for acid-base chemistry in nanoparticle growth (MABNAG),” *Atmos. Chem. Phys.* **13**, 12507–12524.
- Yli-Juuti, T., *et al.*, 2011, “Growth rates of nucleation mode particles in Hyytiälä during 2003–2009: Variation with particle size, season, data analysis method and ambient conditions,” *Atmos. Chem. Phys.* **11**, 12865–12886.
- Yli-Juuti, Taina, *et al.*, 2009, “Characteristics of new particle formation events and cluster ions at K-pusztá, Hungary,” *Boreal Environ. Res.* **14**, 683–698, <https://www.borenav.net/BER/archive/pdfs/ber14/ber14-683.pdf>.
- Ylisirmio, A., L. M. F. Barreira, I. Pullinen, A. Buchholz, J. Jayne, J. E. Krechmer, D. R. Worsnop, A. Virtanen, and S. Schobesberger, 2021, “On the calibration of FIGAERO-ToF-CIMS: Importance and impact of calibrant delivery for the particle-phase calibration,” *Atmos. Meas. Tech.* **14**, 355–367.
- Young, L.-H., S.-H. Lee, V. P. Kanawade, T.-C. Hsiao, Y. L. Lee, B.-F. Hwang, Y.-J. Liou, H.-T. Hsu, and P.-J. Tsai, 2013, “New particle growth and shrinkage observed in subtropical environments,” *Atmos. Chem. Phys.* **13**, 547–564.
- Yu, F., 2011, “A secondary organic aerosol formation model considering successive oxidation aging and kinetic condensation of organic compounds: Global scale implications,” *Atmos. Chem. Phys.* **11**, 1083–1099.
- Yu, F., and G. Luo, 2009, “Simulation of particle size distribution with a global aerosol model: Contribution of nucleation to aerosol and CCN number concentrations,” *Atmos. Chem. Phys.* **9**, 7691–7710.
- Yu, H., L. Ren, X. Huang, M. Xie, J. He, and H. Xiao, 2019, “Iodine speciation and size distribution in ambient aerosols at a coastal new particle formation hotspot in China,” *Atmos. Chem. Phys.* **19**, 4025–4039.
- Yu, H., L. Zhou, L. Dai, W. Shen, W. Dai, J. Zheng, Y. Ma, and M. Chen, 2016, “Nucleation and growth of sub-3 nm particles in the polluted urban atmosphere of a megacity in China,” *Atmos. Chem. Phys.* **16**, 2641–2657.
- Yu, Huan, Robert McGraw, and Shan-Hu Lee, 2012, “Effects of amines on formation of sub-3 nm particles and their subsequent growth,” *Geophys. Res. Lett.* **39**.
- Yu, Huan, *et al.*, 2014, “New particle formation and growth in an isoprene-dominated Ozark forest: From sub-5 nm to CCN-active sizes,” *Aerosol Sci. Technol.* **48**, 1285–1298.
- Yu, Jianzhen, David R. Cocker, Robert J. Griffin, Richard C. Flagan, and John H. Seinfeld, 1999, “Gas-phase ozone oxidation of monoterpenes: Gaseous and particulate products,” *J. Atmos. Chem.* **34**, 207–258.
- Yuan, Bin, Abigail R. Koss, Carsten Warneke, Matthew Coggon, Kanako Sekimoto, and Joost A de Gouw, 2017, “Proton-transfer-reaction mass spectrometry: Applications in atmospheric sciences,” *Chem. Rev.* **117**, 13187–13229.
- Yue, D. L., M. Hu, R. Y. Zhang, Z. B. Wang, J. Zheng, Z. J. Wu, A. Wiedensohler, L. Y. He, X. F. Huang, and T. Zhu, 2010, “The roles of sulfuric acid in new particle formation and growth in the megacity of Beijing,” *Atmos. Chem. Phys.* **10**, 4953–4960.
- Zhang, K. Max, and Anthony S. Wexler, 2002, “A hypothesis for growth of fresh atmospheric nuclei,” *J. Geophys. Res. Atmos.* **107**, AAC 15-1–AAC 15-6.
- Zhang, Renyi, Alexei Khalizov, Lin Wang, Min Hu, and Wen Xu, 2012, “Nucleation and growth of nanoparticles in the atmosphere,” *Chem. Rev.* **112**, 1957–2011.
- Zhang, Renyi, Inseon Suh, Jun Zhao, Dan Zhang, Edward C. Fortner, Xuexi Tie, Luisa T. Molina, and Mario J. Molina, 2004, “Atmospheric new particle formation enhanced by organic acids,” *Science* **304**, 1487–1490.
- Zhang, Renyi, Lin Wang, Alexei F. Khalizov, Jun Zhao, Jun Zheng, Robert L. McGraw, and Luisa T. Molina, 2009, “Formation of nanoparticles of blue haze enhanced by anthropogenic pollution,” *Proc. Natl. Acad. Sci. U.S.A.* **106**, 17650–17654.
- Zhang, Xi, Spyros N. Pandis, and John H. Seinfeld, 2012, “Diffusion-limited versus quasi-equilibrium aerosol growth,” *Aerosol Sci. Technol.* **46**, 874–885.
- Zhao, Bin, *et al.*, 2020, “High concentration of ultrafine particles in the Amazon free troposphere produced by organic new particle formation,” *Proc. Natl. Acad. Sci. U.S.A.* **117**, 25344–25351.
- Zhao, Chuanfeng, Yanan Li, Fang Zhang, Yele Sun, and Pucui Wang, 2018, “Growth rates of fine aerosol particles at a site near Beijing in June 2013,” *Adv. Atmos. Sci.* **35**, 209–217.
- Zhao, D., *et al.*, 2018, “Effects of NO<sub>x</sub> and SO<sub>2</sub> on the secondary organic aerosol formation from photooxidation of  $\alpha$ -pinene and limonene,” *Atmos. Chem. Phys.* **18**, 1611–1628.
- Zhao, J., E. Häkkinen, F. Graeffe, J. E. Krechmer, M. R. Canagaratna, D. R. Worsnop, J. Kangasluoma, and M. Ehn, 2023, “A combined gas- and particle-phase analysis of highly oxygenated organic molecules (HOMs) from  $\alpha$ -pinene ozonolysis,” *Atmos. Chem. Phys.* **23**, 3707–3730.
- Zhao, Jun, Alexei Khalizov, Renyi Zhang, and Robert McGraw, 2009, “Hydrogen-bonding interaction in molecular complexes and clusters of aerosol nucleation precursors,” *J. Phys. Chem. A* **113**, 680–689.
- Zheng, G., C. Kuang, J. Uin, T. Watson, and J. Wang, 2020, “Large contribution of organics to condensational growth and formation of cloud condensation nuclei (CCN) in the remote marine boundary layer,” *Atmos. Chem. Phys.* **20**, 12515–12525.
- Zimmerman, Alyssa, Markus D. Petters, and Nicholas Meskhidze, 2020, “Observations of new particle formation, modal growth rates, and direct emissions of sub-10 nm particles in an urban environment,” *Atmos. Environ.* **242**, 117835.